

BNL-NCS-22500
ERDA/NDC-9/U
NEANDC(US)-201/U
INDC(USA)-77/U
Informal Report
Limited Distribution

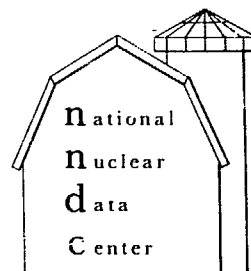
REPORTS TO THE ERDA NUCLEAR DATA COMMITTEE

Edited by
NATIONAL NUCLEAR DATA CENTER
for the
U.S. Energy Research and Development Administration
Nuclear Data Committee

March 1977

MASTER

BROOKHAVEN NATIONAL LABORATORY
ASSOCIATED UNIVERSITIES, INC.
UPTON, NEW YORK 11973



DISTRIBUTION OF THIS DOCUMENT IS UNLIMITED

**REPORTS TO
THE ERDA NUCLEAR DATA COMMITTEE**

March 1977



NOTICE
This report was prepared as an account of work sponsored by the United States Government. Neither the United States nor the United States Energy Research and Development Administration, nor any of their employees, nor any of their contractors, subcontractors, or their employees, makes any warranty, express or implied, or assumes any legal liability or responsibility for the accuracy, completeness or usefulness of any information, apparatus, product or process disclosed, or represents that its use would not infringe privately owned rights.

**Edited by
NATIONAL NUCLEAR DATA CENTER
for the
U.S. Energy Research and Development Administration
Nuclear Data Committee**

**NATIONAL NUCLEAR DATA CENTER
BROOKHAVEN NATIONAL LABORATORY
ASSOCIATED UNIVERSITIES, INC.**

**UNDER CONTRACT NO. EY-76-C-02-0016 WITH THE
UNITED STATES ENERGY RESEARCH AND DEVELOPMENT ADMINISTRATION**

PREFACE

The reports in this document were submitted to the Energy Research and Development Administration Nuclear Data Committee (ERDA-NDC) in March 1977. The reporting laboratories are those having a substantial effort in measuring neutron and nuclear cross sections of relevance to the U.S. applied nuclear energy program. The material contained in these reports is to be regarded as comprised of informal statements of recent developments and preliminary data. Persons wishing to make use of these data should contact the individual experimenter for further details. The data which appear in this document should be quoted only by permission of the contributor and should be referenced as private communication, and not by this document number. Appropriate subjects are listed as follows:

1. Microscopic neutron cross sections relevant to the nuclear energy program, including shielding. Inverse reactions where pertinent are included.
2. Charged particle cross sections, where they are relevant to 1) above, and where relevant to developing and testing nuclear models.
3. Gamma-ray production, radioactive decay, and theoretical developments in nuclear structure which are applicable to nuclear energy programs.
4. Proton and alpha-particle cross sections, at energies of up to 1 GeV, which are of interest to the space program.

These reports cannot be regarded as a complete summary of the nuclear research efforts in the U.S. A number of laboratories, whose research is less programmatically oriented do not submit reports; neither do the submitted reports reflect all the work related to nuclear data in progress at the submitting laboratory.

This compilation has been produced almost completely from master copies prepared by the individual contributors listed in the Table of Contents.

TABLE OF CONTENTS

1.	IDAHO NATIONAL ENGINEERING LABORATORY.	1
	R. L. Heath	
2.	ARGONNE NATIONAL LABORATORY	28
	H. Jackson, A. Smith	
3.	BATTELLE PACIFIC NORTHWEST LABORATORIES	45
	P. Reeder	
4.	BROOKHAVEN NATIONAL LABORATORY	47
	R. E. Chrien	
5.	COLUMBIA UNIVERSITY	67
	W. W. Havens, Jr.	
6.	IOWA STATE UNIVERSITY, AMES LABORATORY	78
	W. L. Talbert, Jr.	
7.	IRT CORPORATION, SAN DIEGO	84
	S. J. Friesenhahn, N.A. Lurie	
8.	LAWRENCE BERKELEY LABORATORY	87
	C. M. Lederer	
9.	LAWRENCE LIVERMORE LABORATORY	88
	J. D. Anderson, J. C. Browne, D. G. Gardner	
10.	LOS ALAMOS SCIENTIFIC LABORATORY	106
	E. T. Journey, H. Motz	
11.	UNIVERSITY OF LOWELL	158
	L. Beghian	
12.	MICHIGAN UNIVERSITY	164
	G. Knoll	
13.	NATIONAL BUREAU OF STANDARDS	170
	C. Bowman	
14.	OAK RIDGE NATIONAL LABORATORY	196
	F. G. Perey, J. C. Gentry	
15.	OHIO UNIVERSITY LABORATORY	222
	R. O. Lane	
16.	UNIVERSITY OF PENNSYLVANIA	240
	F. Ajzenberg-Selove	
17.	RENNSELAER POLYTECHNIC INSTITUTE	242
	R. C. Block	

TABLE OF CONTENTS (CONT'D.)

18.	TRIANGLE UNIVERSITIES LABORATORY	276
	H. Newson	
19.	UNIVERSITY OF WASHINGTON	306
	G. Woodruff	
20.	YALE UNIVERSITY	313
	F. W. Firk	
21.	UNIVERSITY OF KENTUCKY	315
	M. McEllistrem	

The CINDA-type index which follows was prepared
by Gail Waite, National Nuclear Data Center,
Brookhaven National Laboratory, Upton, New York.

ELEMENT S A	QUANTITY	TYPE	ENERGY		DOCUMENTATION		LAB	COMMENTS
			MIN	MAX	REF	VOL PAGE DATE		
H 001	DIFF ELASTIC	EXPT-PROG	27	47	ERDA-NDC-9	240	477	HAR FOWLEN-FORWARD SCT,NDG,
H 001	ABSORPTION	EXPT-PROG	NDG		ERDA-NDC-9	27	477	ANC SMITH-PREV VAL REVISED,WEIGHTED FIT,
HE 003	DIFF ELASTIC	EVAL-PROG	NDG		ERDA-NDC-9	157	477	LAS MALE-CHG INDEP R-MATRIX ANAL,NDG,TBC
HE 003	N, PHOTON	EVAL-PROG	NDG		ERDA-NDC-9	157	477	LAS MALE-CHG INDEP R-MATRIX ANAL,NDG,TBC
HE 004	DIFF ELASTIC	EVAL-PROG	20	47	ERDA-NDC-9	315	477	YAL BOND-R-MATRIX GLOBAL ANAL,NDG,TBP NP
HE 004	POLARIZATION	EXPT-PROG	20	47	ERDA-NDC-9	191	477	LAS LISOWSKI-JANGS,ANAL PWR MEAS,NDG
LI	NONEL GAMMA	EXPT-PROG	10	45	ERDA-NDC-9	197	477	ORL DICKENS-DIFF CS,NDG,TBP NSE,
LI 006	EVALUATION	EVAL-PROG	10	46	ERDA-NDC-9	157	477	LAS MALE-ENDF/B FILES TO BE PREPARED,NDG
LI 006	TOTAL XSECT	EXPT-PROG	10	45	ERDA-NDC-9	29	477	ANL KNITTER-20KEV INTRVL,R-MATRX TBD,NDG
LI 006	ELASTIC SCAT	EXPT-PROG	75	46	ERDA-NDC-9	277	477	TNL PURSEN-INTEG CS GRPH,DATA AT NNCS
LI 006	DIFF ELASTIC	EXPT-PROG	10	45	ERDA-NDC-9	29	477	ANL KNITTER-20KEV INTRVL,R-MATRX TBD,NDG
LI 006	DIFF ELASTIC	EXPT-PROG	40	46	ERDA-NDC-9	222	477	OHM KNOX-M MATRIX ANAL TBD,NDG
LI 006	DIFF ELASTIC	EXPT-PROG	75	46	ERDA-NDC-9	277	477	TNL PURSEN-7ES,PRELIM GRPH,DATA AT NNCS
LI 006	DIFF ELASTIC	EXPT-PROG	11	47	ERDA-NDC-9	200	477	TNL PURSEN-NDG,SMALL ANG MEAS TBD SPHNG
LI 006	DIFF ELASTIC	EXPT-PROG	11	47	ERDA-NDC-9	200	477	TNL VON-BEHRN-2ANG,XCIT FN,NDG,LI7 ANAL
LI 006	POLARIZATION	EXPT-PROG	15	46	ERDA-NDC-9	315	477	YAL CHIU-BANG,ANALYZING PWR CALC TBD,NDG
LI 006	TOT INELASTI	EXPT-PROG	75	46	ERDA-NDC-9	277	477	TNL PURSEN-INTEG CS GRPH,DATA AT NNCS
LI 006	DIFF INELAST	EXPT-PROG	10	45	ERDA-NDC-9	29	477	ANL KNITTER-20KEV INTRVL,R-MATRX TBD,NDG
LI 006	DIFF INELAST	EXPT-PROG	NDG		ERDA-NDC-9	222	477	OHM KNOX-MEAS TBD,NDG,
LI 006	DIFF INELAST	EXPT-PROG	75	46	ERDA-NDC-9	277	477	TNL PURSEN-7ES,00=2,10MEV,PRELIM GRPH,
LI 006	DIFF INELAST	EXPT-PROG	11	47	ERDA-NDC-9	200	477	TNL VON-BEHRN-2ANG,XCIT FN,NDG,LI7 ANAL
LI 006	N, TRITON	EXPT-PROG	47	41	ERDA-NDC-9	100	477	LAS BROWN-INVERSE,EXCIT FN,GRPH,CS TNL
LI 006	N, TRITON	EXPT-PROG	24	45	ERDA-NDC-9	124	477	LAS JARMIE-HE4 DEL USED,NDG,SEE LA-6188,
LI 006	N, TRITON	EXPT-PROG	24	44	ERDA-NDC-9	109	477	HMG ENGDAML-24KEV MEAS,NDG,MORE MEAS TBD
LI 006	N, TRITON	EXPT-PROG	30	43	ERDA-NDC-9	172	477	NBS LAMAZE-LINAC,TOF,PEAK,CS GVN,TBP NSE
LI 006	N, TRITON	EXPT-PROG	40	44	ERDA-NDC-9	172	477	NBS LAMAZE,U235/LIONT,ANAL TBD,NDG
LI 006	N, TRITON	EXPT-PROG	10	45	ERDA-NDC-9	205	477	ORL RENNER-CS MEAS IN 244KEV REGION,NDG
LI 007	ELASTIC SCAT	EXPT-PROG	70	46	ERDA-NDC-9	277	477	TNL PURSEN-INTEG CS GRPH,DATA AT NNCS,
LI 007	DIFF ELASTIC	EXPT-PROG	40	46	ERDA-NDC-9	222	477	OHM KNOX-ANAL OF DATA COMPLETED,NDG,
LI 007	DIFF ELASTIC	EXPT-PROG	70	46	ERDA-NDC-9	277	477	TNL PURSEN-BES,PRELIM GRPH,DATA AT NNCS
LI 007	TOT INELASTI	EXPT-PROG	90	46	ERDA-NDC-9	277	477	TNL PURSEN-INTEG CS GRPH,DATA AT NNCS,
LI 007	DIFF INELAST	EXPT-PROG	NDG		ERDA-NDC-9	222	477	OHM KNOX-478KEV LVL DEL,DIR MEAS TBD,NDG
LI 007	DIFF INELAST	EXPT-PROG	90	46	ERDA-NDC-9	277	477	TNL PURSEN-BES,PRELIM GRPH,DATA AT NNCS
BE 009	EVALUATION	EVAL-PROG	NDG		ERDA-NDC-9	138	477	LAS YOUNG-EVAL TBD,TO BE CFD ENDF,NDG
BE 009	TOTAL XSECT	EXPT-PROG	10	46	ERDA-NDC-9	146	477	LAS AUCHAMPAUGH-VDG,TOF,CS DATA,NDG

ELEMENT S A	QUANTITY	TYPE	ENERGY		DOCUMENTATION			LAB	COMMENTS
			MIN	MAX	REF	VOL	PAGE		
BE 009	DIFF ELASTIC	EXPT-PROG	NDG			ERDA-NDC-9	277 477	TNL PURSER-NDG,TBP NSE	
BE 009	DIFF ELASTIC	EXPT-PROG	15+6	60+0		ERDA-NDC-9	313 477	YAL MCGUIRE+DANG DIFF CS TO BE MEAS,NDG	
BE 009	POLARIZATION	EXPT-PROG	15+6	60+0		ERDA-NDC-9	313 477	YAL MCGUIRE+DANG,ASYMMTRY TO BE MEAS,NDG	
BE 009	DIFF INELAST	EXPT-PROG	NDG			ERDA-NDC-9	277 477	TNL PURSER-NDG,TBP NSE	
BE 009	DIFF INELAST	EXPT-PROG	70+6	75+0		ERDA-NDC-9	277 477	TNL PURSER-CONTINUM PROD CS,NDG,ANAL TBD	
B 010	EVALUATION	EXPT-PROG		10+0		ERDA-NDC-9	197 477	LAS MALE+END/FB FILES TO BE PREPARED,NDG	
B 010	TOTAL XSECT	EXPT-PROG	10+6	14+7		ERDA-NDC-9	100 477	LAS AUCHAMPAUGH+VDG,TOF,CS DATA,NDG	
B 010	DIFF ELASTIC	EXPT-PROG	40+6	80+0		ERDA-NDC-9	223 477	OHIO KNOX+PREV DATA ANAL,NDG,MEAS-TBC,	
B 010	DIFF ELASTIC	EXPT-PROG	NDG			ERDA-NDC-9	200 477	TNL PURSER-NDG,T60 FEB 1977	
B 010	DIFF INELAST	EXPT-PROG	NDG			ERDA-NDC-9	223 477	OHIO KNOX+MEAS TBD,NDG	
B 011	TOTAL XSECT	EXPT-PROG	10+6	14+7		ERDA-NDC-9	100 477	LAS AUCHAMPAUGH+VDG,TOF,CS DATA,NDG	
B 011	DIFF ELASTIC	EXPT-PROG	40+6	80+0		ERDA-NDC-9	223 477	OHIO WHITE+PREV DATA ANAL,NDG,MEAS TBC,	
B 011	DIFF ELASTIC	EXPT-PROG	NDG			ERDA-NDC-9	200 477	TNL PURSER-NDG,T60 FEB 1977	
B 011	DIFF INELAST	EXPT-PROG	NDG			ERDA-NDC-9	223 477	OHIO WHITE+MEAS TBD,NDG,	
C 012	TOTAL XSECT	EXPT-PROG	15+6	14+7		ERDA-NDC-9	100 477	LAS AUCHAMPAUGH+VDG,TOF,CS DATA,NDG	
C 012	DIFF ELASTIC	EXPT-PROG	NDG			ERDA-NDC-9	277 477	TNL PURSER-NDG,SEE NSE 61 P52.	
C 012	DIFF INELAST	EXPT-PROG	NDG			ERDA-NDC-9	277 477	TNL PURSER-NDG,SEE NSE 61 P52.	
C 012	NONEL GAMMAS	EXPT-PROG	10+5	20+7		ERDA-NDC-9	197 477	ORL DICKENS+DIFF CS,NDG,TBP NSE,	
C 013	TOTAL XSECT	EXPT-PROG	10+6	14+7		ERDA-NDC-9	100 477	LAS AUCHAMPAUGH+VDG,TOF,CS DATA,NDG	
C 013	GAMMA,N	EXPT-PROG		90+0		ERDA-NDC-9	33 477	ANL LASZEWSKI+TOF,2ANGS,R=MATRIX ANAL,NDG	
N 014	NONEL GAMMAS	EXPT-PROG	10+5	20+7		ERDA-NDC-9	197 477	ORL DICKENS+DIFF CS,NDG,TBP NSE,	
O 016	DIFF ELASTIC	EXPT-PROG	93+6	15+7		ERDA-NDC-9	200 477	TNL PURSER+12 ES,PHELIM GRPH 6ES,	
O 017	GAMMA,N	EXPT-PROG	45+6	71+0		ERDA-NDC-9	33 477	ANL LASZEWSKI+2ANG,GRPH,R=MATRIX ANAL	
F 019	TOTAL XSECT	EXPT-PROG	50+0	20+7		ERDA-NDC-9	203 477	ORL LARSON+THNS,CS,NDG,ABST ORNL-TM-2612	
F 019	NONEL GAMMAS	EXPT-PROG	10+5	20+7		ERDA-NDC-9	197 477	ORL DICKENS+DIFF CS,NDG,TBP NSE,	
NA 023	TOTAL XSECT	EXPT-PROG	32+4	37+7		ERDA-NDC-9	203 477	ORL LARSON+THNS,CS CFD END/FB,NDG	
NA 023	DIFF INELAST	EXPT-PROG	52+5	42+0		ERDA-NDC-9	128 477	LTI BARNES+INEL FROM G PROD,NDG,TBP PR/C	
NA 023	INELST GAMMA	EXPT-PROG	TR	20+0		ERDA-NDC-9	31 477	ANL SMITH,55UEG,REL U,CFD,NDG,TBP,NSE,	
NA 023	INELST GAMMA	EXPT-PROG	52+5	42+0		ERDA-NDC-9	128 477	LTI BARNES+G PHOD,ANG DISTR,NDG,TBP PR/C	
HG	DIFF ELASTIC	EXPT-PROG	11+7			ERDA-NDC-9	223 477	OHIO FERREN+TUF,OPTMDL PARS,ABST NP/A275,	
HG	NONEL GAMMAS	EXPT-PROG	10+5	20+7		ERDA-NDC-9	197 477	ORL DICKENS+DIFF CS,NDG,TBP NSE,	
HG 024	DIFF ELASTIC	EXPT-PROG	NDG			ERDA-NDC-9	204 477	ORL MOREN+L VALS FROM SCAT,NDG,TBP PR/C,	
AL 027	DIFF ELASTIC	EXPT-PROG	11+7			ERDA-NDC-9	223 477	OHIO FERREN+TUF,OPTMDL PARS,ABST NP/A275,	
AL 027	INELST GAMMA	EXPT-PROG		+0		ERDA-NDC-9	31 477	ANL SMITH,ANAL TBD,NDG,	
AL 027	NONEL GAMMAS	EXPT-PROG	10+5	20+7		ERDA-NDC-9	197 477	ORL DICKENS+DIFF CS,NDG,TBP NSE,	

ELEMENT S A	QUANTITY	TYPE	ENERGY		DOCUMENTATION		LAB	COMMENTS
			MIN	MAX	REF	VOL PAGE DATE		
AL 027	N, PHOTON	EXPT-PROG	15+7		ERDA-NDC-9	88	477	LRL HAIGHT+(N,XP)CS GVN,SPEC CFD STAIMDL
AL 027	N,N PHOTON	EXPT-PROG	15+7		ERDA-NDC-9	88	477	LRL HAIGHT+(N,XP)CS GVN,SPEC CFD STAIMDL
AL 027	N, DEUTERON	EXPT-PROG	15+7		ERDA-NDC-9	88	477	LRL HAIGHT+(N,XD)CS GVN,SPEC CFD STAIMDL
AL 027	N, ALPHA HEAC	EXPT-PROG	15+7		ERDA-NDC-9	88	477	LRL HAIGHT+(N,XA)CS GVN,SPEC CFD STAIMDL
SI	TOTAL XSECT	EXPT-PROG	50+0	73+0	ERDA-NDC-9	203	477	ORL LARSON+THNS,CFD ENDF,ABST ORNLTM5618
SI	DIFF ELASTIC	EXPT-PROG	11+7	26+7	ERDA-NDC-9	223	477	OHO RAPAPORT+JES,DISTR,OPTMOL ,ABST NP/A
SI	NONEL GAMMAS	EXPT-PROG	18+5	20+7	ERDA-NDC-9	197	477	ORL DICKENS+DIFF CS,NDG,TBP NSE,
SI 024	DIFF ELASTIC	EXPT-PROG	NDG		ERDA-NDC-9	223	477	OHO RAPAPORT+OPMOL PAR CA USED,ABST NP/A
SI 028	DIFF INELAST	EXPT-PROG	28+6	42+6	ERDA-NDC-9	129	477	LTJ BARNES+INEL FROM G PROD,NDG.
SI 028	DIFF INELAST	EXPT-PROG	NDG		ERDA-NDC-9	223	477	OHO RAPAPORT+OPMOL PAR CA USED,ABST NP/A
SI 028	INELST GAMMA	EXPT-PROG	28+6	42+6	ERDA-NDC-9	129	477	LTJ BARNES+G PROD,ANG DISTR,NDG.
SI 028	RESON PARAMS	EXPT-PROG		45+0	ERDA-NDC-9	286	477	TNL CLEMENT+R-MATRIX,ANAL,ABST AP102 ND,2
S	DIFF ELASTIC	EXPT-PROG	11+7	26+7	ERDA-NDC-9	223	477	OHO RAPAPORT+JES,DISTR,OPTMOL ,ABST NP/A
S	DIFF ELASTIC	EXPT-PROG	11+7		ERDA-NDC-9	223	477	OHO FERREN+TOF,OPTMOL PARS,ABST NP/A275,
S 032	DIFF ELASTIC	EXPT-PROG	NDG		ERDA-NDC-9	223	477	OHO RAPAPORT+OPMOL PAR CA USED,ABST NP/A
S 032	DIFF INELAST	EXPT-PROG	NDG		ERDA-NDC-9	223	477	OHO RAPAPORT+OPMOL PAR CA USED,ABST NP/A
CL 033	SPECT N,GAMM	EXPT-PROG	40+2		ERDA-NDC-9	97	477	BNL CMRIEN+P-T STAT MDL FAILS,TBP NSE,
CA	DIFF ELASTIC	EXPT-PROG	11+7	26+7	ERDA-NDC-9	223	477	OHO RAPAPORT+JES,DISTR,OPTMOL ,ABST NP/A
CA	DIFF ELASTIC	EXPT-PROG	11+7		ERDA-NDC-9	223	477	OHO FERREN+TOF,OPTMOL PARS,ABST NP/A275,
CA	NONEL GAMMAS	EXPT-PROG	18+5	20+7	ERDA-NDC-9	197	477	ORL DICKENS+DIFF CS,NDG,TBP NSE,
CA 042	DIFF ELASTIC	EXPT-PROG	NDG		ERDA-NDC-9	223	477	OHO RAPAPORT+OPMOL ANAL CA=40,ABST NP/A
CA 042	DIFF INELAST	EXPT-PROG	11+7	26+7	ERDA-NDC-9	227	477	OHO RAPAPORT+INEL XCIT ANAL,NDG,TBP
CA 042	N, GAMMA	EXPT-PROG	NDG		ERDA-NDC-9	202	477	AUA MUSGROVE+ORELA,RES PARS,NDG,TBP NP/A
CA 042	RESON PARAMS	EXPT-PROG		23+0	ERDA-NDC-9	202	477	AUA MUSGROVE+D GVN S WAVE,HC PH,TBP NP/A
CA 043	N, GAMMA	EXPT-PROG	NDG		ERDA-NDC-9	202	477	AUA MUSGROVE+ORELA,RES PARS,NDG,TBP NP/A
CA 043	RESON PARAMS	EXPT-PROG		40+0	ERDA-NDC-9	202	477	AUA MUSGROVE+D GVN S WAVE,HC SW,TBP NP/A
CA 044	N, GAMMA	EXPT-PROG	NDG		ERDA-NDC-9	202	477	AUA MUSGROVE+ORELA,RES PARS,NDG,TBP NP/A
CA 044	RESON PARAMS	EXPT-PROG		17+0	ERDA-NDC-9	202	477	AUA MUSGROVE+D GVN S WAVE,HC PH,TBP NP/A
SC 045	TOTAL XSECT	EXPT-PROG	40+2	20+0	ERDA-NDC-9	49	477	RPI LIOU+MPI LINAC,CURV,2KEV=,7100,TBP
SC 045	TOTAL XSECT	EXPT-PROG	20+3		ERDA-NDC-9	220	477	RPI BICKNELL+TRNS,TOF,CS=,71+0,028,
SC 045	RESON PARAMS	EXPT-PROG	05+3	21+4	ERDA-NDC-9	49	477	RPI LIOU+M-MATRIX,S,P,HC,WN,J,TBL,TBP
TI	EVALUATION	EXPT-PROG	18+5	20+7	ERDA-NDC-9	43	477	ANL PHYLIS+ISOTOPE+ELEMENT,ENDFB9,NDG,
TI	TOTAL XSECT	EXPT-PROG	18+6	50+0	ERDA-NDC-9	29	477	ANL GUENTHER+CFD MDL,NDG,TBP ANL=NDM=24
TI	TOTAL XSECT	EXPT-PROG	18+6	50+0	ERDA-NDC-9	30	477	ANL WALEN+190KEV RSLN,VARY THICKNES,NDG
TI	DIFF ELASTIC	EXPT-PROG	15+6	40+0	ERDA-NDC-9	29	477	ANL GUENTHER+CFD MDL,NDG,TBP ANL=NDM=24

ELEMENT S A	QUANTITY	TYPE	ENERGY		DOCUMENTATION			LAB	COMMENTS
			MIN	MAX	REF	VOL	PAGE		
TI	DIFF INELAST	EXPT=PROG	15*6	40*6	ERDA=NDC-9	29	477	ANL	GUENTHER+CFD MDL,NDG,TBP ANL=NDM=24
TI 046	DIFF INELAST	EXPT=PROG TR	34*6		ERDA=NDC-9	129	477	LTI	BARNES+INEL FROM G PROD,NDG.
TI 046	N ₁ GAMMA	EXPT=PROG	28*3	30*3	ERDA=NDC-9	198	477	AUA	ALLEN+CAPT CS ,2PC RSLN,NDG
TI 046	INELST GAMMA	EXPT=PROG TR	34*6		ERDA=NDC-9	129	477	LTI	BARNES+G PROD,ANG DISTR,NDG.
TI 046	N ₁ PROTON	EVAL=PROG	NDG		ERDA=NDC-9	93	477	ANL	PHYLIS+ENDFB5,NDG,SEE ANL=NDM=27
TI 046	N ₁ PROTON	EXPT=PROG	15*7		ERDA=NDC-9	88	477	LRL	HAIGHT+(N,XP)CS GVN,SPEC CFD STAIMDL
TI 046	N ₁ N PROTON	EXPT=PROG	15*7		ERDA=NDC-9	88	477	LRL	HAIGHT+(N,XP)CS GVN,SPEC CFD STAIMDL
TI 046	N ₁ DEUTERON	EXPT=PROG	15*7		ERDA=NDC-9	88	477	LRL	HAIGHT+(N,XD)CS GVN,SPEC CFD STAIMDL
TI 046	N ₁ ALPHA REAC	EXPT=PROG	15*7		ERDA=NDC-9	88	477	LRL	HAIGHT+(N,XA)CS GVN,SPEC CFD STAIMDL
TI 046	RESON PARAMS	EXPT=PROG	28*3	30*3	ERDA=NDC-9	198	477	AUA	ALLEN+RES CAPT,WNO,WG S WAVE,NDG
TI 047	N ₁ GAMMA	EXPT=PROG	28*3	30*3	ERDA=NDC-9	198	477	AUA	ALLEN+CAPT CS 92PC RSLN,NDG
TI 047	INELST GAMMA	EXPT=PROG TR	34*6		ERDA=NDC-9	129	477	LTI	BARNES+G PROD,ANG DISTR,NDG.
TI 047	N ₁ PROTON	EVAL=PROG	NDG		ERDA=NDC-9	93	477	ANL	PHYLIS+ENDFB5,NDG,SEE ANL=NDM=27
TI 047	RESON PARAMS	EXPT=PROG	28*3	30*3	ERDA=NDC-9	198	477	AUA	ALLEN+RES CAPT,WNO,WG S WAVE,NDG
TI 048	DIFF INELAST	EXPT=PROG TR	34*6		ERDA=NDC-9	129	477	LTI	BARNES+INEL FROM G PROD,NDG.
TI 048	N ₁ GAMMA	EXPT=PROG	28*3	30*3	ERDA=NDC-9	198	477	AUA	ALLEN+CAPT CS ,2PC RSLN,NDG
TI 048	INELST GAMMA	EXPT=PROG TR	34*6		ERDA=NDC-9	129	477	LTI	BARNES+G PROD,ANG DISTR,NDG.
TI 048	N ₁ PROTON	EVAL=PROG	NDG		ERDA=NDC-9	93	477	ANL	PHYLIS+ENDFB5,NDG,SEE ANL=NDM=27
TI 048	N ₁ PROTON	EXPT=PROG	15*7		ERDA=NDC-9	88	477	LRL	HAIGHT+(N,NP)CS GVN,SPEC CFD STAIMDL
TI 048	N ₁ DEUTERON	EXPT=PROG	15*7		ERDA=NDC-9	88	477	LRL	HAIGHT+(N,ND)CS GVN,SPEC CFD STAIMDL
TI 048	N ₁ ALPHA REAC	EXPT=PROG	15*7		ERDA=NDC-9	88	477	LRL	HAIGHT+(N,NA)CS GVN,SPEC CFD STAIMDL
TI 048	RESON PARAMS	EXPT=PROG	28*3	30*3	ERDA=NDC-9	198	477	AUA	ALLEN+RES CAPT,WNO,WG S WAVE,NDG
TI 049	N ₁ GAMMA	EXPT=PROG	28*3	30*3	ERDA=NDC-9	198	477	AUA	ALLEN+CAPT CS ,2PC RSLN,NDG
TI 049	INELST GAMMA	EXPT=PROG TR	34*6		ERDA=NDC-9	129	477	LTI	BARNES+G PROD,ANG DISTR,NDG.
TI 049	RESON PARAMS	EXPT=PROG	28*3	30*3	ERDA=NDC-9	198	477	AUA	ALLEN+RES CAPT,WNO,WG S WAVE,NDG
TI 050	DIFF INELAST	EXPT=PROG TR	34*6		ERDA=NDC-9	129	477	LTI	BARNES+INEL FROM G PROD,NDG.
TI 050	N ₁ GAMMA	EXPT=PROG	28*3	30*3	ERDA=NDC-9	198	477	AUA	ALLEN+CAPT CS ,2PC RSLN,NDG
TI 050	INELST GAMMA	EXPT=PROG TR	34*6		ERDA=NDC-9	129	477	LTI	BARNES+G PROD,ANG DISTR,NDG.
TI 050	RESON PARAMS	EXPT=PROG	28*3	30*3	ERDA=NDC-9	198	477	AUA	ALLEN+RES CAPT,WNO,WG S WAVE,NDG
V 051	EVALUATION	EVAL=PROG	10*6	20*7	ERDA=NDC-9	43	477	ANL	SMITH+ENDFB5,TBP IN ANL=NDM=24.
V 051	TOTAL XSECT	EXPT=PROG	10*6	50*6	ERDA=NDC-9	30	477	ANL	GUENTHER+CS HEAS,NDG,TBP NSE,
V 051	ELASTIC SCAT	EXPT=PROG	10*6	50*6	ERDA=NDC-9	30	477	ANL	GUENTHER+CS HEAS,NDG,TBP NSE,
V 051	DIFF ELASTIC	EXPT=PROG	10*6	50*6	ERDA=NDC-9	30	477	ANL	GUENTHER+CS HEAS,NDG,TBP NSE,
V 051	DIFF ELASTIC	EXPT=PROG	11*7		ERDA=NDC-9	229	477	OWO	FERRER+TOF,OPTMDL PARS,ABST NP/A275,
V 051	DIFF INELAST	EXPT=PROG	10*6	50*6	ERDA=NDC-9	30	477	ANL	GUENTHER+CS HEAS,NDG,TBP NSE,

ELEMENT S A	QUANTITY	TYPE	ENERGY		DOCUMENTATION			LAB	COMMENTS
			MIN	MAX	REF	VOL	PAGE		
V 051	NONEL GAMMAS	EXPT=PHOG	10+5	20+7	ERDA=NDC-9	197	477	ORL DICKENS+DIFF CS,NOG,TBP NSE.	
V 051	NONEL GAMMAS	EXPT=PHOG	10+5	20+7	ERDA=NDC-9	197	477	ORL DICKENS+DIFF CS,NOG,TBP NSE.	
V 051	N ₁ PROTON	EXPT=PHOG	15+7		ERDA=NDC-9	08	477	LRL HAIGHT+(N,NP)CS GVN,SPEC CFD STAIMDL	
V 051	N ₁ N PROTON	EXPT=PHOG	15+7		ERDA=NDC-9	08	477	LRL HAIGHT+(N,NP)CS GVN,SPEC CFD STAIMDL	
V 051	N ₁ DEUTERON	EXPT=PHOG	15+7		ERDA=NDC-9	08	477	LRL HAIGHT+(N,NP)CS GVN,SPEC CFD STAIMDL	
V 051	N ₁ ALPHA REAC	EXPT=PHOG	15+7		ERDA=NDC-9	08	477	LRL HAIGHT+(N,NA)CS GVN,SPEC CFD STAIMDL	
V 051	N ₁ N ALPHA	EXPT=PHOG	15+7		ERDA=NDC-9	08	477	LRL HAIGHT+(N,NA)CS GVN,SPEC CFD STAIMDL	
CR	NONEL GAMMAS	EXPT=PHOG	10+5	20+7	ERDA=NDC-9	197	477	ORL DICKENS+DIFF CS,NOG,TBP NSE.	
CR 050	DIFF INELAST	EXPT=PHOG	84+5	40+0	ERDA=NDC-9	199	477	LTI BARNES+INEL FROM G PROD,NOG,TBP	
CR 050	N ₁ GAMMA	EXPT=PHOG		35+0	ERDA=NDC-9	198	477	AUA KENNY+ORELA,CAPT CS,NOG	
CR 050	INELST GAMMA	EXPT=PHOG	84+5	40+0	ERDA=NDC-9	199	477	LTI BARNES+G PROD CS AT 125 DEG,NOG,TBP	
CR 050	N ₁ PROTON	EVAL=PHOG	10+6	12+7	ERDA=NDC-9	199	477	LAS ARTHUR+P,ALF CS+SPEC,STAINLESS STEEL	
CR 050	N ₁ PROTON	EVAL=PHOG	10+6	12+7	ERDA=NDC-9	199	477	LAS ARTHUR+P,ALF CS+SPEC,STAINLESS STEEL	
CR 050	RESON PARAMS	EXPT=PHOG		35+0	ERDA=NDC-9	198	477	AUA KENNY+RES PARS 100 RES FROM N,G,NOG	
CR 052	DIFF INELAST	EXPT=PHOG	84+5	40+0	ERDA=NDC-9	199	477	LTI BARNES+INEL FROM G PROD,NOG,TBP	
CR 052	N ₁ GAMMA	EXPT=PHOG		35+0	ERDA=NDC-9	198	477	AUA KENNY+ORELA,CS MEAS,NOG	
CR 052	INELST GAMMA	EXPT=PHOG	84+5	40+0	ERDA=NDC-9	199	477	LTI BARNES+G PROD CS AT 125 DEG,NOG,TBP	
CR 052	N ₁ PROTON	EVAL=PHOG	10+6	12+7	ERDA=NDC-9	199	477	LAS ARTHUR+P,ALF CS+SPEC,STAINLESS STEEL	
CR 052	N ₁ PROTON	EVAL=PHOG	10+6	12+7	ERDA=NDC-9	199	477	LAS ARTHUR+P,ALF CS+SPEC,STAINLESS STEEL	
CR 052	RESON PARAMS	EXPT=PHOG		35+0	ERDA=NDC-9	198	477	AUA KENNY+ORELA,RES PARS 100RES,NOG	
CR 053	DIFF INELAST	EXPT=PHOG	84+5	40+0	ERDA=NDC-9	199	477	LTI BARNES+INEL FROM G PROD,NOG,TBP	
CR 053	N ₁ GAMMA	EXPT=PHOG		35+0	ERDA=NDC-9	198	477	AUA KENNY+ORELA,CS MEAS,NOG	
CR 053	INELST GAMMA	EXPT=PHOG	84+5	40+0	ERDA=NDC-9	199	477	LTI BARNES+G PROD CS AT 125 DEG,NOG,TBP	
CR 053	RESON PARAMS	EXPT=PHOG		35+0	ERDA=NDC-9	198	477	AUA KENNY+ORELA,RES PARS 100RES,NOG	
CR 054	DIFF INELAST	EXPT=PHOG	84+5	40+0	ERDA=NDC-9	199	477	LTI BARNES+INEL FROM G PROD,NOG,TBP	
CR 054	N ₁ GAMMA	EXPT=PHOG		35+0	ERDA=NDC-9	198	477	AUA KENNY+ORELA,CS MEAS,NOG	
CR 054	INELST GAMMA	EXPT=PHOG	84+5	40+0	ERDA=NDC-9	199	477	LTI BARNES+G PROD CS AT 125 DEG,NOG,TBP	
CR 054	RESON PARAMS	EXPT=PHOG		35+0	ERDA=NDC-9	198	477	AUA KENNY+ORELA,RES PARS 100RES,NOG	
MN 055	DIFF ELASTIC	EXPT=PHOG	11+7		ERDA=NDC-9	220	477	OHQ FERREN+TUF,OPTMOL PARS,ABST NP/A275.	
MN 055	DIFF INELAST	EXPT=PHOG	10+6	36+0	ERDA=NDC-9	100	477	LTI BARNES+INEL FROM G PROD,NOG,TBP NP/A	
MN 055	ABSORPTION	EXPT=PHOG	NOG		ERDA=NDC-9	27	477	ANC SMITH+PREV VAL REVISED,WEIGHTED FIT.	
MN 055	INELST GAMMA	EXPT=PHOG	10+6	36+0	ERDA=NDC-9	100	477	LTI BARNES+G,PHOG CS,125 DEG,NOG,TBP NP.	
MN 055	NONEL GAMMAS	EXPT=PHOG	20+5	20+7	ERDA=NDC-9	196	477	ORL MORGAN,DIFF CS,CFD ENDF,NOG.	
FE	DIFF ELASTIC	EXPT=PHOG	11+7		ERDA=NDC-9	220	477	OHQ FERREN+TUF,OPTMOL PARS,ABST NP/A275.	
FE	TOT INELAST	EXPT=PHOG		21+0	ERDA=NDC-9	204	477	ORL KINNEY+TOT INEL FROM DNG,NOG,TBP NSE	

ELEMENT S A	QUANTITY	TYPE	ENERGY		DOCUMENTATION			LAB	COMMENTS
			MIN	MAX	REF	VOL	PAGE		
FE	DIFF INELAST	EXPT-PROG	98+5	48+6	ERDA-NDC-9	168	477	LTI BARNES+INEL FROM G PROD,NOG,TBP,	
FE	DIFF INELAST	EXPT-PROG		21+6	ERDA-NDC-9	204	477	ORL KINNEY+ANG DISTR VIA DNG,NOG,TBP NSE	
FE	SPECT N,GAMM	EXPT-PROG NOG			ERDA-NDC-9	207	477	ORL WELLS+FE27 G RAY LVL STUDY,CFD,NOG	
FE	INELST GAMMA	EXPT-PROG	88+5	28+6	ERDA-NDC-9	91	477	ANL SMITH,50KEV RSLN,REL U235,NOG,TBP	
FE	INELST GAMMA	EXPT-PROG	15+7		ERDA-NDC-9	94	477	LRL KOOPMAN+HIGH RESOL GE=LI DET,NOG,TBC	
FE	INELST GAMMA	EXPT-PROG	88+5	48+6	ERDA-NDC-9	168	477	LTI BARNES+G PROD AT 125 DEG,NOG,CFD,TBP	
FE	INELST GAMMA	EXPT-PROG		21+6	ERDA-NDC-9	204	477	ORL KINNEY+3ANG,848KEV G RAY,NOG,TBP NSE	
FE	NONEL GAMMAS	EXPT-PROG	85+5	28+7	ERDA-NDC-9	197	477	ORL CHAPMAN+DIFF CS,NOG,ABST ORNL=TM5416	
FE	NONEL GAMMAS	EXPT-PROG	18+5	28+7	ERDA-NDC-9	197	477	ORL DICKENS+DIFF CS,NOG,TBP NSE.	
FE 054	DIFF INELAST	EXPT-PROG	88+5	48+6	ERDA-NDC-9	168	477	LTI BARNES+INEL FROM G PROD,NOG,TBP,	
FE 054	N, GAMMA	EXPT-PROG	25+3	58+3	ERDA-NDC-9	200	477	AUA ALLEN+CAPT CS ,2PC RSLN,NOG	
FE 054	INELST GAMMA	EXPT-PROG	88+5	48+6	ERDA-NDC-9	168	477	LTI BARNES+G PROD AT 125 DEG,NOG,CFD,TBP	
FE 054	N, PROTON	EVAL-PROG	18+6	12+7	ERDA-NDC-9	139	477	LAS ARTHUR+P,ALF CS+SPEC,STAINLESS STEEL	
FE 054	N,ALPHA REAC	EVAL-PROG	58+6	16+7	ERDA-NDC-9	139	477	LAS ARTHUR+P,ALF CS+SPEC,STAINLESS STEEL	
FE 054	RESON PARAMS	EXPT-PROG	25+3	58+3	ERDA-NDC-9	200	477	AUA ALLEN+CAPT,S WAVE HN,NG STUDY,NOG,	
FE 056	TOTAL XSECT	EXPT-PROG	24+4		ERDA-NDC-9	22	477	RPI CHRIEN+RPI LINAC,57MB,ANAL TBC,	
FE 056	TOTAL XSECT	EXPT-PROG	24+4		ERDA-NDC-9	220	477	RPI BICKNELL+THNS,TOF,CS=,057+.,0038	
FE 056	DIFF INELAST	EXPT-PROG	88+5	48+6	ERDA-NDC-9	168	477	LTI BARNES+INEL FROM G PROD,NOG,TBP,	
FE 056	N, GAMMA	EXPT-PROG	25+3	48+3	ERDA-NDC-9	202	477	AUA ALLEN+RES PARS DRVD,CFD,NOG,SEE NP/A	
FE 056	INELST GAMMA	EXPT-PROG	14+7	15+7	ERDA-NDC-9	94	477	LRL KOOPMAN+RING GEOM,GE=LI DET,TBL,TBC	
FE 056	INELST GAMMA	EXPT-PROG	88+5	48+6	ERDA-NDC-9	168	477	LTI BARNES+G PROD AT 125 DEG,NOG,CFD,TBP	
FE 056	N, PROTON	EVAL-PROG	18+6	12+7	ERDA-NDC-9	139	477	LAS ARTHUR+P,ALF CS+SPEC,STAINLESS STEEL	
FE 056	N,ALPHA REAC	EVAL-PROG	58+6	16+7	ERDA-NDC-9	139	477	LAS ARTHUR+P,ALF CS+SPEC,STAINLESS STEEL	
FE 056	RESON PARAMS	EXPT-PROG	25+3	48+3	ERDA-NDC-9	202	477	AUA ALLEN+S,P,D WAVE PARS,NOG,SEE NP/A	
FE 057	DIFF INELAST	EXPT-PROG	88+5	48+6	ERDA-NDC-9	168	477	LTI BARNES+INEL FROM G PROD,NOG,TBP,	
FE 057	INELST GAMMA	EXPT-PROG	88+5	48+6	ERDA-NDC-9	168	477	LTI BARNES+G PROD AT 125 DEG,NOG,CFD,TBP	
FE 058	SPECT N,GAMM	EXPT-PROG NOG			ERDA-NDC-9	207	477	ORL WELLS+FE29 G RAY LVL STUDY,CFD,NOG	
FE CMP	N, PROTON	EXPT-PROG	15+7		ERDA-NDC-9	88	477	LRL HAIGHT+(N,NP)CS GVN,STAINLESS STEAL	
FE CMP	N, DEUTERON	EXPT-PROG	15+7		ERDA-NDC-9	88	477	LRL HAIGHT+(N,ND)CS GVN,STAINLESS STEAL	
FE CMP	N,ALPHA REAC	EXPT-PROG	15+7		ERDA-NDC-9	88	477	LRL HAIGHT+(N,NA)CS GVN,STAINLESS STEAL	
CO 059	EVALUATION	EVAL-PROG	35+4	48+7	ERDA-NDC-9	139	477	LAS ARTHUR+NEUTRON REACTIONS CALC,NOG	
CO 059	DIFF ELASTIC	EXPT-PROG	11+7		ERDA-NDC-9	223	477	DMD FERREH+TOF,OPTHDL PARS,ABST NP/A275,	
CO 059	DIFF INELAST	EXPT-PROG	11+6	33+6	ERDA-NDC-9	161	477	LTI BARNES+19 LVLS,FROM G PROD,NOG,TBP,	
CO 059	INELST GAMMA	EXPT-PROG	11+6	33+6	ERDA-NDC-9	161	477	LTI BARNES+G PROD,ANG DISTR,NOG,TBP,	
NI	DIFF ELASTIC	EXPT-PROG	11+7		ERDA-NDC-9	223	477	DMD FERREH+TOF,OPTHDL PARS,ABST NP/A275,	

ELEMENT S A	QUANTITY	TYPE	ENERGY		DOCUMENTATION			LAB	COMMENTS
			MIN	MAX	REF	VOL	PAGE		
NI	INELST GAMMA	EXPT=PHOG	15+7		ERDA=NDC-9	94	477	LRL KOOPMAN+HIGH RESOL GE=LI DET,NOG,TBC	
NI	NONEI GAMMAS	EXPT=PHOG	10+5	20+7	ERDA=NDC-9	197	477	ORL DICKENS+DIFF CS,NOG,TBP NSE.	
NI	N,ALPHA REAC	EXPT=PHOG	NOG		ERDA=NDC-9	100	477	LYI BARNES+PULSED IONIZ CH,NOG,TBD.	
NI 058	DIFF INELAST	EXPT=PHOG	14+6	40+0	ERDA=NDC-9	101	477	LTI BARNES+INEL FROM G PROD TBD,TBP,NOG	
NI 058	INELST GAMMA	EXPT=PHOG	14+6	40+0	ERDA=NDC-9	101	477	LTI BARNES+G PROD AT 125 DEG,NOG,TBP	
NI 058	N, PROTON	EVAL=PHOG	10+6	12+7	ERDA=NDC-9	109	477	LAS ARTHUR+P,ALF CS+SPEC,STAINLESS STEEL	
NI 058	N,ALPHA REAC	EVAL=PHOG	50+6	16+7	ERDA=NDC-9	109	477	LAS ARTHUR+P,ALF CS+SPEC,STAINLESS STEEL	
NI 060	DIFF INELAST	EXPT=PHOG	14+6	40+0	ERDA=NDC-9	101	477	LTI BARNES+INEL FROM G PROD TBD,TBP,NOG	
NI 060	INELST GAMMA	EXPT=PHOG	14+6	40+0	ERDA=NDC-9	101	477	LTI BARNES+G PROD AT 125 DEG,NOG,TBP	
NI 060	N, PROTON	EVAL=PHOG	10+6	12+7	ERDA=NDC-9	109	477	LAS ARTHUR+P,ALF CS+SPEC,STAINLESS STEEL	
NI 060	N,ALPHA REAC	EVAL=PHOG	10+6	12+7	ERDA=NDC-9	109	477	LAS ARTHUR+P,ALF CS+SPEC,STAINLESS STEEL	
CU	NONEI GAMMAS	EXPT=PHOG	10+5	20+7	ERDA=NDC-9	197	477	ORL DICKENS+DIFF CS,NOG,TBP NSE.	
CU 063	INELST GAMMA	EXPT=PHOG			ERDA=NDC-9	01	477	ANL SMITH,ANAL TBD,NOG.	
CU 063	N, PROTON	EXPT=PHOG	15+7		ERDA=NDC-9	08	477	LRL HAIGHT+(N,NP)CS GVN,SPEC CFD STAIMDL	
CU 063	N,N PROTON	EXPT=PHOG	15+7		ERDA=NDC-9	08	477	LRL HAIGHT+(N,XP)CS GVN,SPEC CFD STAIMDL	
CU 063	N, DEUTERON	EXPT=PHOG	15+7		ERDA=NDC-9	08	477	LRL HAIGHT+(N,ND)CS GVN,SPEC CFD STAIMDL	
CU 063	N,ALPHA REAC	EXPT=PHOG	15+7		ERDA=NDC-9	08	477	LRL HAIGHT+(N,NA)CS GVN,SPEC CFD STAIMDL	
CU 063	N,N ALPHA	EXPT=PHOG	15+7		ERDA=NDC-9	08	477	LRL HAIGHT+(N,XA)CS GVN,SPEC CFD STAIMDL	
CU 065	INELST GAMMA	EXPT=PHOG			ERDA=NDC-9	01	477	ANL SMITH,ANAL TBD,NOG.	
CU 065	N, PROTON	EXPT=PHOG	15+7		ERDA=NDC-9	08	477	LRL HAIGHT+(N,NP)CS GVN,SPEC CFD STAIMDL	
CU 065	N,N PROTON	EXPT=PHOG	15+7		ERDA=NDC-9	08	477	LRL HAIGHT+(N,XP)CS GVN,SPEC CFD STAIMDL	
CU 065	N, DEUTERON	EXPT=PHOG	15+7		ERDA=NDC-9	08	477	LRL HAIGHT+(N,ND)CS GVN,SPEC CFD STAIMDL	
CU 065	N,ALPHA REAC	EXPT=PHOG	15+7		ERDA=NDC-9	08	477	LRL HAIGHT+(N,NA)CS GVN,SPEC CFD STAIMDL	
CU 065	N,N ALPHA	EXPT=PHOG	15+7		ERDA=NDC-9	08	477	LRL HAIGHT+(N,XA)CS GVN,SPEC CFD STAIMDL	
ZN	INELST GAMMA	EXPT=PHOG	15+7		ERDA=NDC-9	94	477	LRL KOOPMAN+HIGH RESOL GE=LI DET,NOG,TBC	
ZN	NONEI GAMMAS	EXPT=PHOG	10+5	20+7	ERDA=NDC-9	197	477	ORL DICKENS+DIFF CS,NOG,TBP NSE.	
KR	N, GAMMA	EXPT=PHOG	10+0	10+0	ERDA=NDC-9	247	477	RPI FEIGENBAUM+CAPT CS MEAS,NOG.	
KR	RESON PARAMS	EXPT=PHOG	28+1	11+0	ERDA=NDC-9	247	477	RPI FEIGENBAUM+TBL NEW RES OBS.	
KR 078	N, GAMMA	EXPT=PHOG	NOG		ERDA=NDC-9	247	477	RPI FEIGENBAUM+MEAS TBD,NOG.	
KR 080	RESON PARAMS	EXPT=PHOG	11+0		ERDA=NDC-9	247	477	RPI FEIGENBAUM+105,9 CAPT RES OBS	
KR 082	RESON PARAMS	EXPT=PHOG	40+1		ERDA=NDC-9	247	477	RPI FEIGENBAUM+40,05 CAPT RES OBS	
KR 083	RESON PARAMS	EXPT=PHOG	28+1	23+2	ERDA=NDC-9	247	477	RPI FEIGENBAUM+20,06,232.3EV N,G RES OBS	
Y 088	N, GAMMA	EXPT=PHOG	03		ERDA=NDC-9	110	477	LAS SILBERT,NUCLEAR EXPLD SOURCE,NOG,TBD	
Y 088	N, PROTON	EXPT=PHOG	NOG		ERDA=NDC-9	100	477	LAS BRITTY+CALC FROM CHG PARTICLE,NOG,TBC	
Y 089	DIFF ELASTIC	EXPT=PHOG	28+6		ERDA=NDC-9	310	477	KTY MCDANIEL+STRUCTURE STUDY,NOG	

ELEMENT S A	QUANTITY	TYPE	ENERGY		DOCUMENTATION			LAB	COMMENTS
			MIN	MAX	REF	VOL	PAGE		
Y 089	DIFF INELAST	EXPT=PROG	28+6		ERDA=NDC-9	312	477	KTY MCDANIEL+STRUCTURE STUDY,NDG,	
Y 089	N, GAMMA	EXPT=PROG	25+3	18+2	ERDA=NDC-9	198	477	AUA BOLDEMAN+OHELA,CS MEAS,NDG,	
Y 089	N, PROTON	EXPT=PROG	48+6	14+7	ERDA=NDC-9	198	477	LAS BRITT+CALC FROM CHG PARTICL,GRPH,TBC	
Y 089	N,N PROTON	EXPT=PROG	48+6	14+7	ERDA=NDC-9	198	477	LAS BRITT+CALC FROM CHG PARTICL,GRPH,TBC	
ER 090	DIFF ELASTIC	EXPT=PROG	35+6		ERDA=NDC-9	312	477	KTY MCDANIEL+STRUCTURE STUDY,NDG	
ER 090	DIFF INELAST	EXPT=PROG	NDG		ERDA=NDC-9	228	477	OWO RAPAPORT+ISQSPIN EFFECTS,NDG,TBP,	
ER 090	DIFF INELAST	EXPT=PROG	35+6		ERDA=NDC-9	312	477	KTY MCDANIEL+STRUCTURE STUDY,NDG,	
ER 091	TOTAL XSECT	EXPT=PROG	NDG		ERDA=NDC-9	199	477	AUA MUSGROVE+THNS+CAPT,RESPANS DRVD,NDG	
ER 091	N, GAMMA	EXPT=PROG	NDG		ERDA=NDC-9	199	477	AUA MUSGROVE+THNS+CAPT,RESPANS DRVD,NDG	
ER 091	RESON PARAMS	EXPT=PROG	29+5		ERDA=NDC-9	198	477	ORL MACKLIN+292,36EV LVL,WN,NG,TBP,NSE,	
ER 091	RESON PARAMS	EXPT=PROG		28+4	ERDA=NDC-9	199	477	AUA MUSGROVE+THNS+CAPT,AVG D,NG,OVN,	
ER 091	STRNGTH FUNC	EXPT=PROG		28+4	ERDA=NDC-9	199	477	AUA MUSGROVE+S0=,36+-.10 S1=5.7+-.1,0	
ER 092	TOTAL XSECT	EXPT=PROG	NDG		ERDA=NDC-9	202	477	AUA BOLDEMAN+TOT CS,NDG,SEE NP/A263 P389	
ER 092	DIFF ELASTIC	EXPT=PROG	28+6	35+6	ERDA=NDC-9	312	477	KTY MCDANIEL+STRUCTURE STUDY,NDG	
ER 092	DIFF INELAST	EXPT=PROG	28+6	35+6	ERDA=NDC-9	312	477	KTY MCDANIEL+STRUCTURE STUDY,NDG,	
ER 092	DIFF INELAST	EXPT=PROG	28+6		ERDA=NDC-9	323	477	KTY GLASGOW+DIN FROM DNG CFD TO DIN MEAS	
ER 092	N, GAMMA	EXPT=PROG	NDG		ERDA=NDC-9	202	477	AUA BOLDEMAN+CAPT CS,NDG,SEE NP/A263P389	
ER 092	INELST GAMMA	EXPT=PROG	22+6	37+6	ERDA=NDC-9	317	477	KTY GLASGOW+XCIT FN,ANG DIST,BRANCH,J,	
ER 092	INELST GAMMA	EXPT=PROG	32+6		ERDA=NDC-9	323	477	KTY GLASGOW+DIN FROM DNG CFD TO DIN MEAS	
ER 092	RESON PARAMS	EXPT=PROG	NDG		ERDA=NDC-9	202	477	AUA BOLDEMAN+NDG,SEE NP/A263 P389	
ER 092	STRNGTH FUNC	EXPT=PROG	NDG		ERDA=NDC-9	202	477	AUA BOLDEMAN+S0,S1,NDG,SEE NP/A263 P389	
ER 094	TOTAL XSECT	EXPT=PROG	NDG		ERDA=NDC-9	202	477	AUA BOLDEMAN+TOT CS,NDG,SEE NP/A263 P389	
ER 094	DIFF ELASTIC	EXPT=PROG	35+6		ERDA=NDC-9	312	477	KTY MCDANIEL+STRUCTURE STUDY,NDG	
ER 094	DIFF INELAST	EXPT=PROG	33+6		ERDA=NDC-9	312	477	KTY MCDANIEL+STRUCTURE STUDY,NDG,	
ER 094	N, GAMMA	EXPT=PROG	NDG		ERDA=NDC-9	202	477	AUA BOLDEMAN+CAPT CS,NDG,SEE NP/A263P389	
ER 094	INELST GAMMA	EXPT=PROG	22+6	37+6	ERDA=NDC-9	317	477	KTY GLASGOW+XCIT FN,ANG DIST,BRANCH,J,	
ER 094	RESON PARAMS	EXPT=PROG	NDG		ERDA=NDC-9	202	477	AUA BOLDEMAN+NDG,SEE NP/A263 P389	
ER 094	STRNGTH FUNC	EXPT=PROG	NDG		ERDA=NDC-9	202	477	AUA BOLDEMAN+S0,S1,NDG,SEE NP/A263 P389	
NB 090	N, PROTON	EXPT=PROG	NDG		ERDA=NDC-9	198	477	LAS BRITT+CALC FROM CHG PARTICLE,NDG,TBC	
NB 093	DIFF ELASTIC	EXPT=PROG	11+7		ERDA=NDC-9	225	477	OWO FERREH+TUF,OPTMOL PARS,ABST NP/A275,	
NB 093	DIFF ELASTIC	EXPT=PROG	NDG		ERDA=NDC-9	230	477	TNL PURSER+NDG,SMALL ANG MEAS TBP SPRING	
NB 093	DIFF INELAST	EXPT=PROG	NDG		ERDA=NDC-9	280	477	TNL PURSER+NDG,SMALL ANG MEAS TBP SPRING	
NB 093	NONE, GAMMA	EXPT=PROG	18+5	28+7	ERDA=NDC-9	197	477	ORL DICKENS+DIFF CS,NDG,TBP,NSE,	
NB 093	NONE, GAMMA	EXPT=PROG	18+6	28+7	ERDA=NDC-9	204	477	ORL MORGAN,129 DEG,NDG,ABST ORNL=TH-3829	
NB 093	N,N REACTION	EXPT=PROG	18+6	28+7	ERDA=NDC-9	204	477	ORL MORGAN,129 DEG,NDG,ABST ORNL=TH-3829	

ELEMENT S A	QUANTITY	TYPE	ENERGY		DOCUMENTATION			LAB DATE	COMMENTS
			MIN	MAX	REF	VOL	PAGE		
NB 093	N ₁ PROTON	EXPT=PROG	15+7		ERDA=NDC-9	88	477	LRL HAIGHT+(N,XP)CS GVN,SPEC CFD STA1MDL	
NB 093	N _{1,N} PROTON	EXPT=PROG	15+7		ERDA=NDC-9	88	477	LRL HAIGHT+(N,XP)CS GVN,SPEC CFD STA1MDL	
NB 093	N ₁ DEUTERON	EXPT=PROG	15+7		ERDA=NDC-9	88	477	LRL HAIGHT+(N,XD)CS GVN,SPEC CFD STA1MDL	
NB 093	N ₁ ALPHA REAC	EXPT=PROG	15+7		ERDA=NDC-9	88	477	LRL HAIGHT+(N,XA)CS GVN,SPEC CFD STA1MDL	
NB 093	N _{1,N} ALPHA	EXPT=PROG	15+7		ERDA=NDC-9	88	477	LRL HAIGHT+(N,XA)CS GVN,SPEC CFD STA1MDL	
MO	NONEI GAMMAS	EXPT=PROG	10+5	20+7	ERDA=NDC-9	197	477	QDL DICKENS+DIFF CS,NDG,TBP NSE.	
MO 092	DIFF ELASTIC	EXPT=PROG	11+7		ERDA=NDC-9	229	477	OWO FERREN+TUF,OPTMDL PARS,ABST NP/A275,	
MO 092	DIFF ELASTIC	EXPT=PROG	NDG		ERDA=NDC-9	229	477	OWO RAPAPORT+OPTMDL REAL,IMAG E DEP,NDG	
MO 092	DIFF ELASTIC	EXPT=PROG	25+6	60+0	ERDA=NDC-9	319	477	KTY MCDANIEL+3ES,6MEV LEG FIT CURV,	
MO 092	DIFF INELAST	EXPT=PROG	NDG		ERDA=NDC-9	226	477	OWO RAPAPORT+19OSPIN EFFECTS,NDG,TBP,	
MO 092	DIFF INELAST	EXPT=PROG	25+6	60+0	ERDA=NDC-9	319	477	KTY MCDANIEL+3ES,6 MEV LEG FIT CURV	
MO 094	DIFF ELASTIC	EXPT=PROG	25+6	60+0	ERDA=NDC-9	319	477	KTY MCDANIEL+3ES,6MEV LEG FIT CURV,	
MO 094	DIFF INELAST	EXPT=PROG	25+6	60+0	ERDA=NDC-9	319	477	KTY MCDANIEL+3ES,6 MEV LEG FIT CURV	
MO 095	TOTAL XSECT	EXPT=PROG	20+1	10+9	ERDA=NDC-9	242	477	RPI HOCKENBURY+TRNS,NDG,RES PARS DRVD	
MO 095	N ₁ GAMMA	EXPT=PROG	20+1	10+9	ERDA=NDC-9	242	477	RPI HOCKENBURY+8 PC ACC,NDG,RES PARS GVN	
MO 095	RESON PARAMS	EXPT=PROG	16+2	90+2	ERDA=NDC-9	242	477	RPI HOCKENBURY+TBL,WG,WN,WT,0,CFD CALC	
MO 096	DIFF ELASTIC	EXPT=PROG	11+7		ERDA=NDC-9	229	477	OWO FERREN+TUF,OPTMDL PARS,ABST NP/A275,	
MO 096	DIFF ELASTIC	EXPT=PROG	NDG		ERDA=NDC-9	229	477	OWO RAPAPORT+OPTMDL REAL,IMAG E DEP,NDG	
MO 096	DIFF ELASTIC	EXPT=PROG	25+6	60+0	ERDA=NDC-9	319	477	KTY MCDANIEL+3ES,6MEV LEG FIT CURV,	
MO 096	DIFF INELAST	EXPT=PROG	25+6	60+0	ERDA=NDC-9	319	477	KTY MCDANIEL+3ES,6 MEV LEG FIT CURV	
MO 097	TOTAL XSECT	EXPT=PROG	20+1	10+9	ERDA=NDC-9	242	477	RPI HOCKENBURY+TRNS,NDG,RES PARS DRVD	
MO 097	N ₁ GAMMA	EXPT=PROG	20+1	10+9	ERDA=NDC-9	242	477	RPI HOCKENBURY+8 PC ACC,NDG,RES PARS GVN	
MO 097	RESON PARAMS	EXPT=PROG	71+1	56+2	ERDA=NDC-9	242	477	RPI HOCKENBURY+TBL,WG,WN,WT,0,CFD CALC	
MO 098	DIFF ELASTIC	EXPT=PROG	11+7		ERDA=NDC-9	229	477	OWO FERREN+TUF,OPTMDL PARS,ABST NP/A275,	
MO 098	DIFF ELASTIC	EXPT=PROG	NDG		ERDA=NDC-9	229	477	OWO RAPAPORT+OPTMDL REAL,IMAG E DEP,NDG	
MO 098	DIFF ELASTIC	EXPT=PROG	28+6		ERDA=NDC-9	319	477	KTY MCDANIEL+1E,NDG.	
MO 098	DIFF INELAST	EXPT=PROG	28+6		ERDA=NDC-9	319	477	KTY MCDANIEL+STRUCTURE STUDY,NDG,	
MO 100	DIFF ELASTIC	EXPT=PROG	11+7		ERDA=NDC-9	229	477	OWO FERREN+TUF,OPTMDL PARS,ABST NP/A275,	
MO 100	DIFF ELASTIC	EXPT=PROG	NDG		ERDA=NDC-9	229	477	OWO RAPAPORT+OPTMDL REAL,IMAG E DEP,NDG	
MO 100	DIFF ELASTIC	EXPT=PROG	28+6	60+0	ERDA=NDC-9	319	477	KTY MCDANIEL+3ES,6MEV LEG FIT CURV,	
MO 100	DIFF INELAST	EXPT=PROG	28+6	60+0	ERDA=NDC-9	319	477	KTY MCDANIEL+3ES,6 MEV LEG FIT CURV,	
TC 099	TOTAL XSECT	EXPT=PROG	55+1	71+2	ERDA=NDC-9	243	477	RPI LITTLE+TRNS,USED TO NORM CAPT DATA,	
TC 099	N ₁ GAMMA	EXPT=PROG	40+3	80+4	ERDA=NDC-9	243	477	RPI LITTLE+CAPT YLD,CS GRPH,CFD ENDF	
TC 099	RESON PARAMS	EXPT=PROG	21+2	16+5	ERDA=NDC-9	243	477	RPI LITTLE+28 NEW RES OBS,TBL,	
PD	TOTAL XSECT	EXPT=PROG	90+0	91+2	ERDA=NDC-9	244	477	RPI SINGH+TRANS,NDG	

ELEMENT S A	QUANTITY	TYPE	ENERGY		DOCUMENTATION			LAB	COMMENTS
			MIN	MAX	REF	VOL	PAGE		
PD	N, GAMMA	EXPT-PROG	58*8	91*2	ERDA-NDC-9	244	477	RPI SINGH-CAPT,NDG,	
PD	RESON PARAMS	EXPT-PROG	58*8	91*2	ERDA-NDC-9	244	477	RPI SINGH-TOF SPEC,TBL 105,107 RES,	
PD 105	TOTAL XSECT	EXPT-PROG	NDG		ERDA-NDC-9	244	477	RPI SINGH-CAPT,MEAS CFD PD 107,	
PD 105	N, GAMMA	EXPT-PROG	NDG		ERDA-NDC-9	244	477	RPI SINGH-TRNS,NDG	
PD 105	RESON PARAMS	EXPT-PROG	NDG		ERDA-NDC-9	244	477	RPI SINGH- RLS ES CFD PD 107,0 SAME PRED	
PD 107	RESON PARAMS	EXPT-PROG	52*8	91*2	ERDA-NDC-9	244	477	RPI SINGH- RLS ES CFD PD 105,0 SAME PRED	
AG	NONEL GAMMAS	EXPT-PROG	10*5	20*7	ERDA-NDC-9	197	477	ORL DICKENS-DIFF CS,NDG,TBP NSE,	
CD	INELST GAMMA	EXPT-PROG	15*7		ERDA-NDC-9	94	477	LRL KOOPMAN-HIGH RESOL GE-LI DET,NDG,TBC	
CD 110	INELST GAMMA	EXPT-PROG	15*7		ERDA-NDC-9	94	477	LRL KOOPMAN-RING GEOM,GE-LI DET,TBL,TBC	
CD 112	INELST GAMMA	EXPT-PROG	15*7		ERDA-NDC-9	94	477	LRL KOOPMAN-RING GEOM,GE-LI DET,TBL,TBC	
CD 114	INELST GAMMA	EXPT-PROG	15*7		ERDA-NDC-9	94	477	LRL KOOPMAN-RING GEOM,GE-LI DET,TBL,TBC	
CD 116	INELST GAMMA	EXPT-PROG	15*7		ERDA-NDC-9	94	477	LRL KOOPMAN-RING GEOM,GE-LI DET,TBL,TBC,	
IN	DIFF ELASTIC	EXPT-PROG	11*7		ERDA-NDC-9	229	477	OHQ FERRER-TOF,OPTMOL PARS,ABST NP/A275,	
IN 115	TOT INELASTI	EVAL-PROG	NDG		ERDA-NDC-9	92	477	ANL SMITH,EVAL FOR ENDFB5,SEE ANL-NOM-20	
IN 115	DIFF INELAST	EVAL-PROG	NDG		ERDA-NDC-9	92	477	ANL SMITH,EVAL FOR ENDFB5,SEE ANL-NOM-20	
SN	INELST GAMMA	EXPT-PROG	15*7		ERDA-NDC-9	94	477	LRL KOOPMAN-HIGH RESOL GE-LI DET,NDG,TBC	
SN	NONEL GAMMAS	EXPT-PROG	10*5	20*7	ERDA-NDC-9	197	477	ORL DICKENS-DIFF CS,NDG,TBP NSE,	
SN 116	DIFF ELASTIC	EXPT-PROG	10*6		ERDA-NDC-9	330	477	KTY HARPER-14ANG,OPTMOL CALC T8D,T8C,NDG	
SN 118	DIFF ELASTIC	EXPT-PROG	NDG		ERDA-NDC-9	229	477	OHQ RAPAPORT-ISOPIN FORBIDDEN,T8D,	
SN 118	DIFF ELASTIC	EXPT-PROG	11*7		ERDA-NDC-9	229	477	OHQ RAPAPORT-ANG DIST,OPMOL ANAL T8D,NDG	
SN 118	DIFF ELASTIC	EXPT-PROG	10*6		ERDA-NDC-9	330	477	KTY HARPER-14ANG,OPTMOL CALC T8D,T8C,NDG	
SN 118	DIFF INELAST	EXPT-PROG	NDG		ERDA-NDC-9	229	477	OHQ RAPAPORT-TOF,82,5DEG,XCIT FN,NDG,	
SN 118	DIFF INELAST	EXPT-PROG	NDG		ERDA-NDC-9	229	477	OHQ RAPAPORT-ISOSPIN EFFECTS,NDG,T8P,	
SN 118	N, PHOTON	EXPT-PROG	NDG		ERDA-NDC-9	229	477	OHQ RAPAPORT-ISOPIN FORBIDDEN,T8D,	
SN 120	DIFF ELASTIC	EXPT-PROG	11*7		ERDA-NDC-9	229	477	OHQ FERRER-TOF,OPTMOL PARS,ABST NP/A275,	
SN 120	DIFF ELASTIC	EXPT-PROG	NDG		ERDA-NDC-9	229	477	OHQ RAPAPORT-TOF,82,5DEG,XCIT FN,NDG,	
SN 120	DIFF ELASTIC	EXPT-PROG	11*7		ERDA-NDC-9	229	477	OHQ RAPAPORT-ANG DIST,OPMOL ANAL T8D,NDG	
SN 120	DIFF ELASTIC	EXPT-PROG	10*6		ERDA-NDC-9	330	477	KTY HARPER-14ANG,OPTMOL CALC T8D,T8C,NDG	
SN 120	DIFF INELAST	EXPT-PROG	NDG		ERDA-NDC-9	229	477	OHQ RAPAPORT-TOF,82,5DEG,XCIT FN,NDG,	
SN 120	DIFF INELAST	EXPT-PROG	NDG		ERDA-NDC-9	229	477	OHQ RAPAPORT-ISOSPIN EFFECTS,NDG,T8P,	
SN 120	N, PHOTON	EXPT-PROG	NDG		ERDA-NDC-9	229	477	OHQ RAPAPORT-ISOPIN FORBIDDEN,T8D,	
SN 122	DIFF ELASTIC	EXPT-PROG	NDG		ERDA-NDC-9	229	477	OHQ RAPAPORT-TOF,82,5DEG,XCIT FN,NDG,	
SN 122	DIFF ELASTIC	EXPT-PROG	11*7		ERDA-NDC-9	229	477	OHQ RAPAPORT-ANG DIST,OPMOL ANAL T8D,NDG	
SN 122	DIFF ELASTIC	EXPT-PROG	10*6		ERDA-NDC-9	330	477	KTY HARPER-14ANG,OPTMOL CALC T8D,T8C,NDG	
SN 122	DIFF INELAST	EXPT-PROG	NDG		ERDA-NDC-9	229	477	OHQ RAPAPORT-TOF,82,5DEG,XCIT FN,NDG,	

ELEMENT S A	QUANTITY	TYPE	ENERGY		DOCUMENTATION			LAB	COMMENTS
			MIN	MAX	REF	VOL	PAGE		
SN 122	DIFF INELAST	EXPT=PROG	NDG		ERDA=NDC=9	226	477	QHO	RAPAPORT+ISOSPIN EFFECTS,NDG,TBP,
SN 122	N, PROTON	EXPT=PROG	NDG		ERDA=NDC=9	226	477	QHO	RAPAPORT+ISOPIN FORBIDDEN,TBD,
SN 124	DIFF ELASTIC	EXPT=PROG	NDG		ERDA=NDC=9	226	477	QHO	RAPAPORT+TOP,82,5DEG,XCIT FN,NDG,
SN 124	DIFF ELASTIC	EXPT=PROG	11*7		ERDA=NDC=9	226	477	QHO	RAPAPORT+ANG DIST,OPMDL ANAL TBD,NDG
SN 124	DIFF ELASTIC	EXPT=PROG	10*6		ERDA=NDC=9	330	477	KTY	HARPEM+14ANG,OPTMDL CALC TBD,TBC,NDG
SN 124	DIFF INELAST	EXPT=PROG	NDG		ERDA=NDC=9	226	477	QHO	RAPAPORT+TOP,82,5DEG,XCIT FN,NDG,
SN 124	DIFF INELAST	EXPT=PROG	NDG		ERDA=NDC=9	226	477	QHO	RAPAPORT+ISOSPIN EFFECTS,NDG,TBP,
SN 124	N, PROTON	EXPT=PROG	NDG		ERDA=NDC=9	226	477	QHO	RAPAPORT+ISOPIN FORBIDDEN,TBD,
TE 130	SPECT N,GAMM	EXPT=PROG	NDG		ERDA=NDC=9	32	477	BNL	KOENE+STRUCTURE STUDY,LVL SCH,NDG,
CS 133	TOTAL XSECT	EXPT=PROG	20*1	10*3	ERDA=NDC=9	242	477	RPI	HOCKENBURY+TRNS,NDG,RES PARS DRVD
CS 133	N, GAMMA	EXPT=PROG	20*1	10*3	ERDA=NDC=9	242	477	RPI	HOCKENBURY+8 PC ACC,NDG,RES PARS GVN
CS 133	RESON PARAMS	EXPT=PROG	40*1	30*2	ERDA=NDC=9	242	477	RPI	HOCKENBURY+TBL,WG,HN,HT,D,CFO CALC
BA 134	SPECT N,GAMM	EXPT=PROG	NDG		ERDA=NDC=9	32	477	BNL	KOENE+STRUCTURE STUDY,LVL SCH,NDG,
CE 136	SPECT N,GAMM	EXPT=PROG	NDG		ERDA=NDC=9	32	477	BNL	KOENE+STRUCTURE STUDY,LVL SCH,NDG,
CE 140	N, GAMMA	EXPT=PROG	NDG		ERDA=NDC=9	199	477	AUA	MUSGROVE+CS MEAS,NDG,RES PARS DRVD,
CE 140	RESON PARAMS	EXPT=PROG		60*4	ERDA=NDC=9	199	477	AUA	MUSGROVE+S WAVE AVG D,WG GVN,
CE 140	STRNGTH FUNC	EXPT=PROG		60*4	ERDA=NDC=9	199	477	AUA	MUSGROVE+S $\theta=(3,1+0.9)=4,$
PR 141	TOTAL XSECT	EXPT=PROG	10*0	10*3	ERDA=NDC=9	247	477	RPI	FEIGENBAUM+TRNS,NDG,TO NORMALIZE N,G
PR 141	N, GAMMA	EXPT=PROG	10*0	10*3	ERDA=NDC=9	247	477	RPI	FEIGENBAUM+CAPT,MEAS,ANAL TBD,NDG
ND 142	N, GAMMA	EXPT=PROG		+3	ERDA=NDC=9	199	477	AUA	MUSGROVE+ORELA,CS MEAS,NDG,TBP NP/A,
ND 142	RESON PARAMS	EXPT=PROG		+3	ERDA=NDC=9	199	477	AUA	MUSGROVE+S WAVE WND,WG,NDG,TBP NP/A
ND 143	TOTAL XSECT	EXPT=PROG	20*1	10*3	ERDA=NDC=9	242	477	RPI	HOCKENBURY+TRNS,NDG,RES PARS DRVD
ND 143	N, GAMMA	EXPT=PROG		+3	ERDA=NDC=9	199	477	AUA	MUSGROVE+ORELA,CS MEAS,NDG,TBP NP/A,
ND 143	N, GAMMA	EXPT=PROG	20*1	10*3	ERDA=NDC=9	242	477	RPI	HOCKENBURY+8 PC ACC,NDG,RES PARS GVN
ND 143	RESON PARAMS	EXPT=PROG		+3	ERDA=NDC=9	199	477	AUA	MUSGROVE+S WAVE WND,WG,NDG,TBP NP/A
ND 143	RESON PARAMS	EXPT=PROG	55*1	71*2	ERDA=NDC=9	242	477	RPI	HOCKENBURY+TBL,WG,HN,HT,D,CFO CALC
ND 144	N, GAMMA	EXPT=PROG		+3	ERDA=NDC=9	199	477	AUA	MUSGROVE+ORELA,CS MEAS,NDG,TBP NP/A,
ND 144	RESON PARAMS	EXPT=PROG		+3	ERDA=NDC=9	199	477	AUA	MUSGROVE+S WAVE WND,WG,NDG,TBP NP/A
ND 145	N, GAMMA	EXPT=PROG		+3	ERDA=NDC=9	199	477	AUA	MUSGROVE+ORELA,CS MEAS,NDG,TBP NP/A,
ND 145	RESON PARAMS	EXPT=PROG		+3	ERDA=NDC=9	199	477	AUA	MUSGROVE+S WAVE WND,WG,NDG,TBP NP/A
ND 146	N, GAMMA	EXPT=PROG		+3	ERDA=NDC=9	199	477	AUA	MUSGROVE+ORELA,CS MEAS,NDG,TBP NP/A,
ND 146	RESON PARAMS	EXPT=PROG		+3	ERDA=NDC=9	199	477	AUA	MUSGROVE+S WAVE WND,WG,NDG,TBP NP/A
ND 148	N, GAMMA	EXPT=PROG		+3	ERDA=NDC=9	199	477	AUA	MUSGROVE+ORELA,CS MEAS,NDG,TBP NP/A,
ND 148	RESON PARAMS	EXPT=PROG		+3	ERDA=NDC=9	199	477	AUA	MUSGROVE+S WAVE WND,WG,NDG,TBP NP/A
ND 150	N, GAMMA	EXPT=PROG		+3	ERDA=NDC=9	199	477	AUA	MUSGROVE+ORELA,CS MEAS,NDG,TBP NP/A,

ELEMENT S A	QUANTITY	TYPE	ENERGY		DOCUMENTATION			LAB	COMMENTS
			MIN	MAX	REF	VOL	PAGE		
ND 150	RESON PARAMS	EXPT=PROG			03	ERDA=NDC-9	199	477	AUA MUSGROVE+S HAVE HNO ₃ ,HG,NDG,TBP NP/A
SM 148	DIFF INELAST	EXPT=PROG	25+6			ERDA=NDC-9	321	477	KTY HCELLISTHEM+ANOMALOUS DATA SUPPORTED
SM 152	DIFF INELAST	EXPT=PROG	25+6			ERDA=NDC-9	321	477	KTY HCELLISTHEM+ANOMALOUS DATA SUPPORTED
SM 152	INELBT GAMMA	EXPT=PROG	25+6			ERDA=NDC-9	321	477	KTY HCELLISTHEM+ANOMALOUS DATA SUPPORTED
HO 165	SPECT N,GAMM	EXPT=PROG	20+3			ERDA=NDC-9	08	477	BNL MCCLUMC+KES SPEC,NDG,SPIN,PI 430KEV,
HO 165	RESON PARAMS	EXPT=PROG	20+3			ERDA=NDC-9	08	477	BNL MCCLUMC+SPIN,PI 430KEV=2+.CFU.
ER 164	SPECT N,GAMM	EXPT=PROG	20+3	24+4		ERDA=NDC-9	08	477	BNL GREENWOOD+HFBR,G,2ES,CFD OTH,NDG
ER 166	SPECT N,GAMM	EXPT=PROG	20+3	24+4		ERDA=NDC-9	08	477	BNL GREENWOOD+HFBR,G,2ES,CFD OTH,NDG
EM 168	SPECT N,GAMM	EXPT=PROG	20+3	24+4		ERDA=NDC-9	08	477	BNL GREENWOOD+HFBR,G,2ES,CFD OTH,NDG
EM 170	SPECT N,GAMM	EXPT=PROG	20+3	24+4		ERDA=NDC-9	08	477	BNL GREENWOOD+HFBR,G,2ES,CFD OTH,NDG
YM 169	N, GAMMA	EXPT=PROG	37+3	30+0		ERDA=NDC-9	110	477	LAS DRAKE+PRELIM ANAL,TBC,NDG.
LU	N, GAMMA	EXPT=PROG	NDG			ERDA=NDC-9	110	477	LAS DRAKE+NDG,TBD ORELA.
LU 179	N2N REACTION	EXPT=PROG	15+7			ERDA=NDC-9	91	477	LRL NETHAWAY+ISON RATIO GVN,CFD CALC,
TA 181	DIFF ELASTIC	EXPT=PROG	11+7			ERDA=NDC-9	220	477	OHQ FERREH+TUF,OPTMOL PARS,ABST NP/A279.
TA 181	NONEL GAMMAS	EXPT=PROG	10+5	20+7		ERDA=NDC-9	197	477	ORL DICKENS+DIFF CS,NDG,TBP NSE.
W 182	TOTAL XSECT	EXPT=PROG	10+6	40+0		ERDA=NDC-9	30	477	ANL GUENTHER+ROT,VIB XCIT,THESIS TBP,NDG
W 182	ELASTIC SCAT	EXPT=PROG	10+6	40+0		ERDA=NDC-9	30	477	ANL GUENTHER+ROT,VIB XCIT,THESIS TBP,NDG
W 182	DIFF ELASTIC	EXPT=PROG	10+6	40+0		ERDA=NDC-9	30	477	ANL GUENTHER+ROT,VIB XCIT,THESIS TBP,NDG
W 182	DIFF INELAST	EXPT=PROG	10+6	40+0		ERDA=NDC-9	30	477	ANL GUENTHER+ROT,VIB XCIT,THESIS TBP,NDG
W 182	SPECT N,GAMM	EXPT=PROG	NDG			ERDA=NDC-9	07	477	BNL STELTS+PAIR SPEC,HIGHER EXCIT,NDG
W 182	INELBT GAMMA	EXPT=PROG	10+6	40+0		ERDA=NDC-9	30	477	ANL GUENTHER+ROT,VIB XCIT,THESIS TBP,NDG
W 182	RESON PARAMS	EXPT=PROG	NDG			ERDA=NDC-9	07	477	BNL STELTS+PAIR SPEC,40 SPIN STATES,NDG
W 184	TOTAL XSECT	EXPT=PROG	10+6	40+0		ERDA=NDC-9	30	477	ANL GUENTHER+ROT,VIB XCIT,THESIS TBP,NDG
W 184	ELASTIC SCAT	EXPT=PROG	10+6	40+0		ERDA=NDC-9	30	477	ANL GUENTHER+ROT,VIB XCIT,THESIS TBP,NDG
W 184	DIFF ELASTIC	EXPT=PROG	10+6	40+0		ERDA=NDC-9	30	477	ANL GUENTHER+ROT,VIB XCIT,THESIS TBP,NDG
W 184	DIFF INELAST	EXPT=PROG	10+6	40+0		ERDA=NDC-9	30	477	ANL GUENTHER+ROT,VIB XCIT,THESIS TBP,NDG
W 184	INELBT GAMMA	EXPT=PROG	10+6	40+0		ERDA=NDC-9	30	477	ANL GUENTHER+ROT,VIB XCIT,THESIS TBP,NDG
W 186	TOTAL XSECT	EXPT=PROG	10+6	40+0		ERDA=NDC-9	30	477	ANL GUENTHER+ROT,VIB XCIT,THESIS TBP,NDG
W 186	ELASTIC SCAT	EXPT=PROG	10+6	40+0		ERDA=NDC-9	30	477	ANL GUENTHER+ROT,VIB XCIT,THESIS TBP,NDG
W 186	DIFF ELASTIC	EXPT=PROG	10+6	40+0		ERDA=NDC-9	30	477	ANL GUENTHER+ROT,VIB XCIT,THESIS TBP,NDG
W 186	DIFF INELAST	EXPT=PROG	10+6	40+0		ERDA=NDC-9	30	477	ANL GUENTHER+ROT,VIB XCIT,THESIS TBP,NDG
W 186	INELBT GAMMA	EXPT=PROG	10+6	40+0		ERDA=NDC-9	30	477	ANL GUENTHER+ROT,VIB XCIT,THESIS TBP,NDG
OS 190	SPECT N,GAMM	EXPT=PROG	25+2	20+3		ERDA=NDC-9	00	477	BNL CASTEN+2ES,FRAG NILSSON MDL,NDG,
IR 191	N, GAMMA	EXPT=PROG	NDG			ERDA=NDC-9	110	477	LAS DRAKE+NDG,TBD ORELA.
IR 193	N, GAMMA	EXPT=PROG	NDG			ERDA=NDC-9	110	477	LAS DRAKE+NDG,TBD ORELA.

ELEMENT S A	QUANTITY	TYPE	ENERGY		DOCUMENTATION			LAB	COMMENTS
			MIN	MAX	REF	VOL	PAGE		
PT 192	SPECT N,GAMM	EXPT=PROG	25	02	ERDA=NDC=9	99	477	BNL CIZENSKI+HFBR,PT193	LVL SCHEME,NOG
PT 195	SPECT N,GAMM	EXPT=PROG	28	03	ERDA=NDC=9	99	477	BNL CIZENSKI+HFBR,PT196	LVL SCHEME,NOG
AU 197	NONEL GAMMAS	EXPT=PROG	18	05	28	07	ERDA=NDC=9	197	477 ORL DICKENS+DIFF CS,NOG,TBP NSE.
PB	INELST GAMMA	EXPT=PROG	15	07	ERDA=NDC=9	94	477	LRL KOOPMAN+HIGH RESOL GE=LI DET,NOG,TBC	
PB	NONEL GAMMAS	EXPT=PROG	18	05	28	07	ERDA=NDC=9	197	477 ORL DICKENS+DIFF CS,NOG,TBP NSE.
PB 204	INELST GAMMA	EXPT=PROG	NOG		ERDA=NDC=9	31	477	ANL SMITH+ANAL T8D,NOG,	
PB 206	DIFF ELASTIC	EXPT=PROG	68	05	18	06	ERDA=NDC=9	30	477 ANL SMITH+CS MEAS,MDL PRED U238 CS,NOG,
PB 206	DIFF ELASTIC	EXPT=PROG	11	07	ERDA=NDC=9	229	477	DHO FERREN+TOF,OPTMDL PARS,ABST NP/A279.	
PB 207	TOTAL XSECT	EXPT=PROG	48	09	ERDA=NDC=9	209	477	ORL HOREN+NOG,MAG DIPOLE ST,TBP BAP 4-77	
PB 207	DIFF ELASTIC	EXPT=PROG	68	05	18	06	ERDA=NDC=9	30	477 ANL SMITH+CS MEAS,MDL PRED U238 CS,NOG,
PB 207	DIFF ELASTIC	EXPT=PROG	48	09	ERDA=NDC=9	209	477	ORL HOREN+NOG,MAG DIPOLE ST,TBP BAP 4-77	
PB 207	SPECT N,GAMM	EXPT=PROG	18	06	ERDA=NDC=9	207	477	ORL RAMAN+MI,SI,E2 DATA,NOG,TBP BAP 4-77	
PB 207	RESON PARAMS	EXPT=PROG	98	04	13	09	ERDA=NDC=9	209	477 ORL HOREN+,WN,HC,MAG DIPOLE,TBP BAP 4-77
PB 208	DIFF ELASTIC	EXPT=PROG	68	05	18	06	ERDA=NDC=9	30	477 ANL SMITH+CS MEAS,MDL PRED U238 CS,NOG,
PB 208	DIFF ELASTIC	EXPT=PROG	NOG		ERDA=NDC=9	226	477	DHO RAPAPORT+OPTMDL PARS,CFD P DATA,NOG	
PB 208	TOT INELASTI	EXPT=PROG	49	06	88	06	ERDA=NDC=9	196	477 ORL DICKENS,DIN,SIN FROM DNG,NOG,TBP NSE
PB 208	DIFF INELAST	EXPT=PROG	49	06	88	06	ERDA=NDC=9	196	477 ORL DICKENS,DIN,SIN FROM DNG,NOG,TBP NSE
PB 208	DIFF INELAST	EXPT=PROG	11	07	26	07	ERDA=NDC=9	227	477 DHO RAPAPORT+INEL XCIT ANAL,NOG,TBP
PB 208	N, GAMMA	EXPT=PROG	NOG		ERDA=NDC=9	208	477	ORL MACKLIN+TOE,STELLAR T,NOG,TBP AJ,	
PB 208	INELST GAMMA	EXPT=PROG	49	06	88	06	ERDA=NDC=9	196	477 ORL DICKENS,TOE,VOG,G SPECT,NOG,TBP NSE
PB 208	RESON PARAMS	EXPT=PROG			83	09	ERDA=NDC=9	200	477 ORL MACKLIN+STELLAR T,2 NEW RES,TBP AJ
BI 209	DIFF ELASTIC	EXPT=PROG	68	05	18	06	ERDA=NDC=9	30	477 ANL SMITH+CS MEAS,MDL PRED U238 CS,NOG,
BI 209	DIFF ELASTIC	EXPT=PROG	11	07	ERDA=NDC=9	229	477	DHO FERREN+TOF,OPTMDL PARS,ABST NP/A279.	
BI 209	TOT INELASTI	EXPT=PROG	54	06	ERDA=NDC=9	196	477	ORL DICKENS,SIN FROM DNG,NOG,TBP NSE,	
BI 209	INELST GAMMA	EXPT=PROG	54	06	ERDA=NDC=9	196	477	ORL DICKENS,TOE,VOG,G SPECT,NOG,TBP NSE	
TM 229	FISSION	EXPT=PROG	18	08	18	01	ERDA=NDC=9	69	477 COL LUERS+REL U235,GRPH,ANAL TBC,
TM 229	FRAG SPECTRA	EXPT=PROG	NOG		ERDA=NDC=9	70	477	COL LUERS+CDINC FRAG E MEAS,ANAL T8D,NOG	
TM 229	RESON PARAMS	EXPT=PROG	18	08	18	01	ERDA=NDC=9	69	477 COL LUERS+DR,JEV,FISS AREAS TBC,
TM 230	SPECT N,GAMM	EXPT=PROG	14	08	ERDA=NDC=9	93	477	BNL CHRIEN+M231 LVL STUDY,NOG	
TM 232	DIFF INELAST	EXPT=PROG	NOG		ERDA=NDC=9	162	477	LTI BARNES+INEL FROM G FROD,NOG	
TM 232	N, GAMMA	EXPT=PROG	26	03	88	09	ERDA=NDC=9	200	477 ORL MACKLIN+ORELA,NOG,RES PARS DRYO,
TM 232	SPECT N,GAMM	EXPT=PROG	28	03	24	04	ERDA=NDC=9	93	477 BNL CHRIEN+RES,TH 233 LVL SCHEME,NOG,
TM 232	INELST GAMMA	EXPT=PROG	NOG		ERDA=NDC=9	162	477	LTI BARNES+G PROD MEAS T8D,NOG	
TM 232	FISSION	EXPT=PROG	18	03	38	07	ERDA=NDC=9	97	477 LRL BEHRENS+REL,U235,IONIZ CH,NOG,
TM 232	FISSION	EXPT=PROG	18	08	18	02	ERDA=NDC=9	249	477 RPI BLOCK+1/Y NF CS GVN,CFD OTH.

ELEMENT S A	QUANTITY	TYPE	ENERGY		DOCUMENTATION			LAB	COMMENTS
			MIN	MAX	REF	VOL	PAGE		
TM 232	RESON PARAMS	EXPT=PROG	26+3	18+4	ERDA=NDC-9	200	477	ORL	MACKLIN+AVG WG FOR 50RES2,8-9,0KEV,
TM 232	STRENGTH FUNC	EXPT=PROG	26+3	18+4	ERDA=NDC-9	200	477	ORL	MACKLIN+S,P,D HAVE STF GVN,
TM 232	PHOTO-FISSN	EXPT=PROG	68+6	18+7	ERDA=NDC-9	199	477	LRL	BERMAN+PRELIM ANAL,NDG,TBC,
U 233	FISS YIELD	EVAL=PROG	25+2	14+7	ERDA=NDC-9	198	477	LAS	MADLAND+DISTR OF FP YLOS,7ES,GRPH,
U 233	PHOTO-FISSN	EXPT=PROG	68+6	18+7	ERDA=NDC-9	199	477	LRL	BERMAN+PRELIM ANAL,NDG,TBC,
U 234	SPECT N,GAMM	EXPT=PROG	59+0	49+1	ERDA=NDC-9	202	477	BNL	CHRIVEN+HEBR,G,SES,U235 LVL STUDY,NDG
U 234	FISSION	EXPT=PROG	18+5	18+7	ERDA=NDC-9	28	477	ANL	MEADOWS,REL U235,NDG
U 234	PHOTO-FISSN	EXPT=PROG	68+6	18+7	ERDA=NDC-9	199	477	LRL	BERMAN+PRELIM ANAL,NDG,TBC,
U 235	EVALUATION	EVAL=PROG	82+1	25+4	ERDA=NDC-9	214	477	ORL	PEELE,RES PARS ENDF4B,ABST ORNL 4955
U 235	DIFF INELAST	EXPT=PROG	NDG		ERDA=NDC-9	198	477	LTI	BARNES+INEL FROM G PROD,NDG,
U 235	INELST GAMMA	EXPT=PROG	NDG		ERDA=NDC-9	198	477	LTI	BARNES+G PROD MEAS TBD,NDG,
U 235	FISSION	EXPT=PROG	18+5	18+7	ERDA=NDC-9	28	477	ANL	MEADOWS,U234,246,PU242,259 RATIO,NDG
U 235	FISSION	EXPT=PROG	28+5	38+5	ERDA=NDC-9	28	477	ANL	POENITZ,LIQ SCINT,NO STRUCT,CFD,NDG
U 235	FISSION	EXPT=PROG	28+5	82+6	ERDA=NDC-9	28	477	ANL	POENITZ,IONIZ CH,CFO OTH,ENDF,NDG,
U 235	FISSION	EXPT=PROG	18+3	38+7	ERDA=NDC-9	197	477	LRL	BEHRENS+RATIO TO TH,NP,PU,AM,
U 235	FISSION	EXPT=PROG		38+4	ERDA=NDC-9	111	477	LAS	KEYNDHTM+SHAPE+AREA ANAL DATA+OTH,
U 235	FISSION	EXPT=PROG	14+5	96+5	ERDA=NDC-9	104	477	MMG	DAVIS+DIFF FISS CS MEAS,4ES,VALS GVN
U 235	FISSION	EXPT=PROG	FISS		ERDA=NDC-9	102	477	MMG	DAVIS+CF 292 SOURCE 1,215+-,017B,CFO
U 235	FISSION	EXPT=PROG	68+0	38+4	ERDA=NDC-9	172	477	NBS	LAMAZE,REL LI NT,TO BE ANAL,NDG,
U 235	FISSION	EXPT=PROG	78+5	35+6	ERDA=NDC-9	173	477	NBS	CARLSON+REL NP237,ANAL,MEAS TBC,NDG,
U 235	FISSION	EXPT=PROG	25+2		ERDA=NDC-9	174	477	NBS	SCHRACK+U300 VS U02 NFY,CHEM EFFECT,
U 235	FISSION	EXPT=PROG	FISS		ERDA=NDC-9	178	477	NBS	GRUNDL+CF 292SOURCE,CFO ENDF,
U 235	FISSION	EXPT=PROG	FISS		ERDA=NDC-9	180	477	NBS	GILLIAM+PU239,U238 RATIOS GVN,ISNF,
U 235	FISSION	EXPT=PROG	28+6	25+7	ERDA=NDC-9	200	477	ORL	DIFILIPPO+U238/U239,NDG,SEE 76ANL,
U 235	F NEUT DELAY	EXPT=PROG	25+2		ERDA=NDC-9	174	477	NBS	SCHRACK+U300 VS U02 NFY,TBD,NDG,
U 235	F NEUT DELAY	EXPT=PROG	NDG		ERDA=NDC-9	300	477	HAU	ECCLESTON+EQUILIB SPEC,YLOS CFO OTH
U 235	FISS PROD GS	EXPT=PROG	25+2		ERDA=NDC-9	174	477	NBS	SCHRACK+U300 VS U02 NFY,TBD,NDG,
U 235	FISS PROD BS	EXPT=PROG	FISS		ERDA=NDC-9	85	477	ION	WOMN+XR FP+DAUGHTERS B BRANCHING,
U 235	FISS YIELD	EXPT=PROG	85+0	95+0	ERDA=NDC-9	70	477	COL	LUERS+MASS DISTR GRPH,ANAL TBC,
U 235	FISS YIELD	EVAL=PROG	25+2	14+7	ERDA=NDC-9	140	477	LAS	MADLAND+DISTR OF FP YLOS,7ES,GRPH,
U 235	FISS YIELD	EXPT=PROG	25+2		ERDA=NDC-9	174	477	NBS	SCHRACK+U300 VS U02 NFY,CHEM EFFECT,
U 235	FISS YIELD	EVAL=PROG	FAST		ERDA=NDC-9	180	477	NBS	GILLIAM+FISS YLOS,TBL,FP HL GVN,
U 235	FRAG SPECTRA	EXPT=PROG	NDG		ERDA=NDC-9	67	477	COL	LUERS+PULSE HT DATA,CFO GEEL,NDG,TBC
U 235	FRAG SPECTRA	EXPT=PROG	85+0	95+0	ERDA=NDC-9	70	477	COL	LUERS+TOI KE DISTR,GRPH,ANAL TBC
U 235	FRAG SPECTRA	EXPT=PROG		18+2	ERDA=NDC-9	115	477	LAS	MOSES+ANG DISTR FISS FRAG TO BE MEAS

ELEMENT S A	QUANTITY	TYPE	ENERGY		DOCUMENTATION			LAB	COMMENTS
			MIN	MAX	REF	VOL	PAGE		
U 235	RESON PARAMS	EXPT=PHOG	NOG		ERDA=NDC-9	67	477	COL LUERS+LEVEL SPACING STUDY TBC,NDG	
U 235	RESON PARAMS	EXPT=PHOG	10+2	40+4	ERDA=NDC-9	111	477	LAS KEYNORTH+AVG WF CALC,GRPHS,	
U 235	PHOTO-FISSN	EXPT=PHOG	60+6	18+7	ERDA=NDC-9	99	477	LRL BERMAN+PRELIM ANAL,NDG,TBC	
U 236	SPECT N,GAMM	EXPT=PHOG	55+0		ERDA=NDC-9	94	477	BNL CHRIEN+LVL SCHEME U237,ANAL TBC,NDG	
U 236	FISSION	EXPT=PHOG	10+5	10+7	ERDA=NDC-9	28	477	ANL MEADOWS,REL U239,NDG	
U 236	PHOTO-FISSN	EXPT=PHOG	60+6	18+7	ERDA=NDC-9	99	477	LRL BERMAN+PRELIM ANAL,GRPH NU,TBC,	
U 238	EVALUATION	EVAL=PHOG	10+5	20+7	ERDA=NDC-9	45	477	ANL PENNINGTON+ENDFB5,NG,NF,INEL,NDG,TBP	
U 238	TOTAL XSECT	THEO=PHOG		+0	ERDA=NDC-9	30	477	ANL SMITH+CS CALC FROM PB,BI DEL,NDG	
U 238	TOTAL XSECT	EXPT=PHOG	52+1	40+3	ERDA=NDC-9	209	477	ORL OLSEN+TRNS,7 SAMPLES,NDG,TBP NSE,	
U 238	DIFF ELASTIC	THEO=PHOG		+0	ERDA=NDC-9	30	477	ANL SMITH+CS CALC FROM PB,BI DEL,NDG	
U 238	POINTAL SCAT	EXPT=PHOG	52+1	11+3	ERDA=NDC-9	209	477	ORL OLSEN+RADIUS=(.964+-,.005)=12,TBP NSE	
U 238	DIFF INELAST	THEO=PHOG		+0	ERDA=NDC-9	30	477	ANL SMITH+CS CALC FROM PB,BI DEL,NDG	
U 238	DIFF INELAST	EXPT=PHOG	90+5	31+0	ERDA=NDC-9	101	477	LTI BARNES+DATA TO BE ANAL,NDG,TBP,	
U 238	DIFF INELAST	EXPT=PHOG	10+6	15+0	ERDA=NDC-9	101	477	LTI BARNES+INEL FROM G PROD,NDG	
U 238	DIFF INELAST	EXPT=PHOG	10+5	15+0	ERDA=NDC-9	101	477	LTI BARNES+EXCIT FN,CS,CFD ENDF,NDG,TBC	
U 238	SPECT N,GAMM	EXPT=PHOG	25+2	+3	ERDA=NDC-9	94	477	BNL CHRIEN+U239 LVL STUDY,SPIN ASSIGN,	
U 238	SPECT N,GAMM	EXPT=PHOG	67+0	81+2	ERDA=NDC-9	201	477	RPI KOBAYASHI+CAPT YLD CURVS,CFD ENDF	
U 238	INELST GAMMA	EXPT=PHOG	10+6	15+0	ERDA=NDC-9	101	477	LTI BARNES+PRELIM MEAS,ANAL TBC,NDG,	
U 238	NXN REACTION	EXPT=PHOG	15+7	27+7	ERDA=NDC-9	111	477	LAS VEESER,(N,3N),(N,4N)GRPH,CFD OTH,	
U 238	FISSION	EXPT=PHOG	FISS		ERDA=NDC-9	109	477	NBS GILLIAM+U238/U239=.093+-+.4PC,ISNF,	
U 238	FISSION	EXPT=PHOG	20+6	23+7	ERDA=NDC-9	208	477	ORL DIFILIPPO+REL U235,NDG,SEE 76ANL,TBC	
U 238	FISSION	EXPT=PHOG	60+2	10+9	ERDA=NDC-9	210	477	ORL DIFILIPPO+AVG CS CFD OTH,NDG,TBP NSE	
U 238	FISSION	EXPT=PHOG	30+0	10+9	ERDA=NDC-9	249	477	RPI SLOVACEK+IONIZ CH,NDG,TH CS CALC,	
U 238	RES INT FISS	EXPT=PHOG	40+1	10+9	ERDA=NDC-9	249	477	RPI SLOVACEK+RIF =1.30+-,.15 MB,	
U 238	FISS YIELD	EXPT=PHOG	15+6	77+0	ERDA=NDC-9	57	477	ANL GLENDENIN+6ES,MASS DISTR,YLD GRPHS,	
U 238	FISS YIELD	EVAL=PHOG	FAST		ERDA=NDC-9	100	477	NBS GILLIAM+FISS YLDS,TBL,FP HL GVN,	
U 238	RESON PARAMS	EXPT=PHOG		+3	ERDA=NDC-9	94	477	BNL CHRIEN+U239 LVL STUDY,SPIN ASSIGN,	
U 238	RESON PARAMS	EXPT=PHOG	52+1	40+3	ERDA=NDC-9	209	477	ORL OLSEN+BHM FIT,AVG NG,NG 3ES,TBP NSE	
U 238	RESON PARAMS	EXPT=PHOG	30+0	10+9	ERDA=NDC-9	249	477	RPI SLOVACEK+WF 3 RES ES GVN,TBP NSE,	
U 238	RESON PARAMS	EXPT=PHOG	67+0	81+2	ERDA=NDC-9	201	477	RPI KOBAYASHI+5 RES S WAVE,	
U 238	STRNGTH FUNC	EXPT=PHOG	52+1	11+3	ERDA=NDC-9	209	477	ORL OLSEN+AVG SB=(.968+-,.036)=4,TBP NSE	
U 238	PHOTO-FISSN	EXPT=PHOG	60+6	18+7	ERDA=NDC-9	99	477	LRL BERMAN+PRELIM ANAL,NU,GRPH,TBC	
U 238	PHOTO-FISSN	THEO=PHOG	90+6	11+7	ERDA=NDC-9	112	477	LAS BRITT+STATHOL CALC CFD EXPT,GRPH,	
NP 237	FISSION	EXPT=PHOG	10+3	30+7	ERDA=NDC-9	97	477	LRL BEHRENS+REL,U235,PRELIM DATA,CFD,	
NP 237	FISSION	EXPT=PHOG	70+5	35+0	ERDA=NDC-9	175	477	NBS CARLSON+REL U 235,ANAL,MEAS TBC,NDG,	

ELEMENT S A	QUANTITY	TYPE	ENERGY		DOCUMENTATION			LAB	COMMENTS
			MIN	MAX	REF	VOL	PAGE		
NP 237	NUBAR, (NU)	EXPT=PROG	10+6	15+7	ERDA=NDC-9	113	477	LAS VEESER, 6ES, FROM FIT NUM 2, 634+-, 148EN	
NP 237	FISS YIELD	EVAL=PROG	FAST		ERDA=NDC-9	188	477	NBS GILLIAM+FISS YLOS, TBL, FP HL GVN,	
NP 237	PHOTO-FISSN	EXPT=PROG	60+6	18+7	ERDA=NDC-9	99	477	LRL BERMAN+PRELIM ANAL, NDC, TBC	
PU 239	DIFF INELAST	EXPT=PROG	NDG		ERDA=NDC-9	162	477	LTI BARNES+INEL FROM G PROD, NDC	
PU 239	INELST GAMMA	EXPT=PROG	NDG		ERDA=NDC-9	162	477	LTI BARNES+G PROD MEAS T8D, NDC,	
PU 239	FISSION	EXPT=PROG	15+5	18+7	ERDA=NDC-9	28	477	ANL MEADOWS, REL U235, NDC	
PU 239	FISSION	EXPT=PROG	14+5	96+9	ERDA=NDC-9	164	477	MWG DAVIS+DIFF FISS CS MEAS, 4ES, VALS GVN	
PU 239	FISSION	EXPT=PROG	FISS		ERDA=NDC-9	169	477	MWG DAVIS+CF 252 SOURCE 1, 790+-, 0348, CFO	
PU 239	FISSION	EXPT=PROG	FISS		ERDA=NDC-9	169	477	NBS GILLIAM+PU239/U235=1, 15+-4PC, ISNE,	
PU 239	FISS YIELD	EVAL=PROG	FAST		ERDA=NDC-9	188	477	NBS GILLIAM+FISS YLOS, TBL, FP HL GVN,	
PU 239	FRAG SPECTRA	EXPT=PROG	NDG		ERDA=NDC-9	78	477	COL LUERS+DOUBLE E MEAS T8D, NDC,	
PU 240	N, GAMMA	EXPT=PROG	28+2	35+9	ERDA=NDC-9	209	477	ORL WESTON+REL 0, LI, NDC, CFD ENDF, TBP NSE	
PU 240	SPECT N, GAMM	EXPT=PROG	NDG		ERDA=NDC-9	98	477	BNL CHRIEN+PU243 STUDY, RES CAPT DATA, NDC	
PU 240	F NEUT DELAY	EXPT=PROG	NDG		ERDA=NDC-9	308	477	WAL ECCLESTON+EQUILIB SPEC TO BE MEAS,	
PU 241	FISSION	EXPT=PROG	88+0	70+4	ERDA=NDC-9	97	477	LRL CARLSON+CFD ENDF, NDC, SEE UCRL-78696,	
PU 242	SPECT N, GAMM	EXPT=PROG	NDG		ERDA=NDC-9	98	477	BNL CHRIEN+PU243 STUDY, RES CAPT DATA, NDC	
PU 242	FISSION	EXPT=PROG	18+5	18+7	ERDA=NDC-9	28	477	ANL MEADOWS, REL U235, NDC	
PU 244	SPECT N, GAMM	EXPT=PROG	NDG		ERDA=NDC-9	98	477	BNL CHRIEN+PU243 STUDY, RES CAPT DATA, NDC	
PU 244	FISSION	EXPT=PROG	18+3	38+7	ERDA=NDC-9	97	477	LRL BEHRENS+REL, U235, IONIZ CH, NDC,	
AM 241	FISSION	EXPT=PROG	18+3	38+7	ERDA=NDC-9	97	477	LRL BEHRENS+REL, U235, PRELIM DATA, CFD,	
AM 241	FISSION	EXPT=PROG	NDG		ERDA=NDC-9	210	477	ORL GABBS+MEAS T8D, NDC,	
AM 242	N, GAMMA	EXPT=PROG	NDG		ERDA=NDC-9	110	477	LAS SILBERT, NUCLEAR EXPLO SOURCE, NDC, T8D	
CM 243	ABSORPTION	EXPT=PROG	25+2		ERDA=NDC-9	210	477	ORL BEMIS+2200M/S CS=NF +NG CS, TBP NSE,	
CM 243	RES INT ABS	EXPT=PROG	25+2		ERDA=NDC-9	210	477	ORL BEMIS+CD FILTER, RIA=RIF+RIG, TBP NSE	
CM 243	N, GAMMA	EXPT=PROG	25+2		ERDA=NDC-9	210	477	ORL BEMIS+2200M/S CS=130, 7+-9, 68, TBP NSE	
CM 243	RES INT CAPT	EXPT=PROG	25+2		ERDA=NDC-9	210	477	ORL BEMIS+CD FILTER, #214, 7+-20, 3, TBP NSE	
CM 243	FISSION	EXPT=PROG	25+2		ERDA=NDC-9	210	477	ORL BEMIS+2200M/S CS=609, 6+-25, 98	
CM 243	RES INT FISS	EXPT=PROG	25+2		ERDA=NDC-9	210	477	ORL BEMIS+CD FILTER, #1575+-1368, TBP NSE	
CM 245	FISSION	EXPT=PROG	18+2	35+1	ERDA=NDC-9	99	477	LRL BROWNE+LINAC, THR VAL GVN, TBP NSE,	
CM 245	FISSION	EXPT=PROG	NDG		ERDA=NDC-9	210	477	ORL GABBS+DATA REDUCTION T8D, NDC	
CM 245	RESON PARAMS	EXPT=PROG	18+2	35+1	ERDA=NDC-9	99	477	LRL BROWNE+RES PAR ANAL, TBP NSE, NDC,	
CM 250	N, GAMMA	EXPT=PROG	25+2		ERDA=NDC-9	99	477	LRL LOUGHEED+THR VAL=808, CM 251 MADE,	
BF 249	FISSION	EXPT=PROG	78+5	38+8	ERDA=NDC-9	111	477	LAS SILBERT+REL U235, NDC, TBP NSE,	
CF 249	TOTAL XSECT	EXPT=PROG	58+3	18+9	ERDA=NDC-9	211	477	ORL HARVEY+TRNS., 3PC RSLN, ANAL T8D, NDC	
CF 252	NUBAR, (NU)	EXPT=PROG	SPON		ERDA=NDC-9	27	477	ANC SMITH+MV BATH METHOD, NDC, T8C	

ELEMENT S A	QUANTITY	TYPE	ENERGY		DOCUMENTATION			LAB	COMMENTS
			MIN	MAX	REF	VOL	PAGE		
CF 252	NUBAR ₂ (NU)	EXPT=PROG	SPON			ERDA=NDC-9	107	477	MHG BOZORGHANESH+NU=5,744+-,025.
ES 253	FRAG SPECTRA	EXPT=PROG	SPON			ERDA=NDC-9	127	477	LAS MOSES+ANG DISTR FISS FRAG TO BE MEAS

IDAHO NATIONAL ENGINEERING LABORATORY
IDAHO FALLS, IDAHO

A. DATA COMPILATION AND EVALUATION ACTIVITIES

1. A File of Actinide-Isotope Decay Data For ENDF/B: (C. W. Reich)

In recognition of the need for a commonly available base of evaluated nuclear decay data for use in a variety of reactor-related applications, the scope of the Evaluated Nuclear Data File (ENDF/B) was expanded several years ago to include such information. The first general category of nuclides whose detailed decay data were incorporated into ENDF/B were the fission-product nuclides; these data appeared in the Fission-Product File of Version IV of ENDF/B¹. The increasing importance of the actinides in many areas of reactor technology has led to a decision to produce an Actinide File to be included in ENDF/B-V. We have had the responsibility for preparing the decay data for this file.

The Actinide File contains nuclear data for 46 isotopes and isomeric states. The following is a listing of these 46:

U - 232, 233, 234, 235, 236, 237, 238, 239

Np - 236, 236m, 237, 238, 239

Pu - 236, 237, 238, 239, 240, 241, 242, 243, 244

Am - 240, 241, 242, 242m, 243, 244, 244m

Cm - 241, 242, 243, 244, 245, 246, 247, 248, 249

Bk - 249, 250

Cf - 249, 250, 251, 252, 253

Es - 253

These decay data have been worked up in the expanded data content adopted for the Version-V ENDF/B decay data².

-
- (1) C. W. Reich, R. G. Helmer and M. H. Putnam, Radioactive-Nuclide Decay Data for ENDF/B, ANCR-1157, (August 1974).
 - (2) C. W. Reich, R. G. Helmer and R. L. Bunting, Nuclear Technology Division Annual Progress Report for Period Ending June 30, 1975, ANCR-1255 (February 1976), 25-26.

2. A File of Evaluated Decay-Scheme Data For NRC: (R. L. Bunting,
N. C. Dyer, M. A. Lee*, M. H. Putman)

A data file of recently evaluated radionuclide decay data is being prepared for the Nuclear Regulatory Commission. This file contains data on 111 nuclides.

It is tailored to satisfy the radionuclide decay-data needs for the quantitative monitoring of radionuclides associated with nuclear power plant operations and the calculation of radiation doses from nuclear power plant effluents.

The report contains the following data classifications.

1. Nuclide Identification
2. Half-life
3. Decay Modes (β^- , β^+ , ϵ , α , IT)
 - a. Associated branching ratios
4. Average Energy per Disintegration (electron, photon, α)
5. Gamma-ray Intensity Normalization
6. Gamma-ray Listing
 - a. Energy
 - b. Relative and/or absolute gamma-ray intensity
 - c. Assay flags

The associated uncertainties in the reported values are also included.

The average energy per disintegration is calculated for three categories, electron, photon and alpha. The average electron energy includes contributions from the beta spectrum as well as conversion and Auger electrons. The latter two contributions are processed into the file from known γ -ray multipolarity and electron-capture data. The average photon energy includes the contributions of the γ -spectrum and x-rays and annihilation radiation from other decay processes. Nuclear recoil effects are considered in calculating the average α -energy.

The γ -spectra from the nuclides of interest for this file are frequently complex. In order to present a useful γ -ray listing, the output list can be controlled by the value of the γ -ray intensity code.

* Summer Faculty participant from Wartburg College, Waverly, Iowa

This code indicates the height of the γ -ray above background in a single source spectrum. A summary of the intensity code is given below:

<u>Intensity Code</u>	<u>Peak-to-Background Ratio (PBR)</u>
1	$PBR \geq 10$
2	$10 > PBR \geq 5$
3	$5 > PBR \geq 2$
4	$PBR < 2$

Only γ rays with intensity codes 1 or 2 are output for the NRC file. For each γ -ray emitting nuclide on the file, one or two γ rays have been flagged by the compilers as the "assay γ rays." These "assay γ rays" will uniquely identify the presence of the nuclide in question.

In selecting these, consideration has been given to the problem of the existence of γ rays of similar energy from the decay of other radionuclides known (or suspected) to be present in known power plant radionuclide samples, which can cause problems in the quantitative assay of these activities.

Several summary appendices are included in this report. These summaries contain various sorts of the E_{γ} , I_{γ} , $T_{1/2}$ and Identification records to further aid the user of these data.

B. NUCLEAR LEVEL-SCHEMES STUDIES

1. Decay of ^{128}Cs : (R. C. Greenwood, R. G. Helmer, C. W. Reich, R. J. Gehrke, R. A. Anderl)

As a part of our program of nuclear structure studies of neutron-deficient isotopes off the line of stability, samples of $^{128}\text{Ba-Cs}$ have been produced at the C. P. Anderson Meson Physics Facility (LAMPF) by irradiation of praseodymium metal with ~ 800 MeV protons. These targets were shipped to the INEL where the barium fraction was chemically extracted and the mass-128 fraction was obtained from an isotope separator. The resulting samples included only the radioactive isotopes ^{128}Ba and the daughter ^{128}Cs .

Gamma-ray spectra obtained during a continuous Ba-Cs chemical separation were used¹ to identify twelve γ rays associated with the ^{128}Ba (2.4 d) activity. The remaining γ rays are given in Table B-1 and are associated with the ^{128}Cs (4 m) decay.

Measurements were made of the γ - γ coincidence spectra with gates on the peaks at 442, 511, 526, 590, 1030 and 1140 keV. In addition to establishing many γ - γ coincidence relationships, these spectra can be used to determine the absence of many other γ - γ coincidences. For this particular decay scheme, the "no coincidence" result does really mean that the γ ray does not populate any level at, or above, that depopulated by the gating γ ray. From this fact, the γ - γ coincidence data can be used to place many γ rays in the level scheme.

The γ - γ coincidence results are also used to determine the absolute β^+ branching ratios to the levels at 969 and 1999 keV and the relative β^+ intensities to the levels at 442 and 1582 keV.

The decay scheme deduced from these data is shown in Fig. B-1. The seven transitions at the left-hand side of the figure are placed tentatively since only one transition is seen from each level. The remainder of the scheme is quite well determined. The spins and parities of the states below 1200 keV are known from previous experiments and those for the states above 1200 keV are deduced from the electron-capture population and γ ray depopulation of the levels.

(1) R. G. Helmer, R. J. Gehrke, R. C. Greenwood, C. W. Reich and L. D. McIsaac, Nucl. Phys. A258, 83 (1976).

Table B-1

¹²⁸Cs γ-ray energies and intensities

<u>Energy (keV)</u>	<u>Relative intensity^a</u>	<u>Placement in scheme</u>
442.873 + .009	100.	442 - 0
459.98 + .04	0.123 + .015	1429 - 969
511.	492. + 15	β+
526.577 + .010	9.01 + .18	969 - 442
570.07 + .03	0.115 + .017	1999 - 1429
590.239 + .019	0.250 + .007	1033 - 442
613.473 + .012	1.32 + .03	1582 - 969
688. + 1. b	0.017 + .007 ^b	2272 - 1582
966.5 + .3 b	0.12 + .02 ^b	1999 - 1033
969.465 + .019	2.34 + .05	969 - 0
986.65 + .03	0.133 + .010	1429 - 442
1030.170 + .022	0.812 + .017	1999 - 969
1081.14 + .06	0.076 + .007	2510 - 1429
1140.05 + .03	4.26 + .09	1582 - 442
1157.61 + .12	0.031 + .004	2127 - 969
1162.00 + .07	0.036 + .004	2591 - 1429
1203.64 + .08	0.034 + .004	2633 - 1429
1239.64 + .06	0.049 + .003	2272 - 1033
1283.43 + .07	0.043 + .006	(1726 - 442)
1303.34 + .03	0.440 + .013	2272 - 969
1392.53 + .07	0.059 + .005	2361 - 969
1434.45 + .07	0.049 + .004	1877 - 442
1461.1 + .2	0.14 + .02	2430 - 969
1477.66 + .09	0.036 + .004	2510 - 1033
1512.98 + .03	0.198 + .011	2482 - 969
1541.21 + .05	0.066 + .008	2510 - 969
1556.73 + .06	0.053 + .004	1999 - 442
1600.06 + .14	0.019 + .004	2633 - 1033
1629.07 + .04	0.498 + .014	2598 - 969
1663.61 + .04	0.094 + .004	2633 - 969
1684.13 + .04	0.416 + .013	2127 - 442
1804.12 + .14	0.022 + .003	2837 - 1033
1810.20 + .13 doublet	0.04	
1829.86 + .10	0.025 + .002	2272 - 442
1837.20 + .17	0.013 + .002	
1868.06 + .11	0.028 + .003	2837 - 969
1918.83 + .05	0.137 + .007	2361 - 442
1978.06 + .05	0.172 + .005	2420 - 442
1987.84 + .05	0.098 + .007	2430 - 442
2039.56 + .05	0.115 + .006	2482 - 442
2067.71 + .14	0.020 + .003	2510 - 442
2078.18 + .07	0.043 + .004	2521 - 442
2141.24 + .19	0.027 + .009	3110 - 969
2148.61 + .09	0.184 + .007	2591 - 442

Table B-1 (Continued)

<u>Energy (keV)</u>	<u>Relative intensity^a</u>	<u>Placement in scheme</u>
2155.63 + .04	0.568 + .017	2598 - 442
2190.15 + .05	0.211 + .007	2633 - 442
2255.50 + .16	0.009 + .002	
2275.53 + .06	0.059 + .002	2718 - 442
2314.47 + .56	0.006 + .002	
2361.91 + .10	0.22 + .02	2361 - 0
2363.6 + .4 ^b	0.043 + .011 ^b	(2806 - 442)
2394.33 + .06	0.090 + .003	2837 - 442
2416.41 + .06	0.128 + .004	2859 - 442
2430.55 + .08	0.023 + .004	2430 - 0
2466.69 + .24	0.008 + .002	
2482.58 + .12	0.015 + .002	2482 - 0
2510.60 + .11	0.016 + .002	2510 - 0
2564.53 + .15	0.008 + .001	
2591.43 + .10	0.024 + .002	2591 - 0
2632.94 + .08	0.025 + .002	2633 - 0
2650.69 + .31	0.008 + .002	(3099 - 442)
2667.42 + .13	0.012 + .003	3110 - 442
2837.64 + .09	0.023 + .001	2837 - 0
2859.26 + .09	0.023 + .002	2859 - 0
2937.33 + .12	0.010 + .002	
3104.05 + .26	0.008 + .001	

^aAbsolute γ -ray intensities, $\gamma/100$ decays, can be obtained by multiplying these values by (0.258 ± 0.013)

^bValues are from γ - γ coincidence measurements.

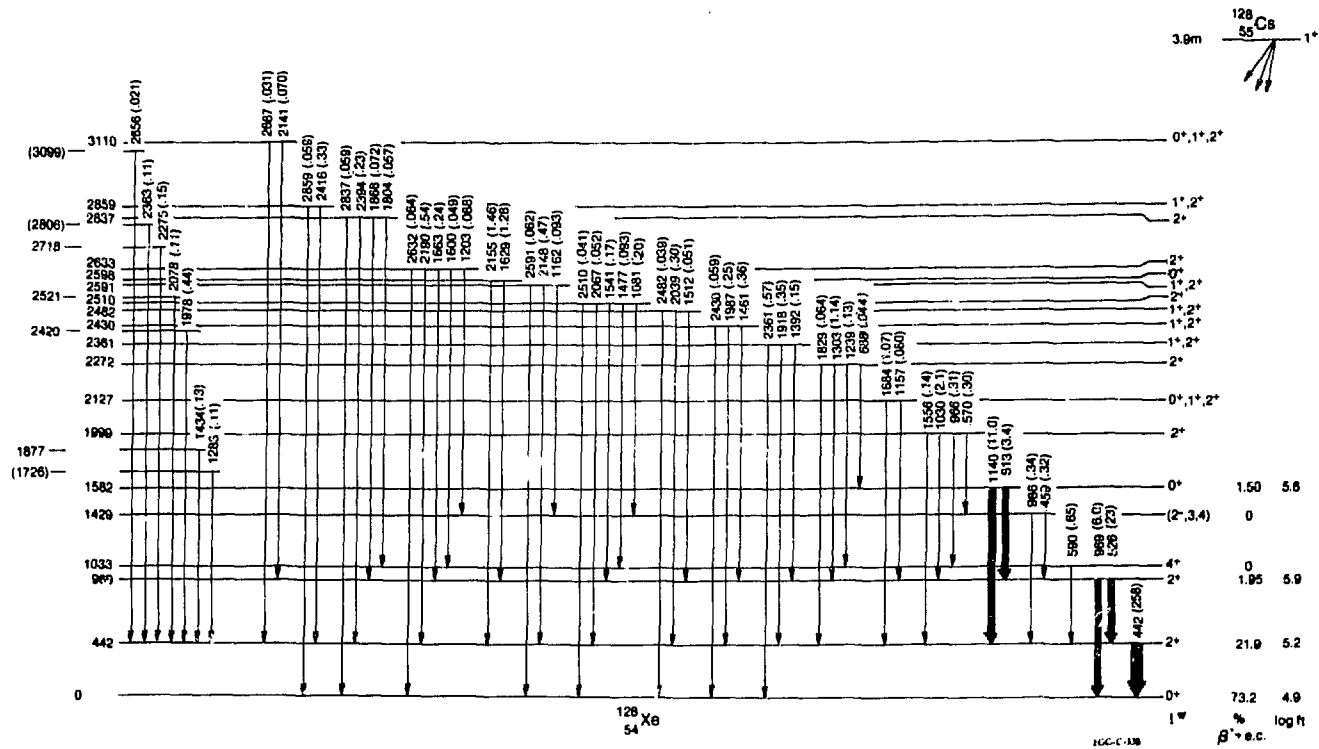


Figure B-1. Proposed decay scheme of ^{128}Cs . The energies are in keV and the γ -ray intensities are per 100 decays.

2. Half-Lives of ^{134}La And $^{132-135}\text{Ce}$: (R. J. Gehrke and R. G. Helmer)

The half-lives of ^{134}La and $^{132-135}\text{Ce}$ have been measured by means of γ -ray spectrometry with Ge(Li) detectors. All of the sources used were samples produced at the Clinton P. Anderson Meson Physics Facility (LAMPF) by the spallation reaction with ~ 800 MeV protons bombarding praseodymium metal foils. The cerium was separated from the praseodymium foils by preferentially extracting Ce(IV) out of 10 M HNO_3 into di-(2-ethylhexyl) orthophosphoric acid (HDEHP). Isotopically purified ^{134}Ce samples were produced with the INEL isotope separator. The ^{134}La sample was obtained from chemically and isotopically purified ^{134}Ce by oxidizing ^{134}Ce to the +4 oxidation state and extracting it into HDEHP leaving the ^{134}La in the aqueous medium. The decay of the ^{134}La was observed by measurements of the gross γ -ray counting rate from a Ge(Li) detector. The half-lives of all of the cerium isotopes were determined by following the decay of the stronger γ -ray peaks in the Ge(Li) spectra. Since both chemical and isotopic separations were carried out, the activity of each isotope was expected to follow a pure exponential decay.

Our measured values of the half-lives of ^{134}La and $^{132-135}\text{Ce}$ are given in Table B-2. The reduced- χ^2 values for the least-squares fits are also given in this table. They generally support the assumption of a single component in the cases with more than five data points. The systematic errors given are intended to be reasonable estimates of the magnitudes of these errors and are based on the physical conditions of the experiments or on the performance of the electronic circuitry. Generally, where several previous measurements exist they are inconsistent. As an example, previous half-life values of ^{134}Ce vary from 72.0 ± 0.5 to 81 ± 2 hr. The average ($1/\sigma^2$ weighted) of the six previous values with assigned errors is 73.76hr and has a reduced- χ^2 value of 12.5, compared to the expected value of ~ 1.0 . Similarly, the previous ^{135}Ce values vary from 17.5 ± 0.4 to 22 ± 0.7 hr. These gross discrepancies indicate the presence of systematic errors in some of the experiments which were underestimated or not taken into account. Because our cerium sources were chemically and isotopically purified and because each radionuclide was counted with Ge(Li) spectrometers to resolve the cerium γ -rays from any contaminating radiations, (e.g. ^{132}La in ^{132}Ce , ^{133}La in ^{133}Ce or ^{132}Ce in ^{133}Ce), the present measurements should provide more accurate half-life values.

Table B-2. Half-life values for ^{134}La and $^{132-135}\text{Ce}$ from the present investigation

Isotope	# of Data Points Fit	Time Observed (half-lives)	γ -ray peak Observed [E(keV)]	Least-squares fit		Averaged Data Error Components		Half-life
				ϵ^a	half-life	Statistical	Systematic	
^{134}La	80	4.5	Total Spectrum	0.84	6.45 ± 0.06 min	0.06 min	0.10 min	5.45 ± 0.16 min
^{132}Ce	5	11	155	4.18	3.51 ± 0.11 hr	0.05 hr	0.056 hr	3.51 ± 0.11 hr
			180	3.69	3.51 ± 0.05 hr			
^{133}Ce	3	7	130	0.35	4.91 ± 0.05 hr	0.06 hr	0.33 hr	4.93 ± 0.39 hr
			785	11.6	5.17 ± 0.26 hr			
			1584	0.57	4.94 ± 0.18 hr			
			2016	0.54	4.80 ± 0.19 hr			
^{134}Ce	11	9	511	4.96	75.80 ± 0.09 hr	0.15 hr	0.76 hr	75.9 ± 0.9 hr
			563	0.90	76.64 ± 1.59 hr			
			604	2.12	76.23 ± 0.31 hr			
^{135}Ce	14	2.5	206	1.02	17.731 ± 0.038 hr	0.13 hr	0.18 hr	17.76 ± 0.31 hr
			265	0.93	17.756 ± 0.016 hr			
			300	1.17	17.787 ± 0.025 hr			

3. Decay of ^{134}La : R. C. Greenwood, C. W. Reich, R. G. Helmer, R. J. Gehrke, R. A. Anderl and J. D. Baker*

The properties of nuclides in the mass region $50 < Z, N < 82$ are of considerable current interest because of the information which they provide concerning the collective potential-energy surfaces and how these surfaces vary with both proton and neutron number. In a continuing effort to systematically study the decay properties of such nuclei, a source of ^{134}Ce - ^{134}La was produced by spallation in Pr-metal targets using ~ 890 -MeV protons from the Clinton P. Anderson Meson Physics Facility (LAMPF). After bombardment, the irradiated foils were transported to the INEL for study.

The Ce fraction was chemically separated from the other spallation products and the Pr. Following the chemical separation, the residual fraction of Ce was mass separated. A surface-ionization-type ion source was employed in these separations and a complete separation typically took ~ 4 -6 hours.

The spectrum of γ rays emitted in the ^{134}Ce - ^{134}La decay chain was measured using the mass-separated ^{134}Ce - ^{134}La sample with a Ge(Li) detector. A listing of the average energies and intensities (relative) of the γ -ray transitions which could be associated with the ^{134}La decay in the present work is given in Table B-3. To assist in the determination of absolute photon emission rates in the $^{134}\text{Ce} \rightarrow ^{134}\text{La} \rightarrow ^{134}\text{Ba}$ decay chain, it is necessary to know the relative intensities of the K x-radiation from La and Ba. This was accomplished using a Si(Li) photon detector. Gamma-ray coincidence spectra were measured for several of the strongest γ -ray lines in the ^{134}La spectrum. These lines were those at 563, 604, 1211, 1424, 1483, 1554, and 1732 keV (in a 180° geometry), as well as the 511-keV annihilation-radiation peak (in a 90° geometry).

A decay scheme for ^{134}La is quite readily constructed from the data obtained in the present study. The extensive γ - γ coincidence relationships generally give quite unambiguous evidence as to the placement of γ -ray transitions in the ^{134}Ba level scheme. These coincidence data are further supplemented by the noncoincident γ -ray transitions, which are therefore inferred to be ground-state transitions. Since the decay energy of ^{134}La is quite well known ($Q = 3720 \pm 25$ keV) we can also infer that those γ -ray transitions with energies ≥ 3140 keV must populate the ^{134}Ba ground state, while those transitions with energies ≥ 2580 keV must populate either the ground state or the 604-keV first excited state (assuming that the second excited state in ^{134}Ba is at 1167 keV). The placement of other γ -ray transitions, which were not sufficiently intense to be observed in the

* Allied Chemical Corporation

Table B-3. γ -ray energies and intensities from ^{134}La decay.

γ -ray Energy (keV) ^a	Error (keV)	Relative γ -ray intensity ^b	Error (%)
Ba K-x		7020.	8.
475.33	0.21	1.27	30.
511. (Ann)		29130.	4.
563.226	0.013	86.7	2.5
592.577	0.038	3.98	7.
604.699	0.012	1218.7	2.5
659.85	0.09	0.62	10.
718.709	0.028	2.90	7.
795.907	0.032	1.83	7.
861.286	0.047	0.99	10.
920.347	0.024	4.32	5.
991.725	0.042	1.38	7.
1038.68	0.05	0.91	7.
(1103.4)	0.5	0.2	50.
1155.826	0.022	4.68	5.
1162.1	0.1	18.5	7.
1168.63	0.08	5.2	20.
1184.92	0.12	0.42	15.
1211.145	0.026	28.59	2.5
(1243.84)	0.21	0.54	20.
(1255.06)	0.26	0.35	40.
1307.0	0.7	0.18	50.
1320.701	0.028	19.80	2.5
1347.34	0.05	1.18	5.
1368.96	0.07	0.74	10.
1396.730	0.029	8.55	2.5
1402.889	0.034	2.47	5.
1424.506	0.030	45.4	2.5
1431.35	0.13	0.54	20.
1483.516	0.031	35.9	2.5
1488.29	0.27	1.05	20.
1528.54	0.07	0.64	10.
1554.934	0.032	100.0	2.5
1560.42	0.48	1.18	30.
1579.92	0.15	1.14	20.
1591.1	1.1	6.22	30.
1649.68	0.16	0.29	15.
1660.57	0.07	0.73	10.
(1674.6)	0.5	0.14	40.
1683.33	0.07	0.77	10.
1719.04	0.05	1.50	5.
1732.129	0.035	56.6	2.5
1749.41	0.13	0.34	15.
1765.71	0.22	0.53	20.
1774.353	0.036	11.55	2.5
(1800.8)	0.5	0.084	40.
1836.43	0.15	0.40	15.

Table B-3 (Continued)

γ -ray Energy (keV) ^a	Error (keV)	Relative γ -ray intensity ^b	Error (%)
1859.43	0.06	0.86	7.
1883.74	0.12	0.80	10.
1893.20	0.08	0.56	10.
(1918.0)	0.5	0.16	40.
1932.16	0.06	1.07	7.
1959.956	0.043	23.55	2.5
1966.07	0.12	1.03	15.
1995.133	0.044	21.57	2.5
2029.191	0.044	9.49	2.5
2051.55	0.10	1.42	10.
(2064.4)	0.5	0.15	30.
2088.24	0.05	14.0	5.
2091.99	0.10	2.38	10.
2104.11	0.06	0.75	7.
2124.482	0.050	7.50	2.5
2143.222	0.050	3.87	5.
2156.03	0.08	1.01	10.
(2159.5)	0.5	0.06	100.
2223.781	0.048	4.38	2.5
2240.4	0.6	0.12	30.
2246.67	0.35	0.13	30.
2282.290	0.054	2.12	5.
2312.91	0.07	0.54	7.
2334.7	0.4	0.45	20.
2345.56	0.21	0.155	15.
2442.68	0.26	0.104	20.
2464.15	0.13	0.174	15.
2482.24	0.17	0.145	15.
2564.84	0.07	1.36	5.
2570.87	0.054	4.56	2.5
2599.84	0.06	0.68	7.
2656.11	0.18	0.115	15.
2667.37	0.09	0.270	7.
2696.54	0.07	0.73	7.
2722.51	0.25	0.109	15.
(2748.1)	0.5	0.02	100.
2758.90	0.32	0.110	15.
2764.16	0.08	0.334	10.
2788.72	0.21	0.075	15.
2803.51	0.32	0.069	15.
2824.08	0.25	0.081	20.
2828.05	0.28	0.082	20.
2851.05	0.12	0.268	7.
2866.44	0.24	0.057	15.

Table B-3 (Continued)

γ -ray Energy (keV) ^a	Error (keV)	Relative γ -ray intensity ^b	Error (%)
2894.92	0.14	0.100	10.
2938.92	0.15	0.68	7.
3027.11	0.18	0.147	10.
3061.33	0.15	0.147	10.
3086.59	0.15	0.082	15.
3160.04	0.15	0.135	10.
3245.84	0.19	0.055	20.
3327.18	0.15	0.139	10.
3449.46	9.18	9.143	10.

^a Parentheses around a γ -ray energy indicate a tentative assignment.

^b These values must be multiplied by a factor 4.14×10^{-3} to convert to absolute intensities (in $\gamma/100$ disintegrations). Since the uncertainty in this conversion factor is $\pm 4.1\%$, this should be added in quadrature to the error assigned to the relative intensities to obtain the total error assigned to the absolute intensity values.

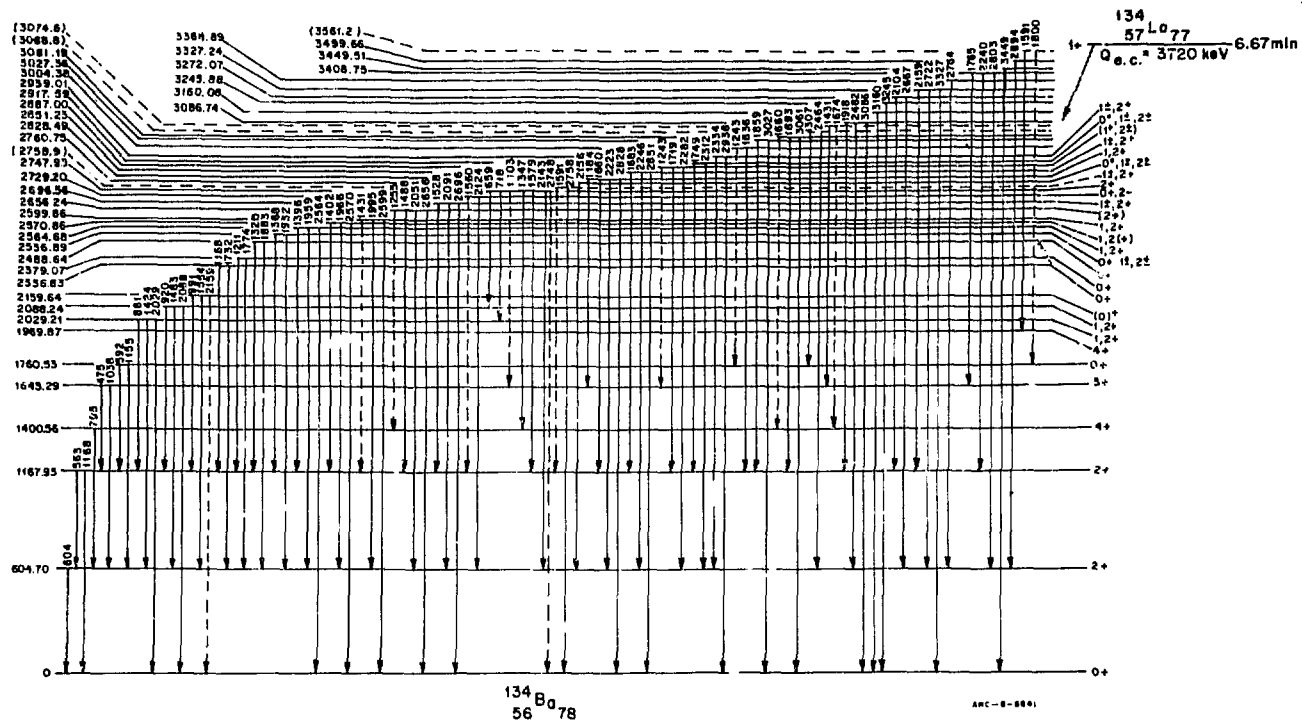


Figure B-2. Proposed decay scheme for ^{134}La . Spin and parity assignments are listed only for those states below 3.0 MeV.

coincidence spectra or by the energy limits noted above, was facilitated by the high precision attained for the γ -ray energy measurements. Such γ -ray transitions could then generally be placed in the level scheme from the Ritz combination principle. The decay scheme of ^{134}La which was proposed from the present data, using the considerations cited above, is shown in Fig. B-2.

4. K Conversion Coefficients of γ -Rays Above 800 keV From ^{182}Ta Decay: (R. G. Helmer)

The relative intensities of the K-shell internal-conversion electrons above 800 keV from the decay of ^{182}Ta (115 d) have been measured for all of the known γ -ray transitions except that at 1180 keV. These measurements were made with a $\pi\sqrt{2}$ iron-free magnetic spectrometer. Each K-line was measured once or twice at a resolution R of 0.10% and once at either 0.075% (for complex peaks) or 0.20% (for single lines). The results of these measurements are shown in columns 2-5 of Table B-4. The results from the various resolutions are reasonably consistent. The uncertainties in the averages range from 0.5 to 20%.

Ten γ -ray spectra of ^{182}Ta were measured on Ge(Li) detectors and analyzed to obtain the relative intensities of the high-energy lines. The results from these measurements are given in column 6 of Table B-4. The intensities are quoted relative to 1221-keV line and the uncertainty in the efficiency is taken to be zero at this energy, 0.3% within 25 keV, 0.7% within 50 keV and 1.0% elsewhere. These are the uncertainties applied after averaging results from three source-detector distances on one detector and two distances on another detector.

The K-conversion-electron intensities and the γ -ray intensities were normalized to give the K-conversion coefficients given in column 7 of the table. The quoted uncertainties are generally a factor of 3 or more smaller than the best previous measurements. Comparisons of these conversion coefficients with the theoretical values for ten transitions which have pure multiplicities show excellent agreement and indicate that the uncertainties are realistic. The best multipolarity determinations for the remaining twelve transitions will require a complete reanalysis of the published angular correlation and angular distribution (low temperature) results in conjunction with these internal-conversion coefficients.

Table B-4

Summary of K-conversion-electron data for ^{182}Ta decay.

γ -ray energy (keV)	Relative K-line intensity				Average	Relative γ - ray intensity	K-conversion Coefficient
	R = 0.75%	R = 0.10%	R = 0.20%	Average			
891.961		0.32 (3)		0.33(2)	0.33(2)	0.212(25)	3.94(53)
927.973		3.62 (3)		3.70(3)	3.66(4)	2.30 (3)	4.03(7)
959.709		4.54 (5)		4.69(4)	4.63(7)	1.29 (2)	9.08(20)
1001.674		10.66 (6)	10.59(8)	10.79(8)	10.68(5)	7.63 (8)	3.54(4)
1044.388		1.48 (3)		1.52(2)	1.51(2)	0.877(17)	4.36(10)
1113.38	1.99(15)	1.94 (5)	1.98(4)		1.97(3)	1.65 (2)	3.02(6)
1121.276	150.9 (6)	152.9 (5)	152.9 (3)	152.9 (8)	152.7 (8)	129.3 (14)	2.99(4)
1157.288	6.78(9)	6.54 (8)	6.65(7)		6.65(6) }	3.67 (4)	7.0 a
1158.057	1.00(33)	1.35 (46)	1.07(33)		1.10(21) }		2.2 a
1180.76						0.322(19)	3.0 (15) ^b
1189.024	91.6 (9)	92.9 (10)	92.5 (6)		92.4 (8)	60.3 (4)	3.88(4)
1221.379	100.0 (5)	100.3 (4)	99.7 (4)	100.0 (6)	\approx 100.0	\approx 100.0 (8)	\approx 2.53
1223.777	1.05(42)	0.88 (13)	0.72(8)		0.77(7)	0.8	2.4 (4)
1230.989	41.6 (3)	42.5 (2)	42.3 (2)	42.1 (3)	42.2 (2)	42.56 (20)	2.50(2)
1257.392	5.47(14)	5.23 (21)	5.32(31)		5.39(11)	5.52 (4)	2.47(5)
1273.703	2.88(7)	2.74 (3)	2.78(3)		2.77(3)	2.41 (3)	2.91(5)
1289.128	21.5 (7)	20.4 (9)			21.1 (6)	5.00 (6)	10.68(33)
1342.70		0.86 (3)	0.83(3)		0.84(2)	0.931(12)	2.28(6)
1373.806		1.31 (3)		1.31(2)	1.31(2)	0.812(10)	4.08(8)
1387.772		0.470(15)		0.47(1)	0.47(1)	0.261(5)	4.56(13)
1410.08		0.150(15)		0.14(2)	0.15(1)	0.149(6)	2.55(20)
1453.092		0.170(15)		0.18(1)	0.18(1)	0.104(4)	4.38(30)

^a These two values are based on a published decomposition of the 1158-keV γ -ray peak.

^b Based on the L-electron line intensity and an assumed K/L ratio.

5. Absolute γ -Ray Branching And Half-Life of ^{250}Bk : (R. J. Gehrke, R. G. Helmer, C. W. Reich, J. D. Baker*)

As part of an investigation of the decay of 3.2 h ^{250}Bk we have measured the absolute intensity (or branching ratio) of the 989- and the 1028 + 1031 - keV γ rays and the ^{250}Bk half-life. These experiments were performed with a $4\pi\beta$ - γ coincidence system and a Ge(Li) spectrometer whose absolute photopeak efficiency had been determined previously.

The sources were prepared by chemically extracting the ^{250}Bk from the ^{254}Es (275.7 d) parent activity. This was accomplished by oxidation of Bk to the +4 oxidation state using 10M HNO_3 -0.1M NaBrO_3 and extracting into an equal volume of 0.1 M HDEHP in heptane³. Possible³ traces of entrained Es were eliminated by washing the HEDHP once with an equal volume of fresh 10 M HNO_3 -0.1M NaBrO_3 . Bk was then back extracted into 6M HNO_3 containing several drops of 30% H_2O_2 . The Bk source was made relatively massless by using successively anion-exchange and cation-exchange techniques.

The ^{250}Bk activity was deposited as a small droplet on thin conducting films of VYNS and taken to dryness with a heat lamp. The VYNS films were typically 40 $\mu\text{g}/\text{cm}^2$ thick with gold layers of 25 $\mu\text{g}/\text{cm}^2$ thickness deposited on each side by vacuum evaporation. Alpha counting of the residual activity (i.e. ^{250}Cf and ^{254}Es after the ^{250}Bk decayed) indicated that the chemical separation of the ^{254}Es from the ^{250}Bk was extremely good. At the time of separation the activities of $^{250}\text{Bk}/^{254}\text{Es}$ were $>300,000/1$. Three sets of experiments were run to determine the absolute γ -ray branch through the 989 and 1028 + 1031 - keV γ rays. For each experiment the ^{250}Bk source was counted with the Ge(Li) spectrometer and the $4\pi\beta$ - γ coincidence system.

In the first experiment the ^{250}Bk was counted with the $4\pi\beta$ - γ coincidence system to determine the source disintegration rate. The beta- and γ -ray counts were corrected for dead time and background. The coincidence counts were corrected for dead time, background and accidental coincidences. The beta chamber efficiency (i.e., ratio of γ -ray and coincidence counts) was 95.5%. The γ -ray branching ratios were calculated from the Ge(Li) γ -ray peak intensities and these disintegration rates.

The second experiment employed two techniques for measuring the sample disintegration rate. The first technique was the same as that used in the first experiment. The chamber efficiency was 96.5%. The second technique involved taking data with beta chamber bias from 2800 to 3300 volts. This range produced beta chamber efficiencies of from 57 to 97%. The source disintegration rate was then determined by extrapolating to a chamber efficiency of 100%.

* Allied Chemical Corporation

For each of these three experiments, the γ -ray emission rate of the sample was determined for the 989- and 1028 + 1031 - keV transitions. This was done by counting the samples at 10 cm from a 65-cm³ closed-ended coaxial Ge(Li) spectrometer. The sample was counted in two orientations to minimize the uncertainty in the source-detector distance. Since the statistical uncertainty in each of these peaks was $\leq 2\%$, the ratio of measured values was adjusted to correspond to the much more precise ratio previously determined (from measurements with a ²⁵⁴Es-²⁵⁰Bk source). The adjustments were 0.0, 0.15 and 0.5% in the three cases. The resulting branching ratios are given in Table B-5. Typical values of the uncertainties considered in the individual values in Table B-5 are: statistical error in Ge(Li) peak areas, 1-2%; source position, 0.25%; adjustment to precise relative intensities, 0-0.25%; sample disintegration rate, 0.2-0.3%; and decay corrections, 0.08-0.50%. After averaging the three values, an uncertainty of 1.5% was added from the Ge(Li) detector efficiency curve. The latter is the dominant single error and several of the errors from the γ -ray counting exceed the error in the disintegration rate.

The system used to measure the ²⁵⁰Bk half-life consists of a 4 π β - γ proportional chamber with associated preamplifiers and fast discriminators. Following the fast discriminator, there are two parallel electronic pulse-processing systems. One system is a conventional 4 π β - γ system with fixed (and long) pulse width, to produce a constant dead time τ . The other system is being developed for sources which have very high count rates (e.g., β -rates of 100,000 c/s). With this system the pulse widths vary and the associated dead times are measured directly by gating the pulses of an internal 8 MHz clock.

The ²⁵⁰Bk activity was followed for over 20 half-lives by counting the source for a preset count time (600 s) alternately with the fixed pulse width and the variable pulse width systems. The time between the end of one count and the start of the next count was 300 s. The counts were corrected for dead time and background. The residual activity in the source, i.e. the background, was determined four days after the last half-life count was made. The data were analyzed by performing a non-linear least squares fit to the data with a one-component exponential. Because of the presence of a residual activity, above the background subtracted, the data were also fitted with the sum of two exponential terms. The results of these fits are given in Table B-6. Fits were made to the data from the bet. chamber for both electronic systems and to the computed disintegration rates, N_0 , from the fixed dead time system.

The $1/\sigma^2$ -weighted average of the N_0 run(1 decay component only), fixed-pulse-width N_β data (2 components) and variable pulse width N_β data (2 components) gives a half-life of (192.40 + 0.08) m. We assign a systematic error of ± 0.2 m which is intended to include possible errors in background subtraction and fitting of the second component.

This gives a final half-life of (192.40 ± 0.22) m for ^{250}Bk . The large discrepancy between the N_0 half-life and the N_β (exponential components) half-life is believed due to the presence of a second component in the N_0 data. The large errors in these values (due to the very low γ count rates in the $4\pi\beta\text{-}\gamma$ system) precluded a meaningful analysis with two components.

Table B-5

Experimental results of γ -ray branching ratio measurements

<u>^{250}Bk γ-ray branch</u>	<u>1st experiment</u>	<u>2nd experiment</u>	<u>3rd experiment</u>	<u>weighted average</u>	<u>reported *</u>
989-keV	0.450 $_{-7}^{+6}$	0.446 $_{-9}^{+6}$	0.456(10)	0.450(3)	0.450(7)
1028+1031-keV	0.405 $_{-5}^{+5}$	0.401 $_{-4}^{+5}$	0.410 $_{-7}^{+5}$	0.406(3)	0.406(7)

* Weighted average with 1.5% uncertainty in photopeak efficiency added in quadrature to uncertainty due to γ -ray peak, source position, normalization to relative γ -ray intensities and uncertainty in the measured disintegration rate.

Table B-6

 ^{250}Bk half-life measurement with $4\pi\beta\text{-}\gamma$ system

Quantity Measured	Pulse-Processing System	Time Range Included in Fit (hours)	Number of Data Points Included in Fit	Number of $T_{1/2}$ Components Used	ϵ^2	$T_{1/2}$ (minutes)
N_O	fixed pulse width	0-28	56	1	0.48	193.15±0.18*
N_B	fixed pulse width	0-31	62	1	3.66	192.7 ±0.13
N_B	fixed pulse width	2.5-31	57	1	3.49	192.85±0.16
N_B	fixed pulse width	0-21	42	1	1.09	192.54±0.04
N_B	fixed pulse width	2.5-23.5	42	1	1.11	192.67±0.06
N_B	fixed pulse width	0-64.5	125	2	0.90	192.38±0.04*
N_B	variable pulse width	0.25-32	62	1	2.94	192.70±0.10
N_B	variable pulse width	0.25-64.7	123	2	0.83	192.39±0.04*

* The $1/\sigma^2$ weighted average of the half-lives marked with an asterisk equals 192.40 m with $\sigma_{\text{internal}} = 0.03$ m and $\sigma_{\text{external}} = 0.08$ m. $\sigma_{\text{external}} = \epsilon(\sigma_{\text{internal}})$. Uncertainty in the reported half-life, 0.22 m, results from adding in quadrature the 0.08 m uncertainty and the 0.2 m systematic uncertainty due to possible errors in the background subtraction and fitting of a 2nd component.

C. MEASUREMENT TECHNIQUES AND STANDARDS

1. High-Counting Rate $4\pi\beta\text{-}\gamma$ Coincidence System : (L. O. Johnson and R. J. Gehrke)

A high-counting rate $4\pi\beta\text{-}\gamma$ coincidence system has been designed and built. This system is capable of determining source disintegration rates as high as 500,000 D/S to an accuracy of $\pm 0.1\%$. The system has been developed to make high-precision measurements of γ -ray branching ratios of fission-product and other nuclides for applications involving quantitative radionuclide assay.

β and γ pulse widths correspond to the length of time that the amplifier output exceeds the discriminator level. A digital minimum-width circuit guarantees that no pulse width will be less than the required resolving time of 250 ns. Coincidences are determined with an overlap coincidence circuit. The accumulative dead times of each of the β , γ , and coincidence channels is measured and recorded simultaneously with the raw count data. Correction equations to account for dead-time losses and accidental coincidences have been developed. These equations seem to be very straightforward.

The high-counting-rate performance of two systems were compared. One system is a conventional fixed-pulse-width (τ) system with τ (for β and γ) = 4 μ sec and a coincidence resolving time of $\tau_R = 250 \times 10^{-9}$ sec. The other system is the variable-pulse-width system described above. For a source of 556,000 D/S the percentage beta channel dead time was 65% for the fixed- τ system and 20% for the variable- τ system. The deviation of the measured activity from the activity as determined from weighed aliquots was +6% for the fixed τ system and -0.7% for the variable- τ system. We believe the 0.7% deviation can be reduced to $<0.1\%$. For count rates below 100,000 D/S the fixed pulse width system and variable pulse width system agree to within 0.1%.

2. Precise Relative γ -Ray Intensity Measurements: (R. J. Gehrke, R. G. Helmer, R. C. Greenwood)

Over the past several years most experimenters have used Ge(Li), and recently intrinsic Ge, detectors for γ -ray spectrometry. Since each of these detectors is essentially unique, the peak efficiency must be determined experimentally for every detector. One standard method of measuring the energy dependence of the absolute efficiency is to make measurements with a series of separate sources, each of which has a known γ -ray emission rate. A second method is to use a single isotope (or a small number of isotopes) that provides a series of lines of known relative intensity. This technique is much faster, although it is limited to providing only the relative detector efficiency. To aid in such

calibrations we have made precise relative γ -ray intensity measurements for a series of isotopes that can then be used for efficiency calibration of other detectors. These measurements have been made on two Ge(Li) detector systems.

The experimental techniques used in this work have been discussed previously.^{1,2} Special care has been taken to provide a consistent method of analyzing the γ -ray peaks including the background determination; errors have been treated in a well defined manner; and corrections for coincidence summing have been made.

Measurements of the γ -ray spectra have been completed for the following 12 samples: ^{56}Co , ^{75}Se , ^{82}Br , ^{110}Ag , ^{125}Sb , ^{133}Ba , $^{140}\text{Ba-La}$, $^{144}\text{Ce-Pr}$, ^{152}Eu , ^{166}Ho , ^{169}Yb and ^{182}Ta . All of these spectra have been analyzed and the results have been tabulated for over half of the isotopes. Table C-1 gives the results for eight isotopes. With this information, it is expected that the relative efficiency of a Ge(Li) detector can be determined to $\sim 3\%$ between 300 and 1500 keV and $\sim 5\%$ outside of this range.

¹ R. G. Helmer, J. E. Cline and R. C. Greenwood, The Electromagnetic Interaction in Nuclear Spectroscopy, edited by W. D. Hamilton (North-Holland, Amsterdam, 1975), Chapter 17.

² R. C. Greenwood, R. G. Helmer, JW Rogers, N. D. Dudey, R. J. Popek, L. S. Kellogg and W. H. Zimmer, Nucl. Tech. 25, 274 (1975).

Table C-1

Relative γ -Ray Intensities

<u>Isotope</u>	<u>γ-Ray Energy (keV)</u>	<u>Relative γ-Ray Intensity</u>	<u>Isotope</u>	<u>γ-Ray Energy (keV)</u>	<u>Relative γ-Ray Intensity</u>	
⁷⁵ Se	66	1.86 (9)		706	17.67 (12)	
	96	5.9 (3)		744	4.92 (4)	
	121	29.8 (9)		763	23.60 (16)	
	136	102.2 (30)		818	7.73 (5)	
	198	2.53 (8)		884	76.9 (5)	
	264	≈ 100.0 (15)		937	36.22 (25)	
	279	42.4 (6)		1384	25.70 (18)	
	303	2.21 (3)		1475	4.21 (3)	
	400	19.1 (3)		1505	13.84 (12)	
				1562	1.250(9)	
	⁸² Br	92	0.86 (4)	¹³³ Ba	53	3.54 (18)
		221	2.71 (8)		80	49.2 (26)
		273	0.96 (3)		160	1.08 (4)
		554	84.7 (6)		223	0.745(24)
606		1.421(13)	276		11.7 (4)	
619		52.0 (4)	302	29.76 (20)		
698		34.1 (3)	356	≈ 100.0 (8)		
776		≈ 100.0 (8)	383	14.36 (10)		
827		28.8 (2)	¹⁴⁰ Ba-La	162	5.83 (20)	
1007		1.522(14)		304	3.89 (5)	
1043		32.55 (25)		328	21.4 (3)	
1072	0.086(6)	423		2.80 (3)		
1081	0.745(9)	432		3.07 (3)		
1180	0.12 (15)	437		1.72 (2)		
1317	31.74 (24)	487		47.6 (5)		
1474	19.53 (15)	537		22.00 (23)		
1650	0.889(8)	751		4.64 (5)		
1779	0.136(2)	815		24.85 (25)		
1956	0.047(1)	867	5.89 (6)			
^{110m} Ag	446	3.86 (3)	919	2.90 (4)		
	620	2.93 (2)	925	7.41 (8)		
	657	≈ 100.0 (7)	1596	≈ 100.0 (9)		
	677	11.31 (8)	2347	0.981(16)		
	686	6.85 (5)	2521	3.62 (7)		
			2547	0.109(3)		
			2899	0.069(2)		
			3118	0.028(1)		

Table C-1 (Continued)

<u>Isotope</u>	<u>γ-Ray Energy (keV)</u>	<u>Relative γ-Ray Intensity</u>	<u>Isotope</u>	<u>γ-Ray Energy (keV)</u>	<u>Relative γ-Ray Intensity</u>
^{166}Ho	80	21.4 (11)	116	1.26 (4)	
	184	128. (4)	152	20.5 (6)	
	215	5.15 (16)	156	7.78 (23)	
	280	51.5 (16)	179	9.1 (3)	
	300	6.36 (20)	198	4.31 (18)	
	365	4.23 (4)	222	21.9 (7)	
	410	19.55 (13)	229	10.6 (3)	
	451	5.11 (4)	264	10.5 (3)	
	529	16.36 (12)	928	1.80 (3)	
	570	9.53 (7)	959	1.00 (2)	
	670	9.43 (7)	1001	5.90 (6)	
	691	2.31 (2)	1044	0.676(15)	
	711	95.3 (6)	1121	≅100.0 (8)	
	736	9.673(10)	1157 ^a	2.85 (4)	
	752	21.21 (1 ^a)	1189	46.6 (7)	
	778	5.28 (4)	1221	77.6 (7)	
	810	≅100.0 (8)	1230	33.0 (3)	
	830	16.97 (12)	1257	4.25 (4)	
	875	1.253(10)	1273	1.86 (2)	
	950	4.71 (3)	1289	3.86 (5)	
	1146	0.351(3)	1342	0.718(11)	
	1241	1.406(16)	1372	0.629(9)	
	1282	0.309(5)	1387	0.202(4)	
	1400	0.858(8)	1410	0.112(6)	
	1427	0.852(13)	1453	0.79 (3)	
	^{169}Yb	63	116. (6)		
93		7.1 (4)			
109		43.5 (15)			
118		5.31 (16)			
130		32.0 (10)			
177		62.2 (19)			
197		≅100.0 (30)			
240		0.337(17)			
261		4.69 (14)			
307		27.5 (8)			
^{182}Ta	65	15.4 (20)			
	67	125. (6)			
	84	7.6 (4)			
	100	40.9 (12)			
	113	5.42 (17)			

^a Doublet

D. INTEGRAL CROSS-SECTION MEASUREMENTS IN THE CFRMF

1. Integral Cross Section Measurements On ^{241}Am in the CFRMF: (E. H. Turk, Y. D. Harker)

A sample of ^{241}Am was irradiated in the Coupled Fast Reactivity Measurements Facility (CFRMF) for the purpose of measuring this nuclide's integral capture and fission cross sections in a fast reactor type neutron spectrum. Post irradiation analysis of the induced activity has been performed using gamma spectrometry to determine the buildup of ^{140}La and using alpha spectrometry to determine the buildup of ^{242}Cm . The ^{140}La analysis has been completed and from the measured activity and assuming a mass 140 chain yield of 5.77% a fission cross section of 504 ($\pm 12\%$) millibarns was determined. The ^{242}Cm analysis to determine the capture cross section is still in progress.

2. Integral Cross Section Measurements on ^{242}Pu in the CFRMF: (E. H. Turk, Y. D. Harker)

A sample containing 30.21 mg ^{242}Pu was irradiated in the Coupled Fast Reactivity Measurements Facility (CFRMF) for the purpose of measuring this nuclide's integral capture and fission cross sections in a fast reactor type neutron spectrum. Post irradiation analysis of the gamma activity was performed using Ge(Li) spectrometry. The analyses resulted in the determination of the buildup of ^{243}Pu and ^{140}La . From the former activity a capture cross section of 159 ($\pm 10\%$) millibarns was determined. From the latter activity and assuming a fission chain yield for mass 140 of 5.98% a fission cross section of 609 ($\pm 12\%$) millibarns was determined. Corrections for fissioning in trace contaminants of other Pu isotopes were found to be negligible.

3. Integral Cross Section Measurements of Intermediate Mass Nuclides: (Y. D. Harker)

A comprehensive program to measure integral cross sections of intermediate mass nuclides (primarily fission product class) has been in progress. This activity includes measurements in the Coupled Fast Reactivity Measurements Facility (CFRMF) and Experimental Breeder Reactor II (EBR II). A summary report covering the results of this program is being prepared and will describe the measurements (reactivity, activation and transmutation) performed on over 100 different samples and sample configurations. The final report will be available by Dec. 1977; however, a summary of these data will be submitted prior to this to those individuals giving review papers on the appropriate subject matter at the Second Advisory Group Meeting on FPNP to be held at Petten, Netherlands, Sept. 5-9, 1977.

E. MEASUREMENT OF $\bar{\nu}$ FOR ^{252}Cf : (J. R. Smith, S. D. Reeder)

A measurement of $\bar{\nu}$ for ^{252}Cf , using the manganese bath method, is underway at INEL. Two manganese baths have been set up, one a 42-in. x 42-in. cylinder (capacity 914 liter) and the other a 20-in. diam. sphere (65.5 liter capacity). Piping is such that the MnSO_4 solution can be pumped from either bath to a pair of on-line counters in a flow counting mode or samples can be drawn from either bath to be counted in a batch mode operation. This arrangement will make possible the comparison and calibration of fairly weak sources, and also a search for systematic differences between the batch counting and flow counting techniques. The NBS double fission chamber ¹ has been selected for use in the fission rate determination. Two of these have been loaded with ^{252}Cf foils, prepared by Hal Adair of ORNL, using the self-transfer method. Measurements of neutron yield have begun. Selection of electronic equipment is underway for fission rate determination by fission-fission coincidences, neutron fission coincidences, and 2π fission counting. The value for σ_H/σ_{Mn} , reported to the ENDC in the previous report as 0.02506, has been revised to $0.02503 \pm 0.23\%$, based on weighted fitting of the data. The present results agree well with Axton's revised² value of $0.02495 \pm 0.35\%$ in terms of error overlap, but is about 0.36% higher. The higher σ_H/σ_{Mn} value would raise Axton's source measurements by about 0.15%

-
- (1) J. A. Grundl et al, Nucl Tech. Vol 25, P 237 (Feb. 1975).
(2) E. J. Axton, Private Communication.

ARGONNE NATIONAL LABORATORY

A. NEUTRON PHYSICS

1. The U-234, U-236, Pu-242 and Pu-239 Fission Cross Sections Relative to U-235: (J. W. Meadows)

The U-234/U-235, U-236/U-235 and Pu-242/U-235 fission cross section ratios have been measured from threshold to 10 MeV. The Pu-239/U-235 ratio has been measured from 0.15 to 10 MeV. Some results have been reported.¹

2. Measurements of the Fast Neutron Fission Cross Section of ²³⁵U (W. P. Poenitz)

The ²³⁵U fast-fission cross section appears generally well established to within $\pm 3\%$ from 10 keV to 15 MeV (1). However, some local problem areas and discrepancies between measurements exist:

1. Near 270 keV the data of Wasson (1) disagrees by up to 15% with that of Poenitz, Szabo et al. and Robertson et al. (2).
2. Data of Hanson et al. disagrees in shape between 1-2 MeV with that of Czirr and Sidhu, Poenitz, and Szabo et al. (2).
3. Data of Szabo et al. (2) are 3-5% lower than most other sets in the range 3-5 MeV.
4. Data of Hanson et al. appear to differ in energy scale from that of Czirr and Sidhu and Lengers et al. (2) in the region of the second chance fission threshold.

A series of measurements were carried out in an effort to resolve some of these problems. The shape of the ²³⁵U fission cross section was measured with high resolution between 200-300 keV by detecting prompt fission gamma rays with a large liquid scintillator. Absolute measurements were made between 0.2-8.2 MeV using an ionization chamber and a Black Neutron Detector (BNP) (3). Two ²³⁵U samples of ~ 200 gm/cm² thickness were used back to back. The mass determination was based on low-geometry alpha counting and a ²³⁴U half-life of 2.447×10^4 yrs. Three BND sizes were employed ranging from 40 x 40 cm to 6 x 5 cm. The ⁷Li(p,n) reaction was used below 4.5 MeV and the D(d,n) at higher energies. The results of the present measurements indicate that:

¹ The Fission Cross Section of Uranium and Plutonium Isotopes Relative to U-235, J. W. Meadows, NEANDC/NEACRP Specialists Meeting on Fast Neutron Fission Cross Sections of U-233, U-235, U-238 and Pu-239, June 28-30, 1976. ANL-76-90.

1. No structure is present in the cross section between 200-300 keV such as was reported by Wasson. Present results agree very well with previous results from this group and with those of Szabo et al. and Robertson et al.
2. Absolute cross section results below 1 MeV are 2-4% higher than proposed for ENDF/B-V by Bhat (2). The evaluation apparently was weighted by the Wasson results.
3. The present results support those of Szabo et al. between 3-5 MeV. The latter are 3-5% lower than reported by Czirr and Sidhu (normalized to the 14 MeV value of Cance (2)). The present results agree with those of Lengers et al. (2) if the latter are also normalized to the 14 MeV value of Cance.
4. The present results are consistent with those of Hanson et al. within the respective uncertainties however a shape difference between 1-2 MeV and an energy discrepancy near 6 MeV could not be ruled out.
5. The two different energy ranges (above 3 MeV and below 2.5 MeV) measured by Czirr and Sidhu appear to have a different normalization when compared with the present data and that of Szabo et al.

3. Neutron Total and Scattering Cross Sections of ${}^6\text{Li}$
(H. Knitter et al. (CBNM) and A. Smith et al. (ANL))

In a joint effort, total and scattering cross sections have been measured from ~ 0.1 to 4.0 MeV at intervals of ~ 20 keV throughout the energy range. Complimentary methods, samples and techniques have been employed. The maximum of the total cross section at the ~ 250 keV resonance exceeds 11 b. Inelastic scattering has been observed at the higher energies to be larger than given in ENDF/B-IV. The results are being finally corrected for a few percent ${}^7\text{Li}$ content and then will be interpreted in the context of the R-matrix.

4. Measured Fast Neutron Cross Sections of Titanium
(P. Guenther, D. Havel, A. Smith and J. Whalen)

Energy-averaged total neutron cross sections were measured from 1-5 MeV and differential elastic and inelastic scattering cross sections from

¹ Proc. of the NEANDC/NEACRP Specialists Meeting, ANL-76-90.

² See references of 1), above, and its supplement.

³ W. Poenitz, Nucl. Inst. Methods, 109 413 (1973).

1.5-4.0 MeV. Cross sections for the excitation of states at 159, 889, 983, 1430, 1550, 1820, 2009, 2295, 2421 and 2615 keV were obtained. The measured results are consistent with a model concept including vibrational collective excitations. The results will be published as ANL/NDM-24.

5. Fast Neutron Total and Scattering Cross Sections of Vanadium
(P. Guenther, A. Smith and J. Whalen (ANL))

Fast neutron total and elastic and inelastic scattering cross sections of elemental vanadium have been measured in the energy range 1-5 MeV. The experimental results and the associated interpretations are described in a manuscript accepted for publication in Nucl. Sci. and Eng.

6. Comparative Measurements of Fast Neutron Interactions with W-182, 184 and 186: (P. Guenther and A. Smith (ANL))

Total and scattering cross sections and $(n;n',\gamma)$ spectra were concurrently measured over the incident neutron energy range 1-4 MeV. The results clearly show the effects of collective rotational and vibrational excitations. The angular distributions of neutrons resulting from the excitation of the ground-state rotational bands are consistent with calculational results based upon the respective B_2 and B_4 deformations. Relative intensities of the de-excitation gamma-rays clearly trace the vibrational band heads across the three isotopes. The cross sections for the excitations of states above the ground-state rotational band appear to be qualitatively consistent with a statistical-reaction process. The results of this work will be published as a University of Illinois Thesis.

7. Measured and Calculated Neutron Scattering Near A=208 and $E_{in} = 0.8$ MeV: (A. Smith and P. Guenther (ANL))

The differential elastic neutron scattering cross sections of Pb-206, 207, 208 and Bi-209 were measured with relatively broad resolutions from 0.6 to 1.0 MeV. A model deduced from the energy-average of these results was extrapolated to U-238 with only the addition of deformation. Good descriptions of measured U-238 total and scattering cross sections in the few MeV range were achieved including new measurements at 1.5 MeV explicitly made for these comparisons. The implication of this model and the measurements is a total inelastic scattering cross section of U-238 in the MeV range considerably larger than commonly used in applications. Some of these results are available in ANL/NDM-22.

8. Average Fast-Neutron Total Cross Sections
(J. Whalen and A. Smith (ANL))

Precise (better than 1%) total neutron cross sections of a number of structural materials have been measured with broad resolutions (e.g. 150 keV) and varying sample thicknesses from \sim 1-5 MeV. In a number of instances (e.g. titanium) these pseudo-integral results are not consistent with higher resolution results to within large amounts (e.g. 10-20%). The discrepancies may be associated with the relatively very thick samples used in some of the

high resolution measurements involving fluctuating structure far more detailed than the experimental resolutions. These discrepancies are receiving further attention using both theory and experiment.

9. Fast Neutron Gamma-Ray Production from Elemental Iron: $E < 2$ MeV
(D. L. Smith)

Differential-cross-section excitation functions for fast-neutron gamma-ray production from iron have been obtained relative to the ^{235}U fission cross section at 50 keV intervals to 2 MeV with 50 keV incident resolutions. Gamma-ray angular distributions were obtained at 11 selected incident energies. These distributions required significant fourth-order Legendre Polynomial terms casting doubt upon the commonly employed measurement approximation of 4π times the ~ 55 (or 125) deg. cross section. The measured results are compared with previously reported data sets. Details of the work are reported in ANL/NDM-20.

10. Cross Sections for the $^{23}\text{Na}(n;n',\gamma)^{23}\text{Na}$ Reaction
(D. L. Smith)

Cross sections for production of the 0.439 MeV gamma-ray near 55 deg. by the $^{23}\text{Na}(n;n',\gamma)$ reaction have been measured relative to the ^{235}U fission cross section at 50 keV intervals from threshold to 2 MeV with resolutions of about 70 keV. Gamma-ray angular distributions were determined at selected energies in the measured range. The experimental results are compared with those in the literature and with the ENDF/B evaluated file. A report of the work has been submitted for publication in Nucl. Sci. and Eng.

11. $^{27}\text{Al}(n;n',\gamma)^{27}\text{Al}$ and $^{63,65}\text{Cu}(n;n',\gamma)^{63,65}\text{Cu}$ Reactions
(D. L. Smith)

Experimental data has been obtained for each of these reactions to several MeV. The results are now being analyzed.

12. Measurements of the $^{204}\text{Pb}(n;n',\gamma)^{204}\text{Pb}$ Reaction
(D. L. Smith (ANL) and G. C. Neilson et al. (Univ. of Alberta))

Prompt gamma-ray measurements have been made at both ANL and the University of Alberta using isotopically separated samples. The results are being analyzed.

B. CHARGED-PARTICLE REACTIONS

1. Cross Sections for Deuteron-Induced Reactions on ^6Li at Energies Below 1 MeV: (A. J. Elwyn, R. E. Holland, C. N. Davids, L. Meyer-Schützmeister, J. E. Monahan, and F. P. Mooring)

The preparation of a paper detailing the experimental techniques and the results obtained for all reaction channels in $d + ^6\text{Li}$ reactions at

energies between 0.1 and 1 MeV is in progress. Absolute total and differential cross sections for the outgoing protons in the ${}^6\text{Li}(d,p){}^7\text{Li}$ reaction, the alpha particles in the ${}^6\text{Li}(d,\alpha)\alpha$ reaction, and the neutrons in the ${}^6\text{Li}(d,n){}^7\text{Be}$ reaction have been determined to absolute accuracies of 9-15% for deuteron energies ~ 1 MeV. Such data is of importance to the evaluation of ${}^6\text{Li}$ -D as a possible fusion fuel, and at the same time can contribute to the understanding of the nuclear structure of light nuclei, the relative importance of underlying reaction mechanisms, and astrophysical investigations. Cross sections for the three-body breakup reactions $d + {}^6\text{Li} \rightarrow p + t + \alpha$ and $d + {}^6\text{Li} \rightarrow n + {}^3\text{He} + \alpha$ have also been investigated, and the results and interpretations in terms of various final-state interactions will be published separately.

2. Thermonuclear Reaction Rate Parameters for $d + {}^6\text{Li}$ Reactions
(A. J. Elwyn, J. E. Monahan, and F. J. D. Serduke)

A paper with the following abstract has been submitted for publication in Nucl. Sci. and Eng.:

"Thermonuclear reaction-rate and reactivity parameters calculated as a function of kT (for kT values from 1 to 1000 keV) are presented for all of the outgoing channels in nuclear reactions initiated by deuterons on ${}^6\text{Li}$. The results are based on recent experimental $d + {}^6\text{Li}$ reaction cross sections, and a newly derived cross section extrapolation expression."

3. Interference of Direct and Compound Nucleus Processes in ${}^6\text{Li}(d,p)$ and ${}^6\text{Li}(d,n)$ Reactions at Low Energy: (J. E. Monahan and A. J. Elwyn)

The angular distributions of the ground and first-excited state neutrons in the ${}^6\text{Li}(d,n){}^7\text{Be}$ reaction and the corresponding protons in the ${}^6\text{Li}(d,p){}^7\text{Li}$ reaction reflect qualitatively the effects of both compound nucleus and direct-reaction mechanisms in the deuteron energy region below 1 MeV. Traditionally, reactions of deuterons with light nuclei have been interpreted as an incoherent sum of a direct component (calculated e.g. by conventional DWBA methods) and a compound nucleus contribution estimated by use of statistical theories. In the present case, however, a statistical approach is probably unwarranted. Calculations based on a formalism in which the stripping component determined by a DWBA method is added coherently to an R-matrix description of the compound nucleus contribution that involves only a few nuclear levels are being performed. Preliminary results indicate that at least for deuteron energies below 500 keV, such calculations are in reasonable agreement with the data.

4. Elastic Scattering of Deuterons by ${}^6\text{Li}$ at Low Energies
(A. J. Elwyn, R. E. Holland, C. N. Davids, and L. Meyer-Schützmeister)

We have recently completed the measurement of the angular distributions of elastically-scattered deuterons by ${}^6\text{Li}$ from energies near 100 keV to 1 MeV. These results along with those from the recent experimental study of the other reaction channels constitutes a complete investigation of

d + ${}^6\text{Li}$ processes at low energies. Analysis of the data is in progress.

5. The ${}^6\text{Li}(p, {}^3\text{He})\alpha$ Reaction at Proton Energies Below 2 MeV
(A. J. Elwyn, R. E. Holland, C. N. Davids, and L. Meyer-Schützmeister)

Cross sections for reactions between the product nuclei in the primary d + ${}^6\text{Li}$ processes and the ${}^6\text{Li}$ -target material are important for a complete evaluation of d + ${}^6\text{Li}$ reactions for possible thermonuclear applications. We have recently completed the measurement of differential and total reaction cross sections for the ${}^6\text{Li}(p, {}^3\text{He})\alpha$ reaction at energies between 0.1 and 1.5 MeV. Analysis of the data is currently in progress. A study of the equally important ${}^6\text{Li}({}^3\text{He}, p){}^8\text{Be}$ reaction has been started.

C. PHOTO-NUCLEAR PHYSICS

1. ${}^{13}\text{C}$ Ground State Photoneutron Angular Distributions
(R. M. Laszewski, R. J. Holt, and H. E. Jackson)

Very high resolution measurements of the ground state photoneutron cross section for the ${}^{13}\text{C}(\gamma, n){}^{12}\text{C}$ reaction were made for excitations up to 9 MeV at laboratory angles of 90° and 135° using the sub-nanosecond time-of-flight spectrometer at the Argonne high-current linac. Ground state radiation widths for resonances at 7.7, 8.3, and 8.8 MeV were determined by an R-matrix analysis of the data.

2. Direct and Resonance Photoneutron Reactions of ${}^{17}\text{O}$
(R. M. Laszewski, R. J. Holt and H. E. Jackson)

The differential cross section for the ${}^{17}\text{O}(\gamma, n){}^{16}\text{O}$ reaction was measured with high resolution in the excitation energy range 4.5-7.1 MeV and at reaction angles of 90° and 135° . The unique high-current electron linac at Argonne permitted, for the first time, the direct observation of the non resonant component of the photoneutron cross section. The cross section at $\theta = 90^\circ$ is shown in Fig. 1. The dominant features of the excitation function in ${}^{17}\text{O}$ are the asymmetric resonance at $E_\gamma = 4.56$ MeV, the broad M1 excitation at 5.08 MeV, the dip in the cross section at 5.39 MeV and the relatively large non resonant cross section throughout the energy region. A preliminary R-matrix analysis of the data indicates that the background cross section is predominately $p_{3/2}$ in character. In addition, the reduced transition probability for the 5.08 MeV resonance was found to be $B(\text{M1}; 1d_{5/2} \rightarrow 1d_{3/2}) = 1.4 \mu_C^2$, only half the value expected for a pure single-particle transition.

3. Search for the Giant Magnetic Dipole Resonance in ${}^{119}\text{Sn}$
(R. J. Holt, R. M. Laszewski and H. E. Jackson)

The photoneutron cross section for the ${}^{119}\text{Sn}(\gamma, n){}^{118}\text{Sn}$ reaction was measured between 6.8 and 8.2 MeV. Qualitatively, the spectra exhibits a 400-keV wide peak centered at $E_\gamma = 7.6$ MeV. This corresponds roughly with

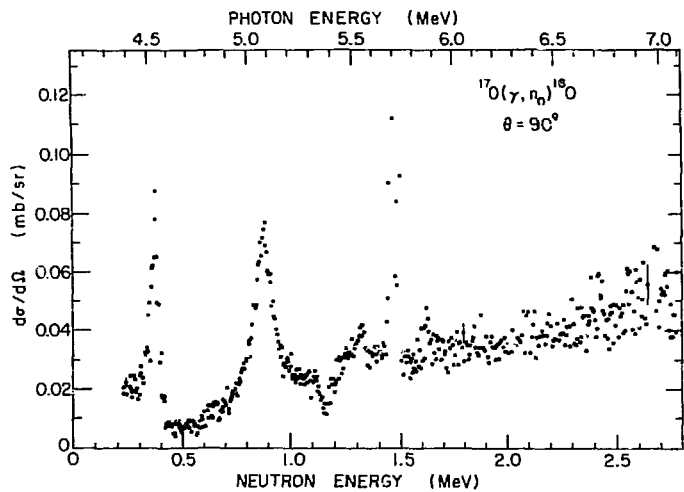


Figure -1. Cross section for the reaction $^{17}\text{O}(\gamma, n)^{16}\text{O}$ at 90 deg.

the resonance structure observed at 7.8 MeV by Winhold et al² at Harwell. The Harwell group suggested that this resonance structure might be the collective M1 resonance which results from $g_{9/2} \rightarrow g_{7/2}$ proton spin-flip transitions. In order to test the notion of an M1 transition in ^{119}Sn , the photoneutron polarization was measured between 7.4 and 7.85 MeV and at a reaction angle of 90° . The polarization vanishes if no M1 or E2 excitations exist in the energy region of interest. Preliminary analysis of the data indicate that the polarization is zero throughout this energy region, hence, the broad resonance structure at 7.6 MeV is predominately E1 in nature.

4. High Resolution Study of the $^{208}\text{Pb}(\gamma, n_0)^{207}\text{Pb}$ Reaction
(R. J. Holt, R. M. Laszewski and H. E. Jackson)

The angular distributions of photoneutrons emitted from resonances in ^{208}Pb were observed with very high resolution using the unique "picopulse" and sub-nanosecond time-of-flight spectrometer at the Argonne high-current electron linac. The photoneutron angular distributions were measured in the neutron energy range of 180 and 1000 keV and at reaction angles of 90° and 135° (see Fig. 2). These data, in conjunction with previous photoneutron polarization measurements, verify the large s-d wave admixtures discovered¹ in the outgoing neutron channels of the 180- and 254-keV resonances. The s-d-wave admixtures were deduced for eight resonances in this energy region. Ground-state radiation widths were extracted from the high-resolution measurements.

5. Evidence for Collective M1 strength in ^{208}Pb Between 8 and 10 MeV
(R. M. Laszewski, R. J. Holt, and H. E. Jackson)

Measurements of the polarization of photoneutrons from the $^{208}\text{Pb}(\gamma, n_0)^{207}\text{Pb}$ reaction were made at a laboratory angle of 90° for excitation energies between 8 and 10 MeV in order to investigate the distribution of M1 and E2 transition strength. Polarizations were determined by elastically scattering the photoneutrons from analyzing targets of ^{16}O and ^{12}C and energies were measured with high resolution (30 keV at $E_n = 1.0$ MeV) using the time-of-flight technique. In order to detect the individual resonances which contribute to the measured polarization, the yield of photoneutrons at 90° was observed with very high resolution (6 keV at 1.0 MeV). We were able to identify seven probable 1^+ resonances at excitations between 8.2 and 9.5 MeV. These resonances have a total strength $B(M1^+) \approx 8.5 \pm .5 \mu^2_0$.

¹ R. J. Holt, R. M. Laszewski and H. E. Jackson, Proceedings of International Conference on the Interactions of Neutrons with Nuclei, edited by E. Sheldon 1. 1278.

² E. J. Winhold, E. M. Bowey, D. B. Garner and B. H. Patrick, Phys. Lett. 32B, 607(1970).

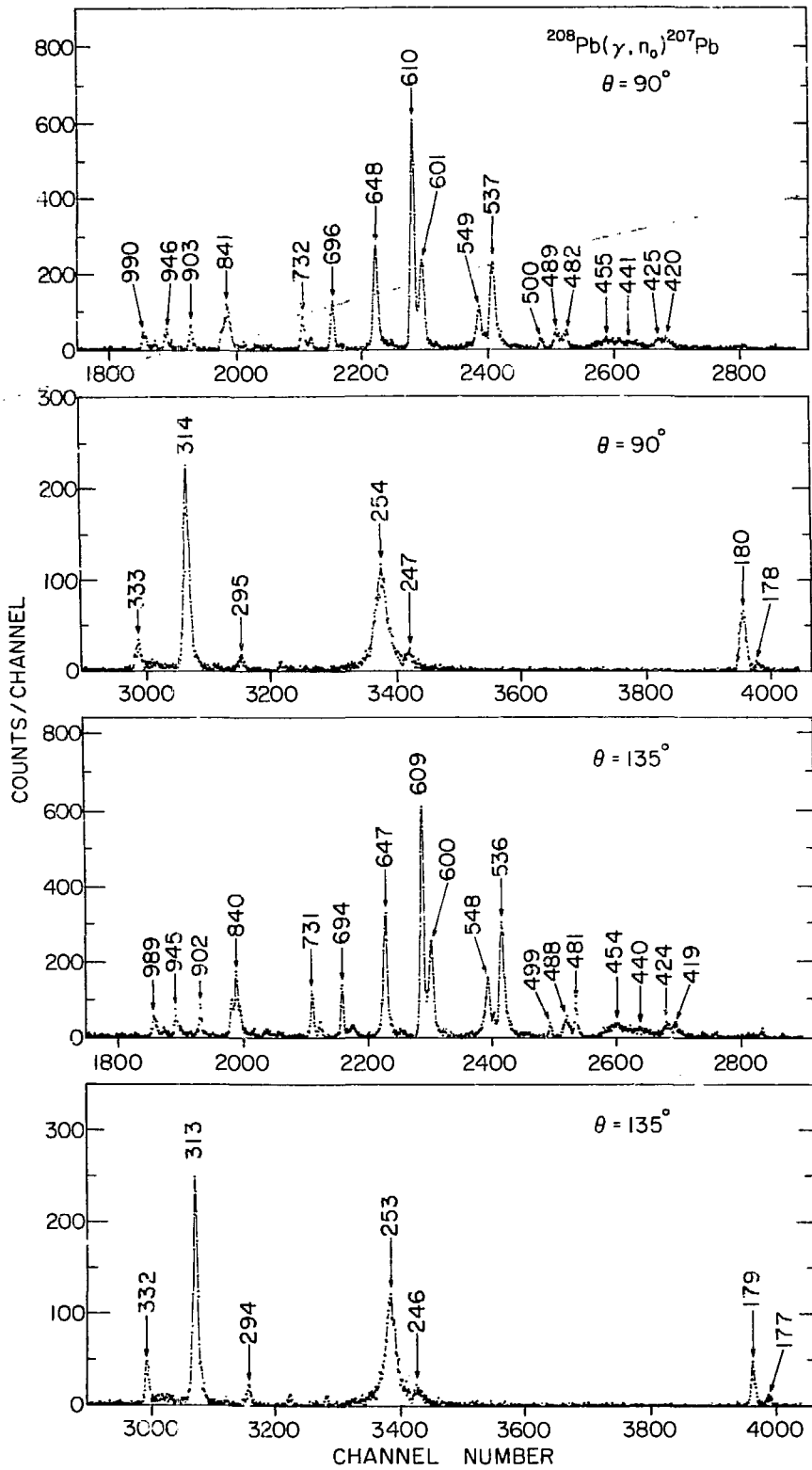


Figure -2. The $^{208}\text{Pb}(\gamma, n_0)^{207}\text{Pb}$ reaction at 90 deg.

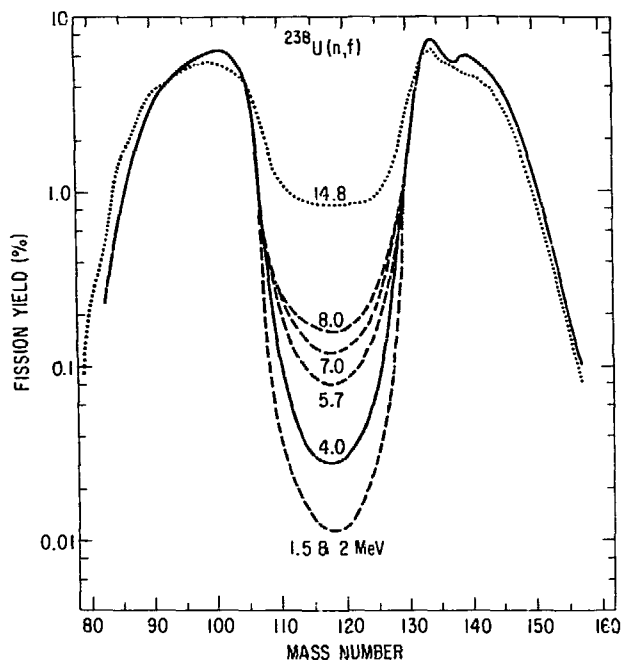


Figure 3. Mass distributions for neutron induced fission of ^{238}U .

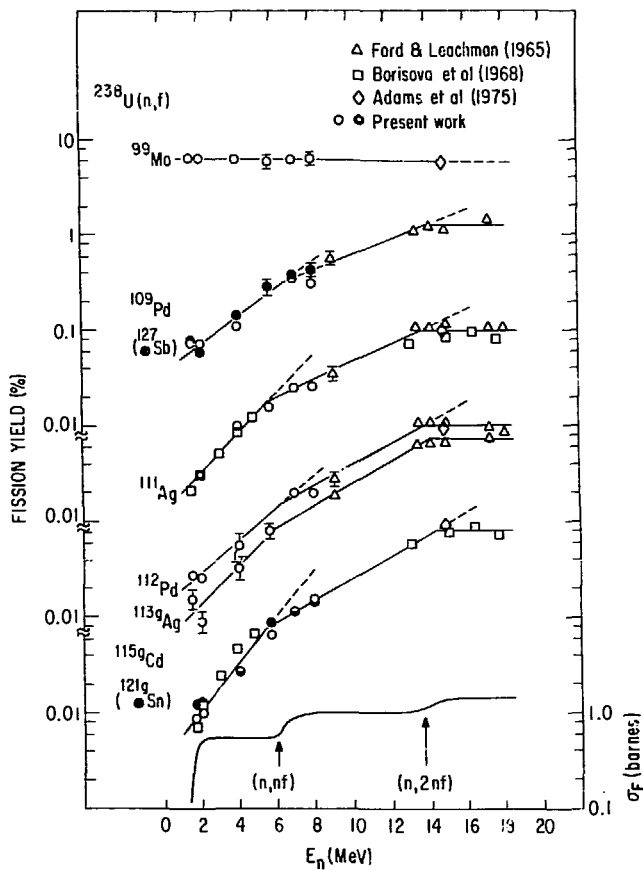


Figure 4. ^{238}U fission yields as function of incident neutron energy.

^{242}Cm is

87.71 ± 0.03 yr

Data for ^{239}Pu has been obtained by specific activity measurements

24126.5 ± 6.5 yr

and by mass spectrographic measurement (isotope dilution) of ^{235}U daughter

24140.5 ± 7 yrs

giving : average of 24133 ± 14 yrs.

Preliminary values (subject to recalculation) have been obtained by specific activity measurement for ^{240}Pu

6570 ± 6 yr

All errors indicated are one standard deviation.

E. FACILITIES AND TECHNIQUES

1. ANL Superconducting Linac

Basic Design

The linac consists of 14 independently-phased resonators of the split-ring type housed in 3 independent cryostats, as shown in the attached Fig. 5. The overall length of the system is 9.5 m and the active length is 4.7 m. It is expected that the system will have an accelerating potential of at least 14 MV and perhaps as high as 20 MV.

Status of Major Components

1. Building addition. Completed.
2. Buncher. Pretandem buncher is to be tested next week, and a complete bunching system will be tested several months thereafter.
3. Cryostat. Design completed. Section A is being fabricated, with completion expected in May 1977. Fabrication of sections C and D will start in April 1977.
4. Refrigeration. A helium refrigerator was ordered in January 1977. Design of a helium distribution system is in progress.
5. RF Controls. Design of resonator-control circuits is complete; fabrication has started and will be completed during 1977. The design of a computer-control system will start soon.

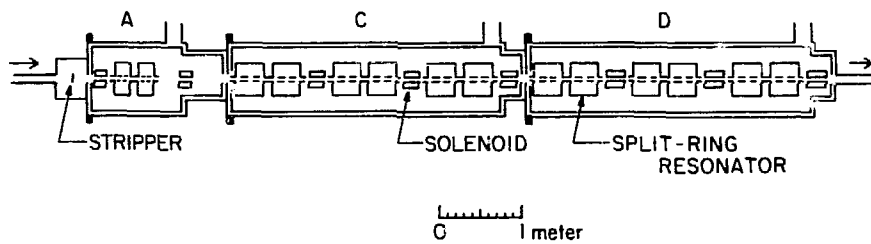


Figure 5. ANL superconducting linac.

6. Resonator. As reported previously, our all-niobium split-ring resonator operated well up to an accelerating field of 3.5 MV/m. On the basis of these good results, fabrication has been started on the inner components of 12 resonators.

In order to reduce fabrication costs and to improve mechanical properties of the resonator housing, we have developed a new fabrication technology in which the housing is made of niobium explosively bonded to copper. The first resonator made in this way is very successful in all respects except that the Q ($\sim 10^8$) is lower than desired. A series of tests aimed at identifying the source of the power loss is in progress and will be completed by ~ February 21.

Schedule

Major parts of the accelerator system will be assembled in late 1977.

It is expected that the first useful beam will be accelerated in April 1978.

2. Determination of the Energy Scale for Monoenergetic Accelerator Used as a Neutron Source: (J. W. Meadows)

Some problems in determining the energy calibration and energy resolution were investigated.¹ The effects of beam energy spread and straggling in thin absorbers were determined by calculation and measurement. The energy calibration was established by the $\text{Li-7}(p,n)\text{Be-7}$ and $\text{B-11}(p,n)\text{C-11}$ thresholds and a time-of-flight measurement. The location of the 2-MeV carbon resonance was determined to be 2078.2 ± 2.8 keV.

3. Calibration of the Neutron Response of Hydrogenous Scintillators (P. Guenther and A. Smith (ANL))

A simple method for the calibration of the neutron response of hydrogenous scintillators relative to the standard ^{252}Cf spectrum has been developed and put into routine application (see ANL/NDM-19 and 21). This development indicated that some structure observed in prompt fission neutron spectra can be attributed to air-attenuation effects.

F. EVALUATIONS AND SPECIAL MEETINGS

1. Evaluation of the $^{115}\text{In}(n;n')^{115\text{m}}\text{In}$ Reaction
(D. L. Smith)

An evaluation of the $^{115}\text{In}(n;n')^{115\text{m}}\text{In}$ reaction for the ENDF/B-V

¹ Determination of the Energy Scale for Neutron Cross Section Measurements Employing Monoenergetic Accelerators, J. W. Meadows, ANL/NDM-25.

dosimetry file has been completed. It is based entirely upon experimental data. The spectrum-averaged cross section in the standard neutron field resulting from ^{235}U fission was calculated from the evaluation and found in good agreement with the results of recent integral measurements. This work is described in ANL/NDM-26.

2. Elemental and Isotopic Titanium Evaluations
(C. Phylis et al. (Bruyeres-le-Chatel) and A. Smith et al. (ANL))

A collaborative effort is providing the elemental evaluated file for ENDF/B-V and selected isotopic files useful in dosimetry and gas-production applications. The (n;p) dosimetry file has been completed and published as ANL/NDM-27. The elemental file is nearing completion with particular attention to the resonance region and high-energy processes of fusion interest.

3. An Evaluated Neutronic File for Vanadium
(A. Smith et al. (ANL), F. Mann (HEDL) and R. Howerton (LLL)).

The file has been completed for ENDF/B-V and documentation will be published as ANL/NDM-24 (in press). The primary emphasis was on the improvement of the high-energy region of fusion interest.

4. U-238 Evaluation
(E. Pennington, W. Poenitz and A. Smith)

A draft version of the ENDF/B-V evaluation has been completed with particular emphasis on (n;gamma), (n;f) and (n;n') reactions. Detailed attention was given to both absolute and ratio results in consideration of the fission and capture processes following, insofar as possible, rigorous numerical evaluation procedures. Consideration of recent microscopic (n;n') results led to large increases in the total inelastic scattering cross section and major changes in the energy transfer elements. Preliminary calculations using ZPR-6 benchmarks were used in iterative adjustment procedures while retaining consistency with microscopic data. An improved description of some integral parameters (e.g. k_{eff}) was obtained relative to ENDF/B-IV. The evaluation and the integral ^{eff} calculations will be described at the forthcoming Annual ANS Meeting.

5. NEANDC/NEACRP Specialists Meeting on Fast Neutron Fission Cross Sections of ^{233}U , ^{235}U , ^{238}U and ^{239}Pu , (ANL-76-90)
(W. Poenitz, A. Smith (Eds.) and P. Guenther)

This Specialists Meeting was held at ANL, June 28-30 (1976). A keynote session dealt with basic theoretical fission concepts and applied needs (fast breeder). Two major technical sessions were devoted to fission-cross-section ratios and absolute-fission cross sections, respectively. A special topics session included discussions of evaluations, cross section averages, unresolved parameters and experimental techniques. Laboratory representation and contributions included LLL, ANL, KFK, ORNL, LASL, NBS, University of Michigan, CBNM, and Cadarache. Two working groups gave detailed consideration to the ratio and absolute problem areas and outlined their conclusions at the summary session. The basis of the working group

discussions was detailed graphical and numerical files assembled from the contributions and from the data-center files. Subsequent to the meeting the extensive graphical material was assembled into a large-scale compendium and issued as a supplement to the proceedings.

BATTELLE - PACIFIC NORTHWEST LABORATORIES

A. DELAYED NEUTRON STUDIES WITH AN ON-LINE MASS SPECTROMETER

1. Delayed Neutron Emission Probabilities (P. L. Reeder, J. F. Wright, and L. J. Alquist)

We have completed our measurements of delayed neutron emission probabilities for 16 isotopes of Br, Rb, I, and Cs and have submitted a paper to Physical Review C.¹ The results are given in Table A-1.

Table A-1. Delayed Neutron Emission Probabilities

<u>Nuclide</u>	<u>P_n</u>	<u>Nuclide</u>	<u>P_n</u>
⁸⁷ Br	2.5 ± .3	¹³⁷ I	8.5 ± .9
⁸⁸ Br	7.4 ± .5	¹³⁸ I	6.0 ± 3.5
⁸⁹ Br	16.9 ± 1.7	¹⁴¹ Cs	.043 ± .007
⁹² Rb	.012 ± .002	¹⁴² Cs	.096 ± .008
⁹³ Rb	1.86 ± .13	¹⁴³ Cs	1.95 ± .14
⁹⁴ Rb	13.7 ± 1.0	¹⁴⁴ Cs	4.3 ± .3
⁹⁵ Rb	11.0 ± .8	¹⁴⁵ Cs	21.8 ± 1.5
⁹⁶ Rb	17.0 ± 1.2		
⁹⁷ Rb	35.9 ± 2.6		

For precursors close to stability the present results are in agreement with other recent measurements, but for precursors farther from stability, the present results tend to be significantly higher.

2. Mean Energy of Delayed Neutrons (P. L. Reeder, J. F. Wright, and L. J. Alquist)

The mean energy of 16 delayed neutron precursors was determined from counting rate ratios of concentric rings of detectors embedded in a polyethylene moderator. The results have been given in a paper submitted to Physical Review C.² and are listed in Table A-2.

Table A-2. Mean Energy of Delayed Neutrons

<u>Nuclide</u>	<u>E_{av}</u>	<u>Nuclide</u>	<u>E_{av}</u>
⁸⁷ Br	.15 ± .01	¹³⁷ I	.53 ± .05
⁸⁸ Br	.33 ± .03	¹⁴¹ Cs	.24 ± .05
⁸⁹ Br	>.71	¹⁴² Cs	.24 ± .06
⁹² Rb	.18 ± .04	¹⁴³ Cs	.35 ± .01
⁹³ Rb	.56 ± .01	¹⁴⁴ Cs	.29 ± .02
⁹⁴ Rb	.57 ± .01	¹⁴⁵ Cs	.46 ± .03
⁹⁵ Rb	.53 ± .01	¹⁴⁶ Cs	.53 ± .07
⁹⁶ Rb	.56 ± .01		
⁹⁷ Rb	>.72		

3. Energy Spectra of Delayed Neutrons (P. L. Reeder and L. J. Alquist)

We have used a ^3He ionization chamber to measure a preliminary energy spectrum for ^{94}Rb . Structure similar to what was reported by Rudstam and Lund³ was observed. We are developing improved thermal neutron shielding, a pulse risetime discrimination system, and computer codes for unfolding the neutron spectra and will soon begin measurements on Rb and Cs precursors. If sufficient counting rates can be obtained, we will also measure spectra for Br, In, and I precursors. G.L. Woodruff and G.W. Eccleston from the University of Washington are planning to measure the delayed neutron energy spectra below 100 keV by use of a proton recoil detector simultaneously with our experiments.

4. Delayed Neutron Emission to Excited States of the Final Nucleus (P. L. Reeder and L. J. Alquist)

We have recently used a large Ge(Li) detector to measure gamma-ray spectra of Rb, In, and Cs delayed neutron precursors and their daughters. Many examples of gamma decay of excited levels of the final nuclide after neutron emission have been observed. From this so-called $\beta n \gamma$ decay process we expect to obtain partial delayed neutron emission probabilities to excited states of the final nuclide.

REFERENCES

1. Reeder, Wright, and Alquist, "Delayed Neutron Emission Probabilities of Separated Isotopes of Br, Rb, I, and Cs," BNWL-SA-5900 Rev. (December 1976).
2. Reeder, Wright, and Alquist, "Average Neutron Energies from Separated Delayed Neutron Precursors," BNWL-SA-5890 Rev. (December 1976).
3. G. Rudstam and E. Lund, "Energy Spectra of Delayed Neutrons from the Precursors ^{79}Zn , ^{80}Ga , ^{81}Ga , ^{94}Rb , ^{95}Rb , ^{129}In , and ^{130}In ," LF-77 (1976).

BROOKHAVEN NATIONAL LABORATORY

A. NEUTRON NUCLEAR PHYSICS

1. Implications of Failure of Porter-Thomas Statistics for Light Nuclides and Its Relevance to Nuclear Energy Programs
(R. E. Chrien and J. Kopecky*)

Applications of nuclear data to energy problems quite often assume the general validity of certain fundamental laws in order to draw conclusions for a specific application. A case in point is the use of the Porter-Thomas width distribution. Recently a paper by W. M. Wilson, H. E. Jackson, and G. E. Thomas** used the properties of this distribution as applied to radiative transitions to deduce certain limits on the size of the radiation width for the 2.8 keV resonance of ^{23}Na . One of the properties employed was the statistical independence (as measured by zero correlation) between widths of neighboring resonances. The relevance arises because of the presence of sodium as a coolant in fast reactors; hence its capture width is of interest. Furthermore the sodium resonance capture width can be used as a gauge to test the ability to measure Γ_γ when $\Gamma_n \gg \Gamma_\gamma$; such a test indicates a woeful deficiency in present techniques, since the measured width varies from 0.35 to 0.60 eV as reported in the literature.

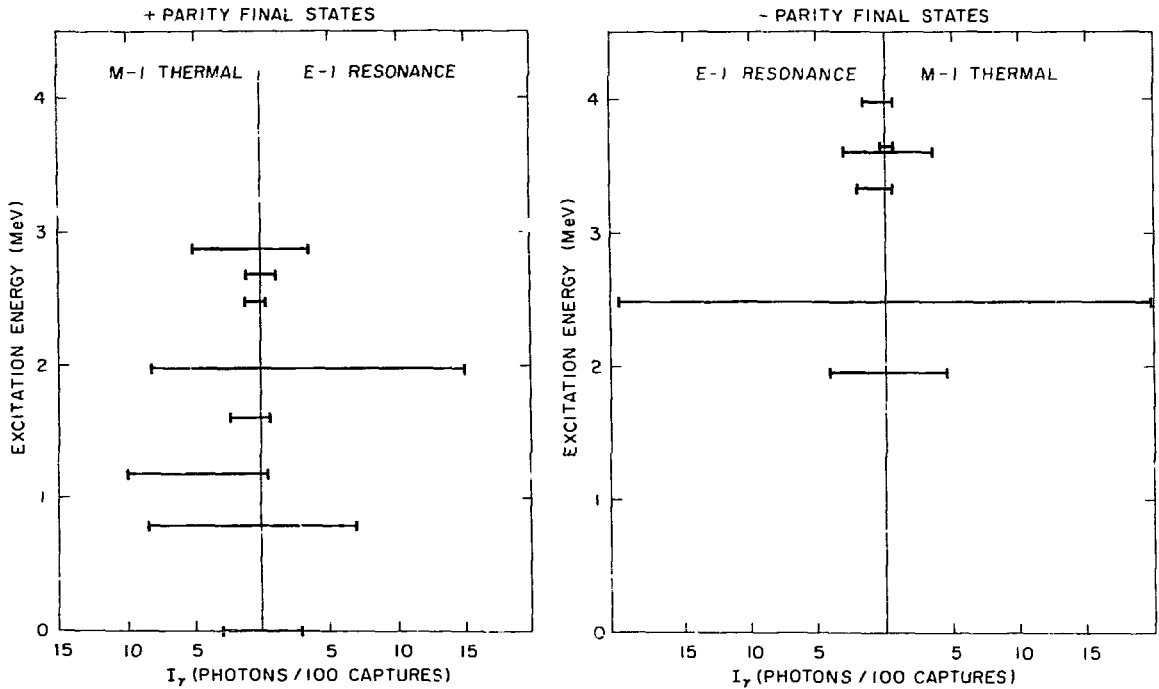
The point of this report is to note the drastic failure of Porter-Thomas statistics in a specific case, namely, $^{35}\text{Cl}(n,\gamma)^{36}\text{Cl}$, and thus to call into question its general validity, at least in light nuclides. We have measured the γ -ray spectrum from the first resonance of ^{35}Cl at 398 eV (presumably $\ell=1$, with $J=2$ or 3^-) and compared it to thermal capture in ^{35}Cl , which is dominated by a nearby 2^+ bound level. In ^{36}Cl there are 18 final states of known spin-parity below 4 MeV in excitation. The transitions to these states are shown in Figs. A-1 and A-2 for the positive and negative parity final states separately. There are two interesting aspects to these figures: 1) The spectral intensities are very similar; the correlation coefficient r between corresponding intensity pairs $\Gamma_{\gamma\lambda 1f}$ and $\Gamma_{\gamma\lambda 2f}$ is $+0.84^{+0.016}_{-0.010}$. This result is in sharp disagreement with the Porter-Thomas hypothesis. 2) E-1's at thermal transform into M-1's at resonance and vice versa. A very direct comparison between M-1 and E-1 strengths is thus possible. In disagreement with a single-particle estimate, the E-1 and M-1 strengths are about equal. This result can be understood on the basis of the giant dipole resonance taking away E-1 strength from the

* Visitor from FOM-ECN, Netherlands Energy Research Foundation, Nuclear Structure Group, Petten (NH)

** Submitted to Nuclear Science and Engineering, September 15, 1976.

5-8 MeV region, while not affecting the M-1 strength.

Thus for light nuclides, the assumption of statistical independence for neighboring resonances is questionable. This fact may make the interpretation of capture spectra for light nuclides much simpler, since it may well be valid that thermal neutron capture spectra may be representation of capture at higher energies (relevant to 74016, 62008, and many others).



Figures A-1 and A-2. Intensities for positive and negative parity final states fed by primary transitions from resonance and thermal capture (2^+) in ^{35}Cl . Note the change from E-1 ($2,3^-$) to M-1 and vice versa, governed by the capture state parity, and the equality of M-1 and E-1 strengths. The high resonance-resonance correlation is obvious.

2. Total Cross Sections of ^{45}Sc
(H. I. Liou, R. E. Chrien, K. Kobayashi (RPI), R. C. Block
(RPI))

Because of the existence of a minimum in the total neutron cross section of scandium near 2 keV, scandium has become widely used in transmission filters, especially at reactor installations. From experience at BNL and elsewhere it has become obvious that the fluxes obtained from these filters are much lower than estimates based on cross section measurements would predict. The cross section of Sc, especially near the 2 keV minimum, was remeasured using the electron linac at the Gaertner Laboratory of Rensselaer Polytechnic Institute. A value of 710 mb was obtained, in sharp contrast to a previously reported value of 50 mb! Extensive chemical checks on the sample revealed no significant impurities. R-matrix curve fitting of the cross section from 400 eV to about 10 keV has been completed, but fits are not satisfactory, as can be seen from Fig. A-3. The best fits are obtained assuming the J=3 channel spin dominates thermal neutron capture. This disagrees with polarized neutron measurements. Table A-1 shows the derived resonance parameters. Further measurements are underway to resolve the problem. (Request #69065)

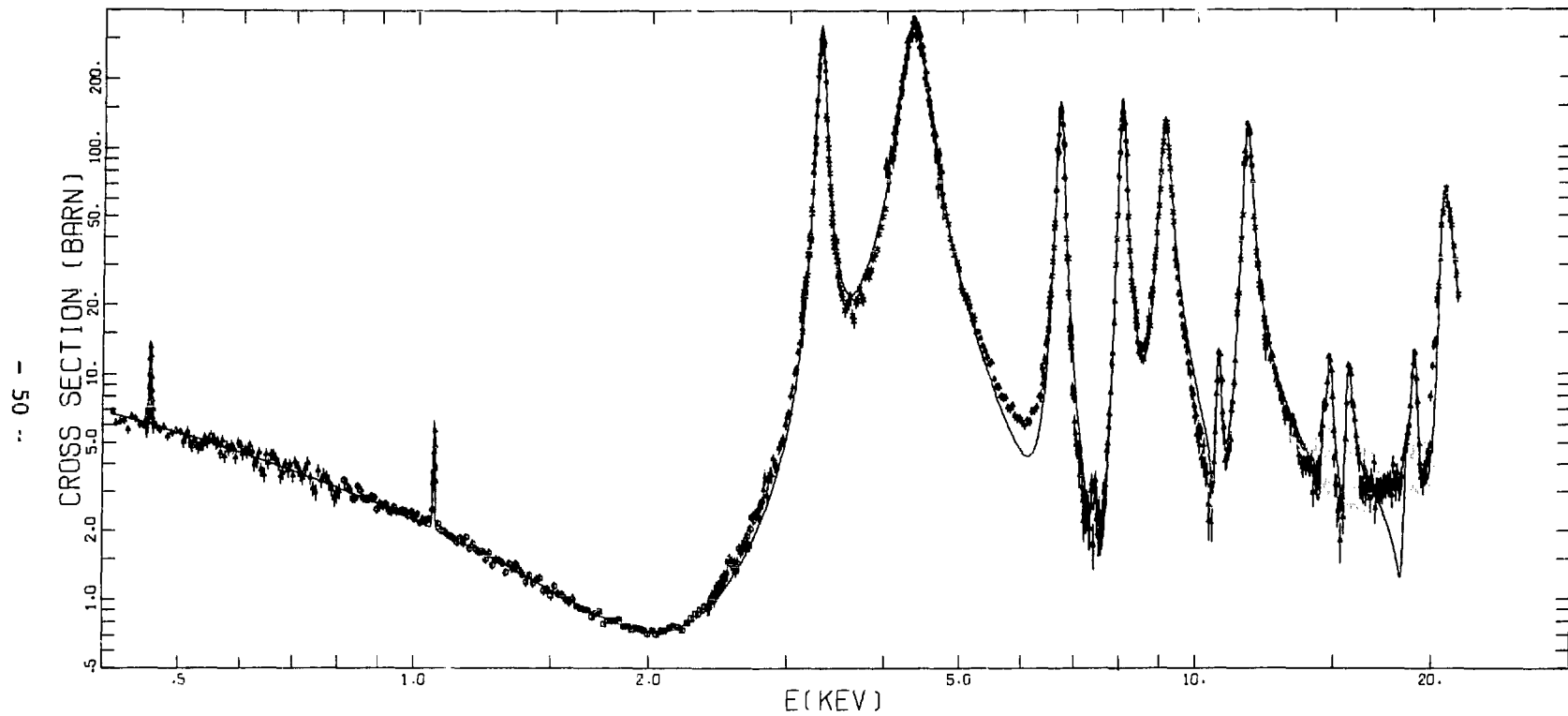


Figure A-3. The best fit scandium cross section up to 20 keV, assuming J=3 dominance at thermal.

Table 1

^{45}Sc

s-wave level parameters: $\gamma = 0.4 \text{ eV}$

E_0 (eV)	Γ_n (eV)	J	E_0 (eV)	Γ_n (eV)	J
-500	4.0 (Γ_n^0)	3	11575	290	4
-220	0.67 (Γ_n^0)	4	14525	20	3
3295	75	3	14740	26	4
4330	340	4	15560	28	4
6684	130	3	17850	5	3
8023	145	4	17880	32	3
9092	300	3	17870	62	4
10625	10	3	20300	80	4
10735	6	4	20300	710	3

p-wave level parameters

E_0 (eV)	$g\Gamma_n$ (eV)
460.6	0.0022
1060.4	0.0050
7377.0	0.4
7458.0	0.4
7548.0	0.25

Resonance parameters for ^{45}Sc derived from shape fits to the total cross section.

3. The Neutron Cross Sections of ^{56}Fe near 24.3 keV
(R. E. Chrien, H. I. Liou, U. Singh (RPI), R. Block (RPI))

Deep penetration of neutrons through iron has long been an interest of shielding engineers, since iron is a common structural and shielding material around neutron sources such as reactors or accelerators. Iron has also been used as a transmission filter to produce quasi-monoenergetic reactor beams at keV energies. The existence of a unique sample of ^{56}Fe --some 27-inches long--enabled us to measure the important cross section minimum near 24.3 keV with considerable accuracy. The measurement was performed with the RPI linac. A preliminary value for the minimum cross section of 57 mb has been obtained. This compares with a value of 420 mb for natural iron. Analysis of this experiment is in progress. (Request #69012, 74049)

4. Nuclear Structure Studies with the (n,γ) Reaction
(B. K. S. Koene and R. E. Chrien)

Levels for N=79

Nuclides near closed shells are of considerable interest theoretically because they are amenable to relatively straightforward model calculations. The Alaga-Paar model, known as the cluster-vibrational model, has had some success in predicting the behavior of such systems. We have attempted to test the model in the case of N=79, or 3 holes in the N=82 shell. The nuclides studied in this program have been ^{131}Te , ^{135}Ba , and ^{137}Ce . Measurements with the chopper time-of-flight facility, and with filtered beams were performed. A large number of low-lying levels were observed, and spin and parities determined. In combining the present data with data from charged particle transfer reactions, and with decay data, fairly complete level schemes were established below an excitation energy of ~ 2 MeV.

These level schemes, with that of ^{133}Xe (obtained from nuclear orientation studies) are well described by the model. The strength of the particle-vibrational interaction shows a gradual increase with mass number.

In the course of these experiments, a rather striking case of direct (potential) capture was uncovered for $^{130}\text{Te}(n,\gamma)^{131}\text{Te}$. The results show a marked correlation between (n,γ) and (d,p) levels of the $\ell=1$ type. The correlation coefficient exceeds 99% for the E^1 energy dependence suggested by potential capture.

5. Actinide Level Schemes

(R. E. Chrien, B. K. S. Koene, J. A. Cizewski, R. F. Casten
W. R. Kane, G. J. Smith, M. L. Stelts (BNL); R. C. Greenwood
(INEL, Idaho); P. Jeuch†; T. von Egidy (RILL, Grenoble);
R. C. Block (RPI); J. Kopecky (ECN); S. Malik (Univ. of Rhode
Island); D. Breitig (Technical Univ. of Munich))

a. Levels in ^{231}Th

The $^{230}\text{Th}(n,\gamma)^{231}\text{Th}$ reaction has been investigated for the capture of neutrons in the 1.427 eV resonance of ^{230}Th . Resonance energy neutrons were provided by a neutron monochromator at the BNL High Flux Beam Reactor. Interference from the decay of 8×10^4 year ^{230}Th was minimized with the use of a very small (50 mg) target, which was sufficient for the experiment because of the very high resonance capture cross section. High resolution spectra of primary and secondary capture gamma rays were obtained with Ge(Li) detectors. Low spin states of ^{231}Th have been identified up to an excitation of ~ 1 MeV. Results obtained on Nilsson levels of ^{231}Th will be compared with those obtained from charged particle transfer reactions and ^{235}U α decay.

b. Levels in ^{233}Th

The results of 2- and 24-keV capture spectra are being combined with data from the (n,e^-) reaction and from highly precise low energy γ -ray data from the Reactor Institute Laue-Langevin. A rather definitive level scheme is in preparation.

c. Low Spin States in ^{235}U

Primary γ rays following neutron capture in ^{234}U at the 5.9 eV, 31.9 eV and 48.8 eV resonances have been studied with the Fast Chopper at the Brookhaven High Flux Beam Reactor. Levels in ^{235}U were identified to an excitation energy of 2.2 MeV. For most of the primary transitions it was possible to distinguish between E1 and M1 multipolarity on the basis of their absolute widths at the different neutron energies. Data from previous thermal-capture work were included in this analysis. The resulting spin-parity restrictions for levels of ^{235}U differ in some instances with earlier rotational-band assignments from charged-particle reactions and thermal neutron capture.

† On leave from RILL, Grenoble.

d. Levels in ^{237}U

Most of the analysis of the $^{236}\text{U}(n,\gamma)^{237}\text{U}$ reaction on the 5.45 eV resonance has been completed and a tentative level scheme up to 1 MeV proposed. γ - γ coincidence experiments are planned as well as conversion electron studies to complement the (n, γ) work. Many of the low-lying levels have been identified as to their Nilsson quantum numbers or as low-lying phonon excitations. A number of problems remain in that low-lying phonon excitations complicate the structure of many states and frequently this will fragment the Nilsson strength into several components. The planned coincidence and electron studies will help resolve these problems.

e. Levels in ^{239}U

Several techniques involving neutron capture were used to study the level structure of ^{239}U . Most recently, these include the study of degree of circular polarization of γ rays emitted following polarized neutron capture (at the Dutch High Flux Reactor, Petten), γ - γ coincidence measurements, and spectra from keV neutron capture. A major revision in the previously accepted decay scheme--the interchange in the spin assignments of the 739 and 746 keV levels--has been made. The polarization data also reveal a closely-spaced doublet in the transition near 3983, a doublet which had been undetected even in the highest resolution primary (n, γ) work. A definitive level scheme is in preparation. Spin assignments made on the basis of these experiments are shown in Table A-2.

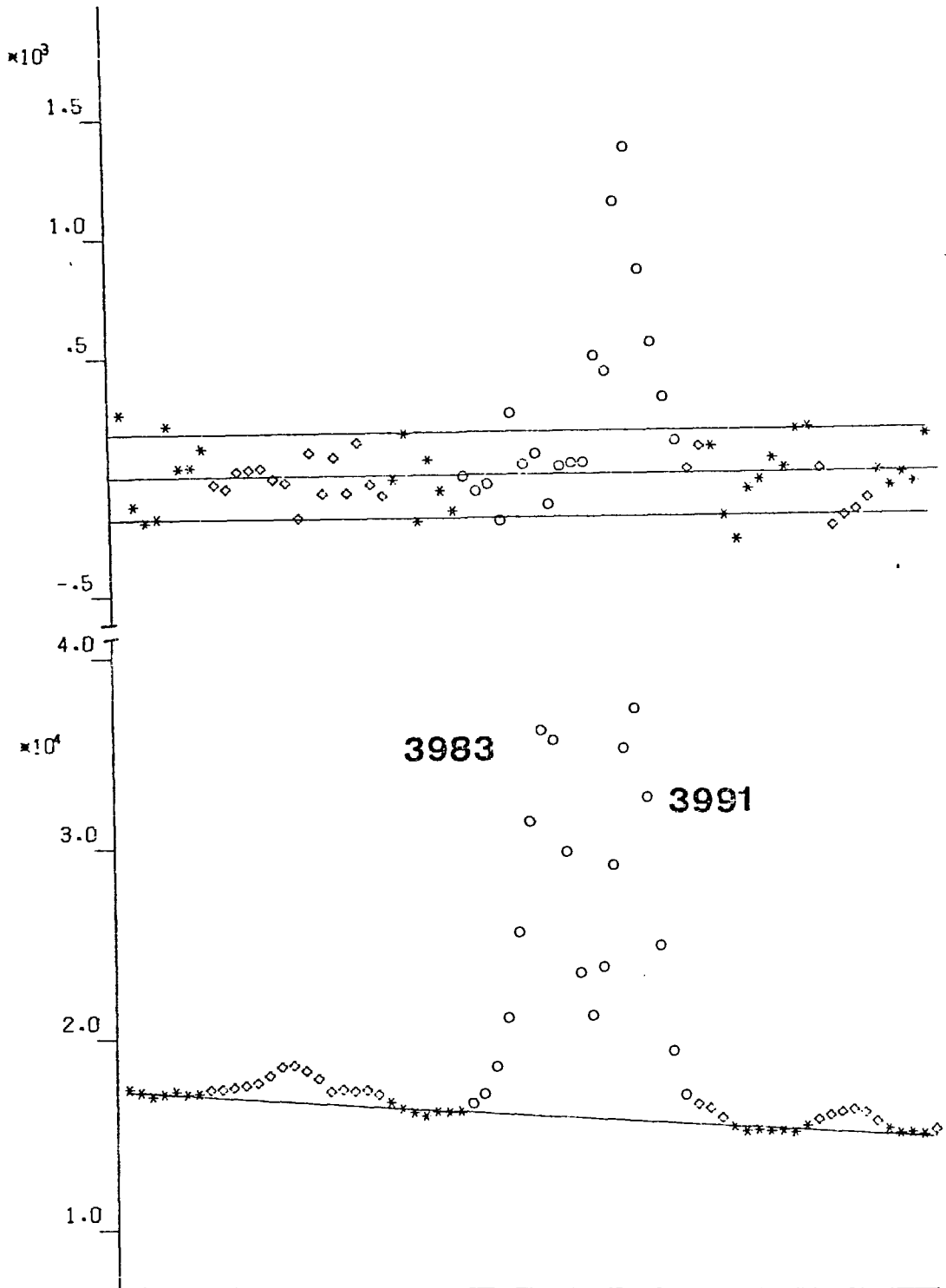


Figure A-4. The singles spectrum (below) and polarization difference signal $N_+ - N_-$ (above) for the 3.9 MeV doublet for thermal capture by ^{238}U . The lack of a negative difference signal for the 3983 transition, which is presumed to feed a $3/2^-$ final state, is strong evidence for a doublet at 824 keV.

Table A-2

E_x (keV)	Previous	Present Experiment
739.2	$3/2^-$	$1/2^-$
745.9	$1/2^-$	$3/2^-$
932.5	n^-	$3/2^-$
961.9	n^-	$3/2^-$
988.5	m^+	$5/2^+$
1025	m^+	$5/2^+, 3/2^+$
1066.6	n^+	$3/2^+$
1152.5	\bar{m}^+	$5/2^+$
1223.3	n^-	$3/2^-$
1237.7	m^+	$5/2^+$
1361.0	$n(-)$	$3/2^-$
1416.9	m^+	$5/2^+$
1509.9	n^-	$3/2^-$

Spin assignments based on the results of circular polarization and γ - γ coincidences for levels in ^{239}U . The states labeled n and m are derived from the experiment of Bollinger et al. (Phys. Rev. C6, 1332 (1972)). The n refers to (1/2 or 3/2); m refers to (1/2, 3/2, or 5/2).

f. Levels in Odd-mass Plutonium Isotopes

Using mostly time-of-flight techniques for resonant capture data have been obtained for capture on ^{240}Pu , ^{242}Pu , and ^{244}Pu leading to levels in ^{241}Pu , ^{243}Pu , and ^{245}Pu . For the latter case, some 14 primary γ -ray lines were observed in resonance capture for a relatively small (~ 1 gm) sample.

The work summarized in 5, a-f above, when complete, will provide a systematic survey for low-spin states and Nilsson orbitals throughout the mass region from A=231 to A=245.

6. Neutron Beam Filters

(R. C. Greenwood (INEL, Idaho) and R. E. Chrien (BNL))

The properties of neutron transmission filters using scandium and iron in combination with other materials have been studied at the HFBR with the aid of several hydrogen-filled proportional recoil counters. The object was to determine the optimum combination of filter materials to enhance the principal beam component (2 keV for scandium and 24 keV for iron) and suppress the transmission through other, higher energy, windows. Optimum combinations proved to be Sc + Ti + Co at 2 keV, and Fe + Al + S at 24 keV. The characteristics of these beams were established with the recoil counter measurements and with γ -sensitive and thermal-neutron sensitive instruments. The results are being checked for consistency against recent total cross section measurements on the filter materials.

7. A Pair Spectrometer for Primary Capture γ -ray Measurements at HFBR

(M. L. Stelts, R. E. Chrien (BNL); P. Ryge*)

A three-crystal pair spectrometer (Ge(Li)-NaI) has been developed for use with the "filtered" neutron beams¹ at the Brookhaven High Flux Beam Reactor. The Ge(Li) diode is a 55-mm diameter by 20-mm thick disc with the γ rays incident on the edge. The peak to continuum ratio exceeds 40:1 at 6 MeV γ -ray energy with a system resolution of 4.5 keV. Used with neutron beams of broad enough energy to average over sufficient capture states to reduce the statistical fluctuations in the partial radiation widths, it is possible to locate all levels of a given band of spin and parity to much higher excitations than has been previously possible. In a study of the $^{182}\text{W}(n,\gamma)$ reaction, 45 states of spin (1/2, 3/2) in ^{183}W were found below 2100 keV excitation, compared with 18 levels found in the most recent work on this nucleus.²

* Princeton Gamma Tech., Princeton, New Jersey.

¹ R.C. Greenwood and R.E. Chrien, Nucl. Instr. and Meth. 138, 125 (1976).

² R.F. Casten and W.R. Kane, Phys. Rev. C7, 419 (1973).

8. Two-keV Average Resonance Neutron Capture Gamma-Ray Population of Levels in ^{166}Ho
(D. A. McClure (Georgia Tech.); M. L. Stelts, R. E. Chrien)

A scandium filtered neutron beam from the High Flux Beam Reactor at Brookhaven, characterized by a flux of $\sim 3 \times 10^7$ n/cm².sec, a full width at half maximum of ~ 0.9 keV and a centroid energy of ~ 2 keV¹ was employed to produce an average resonance neutron-capture gamma-ray spectrum of transitions in ^{166}Ho . This study supports the assignment² of the spin and parity of the 430-keV level as 2^+ and is in disagreement with a recent polarized-neutron capture study³ in which a level at 430-keV excitation energy was assigned spin and parity 4^+ . In addition, approximately 80 other primary transitions were observed and the resulting spin and parity assignments made.

9. Systematic Studies of Low-Spin States in Odd-Er Isotopes from 2- and 24-keV Neutron Capture Reactions
(R. C. Greenwood (INEL, Idaho) and R. E. Chrien)

The primary γ rays emitted as a result of 2- and 24-keV neutron capture in targets consisting of enriched ^{164}Er , ^{166}Er , ^{168}Er and ^{170}Er isotopes have been measured using the filtered neutron beam facility at the HFBR. For each of these isotopes the γ -ray spectra were the result of summing over sufficient compound-nucleus resonance states to average out, to a considerable degree, the large fluctuations (Porter-Thomas) in the primary γ -ray intensities. Thus, we can expect that the primary transitions to all final states with spin values $1/2$ or $3/2$, up to an excitation energy of ~ 2 MeV, are observed in these spectra. Further, in the case of the lighter Er isotopes, the degree of averaging is sufficient to discriminate, on the basis of γ -ray intensities, between transitions having E1 and M1 multipolarities. The results of this work are compared to those obtained in earlier studies of nuclear decay (n,γ) and charged-particle reactions.

¹ R. C. Greenwood and R. E. Chrien, BNL-21582.

² L. M. Bollinger and G. E. Thomas, Phys. Rev. C₂, 1951 (1970).

³ J. J. Bosman, P.P.J. Delhey and H. Postma, Neutron Capture Gamma-Ray Spectroscopy, ed. K. Abrahams (Energy Centrum Nederland, Petten, The Netherlands, c. 1975) 638.

10. Level Schemes of ^{193}Pt and ^{196}Pt

(J. A. Cizewski*, G. J. Smith, M. L. Stelts, R. F. Casten, W. R. Kane, and R. E. Chrien)

The $^{192}\text{Pt}(n,\gamma)^{193}\text{Pt}$ reaction has been investigated at thermal energies at the BNL High Flux Beam Reactor. High resolution spectra of primary and secondary gamma rays were recorded with Ge(Li) detectors. Low spin states of the transitional nucleus ^{193}Pt have been identified up to an excitation of ~ 1 MeV. The structure of ^{193}Pt is compared to that of neighboring transitional nuclei.

The $^{195}\text{Pt}(n,\gamma)^{196}\text{Pt}$ reaction has been investigated using the 2 keV neutron beam at the Brookhaven High Flux Beam Reactor. High resolution spectra of primary and secondary γ rays were recorded. Since the 2 keV neutron beam is fairly broad in energy, the capture process is spread over ~ 40 levels in ^{196}Pt . For 0^- , 1^- capture states, this is sufficient averaging of the Porter-Thomas statistical fluctuations to guarantee primary transitions to all 0^+ , 1^+ , 2^+ states up to ~ 3 MeV in excitation. In particular, about 8 levels below 2 MeV in excitation have been observed, which were not seen in an earlier resonance capture study. Usually a more stringent spin limit can be placed on the final state by studying the secondary transitions. The information from this study will be combined with an earlier investigation of the excited 0^+ states in ^{196}Pt .¹ Results are compared to the current theoretical models for this region of changing deformation.

11. Accurate Transition Probabilities from Resonance Capture

(H. I. Liou, C. M. McCullagh*, R. E. Chrien)

In principle, the measurement of resonance partial widths is the only way to obtain accurate photon strength function data from (n,γ) experiments. In fact the lack of accurate normalizations has been the chief difficulty in past work, which abounds in inaccurate and conflicting values for both E-1 and M-1 radiative strengths. Using the accurately measured $^{197}\text{Au}(n,\gamma)^{198}\text{Au}$ transition intensities, and a comparison method originally developed by R. T. Carpenter at Argonne National Laboratory, values for transition intensities (photons/capture) for a number of targets, including $^{161,162,168,170}\text{Er}$, ^{105}Pd , ^{240}Pu , ^{236}U , ^{234}U , and $^{158,160}\text{Gd}$ were established. The technique is now routinely used for all samples run with the chopper, and will play an important part in re-interpreting older photon strength function experiments.

* Student from SUNY-Stony Brook, New York.

¹ J. A. Cizewski et al. BAPS 21, 558 (1976).

12. Fragmentation of Nilsson Model States in the Hf-Os Region
(R. F. Gasten; R. C. Greenwood (INEL, Idaho); M. R. Macphail
(Manchester); R. E. Chrien, W. R. Kane, G. J. Smith,
J. A. Cizewski)

As a continuation of a broad study of the breakdown of the Nilsson model at high excitation energies (0.5-2.5 MeV) in the Hf-Os region, the $^{190}\text{Os}(n,\gamma)^{191}\text{Os}$ reaction was studied at thermal and 2 keV neutron energies. The experiment was directed toward disclosing all the $1/2^-$ and $3/2^-$ states below about 1700 keV. The use of the average resonance capture technique at 2 keV is ideally suited to such a study since the averaging process for the primary transition intensities essentially guarantees the finding of all such states below some upper limit of excitation energy (here ~ 1700 keV).

The results were analyzed together with existing data from the (d,p) reaction. As expected, extensive fragmentation of the Nilsson states was observed and the systematics previously developed for Hf and W was extended. An attempt was made to continue the interpretation in terms of large and varying hexadecapole moments. In ^{191}Os , analysis showed evidence for a group of positive parity levels which originate in the next higher shell. (This is the most conclusive evidence yet obtained for these states in this mass region.) Their occurrence at low energies, however, is surprising since they are expected to rise in energy as the quadrupole deformation decreases. However, if the hexadecapole deformation also decreases this provides a significant lowering in energy for these states.

Though it is necessary to perform complex coupled channel calculations with quasiparticle-phonon and other interactions to hope to explain the fragmentation systematics in any detail, the series of studies of Hf, W, and Os show that many of the trends in these systematics can be simulated by a simple model in which the hexadecapole deformation (ϵ_4) grows very large in going from ^{179}Hf to $^{183,184}\text{W}$ and then begins to drop in ^{187}W and ^{191}Os , presumably decreasing towards very small values near the Pb nuclei. It is suggested that any future, sophisticated calculations should incorporate such large ϵ_4 deformations in attempting to test this region. Only with such calculations can our simple interpretation be tested as to whether it merely reproduces empirical trends originating in some complex interactions.

Publications:

Casten, R. F., Burke, D., and Hansen, Ole. The $^{180,182}\text{W}$ (t,p) reactions at 15 MeV. Nucl. Phys. A261, 445-452 (1976).

Casten, R. F. et al. States in ^{243}Pu from the (n, γ), (d,p), and (d,t) reactions. Phys. Rev. C14, 912-932 (1976).

Casten, R. F. et al. Study of ^{191}Os by average resonance neutron capture; fragmentation of Nilsson model strength. Nucl. Phys. (submitted).

Chrien, R. E. The failure of the statistical hypothesis for compound nuclear decay. Presented at the Ninth Summer School on Nuclear Physics, "Study of Nuclear Structure by Means of Nuclear Reactions," Mikolajki, Poland, August 30-September 11, 1976.

Chrien, R. E. Monograph on neutron detectors (proposed).

Chrien, R. E. Proceedings of 3rd International Symposium on Neutron Capture γ -Ray Spectroscopy and Related Topics, Brookhaven National Laboratory, Upton, New York, September 18-22, 1978, (proposed).

Chrien, R. E. et al. The failure of the Bohr's compound nucleus hypothesis for the $^{98}\text{Mo}(n,\gamma)^{99}\text{Mo}$ reaction. Phys. Rev. C13, 578-594 (1976).

Chrien, R. E. and Greenwood, R. C. The ^{125}Te (n, γ) reaction at 2 and 24 keV. Proc. 1976 International Conference on the Interaction of Neutrons with Nuclei, Lowell, Mass., July 6-9, 1976, p. 1297.

Chrien, R. E. and Kane, W. R. Nuclear physics at the BNL High Flux Beam Reactor. Proc. 1976 International Conference on the Interaction of Neutrons with Nuclei, Lowell, Mass., July 6-9, 1976, p. 1272.

Chrien, R. E. et al. Population of levels in ^{88}Sr and ^{89}Sr by s- and p-wave neutron capture. Bull. Am. Phys. Soc. II, 21, 536 (1976).

Chrien, R. E., Liou, H. I., and Kopecky, J. Neutron capture in ^{238}U . Proc. 1976 International Conference on the Interaction of Neutrons with Nuclei, Lowell, Mass., July 6-9, 1976, p. 1298.

Cizewski, J. et al. Study of ^{237}U via the (n, γ) reaction. Bull. Am. Phys. Soc. II, 21, 1009 (1976).

Cizewski, J. et al. Low spin states in ^{196}Pt . Bull. Am. Phys. Soc. II, 21, 558 (1976).

Garg, J. B. et al. Resonance neutron capture γ rays from ^{168}Er . Phys. Rev. C13, 1139-1144 (1976).

Gelletly, W., Kane, W. R., and Casten, R. F. Thermal neutron capture on ^{142}Ce . Phys. Rev. C13, 1434-1445 (1976).

Publications: (Cont'd.)

Greenwood, R. C. and Chrien, R. E. Filtered reactor beams for fast neutron capture γ -ray experiments. Nucl. Instr. & Meth. 138, 125-143 (1976).

Greenwood, R. C. and Chrien, R. E. The 2-keV neutron beam facility at HFBR. Bull. Am. Phys. Soc. II, 21, 610 (1976).

Greenwood, R. C., Chrien, R. E., and McCullagh, C. M. Level structure of ^{126}Te . Bull. Am. Phys. Soc. II, 21, 1009 (1976).

Kane, W. R. et al. A new neutron resonance in ^{124}Xe . Bull. Am. Phys. Soc. II, 21, 536 (1976).

Koene, B. K. S. and Chrien, R. E. Low spin states in ^{235}U studied with the (n,γ) reaction. Phys. Rev. (submitted).

Koene, B. K. S. and Chrien, R. E. Low spin states in ^{135}Ba studied with the (n,γ) reaction. Bull. Am. Phys. Soc. II, 21, 1009 (1976).

Koene, B. K. S. et al. Gamma-ray spectroscopy from $^{164}\text{Er}(n,\gamma)^{165}\text{Er}$ at resonance and at 20- and 24-keV neutron energies. Bull. Am. Phys. Soc. II, 21, 658 (1976).

Koene, B. K. S., Liou, H. I., and Chrien, R. E. Primary γ -transitions in ^{235}U from resonance capture. Proc. 1976 International Conference on the Interaction of Neutrons with Nuclei, Lowell, Mass., July 6-9, 1976, p. 1262.

Kopecky, J. et al. The $^{87,88}\text{Sr}(n,\gamma)$ reactions at 2 and 24 keV. Proc. 1976 International Conference on the Interaction of Neutrons with Nuclei, Lowell, Mass., July 6-9, 1976, p. 1287.

Liou, H. I. and Chrien, R. E. Epithermal neutron capture in ^{238}U . Nucl. Science and Engineering (in press).

Rimawi, K. and Chrien, R. E. 24 keV neutron capture studies in Mo isotopes. Phys. Rev. (in press).

B. NATIONAL NEUTRON CROSS SECTION CENTER

1. Data Libraries

NNCSC's role as a data center was expanded in the past year to include responsibility for compilation and evaluation of charged particle reaction and nuclear structure data. In addition, NNCSC has continued its activities in the neutron data area.

During the past year, NNCSC has continued to cover the neutron related literature for CINDA. Data from approximately 110 neutron experiments has been compiled and added to the CSISRS experimental data library. Numerous other set of experimental data compiled by our sister centers at Saclay, Vienna and Obninsk have also been added.

Work continues in preparation for ENDF/B-V. All the checking and processing codes maintained by NNCSC have been upgraded to include new formats and additional tests. A preliminary file of data for the actinides has been assembled and is now being tested by Cross Section Evaluation Working Group (CSEWG) members.

The new edition of BNL-325 Vol. II was distributed in July 1976. A handbook for radioactivity derived from the ENDF/B-IV fission product data files is now in press. Planning for the 4th Edition of BNL-325 Vol. I, Resonance parameters has been started. Proposed additions to the book have been circulated for comments and specifications for physics checking programs have been drawn up. Request have also been sent for latest experimental data with a cut-off date of June '77.

A new activity in charged particle nuclear data has been started. A bibliography of integral charged particle nuclear data has prepared covering the literature published after termination of the work of the Charged Particle Data Group at ORNL. A publication will be made in the next few months. Experimental data compiled at Karlsruhe and Kurchatov has been received by NNCSC. The data is in the same format as the neutron data exchanged by the four neutron data exchanged by the four neutron data centers, making the task of maintaining charged particle nuclear data file much easier.

Work has also started in the nuclear structure data area. NNCSC was assigned the coordinating role for the national and international mass-chain evaluation activity. A U.S. network of evaluation

centers was established and the responsibility for evaluation of mass-chains apportioned among the members. Initially NNCSC will add an evaluator to the center to handle 10 assigned mass-chains.

An international network has also been established. The U.S. network has been instrumental in the encouraging the establishment of new evaluation groups in Germany, United Kingdom, Japan, and Sweden. Some mass-chains have been assigned to these groups. The effort at Utrecht in the low mass region will continue.

NNCSC continues to provide services to the nuclear community. Statistics for those services provided between January 1976 and December 1976 are attached.

2. Data Evaluation and Testing

The evaluation of $^{235}\text{U}(n,f)$ and $^{197}\text{Au}(n,\gamma)$ as cross-section standard has been completed in conjunction with the Normalization and Standards Subcommittee of CSEWG. The re-evaluation and updating of nickel, chromium, manganese, cobalt, gadolinium and gold is nearly complete.

A Monte Carlo study was sponsored by EPRI to analyze thermal reactor benchmark experiments. This use of "exact" neutronics methods has helped to determine actual deficiencies in Uranium-238 capture data.

3. ERDA NDC Secretariat

NNCSC is now the secretariat for the ERDA Nuclear Data committee. As such, we are responsible for editing and publishing committee meeting minutes, status reports and data request list. We also are responsible for the committee documents and distribution lists and for their coordination with the various international nuclear data committees.

Table B-1

Request Statistics for
Experimental Information
Jan. 1, 1976 to Dec. 31, 1976

1. <u>Requests</u>	
a) Number of requests	203
2. <u>Origin of Requests</u>	
a) Government Agencies	6
b) Educational Institutions	28
c) Industry (includes CSEWG members)	18
d) Foreign	9
e) Four-Center Members	35
f) National Laboratories (includes CSEWG members)	107
3. Mode of Requests (may be more than one mode per request)	
a) Magnetic Tapes	90
b) Computer Listing	118
c) Cards	2
d) Plots	20
e) Documentation	98
f) Telephone	0
g) Teletype	1

Table B-2

Request Statistics for
Evaluated Information
Jan. 1, 1976 to Dec. 31, 1976

1. <u>Requests</u>	
a) Number of requests	508
2. <u>Origin of Requests</u>	
a) Government Agencies	30
b) Educational Institutions	62
c) Industry	54
d) Foreign (includes Four- Center Members)	97
e) CSEWG Members	265
3. Mode of Requests (may be more than one mode per request)	
a) Magnetic Tapes	153
b) Computer Listings	101
c) Cards	2
d) Plots	32
e) Documentation	322
f) Telephone	0
g) Teletype	0

COLUMBIA UNIVERSITY

A. Fission Fragment Measurements, B. Luers, J.P. Felvinci, E. Melkonian, W.W. Havens, Jr.

1. Single Fragment Pulse Heights of ^{235}U .

In the last progress report we described our results which were also presented at the Nuclear Cross Sections and Technology Conference held in Washington, D.C. We also mentioned a similar experiment performed at Geel in which no large pulse height effects were found. The run we promised, to obtain more data and thereby improve the statistical accuracy, took place in June-July 1975 and we obtained a 15-fold increase in data resulting in an approximate improvement in statistics by a factor of four. The amount of data we had was now comparable to those at Geel.

To obtain this amount of data we had to use 3 detectors during two separate runs. The conditions were not all the same, and we had to normalize the pulse heights of individual detectors in order to add them together. The experimental arrangement is depicted in Fig. 1.

The results again show statistically significant variation in pulse height, but the expected improvement in significance level did not occur. The effects were localized in the same energy regions as earlier but there seemed to be a decrease in neutron energy resolution. We attribute this to the increased uncertainty in pathlength arising from the fact that the target was no longer perpendicular to the beam but at an angle of 25° . In our opinion, the Geel results did not show the variations we saw because of their poorer neutron energy resolution. The decrease in significance level of our new results confirm our idea that the higher resolution is necessary.

Reviewing our data, we still believe that there are pulse height effects, but that they are probably more complex than we originally thought them to be. Many energy regions have 2.5 - 3.5 standard deviations in the contingency tables, indicating variations in pulse height distributions.

We also are certain that in many regions where we indicated extra levels, there is additional complex structure. Recent evaluation of the polarized neutron experiment by Keyworth¹, and especially the calculations by M.S. Moore², impressively resolved the $J = 3$ and $J = 4$ levels. Some of the new resonances they see, or are indicated on their graphs, were also seen in our work on the variations in pulse height

distribution. (These levels are seen at 9 eV, 17 eV, 18 eV, 26 eV, 32 eV, etc.)

The Los Alamos group obtained a combined level spacing of 0.5 eV for the two spin states. We have earlier reported a level spacing of ~ 0.3 eV which is lower than that obtained by Moore, but not much lower than the 0.38 eV predicted by Garrison³.

In the original interpretation of our data the $J = 4$ levels belong to 2 different K values, both of which are assumed to be good quantum numbers. The level spacing obtained from the analysis of Moore, which is probably correct for $J = 3$, would not give the proper results for $J = 4$ if our assumption that K is a good quantum number is correct, resulting in two different families. Both the Dyson-Mehta Δ_3 statistics and the assumption of a single strength function, and thus a single Porter-Thomas distribution, for neutron widths would be in error for the $J = 4$ set of levels. There would be more small spacings among the $J = 4$ levels and thus more overlapping levels. Because the $J = 4$, $K = 2$ family has larger $\langle g \Gamma_n^0 \rangle$, it would hide many smaller $J = 4$, $K = 1$ levels.

The observation^{1,2} that the fission does not go through the $K = 0^-$ band supports our model which predicts the unavailability of this channel. Other corroborative evidence comes from the missing γ transitions in neutron capture. Transitions in ^{235}U and ^{177}Hf from the compound state to the ground state rotational band seem to be quite inhibited. This appears surprising because, if in the compound state K has a Gaussian distribution, $K = 0$ would be most likely. The transitions in ^{235}U and ^{177}Hf to the ground state band would be high energy $E1$ transitions, which would be highly probable. The inhibition of this transition could be explained in our model by the conservation of K , i.e. the compound state has no $K = 0$ component.

At this point, in our opinion, the experimental evidence is not sufficient to resolve the question of the level spacing for ^{235}U . This is one reason that we are enthusiastically concentrating on the double energy measurements, which in combination with the polarization and alignment experiments would be a great help toward the resolution of this problem.

¹ G.A. Keyworth, Los Alamos Report #LA-UR 76-1418

² G.A. Keyworth, M.S. Moore and J.D. Moses, LASL Report #LA-UR 76-1318

³ J.D. Garrison, Physical Review Letters, 29, p. 1185 (1972).

2. "Thick" Target Measurements (^{235}U).

We described in an earlier section of this progress report that one of the experiments performed in 1975 was the measurement of partial yields from a thick (7 mg/cm^2) ^{235}U target.

The results show that the most energetic group detected, comprising 0. % of the total observed fission fragments was significantly different from the total yield. Increased yield in resonances in this high energy group correlates very strongly with assignments of $J = 4$, $K = 1$ to these resonances in our earlier paper⁴. These assignments were made for those resonances for which energy groups 3, 4, 5 (where 1 is the lowest energy group and 8 is the highest energy group) showed an increased yield. One can understand this correlation if the (E_x, E_y) diagram derived from double energy measurements of the fission fragments is studied⁵. From this graph it can be seen that the most energetic fragments with the longest range will correspond to the masses 90 - 96. The complements of these masses, 140 - 146, are included in the groups (3, 4, 5) mentioned above.

These results indicate definite pulse height effects in the 1.13 eV, 3.19 eV, 7.08 eV resonances. Increased yield in the high energy group is also indicated around 1.7 eV, where no resonance has been reported.

3. ^{229}Th Cross Sections

We have, during the 1976 spring run, also used a thin, $\sim 20 \text{ }\mu\text{g/cm}^2$ ^{229}Th target back to back with a ^{235}U foil. This arrangement will give us the ^{229}Th cross sections normalized to ^{235}U . The preliminary results indicate agreement with our earlier 1970 data, but because of increased statistics, we can identify more levels to higher energies. Figure 2 shows a section of the yield curves to indicate the quality of data. We have tentatively identified more levels than earlier. The present suggested spacing is around 0.3 eV. The average fission width is smaller in ^{229}Th than in other fissile nuclei, and thus we can resolve the levels easier.

The fission areas $\delta_0 \Gamma_f$ are being calculated and will be published as soon as possible.

⁴ Nuclear Cross Sections and Technology, p. 580, NBS Special Publication 425.

⁵ H.W. Schmitt, J.H. Neiler and F.J. Walter, Physical Review, 141, 1146 (1966).

We are also planning to investigate, as soon as feasible, pulse height effects in the ^{229}Th data we already have.

4. Double Energy Measurements

The coincident fission fragment energies have been measured for ^{235}U and ^{229}Th . At this time only the ^{235}U results have been partially analyzed. The method of analysis was the following:

A cumulative sum was calculated for the two individual coincident pulse heights. The 1/4 and 3/4 points were established and the data taken at different runs were normalized to each other using their 1/4 and 3/4 points. These points agree very closely with the reference points in the Schmitt calibration procedure. We then used his constants for ^{235}U to calculate, through the mass dependent formulae, the single fragment kinetic energies and masses. The sum of the coincident energies naturally gave us the total kinetic energies. The relationship between fragment masses and energies, used here, is the usual one which ignores the effects of neutron emission.

In Figure 3(a), the total kinetic energy distribution and in Figure 3(b) the mass distribution is shown for all events.

In an effort to establish differences in total kinetic energy between resonances, the average total kinetic energy was calculated for every neutron energy. We also divided the total kinetic energy distribution into two equal parts of lower and higher energies and calculated the averages for those. These results for the lower half of the total kinetic energy distribution are shown for the 8.5 to 9.5 eV neutron energies on Figure 4(a). The χ^2 for the points is 68.81 for 36 degrees of freedom, resulting in a 0.1% probability that they have the same average. Notice the positive deviations at 9.35 and 8.5 - 8.55 and the negative deviation at 9.27. These are the regions where we claimed levels with $J = 3$ and $J = 4$ spins in our paper.

We also plot the average total kinetic energy (TKE) for this region, Figure 4(b). The positive deviations for the average are at places where we assumed (3,1) levels exist and there is indication in Keyworth papers for this effect. The negative deviations come at the position of the (4,1) levels as expected.

5. Preparations for the 1977 Experiments.

A new data acquisition system based on the PDP-11 computer has been acquired and tested.

The new TOF unit is a 100 MHz CAMAC scaler, preceded by a gate generator, which will allow the 80 MHz clock to be counted between the start and stop pulses. The ADC is a 2048 channel CAMAC octal unit. The ADC and TOF units are connected through a CAMAC interface to the PDP-11 and a 9-track magnetic tape. While the computer is waiting for events, in these low count-rate experiments, it will display the sorted incoming data and will also do some preliminary analysis using the associated disc. This procedure should speed up data analysis considerably as well as improve monitoring during the acquisition of data.

The experiment to be performed will be the double energy measurements from thin deposits of ^{229}Th , ^{235}U , and ^{239}Pu .

B. Multilevel Fits Using the Modified MULTI Code, F. Cohensedgh,
J.P. Felvinci, E. Melkonian, W.W. Havens, Jr.

A study was made toward determining the use and applicability of the Los Alamos developed code MULTI in analyzing the results of the recent Columbia University fission cross section measurement experiments at ORELA. MULTI is a FORTRAN code for least squares fitting of neutron cross section data using the Reich-Moore multi-level formalism. It is expected that the use of this code will establish the limits of the statistical accuracy of the experimental data and hence attempt to test the validity of the recent assumptions regarding dependence of fission cross section data on fragment energy. This determination may be made by considering the degree of consistency among the set of fission cross section resonance parameters obtained from the multi-level fitting of each set of data corresponding to a partial spectrum cut. Of special interest will be the comparison of resonance parameter sets corresponding to the cuts at the main light peak with those at the shoulder of the light peak which suggest a mode of fission different from the mode of the main peaks.

Since MULTI is written to be run on CDC-6600 or 7600 computers, use will be made of the NYU/CDC-6600 facilities, which are available to us.

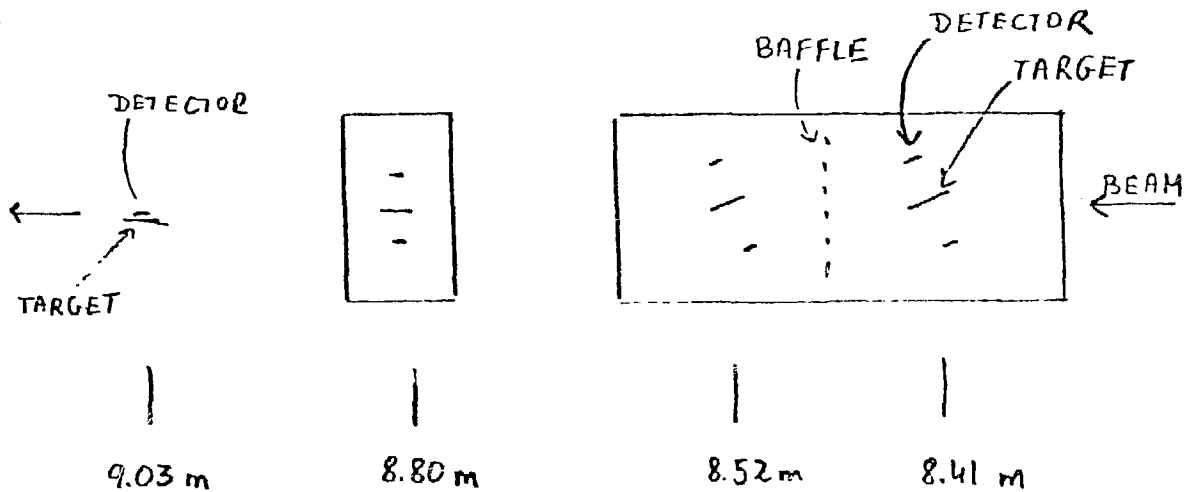


Figure 1(a). Experimental arrangement showing the 1975 ORELA run.

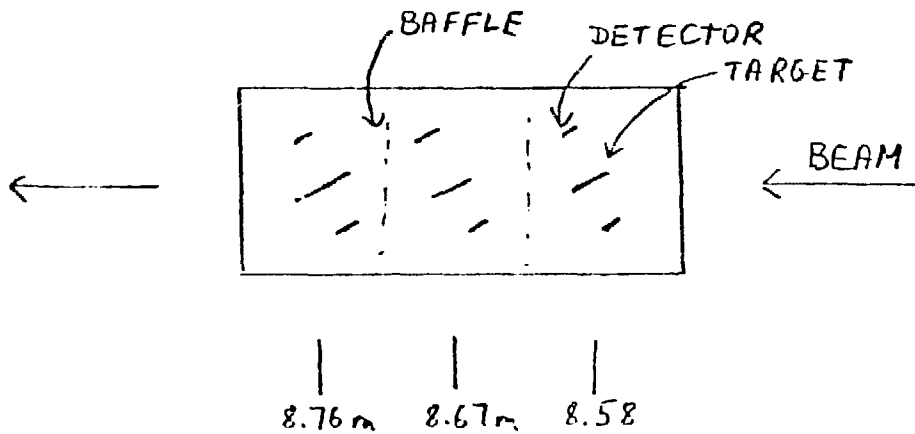


Figure 1(b). Experimental arrangement showing the 1976 ORELA run.

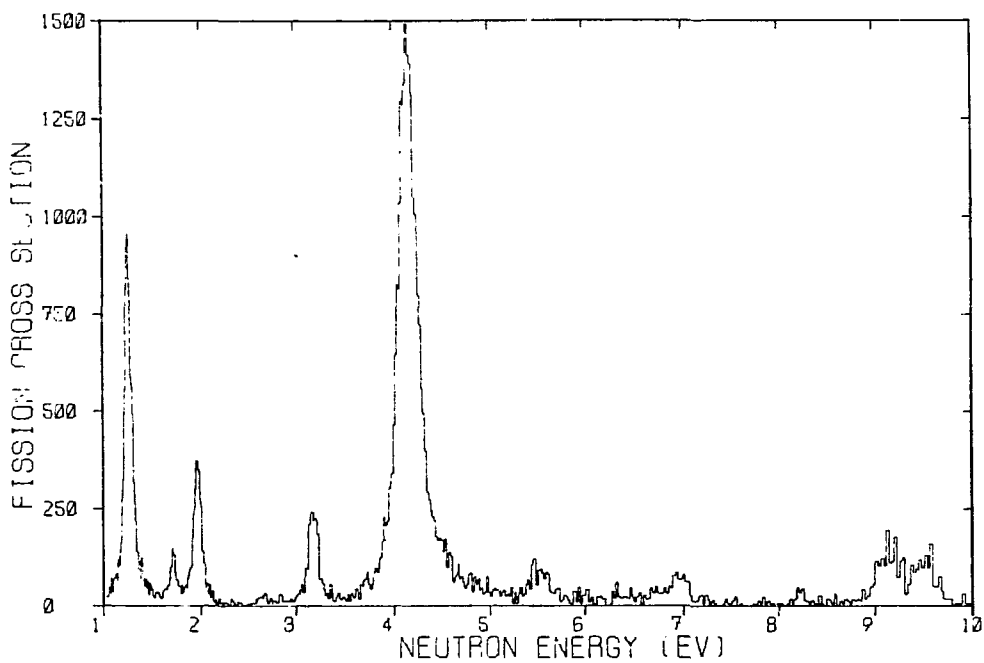


Figure 2. ^{229}Th fission cross section for 1 to 10 eV incident neutron energy. The cross section normalization is preliminary and correct to 20%.

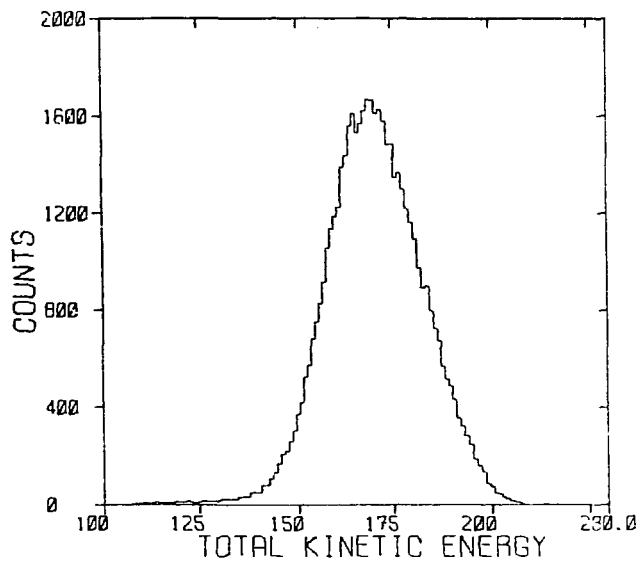


Figure 3(a). Total kinetic energy distribution of ^{235}U for all neutron energies.

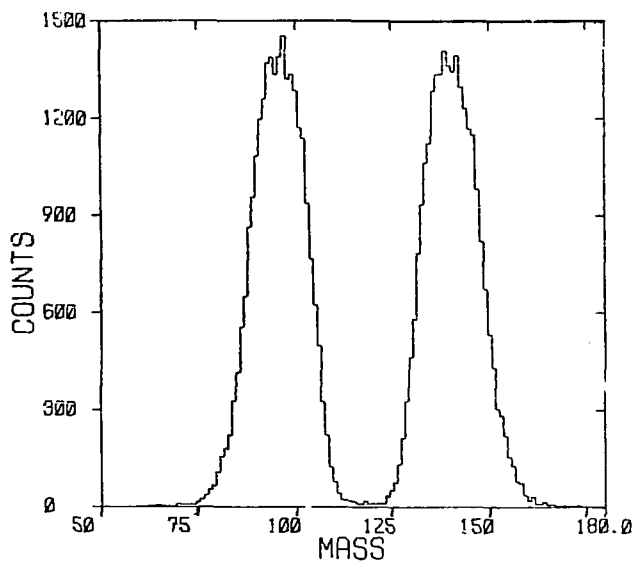


Figure 3(b). Mass distribution of ^{235}U for all neutron energies.

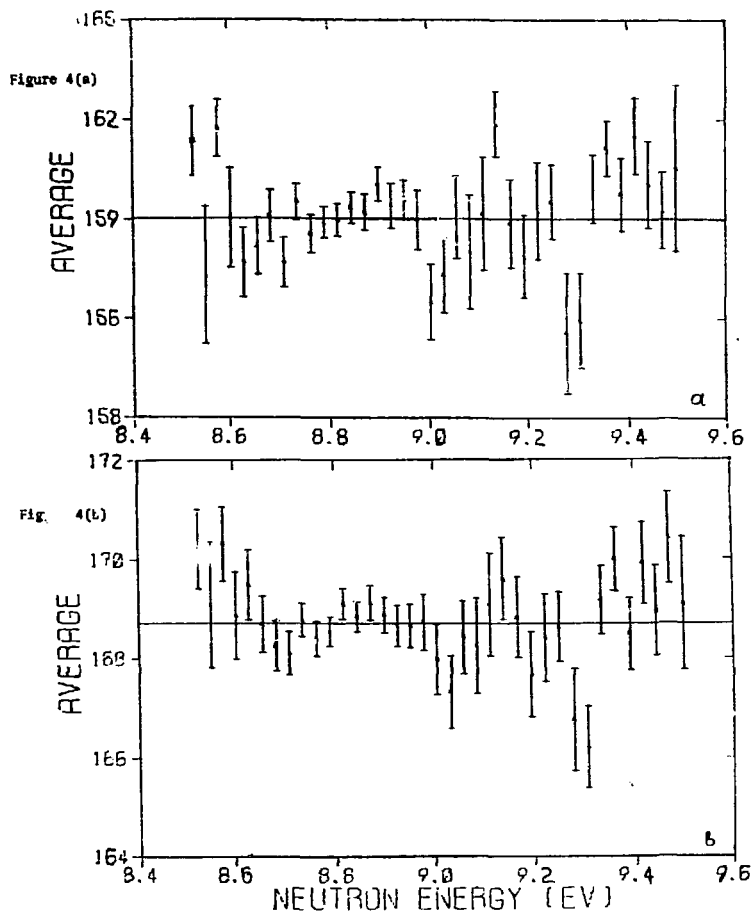


Figure 4(a). Lower half of the average total kinetic energy.

Figure 4(b). Total kinetic energy of ^{235}U for incident neutron energies between 8.5 and 9.5 eV.

AMES LABORATORY-ERDA

A. DECAY STUDIES OF GASEOUS FISSION PRODUCTS AND THEIR DAUGHTERS

1. Decays of ^{88}Kr and ^{88}Rb (R. L. Bunting, W. L. Talbert, Jr., J. R. McConnell, and R. A. Meyer)

The γ rays following the decays of ^{88}Kr and ^{88}Rb have been studied using Ge(Li) detectors and coincidence techniques. In ^{88}Kr decay 81 γ rays were observed and 74 were placed in a level scheme for ^{88}Rb . In ^{88}Rb decay 27 γ rays were observed and all were placed in a level scheme for ^{88}Sr . This work has been published¹ in Phys. Rev. C.

2. Decays of ^{91}Kr and ^{91}Rb (M. D. Glascock, W. L. Talbert, Jr., and C. L. Duke)

The γ rays following the decays of ^{91}Kr and ^{91}Rb have been studied using mass-separated sources produced by the TRISTAN facility. In ^{91}Kr decay 220 γ rays were observed and 218 were placed in a level scheme for ^{91}Rb . In ^{91}Rb decay 109 of the 125 observed transitions were placed in a level scheme for ^{91}Sr . This work has been published² in Phys. Rev. C.

3. On-Line γ - γ Angular Correlations of Transitions in ^{140}Ba
(L. J. Alquist, W. C. Schick, Jr., W. L. Talbert, Jr., and S. A. Williams)

Using sources of mass-separated ^{140}Cs , angular-correlation measurements were made on 12 direct cascades and 5 skip cascades in ^{140}Ba . Definite spin assignments were made for eight levels and tentative spin assignments for five levels. This work has been published³ in Phys. Rev. C.

4. Decay of ^{93}Kr , ^{93}Rb , and ^{93}Sr (C. J. Bischof and W. L. Talbert, Jr.)

Using mass-separated sources obtained at TRISTAN the decay of ^{93}Kr , ^{93}Rb , and ^{93}Sr to levels in ^{93}Rb , ^{93}Sr , and ^{93}Y respectively was observed. In ^{93}Kr decay 203 out of the 217 γ rays observed were placed

¹ Bunting, Talbert, McConnell, and Meyer, Phys. Rev. C 13, 1577 (1976).

² Glascock, Talbert, and Duke, Phys. Rev. C 13, 1630 (1976).

³ Alquist, Schick, Talbert, and Williams, Phys. Rev. C 13, 1277 (1976).

in the ^{93}Rb level scheme. For ^{93}Rb decay 231 out of 243 γ rays were placed and for ^{93}Sr decay 143 out of 162 γ rays were placed. This work has been scheduled to appear in the February 1977 issue of Phys. Rev. C. Tables of γ energies and intensities are too long to reproduce here but have been forwarded to ERDA-NDC.

5. Decay of ^{137}Xe (W. R. Western, John C. Hill, W. L. Talbert, Jr., and W. C. Schick, Jr.)

The decay of ^{137}Xe to levels in the N=82 nucleus ^{137}Cs was studied. Of 94 γ rays observed 83 were placed in a ^{137}Cs level scheme. Tables of γ energies and intensities are too long to reproduce here but have been forwarded to ERDA-NDC. This material has been accepted for publication in Phys. Rev. C and is scheduled to appear in the March 1977 issue.

6. Decay of ^{143}Ba (J. C. Pacer, John C. Hill, D. G. Shirk, and W. L. Talbert, Jr.)

A study at TRISTAN of the decay of ^{143}Ba to levels in ^{143}La has been completed. Of 69 γ rays attributed to ^{143}Ba decay 59 have been placed in the ^{143}La level scheme. This material will be submitted to Phys. Rev. C shortly. The γ ray energies and intensities are too long to be given here but have been forwarded to ERDA-NDC.

B. DECAY STUDIES OF NON-GASEOUS FISSION PRODUCTS

1. Decay of ^{138}I (W. R. Western, John C. Hill, W. C. Schick, Jr., and W. L. Talbert, Jr.)

We reported the first decay scheme for ^{138}I to levels in ^{138}Xe . The iodine was obtained using the "old" TRISTAN target system. A total of eight γ rays observed were placed in the level scheme. This work has been published⁴ in Phys. Rev. C.

2. Decay of ^{136}I (W. R. Western, John C. Hill, W. L. Talbert, Jr., and W. C. Schick, Jr.)

A total of 142 rays were observed in the decay of the 45- and 85-sec isomers of ^{136}I . Of these 116 were placed in a level scheme for ^{136}Xe consisting of 50 excited levels up to 6624 keV. Strong β population was observed to states above 3.5 MeV which are interpreted as neutron particle-hole states. This work has been submitted for publication to

⁴ Western, Hill, Schick, and Talbert, Phys. Rev. C 14, 275 (1976).

Phys. Rev. C. Tables of γ energies and intensities are too long to reproduce here but have been forwarded to ERDA-NDC.

3. Decay Studies of Ag, Cd, and In Fission Products with New In-Beam Ion Source (John C. Hill, T. K. Li, D. R. Margetan, M. L. Gartner, R. L. Gill, and W. L. Talbert, Jr.)

A new in-beam ion source has been developed at TRISTAN and is now on-line for studies of nongaseous fission products. Separated beams of Br, Kr, Rb, Sr, Ag, Cd, In, Sn, Sb, Te, I, Xe, Cs, and Ba have been observed. The ion source consists of a hot graphite cylindrical anode containing ^{235}U oxide. Fission products diffuse from the graphite (at 1500 $^{\circ}\text{C}$) into a plasma where they are ionized prior to acceleration and mass separation. We present below preliminary results from γ singles measurements of the decays of Ag, Cd, and In fission products. Detailed analysis is now in progress. The errors on the γ energies are no more than 1 keV and the intensity errors for strong peaks are no more than 20%.

a. Decay of ^{118}Ag

Preliminary results from ^{118}Ag singles measurements are given in Table B-1. This about triples the present knowledge concerning its transitions.

Table B-1. γ -rays from ^{118}Ag decay.

Energy (keV)	Relative Intensity	Energy (keV)	Relative Intensity
487	100	1939	3.3
678	38	2101	6.2
771	9.6	2278	1.5
781	3.8	2694	1.5
798	6.4	2737	1.6
1060	11	2778	5.8
1127	1.0	2789	9.5
1269	3.0	2894	1.6
1428	1.5	3225	8.0
1535	1.6		

b. Decay of ^{120}Ag

Preliminary results from ^{120}Ag singles measurements are given in Table B-2. The 203 keV γ ray is from the ^{120}Ag isomer whose half-life is 0.4 sec.

Table B-2. γ -rays from ^{120}Ag decay.

Energy (keV)	Relative Intensity	Energy (keV)	Relative Intensity
203	16	1492	1.1
506	100	1588	5.2
555	3.3	2347	3.5
697	41	2995	2.7
817	15	3044	2.3
830	2.7	3053	1.1
925	8.0	3537	1.3
1323	6.2	3881	1.1
1332	17	5526	1.3
1333	4.3	6345	1.1
1407	2.6	6391	1.1
1456	1.0		

c. Decay of ^{126}Cd

No information exists in the literature on the γ decay of ^{126}Cd and nothing is known about excited states in ^{126}In . On the basis of a preliminary analysis we have associated 15 γ rays with ^{126}Cd decay. The results are given in Table B-3.

Table B-3. γ -rays from ^{126}Cd decay.

Energy (keV)	Relative Intensity	Energy (keV)	Relative Intensity
227	3.0	1032	1.1
260	17	1496	0.7
365	2.5	1594	0.5
428	100	1602	0.7
556	4.9	1687	1.0
653	1.1	2371	0.8
667	1.6	3284	0.9
688	4.9		

d. Decay of ^{126}In

The only information available on levels in the semi-magic nucleus ^{126}Sn is from the $^{124}\text{Sn}(t,p)^{126}\text{Sn}$ reaction. We have observed 19 γ rays from the decay of ^{126}In to levels in ^{126}Sn . No decay γ 's from

^{126}In have been reported in the literature. Our results are given in Table B-4 below.

Table B-4. γ -rays from ^{126}In decay.

Energy (keV)	Relative Intensity	Energy (keV)	Relative Intensity
269	4.4	1571	2.5
316	6.4	1637	3.9
632	4.0	2106	1.5
909	27	2111	2.3
970	22	2204	1.9
1024	4.1	3247	2.3
1053	2.4	3345	40
1141	1000	3888	2.6
1230	1.9	3964	1.6
1378	4.2		

e. Decay of ^{128}In

The decay of ^{128}In to levels in ^{128}Sn is of special interest since ^{128}Sn can be described in terms of a doubly-magic ^{132}Sn core plus four neutron holes. Unfortunately no information is available on excited states in ^{128}Sn . We have observed 20 γ rays from ^{128}In decay. Preliminary values of their energies and intensities are given in Table B-5.

Table B-5. γ -rays from ^{128}In decay.

Energy (keV)	Relative Intensity	Energy (keV)	Relative Intensity
68	5.2	1170	100
120	15	1587	3.6
248	5.4	1867	18
257	4.3	1961	3.3
321	8.6	1974	11
832	27	2104	8.9
857	6.2	2258	3.9
869	5.8	3519	19
936	12	3954	5.0
1090	12	4296	14

C. GROUND-STATE β BRANCHING OF FISSION PRODUCTS (F. K. Wohn, M. D. Glascock, W. L. Talbert, Jr., S. T. Hsue, and R. J. Hanson)

The ground-state β branchings for several mass-separated Kr fission products and their daughters have been measured at TRISTAN. These measurements are needed for calculation of fission reactor decay heats. The deduced values of the ground-state β branching expressed as a percentage of decays are: ^{88}Kr , 14 ± 4 ; ^{88}Rb , 78.0 ± 1.2 ; ^{89}Kr , 23 ± 4 ; ^{89}Rb , 25 ± 5 ; ^{90}Kr , 29 ± 4 ; ^{90}Rb , 37 ± 5 ; ^{91}Kr , 10 ± 4 ; ^{91}Rb , 5 ± 5 . This material has been published⁵ in Phys. Rev. C.

⁵ Wohn, Glascock, Talbert, Hsue, and Hanson, Phys. Rev. C 13, 2492 (1976).

IRT CORPORATION

MEASUREMENTS OF FISSION-PRODUCT DECAY HEAT FOR ^{235}U AND ^{239}Pu * (S. J. Friesenhahn and N. A. Lurie)

The thermal neutron fission-product decay heat of ^{235}U and ^{239}Pu has been measured for cooling times of 1 to 10^5 seconds. Irradiation times were 1,000 seconds, 20,000 seconds, 24 hours and 35 days for ^{235}U and 1,000 seconds, 20,000 seconds and 24 hours for ^{239}Pu . The neutrons for the irradiation are provided by spontaneous fission in 10 milligrams of ^{252}Cf . The fission neutron spectrum is thermalized by a water and polyethylene assembly surrounding the terminus of a pneumatic transfer (rabbit) system. The fission sample is encapsulated by cementing between two layers of 0.002-inch mylar. Several tests have indicated that this encapsulation is completely effective in preventing the escape of volatile fission products such as ^{135}Xe . The fissionable material is in the form of 0.001-inch-thick metallic foils.

The fission foil assembly is mounted on the end of a polyethylene rabbit, and at the end of irradiation the rabbit is pneumatically transferred to the center of a very large scintillator. The scintillator consists of 45 liquid-filled plastic cylinders containing a total of 4,000 liters of scintillating solution. At the center of the liquid scintillator is located a 6-inch-diameter NE-110 plastic scintillator. The plastic scintillator was constructed with a reentrant hole to serve as the second terminus of the rabbit system.

The plastic scintillator is directly exposed to the fission foil assembly so that it can record the beta component of the decay heat with high (85 to 92 percent) efficiency. The large mass of the scintillator provides a high (90 to 92 percent) detection efficiency for the gamma-ray component of the decay heat.

The entire system is operated under computer control. The computer determines ambient backgrounds and calibrates the response of the scintillator using a NBS ^{60}Co standard source for which the gamma energy emission rate is known with a precision of ± 2 percent.

The fission rate during irradiation is determined in an auxiliary experiment in which an ion chamber is used to directly measure the fission rate in a very thin (100 microgram/cm²) deposit on a thin (0.00005-inch) nickel foil substrate. The thin substrate allows high bias efficiencies to be obtained (95 to 97 percent) which contributes significantly to the precision of the fission rate determination.

* Work sponsored by the Electric Power Research Institute.

After the fission rate in a foil is determined, it is covered with 0.002-inch mylar to contain the fission products and is returned to the chamber to be irradiated for a time identical to that used for the more massive foils. Since the signal level from these foils is quite small, they are measured with only the plastic scintillator to reduce the effects of ambient background. These data are then normalized to special data points taken with the thick foils using the plastic scintillator only. In this way, the fission rate in the thick foil is determined with high statistical precision.

As of this date, normalized results have been obtained for 24-hour irradiation of ^{235}U only. Comparisons of these results with calculations by Spinrad et al. at Oregon State University based on the ENDF library, are illustrated in Figure 1. As can be seen, the calculations underpredict the decay heat for times less than about 10 seconds. The agreement is quite good up to approximately 2,000 seconds at which time the experiment drops below calculations by about 10 percent. Essentially identical results were found when comparing the present experiment with the calculations of England of Los Alamos Scientific Laboratory.

By performing measurements with and without an iron absorber inside the plastic scintillator, the beta and gamma components of the decay heat are resolved. It appears that the major portion of the disagreement with calculation at long cooling times is in the gamma component. The normalization of the ^{235}U data taken for irradiation times other than 24 hours, is in progress, and it is hoped that these data will shed some light on the source of the disagreement. In addition, beta and gamma-ray spectrum measurements are underway to identify specific isotopes which may be responsible for the disagreement.

The normalization of the ^{239}Pu data is being delayed by the lack of evaporated ion chamber deposits. We expect to receive these within the coming month. Examination of the unnormalized data reveals rather large discrepancies in the shape of the cooling curve, which is undoubtedly due to the inferior knowledge of fission-product yields for this isotope.

Further details on experimental techniques are given in report EPRI NP-180 (February 1976).

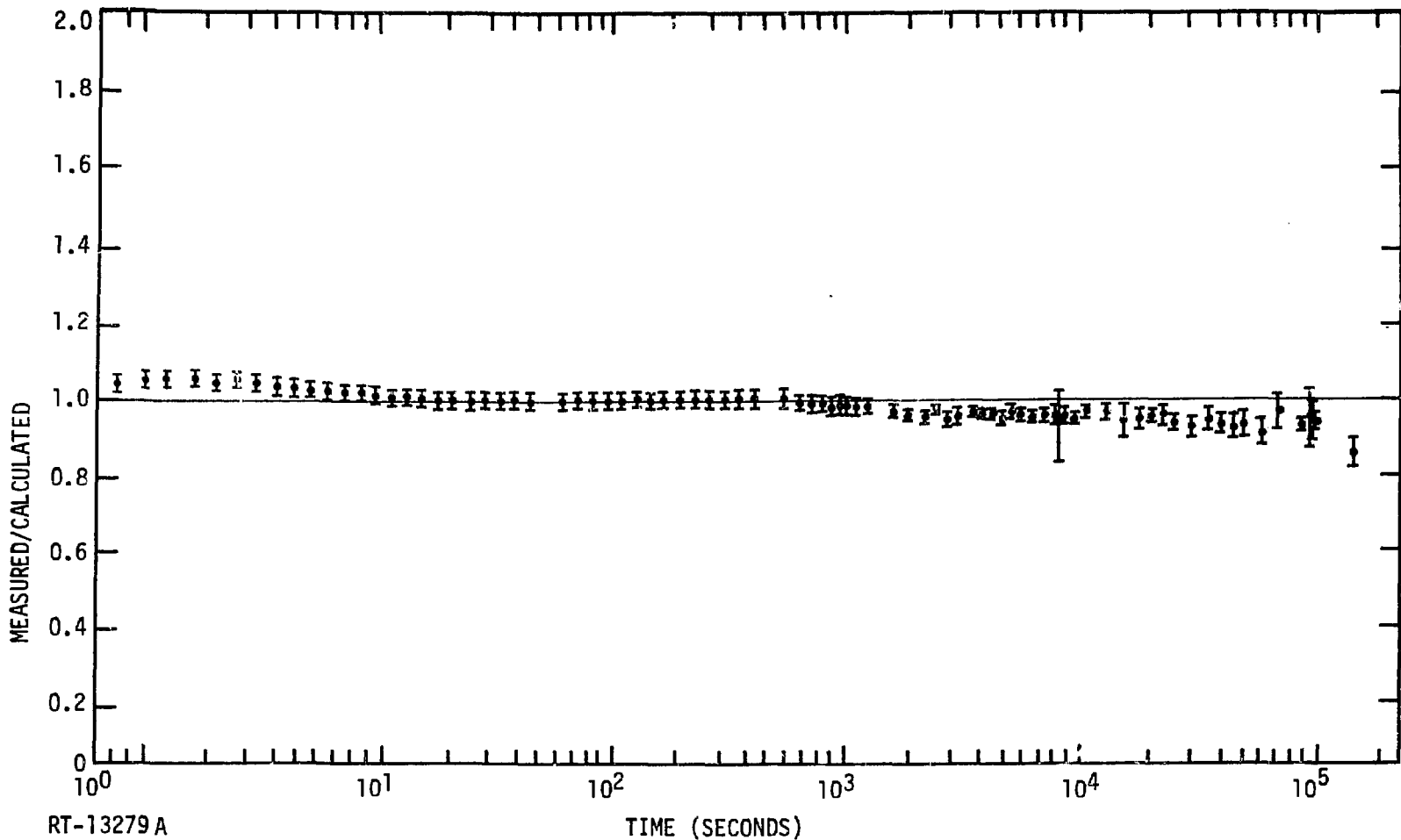


Figure 1. Ratio of measured-to-calculated total decay heat. Calculations are those of Spinrad based on the ENDF/B-IV data library.

LAWRENCE BERKELEY LABORATORY
Nuclear Science Division

DATA COMPILATION - *Table of Isotopes* (C.M. Lederer)

Completion of the 7th edition is planned for the current fiscal year. As of this writing, compilation and evaluation is completed, and final review is well underway. Production of final materials for layout, delayed pending installation of a high-resolution COM camera, has just begun; page layout will be started within a month.

The estimated size of the 7th edition is 1200 pages. The project involved a total of about 42 man-years: 60% of the effort was spent on actual compilation-evaluation work, 20% on data entry, bibliographic work, art work, and other support functions, and 20% on computer programming, development, and managerial tasks.

Future activities of the project will be closely tied to the newly-formed Nuclear Data Network (NDN). LBL has been assigned responsibility for compilation of mass chains 146-152 and 163-194, and has been asked tentatively to take editorial responsibility for the *Radioactivity Handbook*. Work on the first mass-chains is expected to begin this summer, with full effort devoted to the national program beginning in FY 1978.

LAWRENCE LIVERMORE LABORATORY

A. STANDARDS

1. High-Precision Neutron Flux Monitor. (J. B. Czirr and D. W. Shosa)

A totally-absorbing time-of-flight neutron detector was designed to permit flux measurements of standards accuracy in the 1 keV to 1 MeV energy range. The efficiency of the detector is calculated to be a constant over the energy range within $\pm 2\%$. Neutrons are moderated and captured in 4 m³ of compressed ⁶LiH and the capture distribution is sampled with thin slabs of ⁶Li-glass scintillator. The mean capture time is calculated to be approximately 100 nsec. See UCRL-79089 for further details.

B. NUCLEAR DATA APPLICATIONS

1. Studies of (n,xp), (n,xd) and (n,x α) Cross Sections at 15 MeV. (R. C. Haight, S. M. Grimes, J. D. Anderson, K. R. Alvar,* H. H. Barschall* and R. R. Borchers*)

We have continued measurements of hydrogen- and helium-producing reactions of interest to the Division of Magnetic Fusion Energy. A summary of the cross sections measured to date is given in Table B-1.

The spectra of the emitted charged particles have been compared with statistical model calculations. The agreement is particularly sensitive to several parameters of the calculation, namely nuclear level densities, optical model parameters, angular momentum effects and gamma-ray strength functions.

From the measured alpha particle spectrum and angular distribution, we can infer the spectrum of recoils from (n,x α) reactions. These particular recoils constitute the high energy part of the spectrum of recoiling nuclei and hence are important in discussions of displacement damage. The inferred spectrum of recoils in stainless steel 316 from (n,x α) reactions at $E_n = 15$ MeV is given in Figure B-1. Using the experimental data, we avoid making assumptions, which were previously necessary, about the alpha particle angular distributions and spectra.

*University of Wisconsin, Madison, Wisconsin

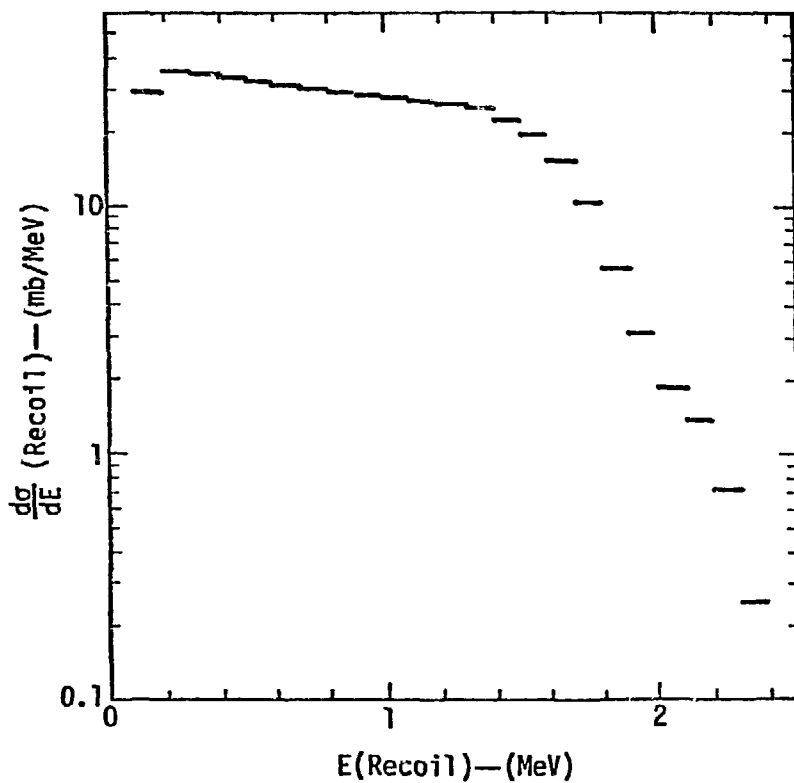


Figure B-1. Stainless steel 316 recoil spectrum from (n,x α) reactions $E_n = 15$ MeV.

Table B-1

Cross Sections at 15-MeV Neutron Energy

<u>Material</u>	<u>Cross Sections (mb)</u>			<u>Reference</u>
	<u>(n,xp)</u>	<u>(n,xd)</u>	<u>(n,xα)</u>	
²⁷ Al	405 \pm 60	19 \pm 8	121 \pm 25	1
⁴⁶ Ti	669 \pm 90	9 \pm 4	98 \pm 18	1
⁴⁸ Ti	85 \pm 16	7 \pm 3	28 \pm 6	1
SS-316 and 304	252 \pm 38	8 \pm 2	48 \pm 7	2
⁶³ Cu	320 \pm 45	<10	56 \pm 10	3
⁶⁵ Cu	86 \pm 12	<10	13.5 \pm 2.6	3
V	91 \pm 14	7 \pm 2	17 \pm 3	4
Nb	51 \pm 8	8 \pm 2	15 \pm 3	4

¹S. M. Grimes, R. C. Haight and J. D. Anderson, "Measurement of Sub-Coulomb Barrier Charged Particles Emitted from Al and Ti Bombarded by 15-MeV Neutrons," UCRL-78314 (1976) - to be published in Nucl. Sci. Eng. (Feb. 1977).

²R. C. Haight, S. M. Grimes and J. D. Anderson, "Hydrogen and Helium Production Cross Sections for 15-MeV Neutrons on Stainless Steels 316 and 304," UCRL-78785 (1976) - to be published in Nucl. Sci. Eng.

³In preparation.

⁴In preparation.

2. Isomer Ratio for the $^{175}\text{Lu}(n,2n)^{174}\text{Lu}$ Reaction at 14.8 MeV
(D. R. Nethaway and D. G. Gardner)

The ratio of the 142-day isomer to the 1204-day ground state of ^{174}Lu produced by the (n,2n) reaction of ^{175}Lu with 14.8 MeV neutrons was measured by following the relative growth and decay of various ^{174}Lu gamma-rays, and by absolute gamma-ray counting. The results were, respectively, 0.47 ± 0.04 and 0.45 ± 0.03 . These results are consistent with the recent LASL value⁵ of 0.475.

The reaction was studied in the incident neutron energy range of 8-16 MeV via statistical model and coupled-channel calculations. We find that the first few rotational bands in ^{174}Lu must be enumerated up to spins of 12 or 13 in order for the calculations to fit the experimental data. This required about 90 levels in ^{174}Lu , so that each band might span the entire spin distribution produced by the 14.8 MeV neutrons. The calculations for various sets of ^{174}Lu levels are shown in Figure B-2. These suggest that even the high spin band members are relatively pure, and that once a gamma-ray cascade is initiated within a band it continues with very little crossing until the lower levels are reached. It is also clear that attempts to extract spin-cutoff parameters from isomer ratio data involving deformed nuclei will yield questionable results, unless a very large number of final levels are considered in the gamma-ray cascade.

3. Radiation Doses from Iron, Concrete and Water as a Function of Mean-Free-Path for 14-MeV Neutrons. (L. F. Hansen, T. T. Komoto, C. Wong and B. A. Pohl)

The extensive use of iron, concrete and water as shielding materials in fast and fusion reactors suggests the importance of being able to predict with accuracy the characteristics of the transmitted neutron and gamma-ray fluxes through these materials. Comparison of these predictions with pertinent experimental results assures their reliability.

The gamma spectra from the interaction of 14-MeV neutrons with 0.9, 2.9 and 4.8 mfp* of iron, 2 and 4 mfp of concrete, and 1.1 and 1.9 mfp of water have been measured using the sphere transmission and time-of-flight techniques. These measurements have been compared with calculations using TARTNP, a coupled neutron-photon Monte Carlo Transport code. The ENDF/B-IV and ENDL libraries for neutrons and gamma rays were used in these calculations. Earlier neutron spectra measurements on all these spherical assemblies were recalculated with TARTNP. These results were in very good agreement with those obtained earlier with TART, where only neutrons were included in the Monte Carlo Transport calculations.

⁵B. Bayhurst et al., Phys. Rev. C12, 451 (1975).

*mfp-mean free path.

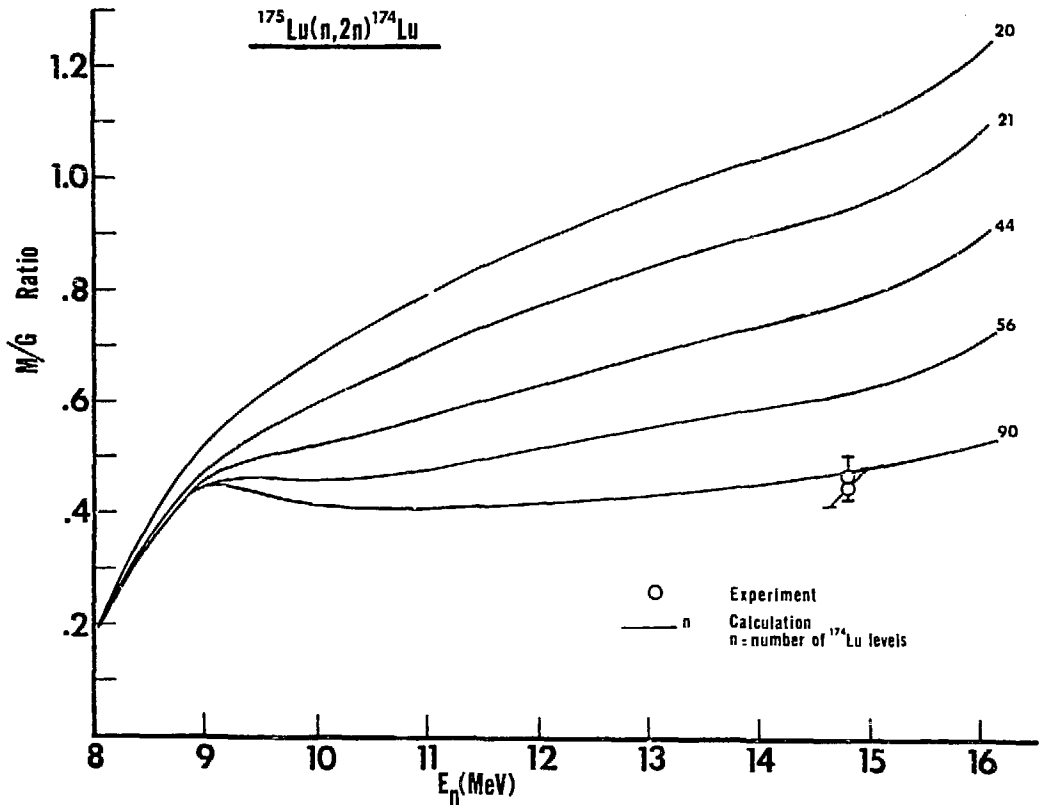


Figure B-2.

The discrepancies between the gamma measurements and calculations for these materials range between 10 and 25%, with both libraries giving similar results. From the neutron and gamma fluences, the radiation doses in tissue have been calculated as a function of mfp for these materials. (This paper was accepted for presentation at the 5th International Conference on Reactor Shielding to be held at Oak Ridge National Laboratory April 18-22, 1977.)

4. Transport of 14-MeV Neutrons Through Fissionable Materials.
(L. F. Hansen, T. T. Komoto, C. Wong and B. A. Pohl)

The neutron and gamma spectra resulting from the interaction of 14-MeV neutrons with ^{232}Th , ^{235}U , ^{238}U and ^{239}Pu have been measured using the sphere transmission and time-of-flight techniques. Because these materials are being used in the design of hybrid reactors (fusion-fission), it is of interest to have assurance that the calculations give a good representation of the interaction of the 14-MeV neutron with these materials.

Spherical assemblies of 1 mfp Th, 0.7 and 1.5 mfp ^{235}U , 0.8 and 2.8 mfp ^{238}U , and 0.7 mfp ^{239}Pu were bombarded with the 14-MeV source positioned at the center of the spheres. The neutron spectra were measured with improved time resolution over earlier measurements. The present results agree well with these earlier measurements. The ^{239}Pu and ^{235}U time spectra showed the presence of delayed gamma radiation presumably from fission fragment isomers, the effect being most pronounced in ^{235}U . The measurements are being compared with TARTNP calculations (coupled neutron-photon Monte Carlo transport code) for neutrons and gamma rays. Preliminary results indicate that the calculations overestimate the gamma production, the discrepancy being largest for ^{239}Pu .

5. Investigation of Gamma-ray Strengths Following Inelastic Proton Scattering on Even-Even Vibrational Nuclei. (R. P. Koopman, L. F. Hansen, and F. S. Dietrich)

A systematic survey of cross-sections for gamma rays de-exciting the low-lying levels of even-even vibration-like nuclei following inelastic proton scattering has been completed. The purpose of these experiments was to provide detailed information on the gamma decays which could be used to test nuclear-modeling codes intended to predict the yields of neutron-induced reactions. It was also desired to test the hypothesis that the production cross-section for the lowest excited-state gamma decay in this class of nuclei is closely equivalent to a measurement of that portion of the inelastic events which is not followed by particle decay. Using the LLL cyclograaff accelerator and Ge(Li) detectors, gammas were detected following 7- to 26-MeV proton bombardment of ^{56}Fe , ^{62}Ni , ^{64}Zn , ^{103}Pd , $^{110,114,116}\text{Cd}$, $^{116,120}\text{Sn}$, and ^{206}Pb . The

excitation function for the low-lying gamma decays of ^{56}Fe is shown in Fig. B-3; qualitatively similar results were found for all of the targets. The 0.847-MeV gamma cross section is in good agreement ($\sim 10\%$) with a value obtained by integrating measured (p,p') spectra⁶ over energy and angle. Preliminary nuclear-modeling calculations (including collective excitation) show that pre-equilibrium reactions are required to explain the data at high bombarding energies (~ 14 MeV), and that isospin effects must be included to reproduce the correct magnitudes of the cross-sections.

6. Measurement of (n,n' γ) Cross Sections Induced by 14-MeV Neutrons on Even-Even Vibration-like Nuclei. (R. P. Koopman, F. S. Dietrich and L. F. Hansen)

A series of (n,n' γ) experiments was performed at the Livermore RTNS facility, using ring geometry and Ge(Li) detectors. Pulsed-beam timing techniques were used to eliminate asynchronous backgrounds and fast-neutron events. Measurements were made on rings of natural Fe, Ni, Zn, Cd, Sn, and Pb; the high resolution of the Ge(Li) detector allowed identification of gammas from the various isotopic constituents of the samples. Data were taken at angles near 50° between the incident neutrons and the gammas for all samples, and additionally near 80° and 125° for several samples. A partial list of cross sections measured for Fe and Cd is given in Table B-2. Because neutron energy varies with angle in a ring-geometry experiment, the data must be corrected to a common energy if the angular distribution is to be inferred. If the total cross section is assumed to behave linearly over the energy range 13.6-14.8 MeV, the cross section and angular dependence of the $2^+ \rightarrow 0^+$ transition in ^{56}Fe are in good agreement with the results of Abbondanno *et al.*⁷, but not those of Lachkar *et al.*⁸ The systematic behavior of the relative strengths of transitions between the low-lying levels is very similar to that observed in (p,p' γ) reactions on the same nuclei.

⁶A. Sprinzak, *et al.*, Nucl. Phys. A203, 280 (1973).

⁷U. Abbondanno *et al.*, J. Nucl. Energy 27, 227 (1973).

⁸J. Lachkar *et al.*, Nucl. Sci. and Eng. 55, 168 (1974).

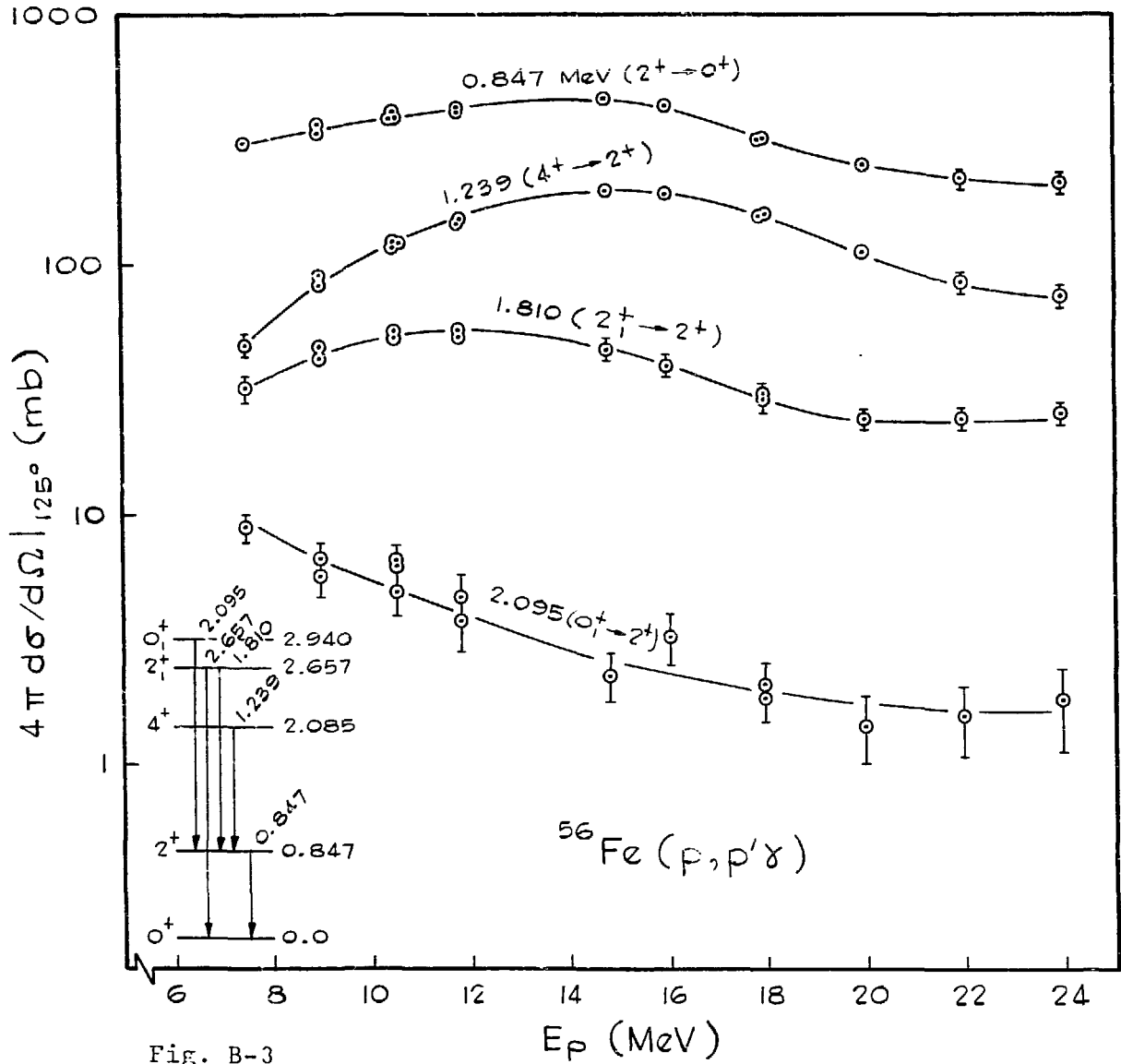


Fig. B-3

Figure B-3.

Table B-2. Differential cross sections in mb/sr for (n,n' γ) reactions producing various gamma rays in Fe and Cd samples. Energies in MeV.

Nucleus	θ	E_n	E_γ	$\sigma_{2^+-0^+}$	E_γ	$\sigma_{4^+-2^+}$	E_γ	$\sigma_{2_1^+-2^+}$
^{56}Fe	124 $^\circ$	13.5	0.847	65 \pm 3	1.239	31 \pm 1	1.810	3.3 \pm 1
	80 $^\circ$	14.3		43 \pm 3		21 \pm 1		2.6 \pm 1
	51 $^\circ$	14.8		50 \pm 3		25 \pm 1		4.0 \pm 1
^{110}Cd	49 $^\circ$	14.8	0.658	149 \pm 6	0.835	75 \pm 4	0.818	8 \pm 2
^{112}Cd	49 $^\circ$	14.8	0.617	114 \pm 6	0.797	59 \pm 2	0.694	7 \pm 2
^{114}Cd	49 $^\circ$	14.8	0.558	45 \pm 2	0.725	12 \pm 2	0.651	10 \pm 1
^{116}Cd	49 $^\circ$	14.8	0.514	39 \pm 12	0.706	35 \pm 7	0.700	2 \pm 6

7. High Energy Fission Cross Section Ratio Measurements.
(J. W. Behrens and J. C. Browne)

We have completed neutron-induced fission cross section measurements on a series of thorium, neptunium, plutonium, and americium isotopes using ionization fission chambers at the LLL 100-MeV electron linear accelerator. Ratios of the cross sections of ^{232}Th , ^{237}Np , ^{244}Pu , and ^{241}Am relative to ^{235}U have been measured as functions of neutron energy over the range .001 to 30 MeV, except where limited by low cross sections on the threshold isotopes. We normalized the results independent of other measurements by using the threshold cross section method. These ratio measurements ⁹⁻¹¹ were obtained in a manner similar to the series of uranium (i.e., $^{233},^{234},^{236},^{238}\text{U}$) and plutonium (i.e., $^{239},^{240},^{241},^{242}\text{Pu}$) isotopes which were presented at the NEANDC/NEACRP Specialists Meeting on Fast Neutron Fission Cross Sections, June 28-30, 1976.¹² Preliminary results for the $^{241}\text{Am}/^{235}\text{U}$ and $^{237}\text{Np}/^{235}\text{U}$ ratios are shown in Figure B-4 and are compared to ratios (line) obtained using the ENDF/B-IV evaluated fission cross-section files.

8. ^{241}Pu Fission Cross Section. (G. W. Carlson, J. W. Behrens and J. B. Czirr)

We have completed a measurement of the fission cross section of ^{241}Pu from 8 eV to 70 keV. The incident neutron spectrum measurement was obtained with a thin ^6Li -glass scintillator. The data were normalized to accepted values near thermal energies. The data exhibit significant discrepancies when compared to the ENDF/B-IV evaluated cross section. See UCRL-78696 for further details.

⁹J. W. Behrens and J. C. Browne, Measurement of the Neutron-Induced Fission Cross Section of ^{241}Am Relative to ^{235}U from 0.001 to 30 MeV, Lawrence Livermore Laboratory, Rept. UCID-17324 (1976).

¹⁰J. W. Behrens, R. S. Newbury, J. C. Browne, and G. W. Carlson, Measurement of the Neutron-Induced Fission Cross Section of ^{244}Pu Relative to ^{235}U from 0.2 to 30 MeV, Lawrence Livermore Laboratory, Rept. UCID-17341 (1976).

¹¹J. W. Behrens, J. W. Magana, and J. C. Browne, Measurement of the Neutron-Induced Fission Cross Section of ^{237}Np Relative to ^{235}U From 0.02 to 30 MeV, Lawrence Livermore Laboratory, Rept. UCID-17370 (1977).

¹²J. W. Behrens and G. W. Carlson, Measurements of Neutron-Induced Fission Cross-Section Ratios Involving Isotopes of Uranium and Plutonium, Proc. NEANDC/NEACRP Specialists Meeting on the Fast Neutron Fission Cross Sections of U-233, U-235, U-238, and Pu-239, Argonne National Laboratory, June 28-30, 1976, Argonne National Laboratory, Rept. ANL-76-90, p. 47.

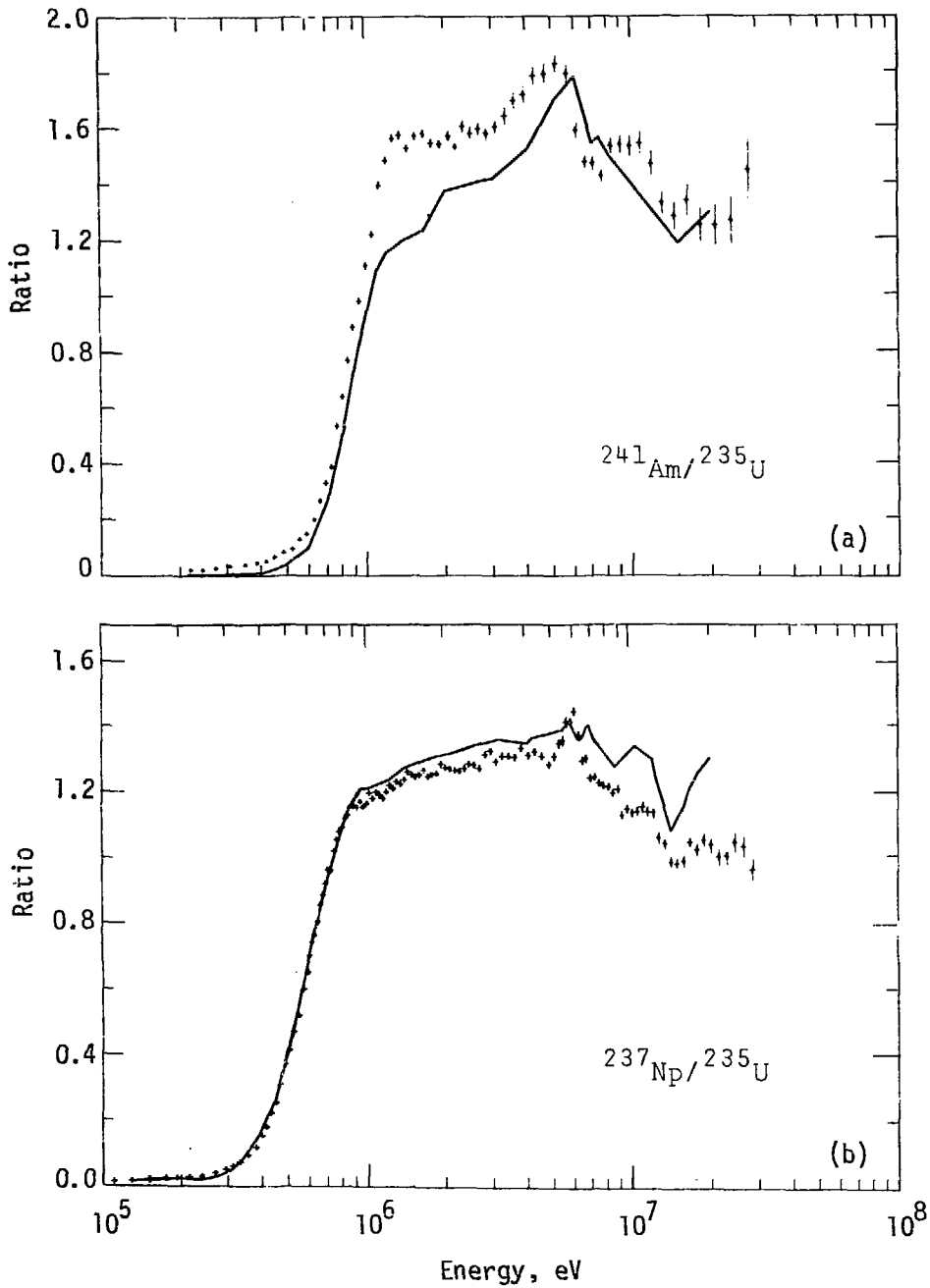


Figure B-4. Preliminary data for the (a) $^{241}\text{Am}/^{235}\text{U}$ and (b) $^{237}\text{Np}/^{235}\text{U}$ fission cross section ratios over the neutron energy range 0.1 MeV to 30 MeV. The lines were obtained using ENDF/B-IV evaluated fission cross sections.

9. ^{245}Cm Fission Cross Section. (J. C. Browne, R. W. Benjamin,* and D. G. Karraker**)

The fission cross section of ^{245}Cm has been measured from 0.01 eV to 35 eV at the LLL 100-MeV linac. By normalizing to previous integral data, a thermal fission cross section of 2143 ± 58 b is obtained. The cross section below 1 eV is non- $1/v$ due mainly to a slightly bound level. The recommended thermal value of 2020 b (BNL-325) differs from our result because it was obtained under the assumption of a $1/v$ energy dependence. Resonance parameter analysis has been completed and a paper is being prepared for submittal to Nuclear Science and Engineering.

10. A New Isotope of Curium: ^{251}Cm . (R. W. Lougheed, J. F. Wild, E. K. Hulet, J. H. Landrum, R. W. Hoff)

We produced this new isotope by neutron capture on ^{250}Cm at the Livermore LPTR reactor. The primary identification was by chemical milking of its beta-decay daughter ^{251}Bk . Its beta-half-life is 16.8 ± 0.2 min, and measured beta-endpoint is 1.42 MeV. We have found a total of thirteen gamma rays from ^{251}Cm , which we have fitted into a consistent decay scheme (Fig. B-5). According to this scheme, Q_{β^-} is also 1.42 MeV. As a by-product of these experiments, an approximate thermal cross-section of 80 barns at a cadmium ratio of 2.84 was measured for neutron capture on ^{250}Cm .

11. A New Isotope of Californium: ^{255}Cf . (R. W. Lougheed, E. K. Hulet, J. Evans, B. Qualheim)

We produced this new beta-emitter by neutron capture on ^{254}Cf at the Vallecitos reactor. We identified and measured ^{255}Cf by chemically milking its daughter, ^{255}Es , at periodic intervals, and subsequently alpha-pulse-height analyzing its granddaughter ^{255}Fm . ^{255}Fm ($\tau_{1/2} = 20$ -hr alpha) reaches equilibrium in a few days with its parent, ^{255}Es ($\tau_{1/2} = 40$ -d beta). Our measured beta half-life for ^{255}Cf is 90 ± 30 minutes.

C. NUCLEAR DATA FOR SAFEGUARDS

1. Photofission Studies with Monoenergetic Photons. (B. L. Berman, R. A. Alvarez, P. Meyer, J. T. Caldwell,** and E. J. Dowdy**)

Preliminary analysis of data acquired to date in this LLL-LASL collaborative program has yielded $(\gamma, n_{\text{total}})$, (γ, n) , $(\gamma, 2n)$ and (γ, f) cross sections for ^{232}Th , ^{235}U , ^{236}U , ^{237}Np , and ^{238}U . Lorentz curves have been fitted to the $\sigma(\gamma, n_{\text{total}})$ data in the giant-resonance region, and the parameters extracted. Similar data have been obtained for ^{233}U and ^{234}U which are presently being analyzed. Figure C-1 shows some

*Savannah River Laboratory, Aiken, South Carolina.

**Los Alamos Scientific Laboratory, Los Alamos, New Mexico.

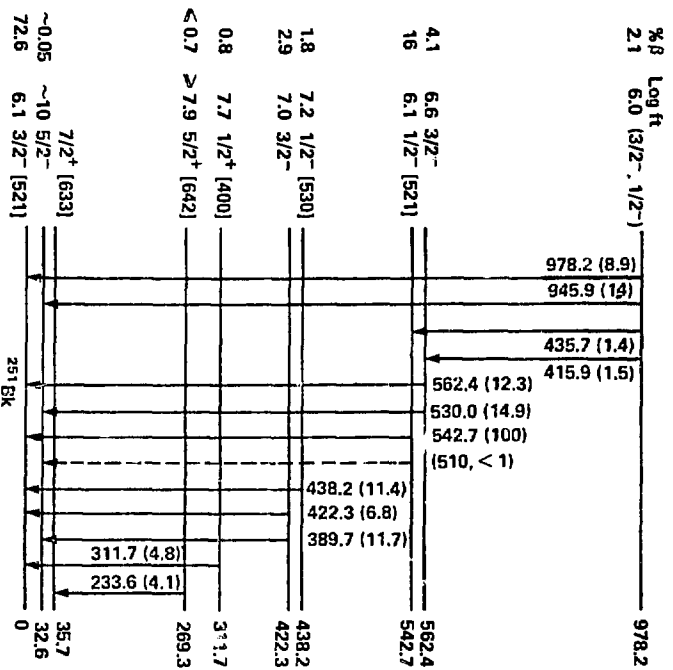
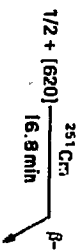


Figure B-5. BETA decay scheme for ^{251}Cm .

representative photofission data for ^{238}U where the cross section has been decomposed into first- and second-chance fission. The prompt fission neutron multiplicity, $\bar{\nu}$, has also been extracted as a function of incident photon energy. Shown in Fig. C-2 are the $\bar{\nu}$ results for ^{236}U along with the evaluated $\bar{\nu}$ for $^{235}\text{U} + n$ for comparison. Fig. C-3 shows the delayed neutron fraction obtained in the present measurement compared with previous results. Further analysis of these photofission data for the actinides is continuing.

D. NUCLEAR DATA COMPILATION

1. Atlas of Photoneutron Cross Sections. (B. L. Berman)

The Bicentennial Edition of the Atlas of Photoneutron Cross Sections Obtained with Monoenergetic Photons has been issued as UCRL-78482. In addition to the graphs of the cross-section data, tables of giant-resonance properties and comparison information from bremsstrahlung data, together with reference lists, are included as well. Figure D-1 shows the current scope of giant-resonance data obtained with monoenergetic photons. The compilation is current as of December, 1976.

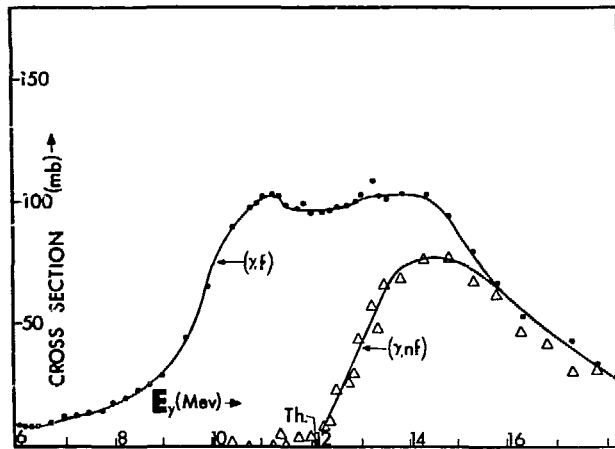


Figure C-1. U-238 photofission.

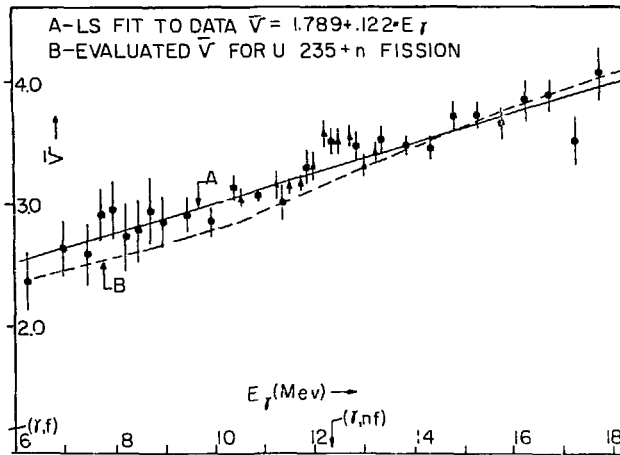


Figure C-2. U-236 photofission.

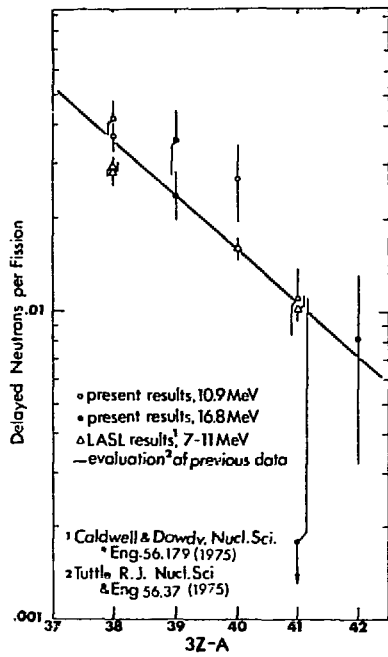


Figure C-3. Delayed neutrons per fission.

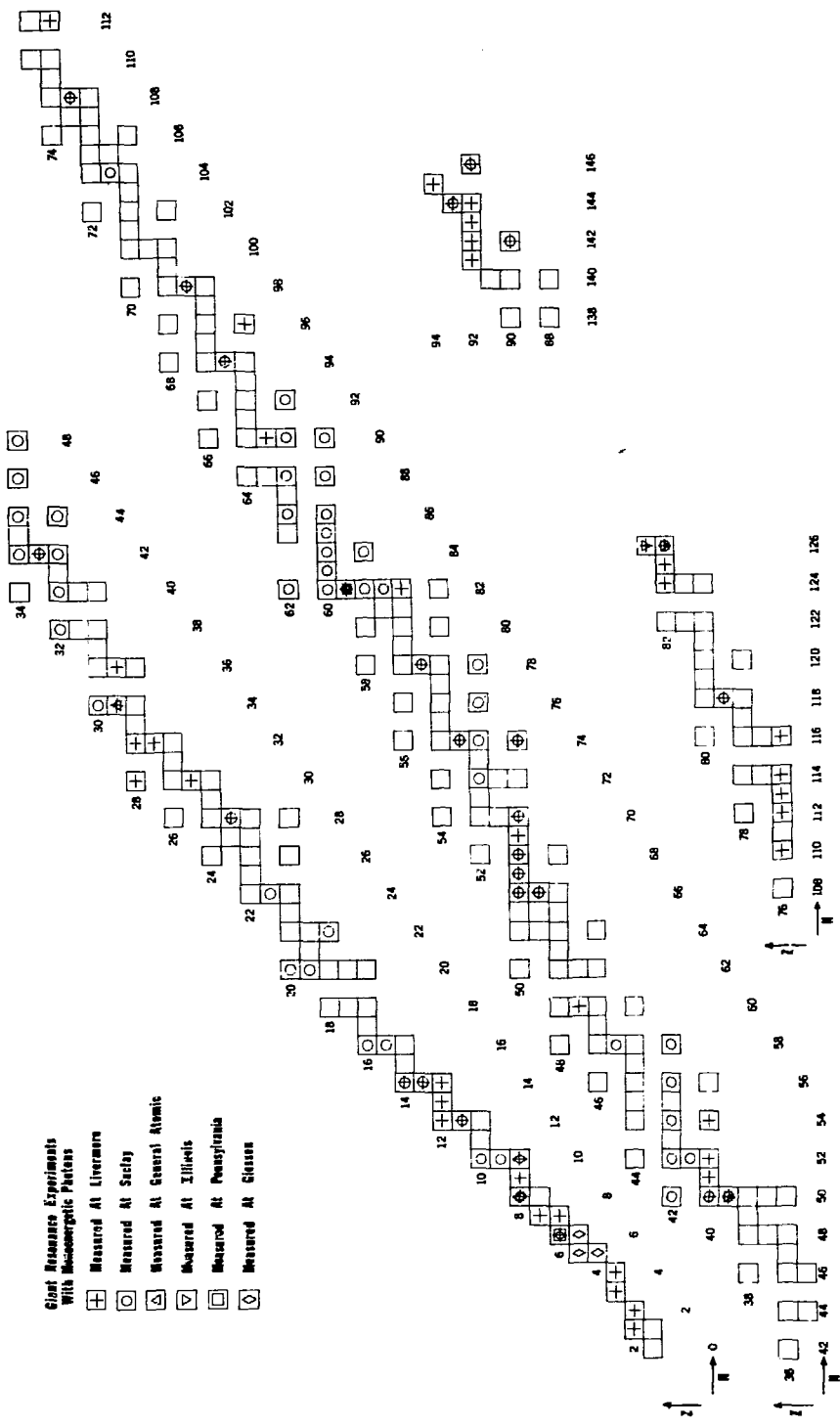


Figure D-1.

LOS ALAMOS SCIENTIFIC LABORATORY

A. NEUTRON CROSS SECTIONS (DIRECT AND INDIRECT)

1. ${}^3\text{H}(\alpha, {}^6\text{Li})\text{n}$ Reaction at Zero Degrees (Brown, Haglund, Jarmie, Ohlsen)

We have completed a set of measurements aimed at resolving the long standing discrepancies in the various measurements of the ${}^6\text{Li}(\text{n}, \alpha)\text{T}$ reaction. This has been done by studying the inverse reaction $\text{T}(\alpha, {}^6\text{Li})\text{n}$, as follows.

Excitation functions for the reaction ${}^3\text{H}(\alpha, {}^6\text{Li})\text{n}$ at 0° (lab) were measured in the energy range covering the resonance corresponding to the 5/2-state in ${}^7\text{Li}$ at 7.46 MeV of excitation. An α -particle beam bombarded a target consisting of a thin Ti-tritide layer on a Ni backing, and, after being spatially separated from the beam in a magnetic field, the ${}^6\text{Li}$ reaction products at 0° were detected by a thin solid-state detector. Data at 14 bombarding energies were obtained for detection of the ${}^6\text{Li}$ group emitted at $\theta_{\text{c.m.}} = 0^\circ$, and data at 11 energies were obtained for the ${}^6\text{Li}$ group emitted at $\theta_{\text{c.m.}} = 180^\circ$. These reaction data were normalized by measuring, simultaneously with the reaction, the yield of the elastically recoiling tritons at $\pm 15^\circ$ and $\pm 30^\circ$ (lab). To obtain absolute differential cross sections from the normalized reaction data, we also measured, in a separate gas-target experiment, excitation functions for ${}^3\text{H}(\alpha, \text{t}){}^4\text{He}$ at 15° and 30° (lab).

The final zero degree data are given in Table A-1 and shown in Fig. A-1 as solid circles. The crosses are from the measurements of Overley et al.,¹ and the solid curves are based on an R-matrix fit of the present and other relevant data.

2. Total Cross Section of ${}^9\text{Be}$, ${}^{10,11}\text{B}$ and ${}^{12,13}\text{C}$ From 1.0 MeV to 14 MeV (Auchampaugh, Ragan; S. Plattard (Bruyeres-le-Chatel); Hill (ORNL))

High-resolution and high-accuracy MeV neutron total cross sections of ${}^9\text{Be}$, ${}^{10,11}\text{B}$ and ${}^{12,13}\text{C}$ have been measured at the LASL Tandem Van de Graaff accelerator using the ${}^9\text{Be}(\text{d}, \text{n})$ reaction to produce a "white" source of neutrons. Fast, nanosecond time-of-flight techniques were used to determine the energy of the neutrons. The ${}^9\text{Be}$, ${}^{10,11}\text{B}$ and ${}^{13}\text{C}$ data cover the energy region from 1.0 MeV to 14 MeV and the ${}^{12}\text{C}$ data the energy region from 1.5 MeV to 14 MeV. The statistical uncertainty

¹ J. C. Overley, R. M. Sealock, and D. H. Ehlers, Nucl. Phys. A221, 573 (1974).

Table A-1 Excitation functions for ${}^3\text{H}(\alpha, {}^6\text{Li})\text{n}$ at 0° (lab). The data are presented as c.m. differential cross sections $\sigma_{\text{c.m.}}$, along with their total standard deviations Δ , for the reaction ${}^6\text{Li}(\text{n}, \text{t}){}^4\text{He}$ at c.m. angles of 0° and 180° and at lab neutron energies E_{n} . The uncertainty in E_{n} is ± 3 keV. The data have been corrected for multiple scattering and beam energy spread.

E_{n} (keV)	$\theta_{\text{c.m.}} = 0^\circ$		$\theta_{\text{c.m.}} = 180^\circ$	
	$\sigma_{\text{c.m.}}$ (mb/sr)	Δ (%)	$\sigma_{\text{c.m.}}$ (mb/sr)	Δ (%)
87	90.9	3.0	---	---
113	103.9	3.2	---	---
140	122.9	2.6	31.0	5.7
165	179.4	2.6	71.8	3.7
191	259.8	2.3	150.0	3.0
204	341.8	2.7	210.6	2.9
218	409.9	1.8	268.2	2.3
232	496.1	2.0	348.6	2.4
244	499.8	2.8	380.6	3.1
257	438.1	2.8	375.6	2.9
270	371.2	2.8	345.8	2.9
296	233.5	2.4	232.3	2.8
322	175.7	2.4	148.3	2.9
398	84.1	2.7	---	---

of each datum point varied from a few percent at the ends of the region to approximately 0.5% in the middle of the region. The systematic error is $\pm 1.7\%$. The neutron energy resolution achieved is approximately $1.4 E^{3/2}$ and the accuracy of the neutron energy scale is given by $\pm 0.060 E \sqrt{1.79 E + 0.75}$ keV where E is in MeV. The data have been corrected for the minor isotopic impurities present in each enriched sample. These data have been forwarded to the National Neutron Cross Section Center at Brookhaven.

The high statistical accuracy of, for example, the ^{11}B has revealed fine structure (peak to valley fluctuations of a few percent) at high excitation energy (around 9 MeV) that correlates with structure observed in charged-particle measurements. The ^{11}B data are presented in Fig. A-2. There are also indications of additional structure that have not been previously seen in the ^{12}B compound nucleus at this excitation energy.

3. Simulation of (n,p) Cross Sections Using Charged Particle Reactions (Britt, Gavron, Goldstone, Schoenmackers, Wilhelmy)

We have begun a study of the feasibility of using direct charged particle reactions as a method for generating simulated neutron induced cross sections. To date our efforts have centered on the n,p reactions. We have measured the probability of proton emission, P_p , as a function of nuclear excitation energy for ^{91}Nb , ^{90}Y and ^{89}Y . These excited nuclei have been produced using the (t, α) reaction on the appropriate targets. The recorded α particle energy defines the residual nuclear excitation energy and the simultaneous measurement of an evaporated proton enables us to determine the probability that the nucleus, from a particular excitation energy, will deexcite by proton emission. The measured proton emission probabilities as a function of nuclear excitation energy are then converted to equivalent n,p cross sections by simply multiplying by the appropriate nonelastic neutron reaction cross section.

The initial reaction studied was the $^{92}\text{Mo}(t,\alpha)^{91}\text{Nb}^*p$. The nucleus ^{91}Nb is a very favorable case for proton emission since it has a high neutron binding energy (12.1 MeV) and a low proton binding energy (5.2 MeV). In the excitation energy region between 5.2 and 12.1 MeV, neutron emission is energetically forbidden and the only substantial de-excitation mode available to the nuclei are gamma decay and proton emission. In this case the proton emission probability reaches the very high level of $P_p \sim 0.35$ at excitation energies near the neutron binding energy. At energies above B_n the neutron channels begin to be important and there is a decrease in the value of P_p . The results obtained from this reaction along with earlier measurements for the $^{91}\text{Zr}(^3\text{He},t)^{91}\text{Nb}^*$ reaction are shown in Fig. A-3. This is a case of possible practical

importance for determining structural damage in fusion reactor environments. To obtain further information that may be of value in calculations of radiation damage effects, we are also able to record the proton emission spectrum as a function of nuclear excitation energy.

We have also measured the proton emission probability from the ^{90}Y nucleus. The neutron and proton binding energies in ^{90}Y are very similar and therefore the Coulomb barrier causes proton emission to be inhibited. However, the nucleus ^{89}Y has a neutron binding energy which is 4.4 MeV above its proton binding energy. Therefore, a reachable "proton window" in ^{90}Y corresponds to excitation energies which allow the evaporation of a neutron from ^{90}Y to the excitation energy gap between B_p and B_n in ^{89}Y . In this case the $^{91}\text{Zr}(t,\alpha)^{90}\text{Y}^*p$ direct reaction simulates the $^{89}\text{Y}(n,p)^{89}\text{Sr}$ cross section which has been measured radio-chemically. However, as can be seen in Fig. A-4, the "proton window" really exists for proton emission from ^{89}Y to form ^{88}Sr . Thus the $^{89}\text{Y}(n,np)^{88}\text{Sr}$ reaction dominates the proton emission process. Unfortunately, the more abundantly formed ^{88}Sr can not be measured radio-chemically since ^{88}Sr is a stable isotope.

Figure A-5 shows our measured proton emission probability for the excited nucleus ^{90}Y . One important thing to note is that even with the very low proton emission probability below 16 MeV excitation energy we are able to obtain adequate statistical accuracy. Once above 16 MeV excitation there is a rise in the P_p value up to the highest excitation energy measured. We have translated these P_p determinations to equivalent $^{89}\text{Y}(n,p+np)$ cross sections by multiplying P_p by optical model calculated nonelastic neutron reaction cross sections. The results are shown on the bottom of Fig. A-5 along with the experimentally measured $^{89}\text{Y}(n,p)^{89}\text{Sr}$ data. The comparison is very gratifying in that it gives experimental credibility to this general charged particle simulation approach. At the lowest region of data overlap the simulated and direct neutron measurement agree. However, as the equivalent neutron bombarding energy is increased the charged particle simulated values diverge from the direct neutron measurements, possibly indicating that at the higher equivalent neutron bombarding energies a substantial fraction of the proton emission probability is coming from what would be the $^{89}\text{Y}(n,np)^{88}\text{Sr}$ reaction. We have also used the $^{90}\text{Zr}(t,\alpha)^{89}\text{Y}^*$ reaction to directly produce the excited ^{89}Y nucleus. In this case the energy difference between the proton and neutron binding energies is 4.4 MeV (as compared with 6.9 MeV for ^{91}Nb) and, therefore, the proton emission probability only reaches a peak of $\sim .05$ as compared with the value of $\sim .35$ in ^{91}Nb .

We believe that these results demonstrate the feasibility of using the (t,α) reaction for generating simulated neutron cross sections in medium mass nuclei. Further experiments are planned to try to extend

the energy range of the measurement, by using higher energy tritons. We also plan to study other targets of practical interest and to carefully study a few cases where $\sigma(n,p)$ is known so that the absolute reliability of the technique can be evaluated.

5. Planned Neutron Capture Cross Section Measurements on Highly-Radioactive Samples by Means of a Nuclear Explosion Source
(Silbert)

We have been exploring methods of measuring neutron capture cross sections of small (~ 1 mg) and highly radioactive samples. Accordingly, plans are being made to measure the capture cross section of a small (1 mg) highly-radioactive (14 Ci) sample of ^{88}Y ($T_{1/2} = 107$ d) in the keV region by employing a nuclear explosion as an intense, single-pulse source at a 15-m flight path, by the time-of-flight technique.² If backgrounds can be suppressed sufficiently, such an experiment utilizing fluor-photomultiplier detectors should be possible. The ^{88}Y sample emits two hard gamma rays per decay, and laboratory measurements would be overwhelmed by this intrinsic gamma-ray flux. In addition, the small size of the available sample would preclude the use of conventional neutron sources.

It is hoped that this technique can also be applied to a small sample of ^{242}Am ($T_{1/2} = 152$ yr), in which the capture measurement would be carried out in competition with the neutrons and gamma rays emitted by the (n,f) reaction, which is expected to have a larger (perhaps 10 x) cross section than the capture cross section.

6. Neutron Capture Cross Sections (Drake, Malanify)

In collaboration with R. L. Macklin (ORNL) we are analyzing Tm capture cross sections for neutrons from 3.7 keV to 3 MeV. We have preliminary results for the continuum part of this neutron energy range. Samples of lutetium, ^{191}Ir , and ^{193}Ir are being fabricated and beam time has been scheduled at the Oak Ridge Electron Linear Accelerator (ORELA) for similar measurements on these isotopes.

7. Unresolved Resonance Parameters for ^{235}U (Keyworth, Moore, Moses; Dabbs and Hill (ORNL))

Several statistical analyses of the fission cross section of ^{235}U have suggested that the well-known fluctuations are due to intermediate structure in fission. If this is the case, then each of the

² "Time-of-Flight Neutron Spectroscopy Using 20-Meter Flight Paths to a Nuclear Device," L. Forman, M. G. Silbert, and A. D. Schelberg, Nucl. Instr. Meth. 128, 607 (1975).

intermediate structure fluctuations should be characterized by a definite compound nucleus spin, as demonstrated by Keyworth, et al.³ for ^{237}Np .

Data obtained on the ORELA in 1974, using the polarized-neutron and polarized-target technique, have been reduced to obtain spin-separated fission cross sections of ^{235}U below 30 keV. The resolved resonance region has been analyzed by shape and area analysis to obtain an improved set of resonance parameters for each spin state. Using the average parameters obtained from the resolved resonance region, we have analyzed these data and capture and fission data measured by others from 0.1 to 30 keV to obtain unresolved s-wave resonance parameters. The average fission widths $\langle\Gamma_{f3}\rangle$ and $\langle\Gamma_{f4}\rangle$ are shown, as a function of neutron energy, in Figs. A-6 and A-7. The non-random behavior of the fluctuations suggests that intermediate structure may be important in both spin states. The analysis is not unique, however, and the results depend strongly on plausible assumptions about the relative constancy of the neutron strength functions for the two s-wave spin states.

8. Measurements of $^{238}\text{U}(n,3n)$ Cross Sections (Veeseer)

We have measured the $^{238}\text{U}(n,3n)$ cross sections from 14.7 to 27.0 MeV using a liquid scintillator tank with 70% efficiency to detect the emitted neutrons. The method is similar to that which we have used in measuring other (n,2n) and (n,3n) cross sections⁴ except that a sizeable background from fission events emitting three neutrons must be measured and subtracted. The circles in Fig. A-8 show the results. Also shown are the results of a similar measurement⁵ done in France at lower energies (closed symbols) as well as our measurements of the $^{238}\text{U}(n,4n)$ cross section at 21 and 22 MeV (triangles).

9. Fission Cross Section of Bk-249 Between 0.7 and 3.0 MeV (Silbert)

Data obtained by LASL experimenters from the underground nuclear explosion Physics-8 have been reduced to yield the

³ G. A. Keyworth, J. R. Lemley, C. E. Olsen, F. T. Seibel, J. W. T. Dabbs, and N. W. Hill, Phys. Rev. C8, 2362 (1973).

⁴ L. R. Veeseer, E. D. Arthur, and P. G. Young, to be published.

⁵ J. Frèhaut and G. Mosinski, Nuclear Cross Sections and Technology (National Bureau of Standards Special Pub. 425, U.S. Government Printing Office, 1975) p. 855.

neutron-induced fission cross section of ^{249}Bk over the threshold region, 0.7 to 3.0 MeV. Fission in the 100 μg sample (prepared and assayed by R. W. Hoff and coworkers at LLL) was measured relative to $^{235}\text{U}(n,f)$. The fission cross section of ^{249}Bk rose from 0.1 b at 0.7 MeV to a plateau of 1.4 b between 1.7 and 3.0 MeV. The half-height position of the threshold was 1.05 MeV. Possible subthreshold fission in ^{249}Bk was obscured by the presence of 2.5 μg of its fissile daughter, ^{249}Cf . A paper on this measurement is scheduled for publication in Nuclear Science and Engineering in May, 1977.

10. Complexity of the Potential Energy Surface for Fission for ^{238}U
(Britt, Gavron, Goldstone, Schoenmackers and Wilhelmy)

For some time we have been puzzling over the interpretation of data on fission probabilities (P_f) for ^{238}U . As discussed in our last report to the Nuclear Data Committee, this is a unique case where we have data from three independent experiments (1) $^{236}\text{U}(t, pf)$ which shows subbarrier resonance structures for $K = 0^+$ bands; (2) $^{238}\text{U}(\gamma, f)$ data which shows subbarrier resonances for $J = 1^-, K = 0$ states and (3) $^{238}\text{U}(\gamma, f)$ data which gives P_f data in the excitation energy range 7-11 MeV. Using our previous hypothesis that fission proceeds through an axially asymmetric first barrier and a mass-asymmetric, axially symmetric second barrier we discovered that resonance fits to the data from (1) and (2) completely determined the barrier parameters. When we then tried to predict the high excitation energy values for P_f we found the calculated values were \sim four times lower than the measurements from (3). This suggested the possibility of additional collective enhancements which would be consistent with an axial deformation at the second barrier.

We communicated this result to the theoretical group of S. G. Nilsson and S. E. Larson at Lund, Sweden and asked them to look into the axial stability of the second barrier. The Lund group has now looked in further detail at the theoretical potential energy surfaces in the vicinity of the second saddle point. The result was rather surprising in that it showed the normal mass asymmetric saddle point was stable toward axial deformations and, thus, could not contribute enough collective enhancement to explain our results, but there appeared an additional second saddle point about 500 keV higher which was axially deformed and probably close to mass symmetric. These two saddle points can be traversed in parallel with the first one dominating the low energy behavior and the second one dominating the high energy behavior. Figure A-9 shows the results of our statistical model calculations with and without the assumption of an additional second saddle point, $E_B^{(2)}$. It is seen that this concept explains the experimental results very nicely.

These results are another indication of the complexity of the potential energy surface associated with fission. Because of the many parameters associated with the theoretical calculations it is not possible for the theoretical groups to completely explore the potential surface and previous calculations had not thought to look for an additional second saddle of this type until the insight gained by attempting to analyze all data in a self consistent manner appeared.

11. Prompt Neutrons from Fission of ^{237}Np (Veaser)

We have measured $\bar{\nu}_p$, the number of prompt neutrons per event, for neutron-induced fission of ^{237}Np . We used a spiral fission chamber to identify the fissions and a liquid scintillator tank with 70% efficiency to detect the fission neutrons. Measurements of $\bar{\nu}_p$ at six energies between 1.0 and 14.7 MeV have an accuracy of about $\pm 2\%$. A least-squares fit to the results gives $\bar{\nu}_p = 2.634 + 0.148 E_n$.

12. Alignment of ^{235}U in the Anti-Ferromagnetic Compound USb (Moses, Keyworth, Moore, Olsen)

We are planning to measure the angular distribution of fragments from the neutron induced fission of ^{235}U for resonances below 100 eV. The purpose of the measurements is to determine the K quantum number, or the mixture of K, for individual resonances. Such measurements have been carried out in the past, notably by Pattenden and Postma,⁶ but the interpretation of their results is ambiguous due to poor energy resolution and limited nuclear orientation in their target.

We hope to produce a very highly aligned ^{235}U target by the interaction of the hyperfine field of the anti-ferromagnetic compound USb with the magnetic moment of ^{235}U nuclei at low temperatures. We are presently pursuing targets in the form of foils thin enough to allow fission fragments to escape. We hope to measure the degree of nuclear alignment produced in such foils by detecting alpha particles from ^{235}U at low temperatures.

If this approach is successful we will fabricate a target consisting of a number of foils, each $\sim 1\text{-mg/cm}^2$ thick, and a number of solid state detectors. The actual measurements using neutron induced fission will be made at the new Weapons Neutron Research (WNR) Facility at the Los Alamos Meson Physics Facility. The unusually high neutron fluxes available with relatively long pulse lengths (.25 to 1 μs) at the WNR Facility will be particularly beneficial in this low count rate experiment. The measurements will be made using a neutron flight path of 35 meters.

⁶ N. J. Pattenden and H. Postma, Nucl. Phys. A167 (1971) 225.

13. Tritium Production from ${}^6\text{Li}(n,\alpha)$ and ${}^7\text{Li}(n,n'\alpha)$ Reactions
(Ragan, Hemmendinger, Shunk, Ellis)

We have performed integral measurements of the tritium production in ${}^6\text{Li}$ and ${}^7\text{Li}$ samples positioned at various radii in a 30-cm radius ${}^6\text{LiD}$ (95% ${}^6\text{Li}$) sphere. The sphere was irradiated by $\sim 10^{16}$ 14-MeV neutrons produced at the center by the $\text{T}(d,n)$ reaction. The tritium analysis, done by Teledyne Isotopes, Westwood, NJ, was accomplished by heating crushed ampules and converting the evolved hydrogen to water. The water was subsequently converted back to hydrogen and the tritium decay rate determined in a gas proportional counter. The processing included quantitative separation of the water sample into several parts so that a number of independent counts could be made. We established Teledyne's accuracy of tritium content in LiH contained in quartz ampules both by test irradiations in a known thermal-neutron fluence and by two cross-checks with the NBS Radiation Standards Section.

Preliminary results for both lithium isotopes appear in Table A-2, which shows specific tritium production as a function of radius in the spherical assembly of ${}^6\text{LiD}$ surrounding the 14-MeV source.

Table A-2

Tritium Production in LiH in a Spherical Assembly of ${}^6\text{LiD}$
Surrounding a Point Source of 14-MeV Neutrons

Radius r [mm]	Tritium Production [$4\pi r^2 \times 10^{-22}$ atoms \cdot (atom Li) $^{-1}$ \cdot (neutron) $^{-1}$]	
	${}^6\text{Li}$ (95.50%)	${}^7\text{Li}$ (99.91%)
50.0	0.344	0.309
76.15	0.504	0.301
126	0.823	0.252
200	0.793	0.209
300	0.308	0.121

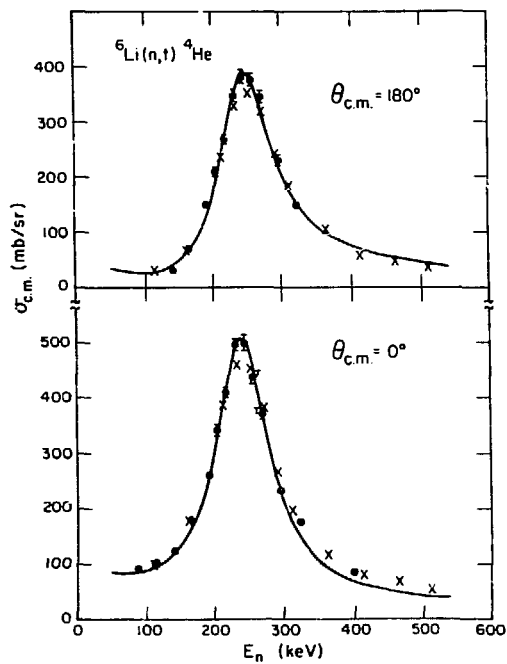


Figure A-1. Excitation function for ${}^3\text{H}(\alpha, {}^6\text{Li})\text{n}$ at 0° and 180° (c.m.). Our data are the solid circles, the crosses are the normalized data of Overley, and the curve is an R-matrix fit.

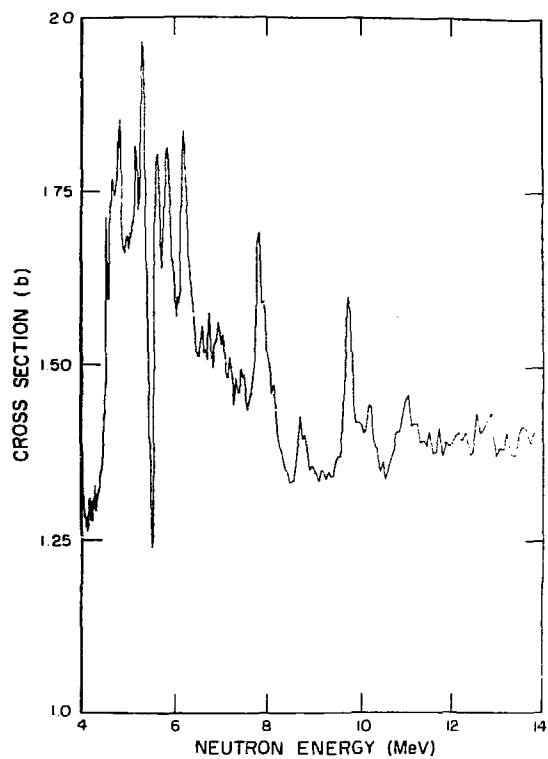


Figure A-2. Total cross section of ^{10}B from 4 MeV to 13.5 MeV. Note the suppressed zero origin on the vertical scale. The data have been averaged over five channels.

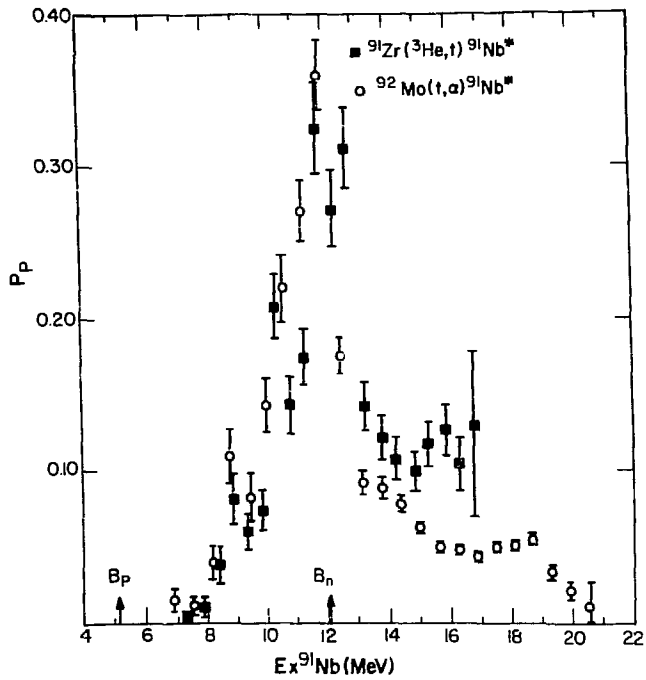


Figure A-3. Experimental proton emission probability in ^{91}Nb following its formation with two different direct reactions.

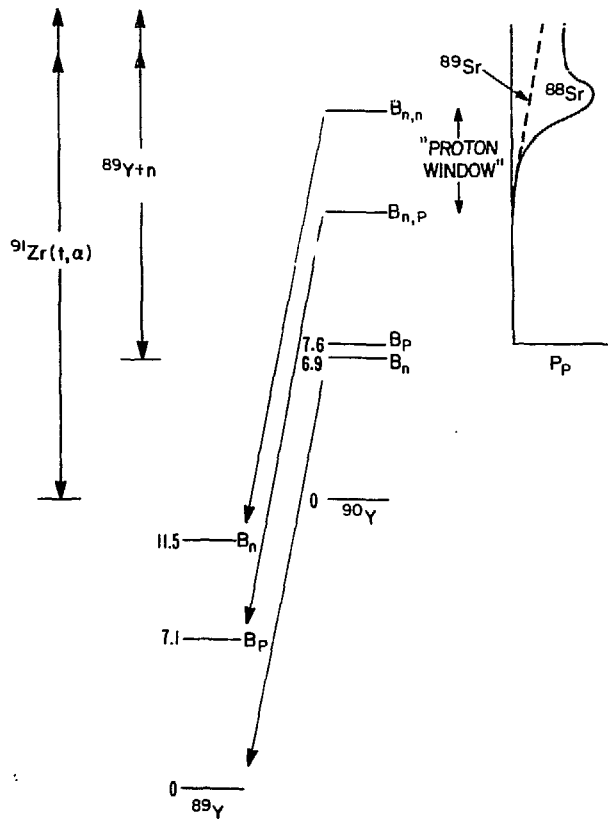


Figure A-4. Energetics of the ^{89}Y and ^{90}Y system emphasizing the region of high proton emission probability.

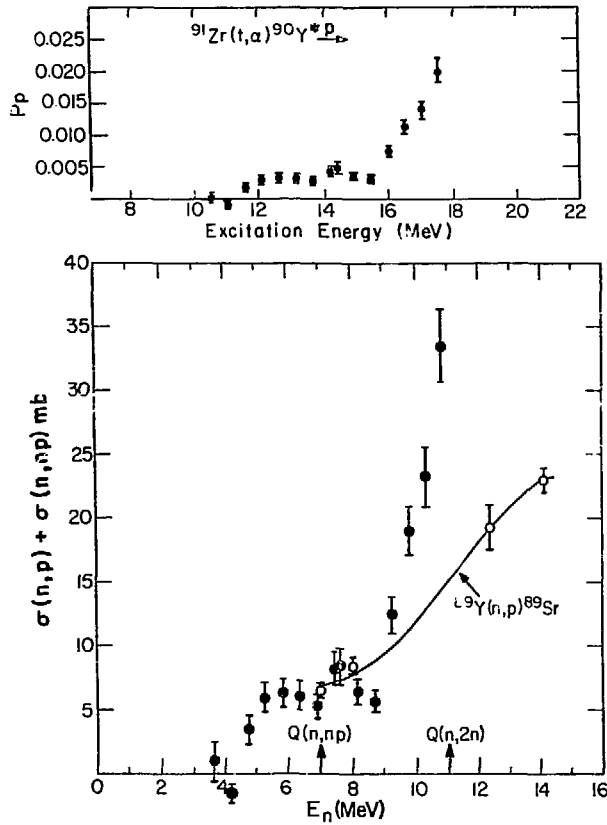


Figure A-5. Proton emission probability as a function of excitation energy in ^{90}Y (top). The charged particle simulated cross section for the $^{89}\text{Y}(n, p + n, np)$ reaction (closed circles) as a function of neutron bombarding energy (bottom). The open circles and solid line are the literature values for the $^{89}\text{Y}(n, p)^{89}\text{Sr}$ cross section.

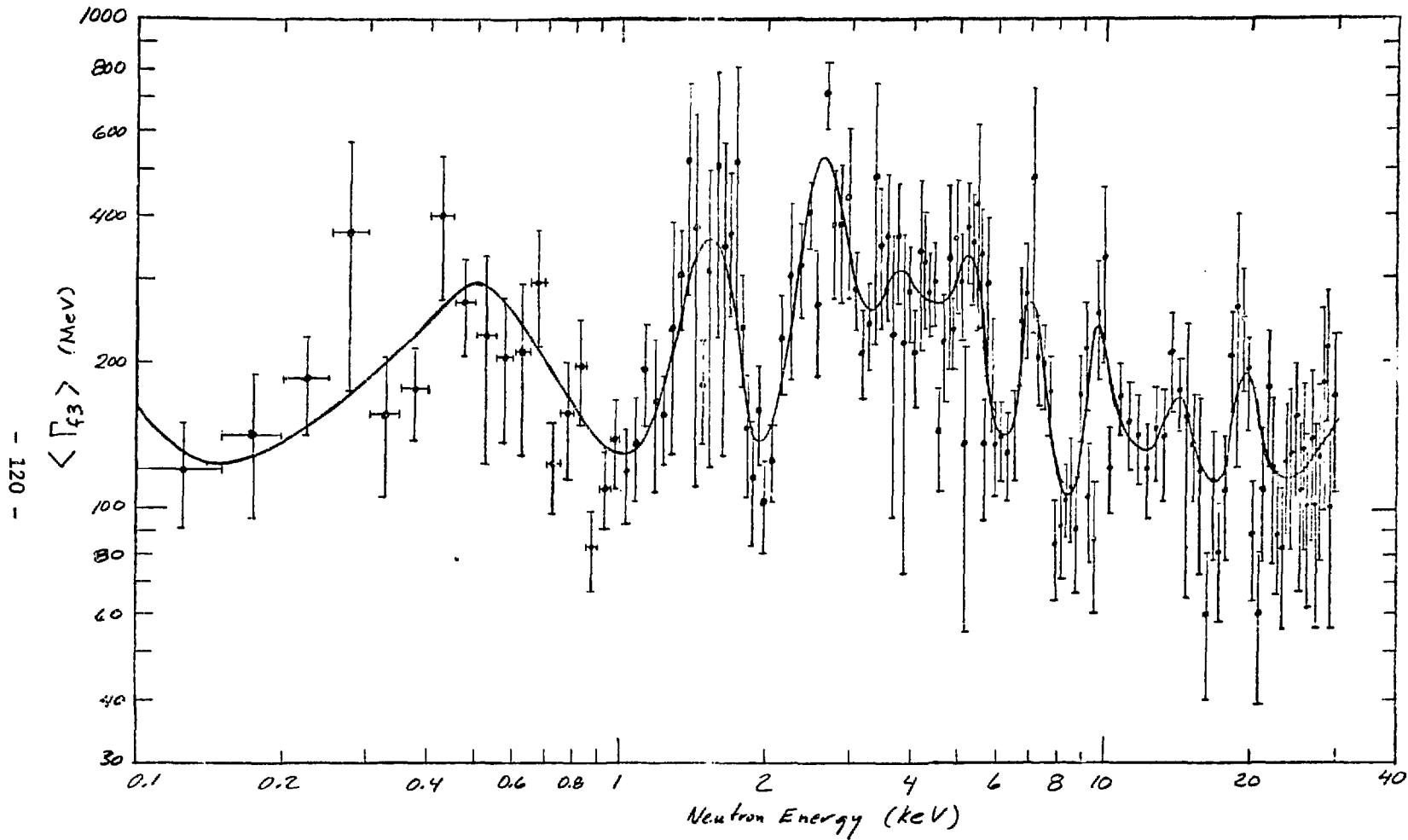


Figure A-6. Average fission width for spin 3^- s-wave neutron-induced resonances in $(^{235}\text{U}+n)$ between 0.1 and 30 keV.

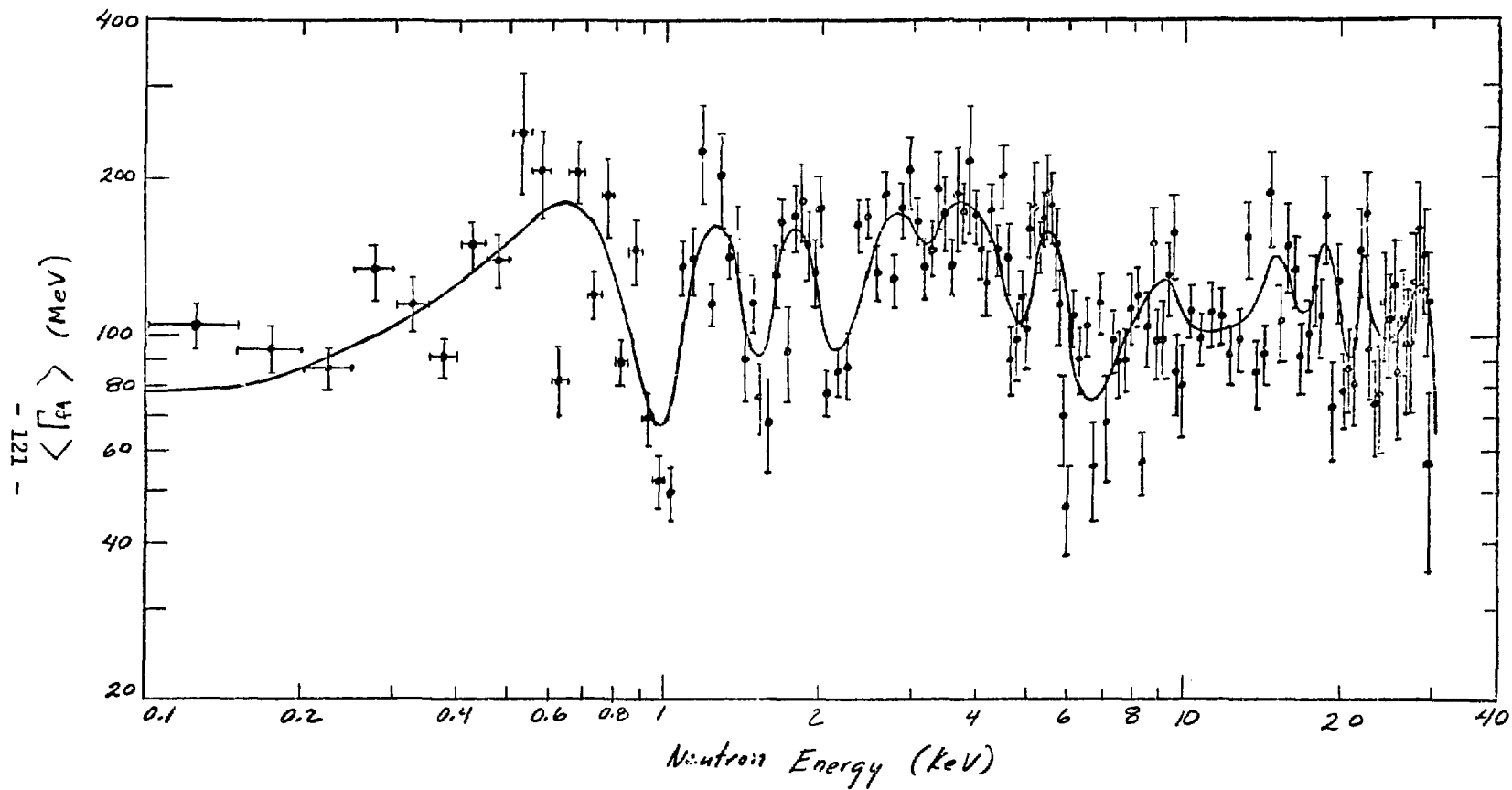


Figure A-7. Average fission width for spin 4^- s-wave neutron-induced resonances in $(^{235}\text{U}+n)$ between 0.1 and 30 keV.

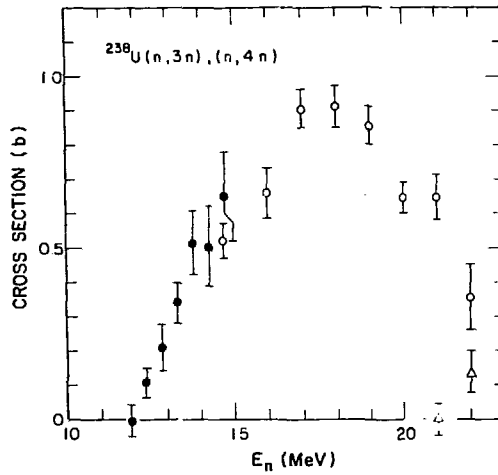


Figure A-8. Cross sections for $^{238}\text{U}(n,3n)$ [round symbols] and for $^{238}\text{U}(n,4n)$ [triangles]. Closed symbols show the results of Frehaut and Mosinski⁵ and open symbols are this work.

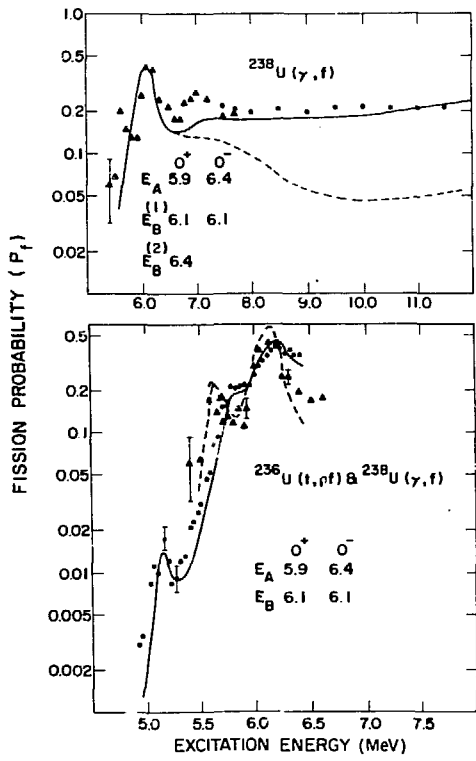


Figure A-9. Fits to ^{238}U fission probability data using microscopic statistical models. Bottom -- resonant fits to low energy (t,pf) [solid circle, solid line] and (γ ,f) [solid triangles, dashed line] data. Top -- dashed curve is non-resonant fit to the photofission data assuming only a mass asymmetric second barrier, $E_B(1)$; solid curve is a fit to the same data assuming an additional axial asymmetric barrier, $E_B(2)$. The listed barrier heights (in MeV) are for the lowest $K = 0^+$ and 0^- channels available at the indicated saddle points.

B. Other Nuclear Data

1. Accurate Measurement of the Proton-Proton Elastic Scattering at 19.700 MeV (Jarmie, Jett)

Proton-proton scattering cross sections have been measured at 19.700 ± 0.015 MeV with a relative error of about 0.4% and a scale error of 0.4%. Thirteen measurements were made in a range of center-of-mass angles of 20° to 90° . The results are presented in Fig. B-1, together with the earlier data of Yntema and White.¹

2. H(t,t)H Scattering at Low Energies (Haglund, Fick, Schmelzbach, Ohlsen, Jarmie, and Brown)

We have measured angular distributions of the differential cross section and vector analyzing power for $H + \bar{t}$ elastic scattering, at center-of-mass energies 1.26, 1.68, 2.19, 2.70, 3.21, and 3.71 MeV. A preliminary phase shift analysis of the data confirms the importance of the tensor and add spin-orbit nucleon-nucleon forces in model calculations for the ${}^4\text{He}$ system in this energy range.

3. ${}^4\text{He}(t,t){}^4\text{He}$ Elastic Scattering (Jarmie, Ohlsen, Hardekopf, Brown, Haglund)

We have investigated multiple scattering corrections for the cross section and analyzing power experiments and the analysis of our data is now complete. In addition to the cross section data presented last year, we have measured analyzing powers as shown in Figs. B-2, B-3, and B-4. The accuracy of these data is ± 0.007 . The combined set of cross sections and analyzing powers will be used to investigate the properties of the ${}^6\text{Li}(n,\alpha)\text{T}$ reaction near the 240 keV resonance by means of an R-matrix analysis. This reaction is of importance in fusion reactor design as well as a neutron standard. A preliminary report of our work has been published.²

4. Analyzing Power in $\bar{t} + {}^3\text{He}$ Elastic Scattering (Jarmie, Haglund, Brown, Hardekopf, and Ohlsen)

As part of a study of the mass-6 system, we have measured angular distributions of the vector analyzing power A_y in $\bar{t} + {}^3\text{He}$ elastic scattering at lab energies of 9.02, 11.05, 13.02, 15.02, 16.05, and

¹ J. L. Yntema and M. G. White, Phys. Rev. 95 1226 (1954).

² R. A. Hardekopf, et al., Los Alamos Scientific Laboratory report LA-6188.

17.02 MeV for c.m. angles between 25° and 155° . Also, excitation functions over the range 14.40 to 17.20 MeV were obtained at c.m. angles 45° , 75° , 105° , and 135° . The experimental method was as follows. A ^3He gas target was bombarded with 77% polarized tritons from the LASL polarized-triton source.³ Scattered tritons were detected in ΔE -E telescopes while recoil ^3He particles were simultaneously detected by recording the singlespectra of the ΔE detectors.

5. Scattering of Polarized Tritons by ^9Be and ^{12}C (Schmelzbach, Hardekopf, Haglund, and Ohlsen)

The differential cross section and the analyzing power A_y for $^9\text{Be}(\vec{t}, t)^9\text{Be}$ and $^{12}\text{C}(\vec{t}, t)^{12}\text{C}$ elastic scattering have been measured at 15 and 17 MeV over the angular range $\theta_{\text{lab}} = 17.5^\circ$ - 165° . The data in the forward hemisphere have been analyzed with a standard optical model. A large depth and conventional geometry parameters for the spin-orbit potential have been found. The results of this analysis are in general agreement with previous work involving polarized tritons and heavy target nuclei, but show important differences with investigations of the scattering of polarized helions on light nuclei. The observed analyzing powers are shown in Figs. B-5 and B-6.

6. States in ^{126}Sb Populated in the β Decay of 10^5 -yr ^{126}Sn (Smith, Bunker, Starner, Orth, Löbner)

We have investigated⁴ the low-energy level structure of the odd-odd nucleus ^{126}Sb by studying the radioactive decay of the long-lived fission product ^{126}Sn (10^5 yr). In the simplest version of the shell model, in which all residual interactions are ignored, the multiplet of states in an odd-odd nucleus that arise from a given proton and neutron configuration are degenerate in energy. However, an effect of both the long-range collective interactions and the short-range neutron-proton interaction is to break this degeneracy, and it is therefore important to establish the systematic trends in the energy ordering of the lowest levels in these nuclei in order that various theoretical formulations of the residual-force interactions can be tested against experiment.

Based on our conversion-electron and γ -ray singles data, γ - γ and γ - e^- prompt and delayed coincidence measurements, and complementary

³ R. A. Hardekopf, Proc. 4th Int. Conf. on Polarization Phenomena in Nuclei, Zurich, Sept. 1975 (Bukhouser Verlag, Basel and Stuttgart 1976) p. 865.

⁴ H. A. Smith, Jr., M. E. Bunker, J. W. Starner, C. J. Orth, and K. E. G. Löbner, Phys. Rev. C13, 387 (1976).

γ -ray energy and intensity balance arguments, an essentially complete decay scheme for ^{126}Sn has been deduced. Also, firm spin and parity assignments have been made for all six of the observed ^{126}Sb levels, significantly extending the systematics of the low-lying energy levels of the odd-odd antimony ($Z=51$) nuclei.

Aside from its basic nuclear structure value, accurate knowledge of the decay radiations of a long-lived fission product such as ^{126}Sn is of value to those concerned with nuclear waste processing and storage, as well as with associated long-range environmental effects. The ^{126}Sn daughter activities, ^{126}Sb (12.4 d) and $^{126}\text{Sb}^m$ (19.0 m) are also under study.

7. Evaporation Residues from the $^7\text{Li},\alpha$ Reaction on ^{197}Au and ^{232}Th
(Britt, Gavron, Goldstone, Schoenmackers, and Wilhelmy)

Considerable effort has gone into the measurement of fission probabilities $P_f = \langle \Gamma_f / (\Gamma_f + \Gamma_n + \Gamma_\gamma) \rangle$ as a function of excitation energy. In these experiments reactions such as ($^3\text{He},d$) were used to produce compound nuclei with excitation energies up to ~ 12 MeV, and the ratio of the coincidence ($^3\text{He},df$) cross section to the singles ($^3\text{He},d$) cross section defined the fission probability. The data yield a direct determination of Γ_n/Γ_f as a function of excitation energy; furthermore, an analysis of P_f with a statistical model allows a determination of the fission barrier parameters.^{5,6}

Recently we attempted to extend the measurements of P_f above ~ 12 MeV excitation by using reactions induced by Li ions, such as ($^6\text{Li},\alpha$) or ($^7\text{Li},\alpha$). These measurements are difficult since at excitation energies above the second chance fission threshold, particularly for targets with $Z > 92$, P_f approaches 1; systematic errors of the order 10% such as present in the previous measurements⁵ then lead to large uncertainties in Γ_n/Γ_f . Preliminary results using 39 MeV ^6Li and ^7Li beams indicated additional experimental problems. In particular, the measured fission probabilities for ($^6\text{Li},\alpha f$) and ($^7\text{Li},\alpha f$) reactions were much lower than expected, indicating that Coulomb breakup and/or reactions on non-fissionable contaminants in the targets generated large contributions to the measured singles ($^6\text{Li},\alpha$) and ($^7\text{Li},\alpha$) cross sections.

⁵ A. Gavron, H. C. Britt, E. Konecny, J. Weber, and J. B. Wilhelmy, Phys. Rev. C 13, 2374 (1976).

⁶ A. Gavron, H. C. Britt, P. D. Goldstone, R. Schoenmackers, J. Weber, and J. B. Wilhelmy, to be published.

It is, however, possible to determine P_f and Γ_n/Γ_f accurately if the cross sections for both fission and neutron evaporation are measured. Then for the (${}^7\text{Li},\alpha$) reaction, for example, Γ_n/Γ_f can be simply obtained from the ratio $\sigma({}^7\text{Li},\alpha xn)/\sigma({}^7\text{Li},\alpha f)$. We have performed initial experiments to measure the cross sections for evaporation residue production following the (${}^7\text{Li},\alpha$) reaction on ${}^{197}\text{Au}$, ${}^{232}\text{Th}$, and ${}^{236}\text{U}$ at $E_{{}^7\text{Li}} = 34$ MeV. The gold target was chosen since at the obtained excitation energies $P_f = 0$; thus the "evaporation residue probability," P_{er} , defined as the ratio $\sigma({}^7\text{Li},\alpha xn)/\sigma({}^7\text{Li},\alpha)$ should be unity.

The measured angular correlation of the evaporation residues is roughly gaussian and centered about the recoil angle determined by the kinematics of the (${}^7\text{Li},\alpha$) reaction. Typical angular correlations from the ${}^{197}\text{Au}({}^7\text{Li},\alpha xn)$ reaction are shown in Fig. B-7 for three excitation energy bins in the excited compound nucleus ${}^{200}\text{Hg}$. The evaporation residue cross section is obtained for each excitation energy bin simply by integrating the angular correlation. For each of the three excitation energy bins shown in Fig. B-7 we obtain a value of $P_{er} = 0.98 \pm 0.05$, indicating that (1) breakup contributions to the singles spectrum are unimportant at this bombarding energy, and (2) the efficiency for detecting the low-energy recoiling heavy ions is very close to unity. (The distributions in Fig. B-7 have different peak values but also have different widths and thus all integrate to the same value.) For ${}^{232}\text{Th}$, the analysis is not so straightforward, since for higher excitation energies the singles spectrum contains contributions from the (${}^7\text{Li},\alpha$) reaction on the carbon backing of the target, and the P_{er} defined by a ratio of the coincidence and singles cross sections is more difficult to interpret. However, for low excitation energies (10-15 MeV) where the contaminants are negligible we obtain $P_{er} = 0.65 \pm .05$. This is consistent with the value of $P_{er} = 0.69$ obtained if Γ_n/Γ_f values taken from systematics⁷ are assumed. In this case we plan also to measure the ${}^{232}\text{Th}({}^7\text{Li},\alpha f)$ cross section to uniquely determine Γ_n/Γ_f for the higher excitation energies.

8. Angular Distribution of Fission Fragments from the Spontaneous Fission of ${}^{253}\text{Es}$ (Moses, Keyworth, Hoffman)

The angular distribution of fission fragments from a state of known total angular momentum I and magnetic quantum number M can be expected to give a value (or distribution of values) of K , the projection of I on the nuclear symmetry axis. For a nucleus in its ground state I is of course known, and the value of M can be restricted by nuclear orientation techniques. To study the role of K in spontaneous

⁷ R. Vandenbosch and J. R. Huizenga, Nuclear Fission (Academic Press, New York, 1973) p. 227.

fission, we are attempting to measure the angular distribution of fragments from the spontaneous fission of oriented ^{253}Es .

We have produced highly aligned Es nuclei by substituting them into the surface layers of a crystal of neodymium ethyl-sulfate, and cooling the crystal to temperatures below 100 mK in a ^3He - ^4He dilution refrigerator. The degree of alignment is monitored by observing the change in the rate of alpha-particle emission along known crystal axes as the sample is cooled. We will detect fission fragments from these sources by exposing a polycarbonate (Lexan) film to the cooled sample, then etching the film to render the tracks visible under a microscope. This technique gives nearly perfect discrimination against the background of alpha particles, and is highly efficient, since it permits us to detect essentially all of the fragments emitted into 2π steradians.

9. Muonic X-Ray Measurements of Nuclear Charge Radii in the Mass-60 Region (Shera, Wohlfahrt)

The x rays emitted when a negative muon is captured by an atomic nucleus provide a very sensitive tool for investigating the nuclear charge distribution. As part of a continuing muonic x-ray program, the muonic $2p_{3/2} \rightarrow 1s_{1/2}$ and $2p_{1/2} \rightarrow 1s_{1/2}$ transition energies for the 16 separated isotopes Fe-54,56,57,58, Co-59, Ni-58,60,61,62,64, Cu-63,65 and Zn-64,66,68,70 have been measured in the stopped-muon channel of LAMPF. Subsets of three different nuclides were measured simultaneously to extract precise values of isotope and isotone shifts. Equivalent-charge-radii differences between isotopes were determined from the Ford-Wills radial moments $\langle r^{1.55} \rangle$ with accuracies of about $\pm 10^{-3}$ fm. Details of the measurements, together with results for all isotopes, appear in Ref. 8. Isotope shift data for all the nuclei studied are summarized in the lower half of Fig. B-8, in which values for the differences in charge radii, ΔR_k , between isotopes differing by both $\Delta n=1$ and $\Delta n=2$ are plotted. The isotope shift values are plotted below the isotope pairs (in the upper half of the figure) to which they correspond. Two effects are readily apparent: 1) The isotope shifts between even nuclei ($\Delta n=2$) form an approximately linear sequence--strikingly independent of Z--as n increases from 28 to 40. The cause of this systematic behavior is not presently understood. 2) A pronounced even-odd staggering exists for the $\Delta n=1$ shifts. This effect, which has been observed in other optical and muonic isotope shift studies, is also evident in our isotone shift data. Detailed Hartree-Fock predictions of the nuclear charge distribution of these nuclei are also presented in Ref. 8.

⁸ E. B. Shera *et al.*, Phys. Rev. C14, 731 (1976).

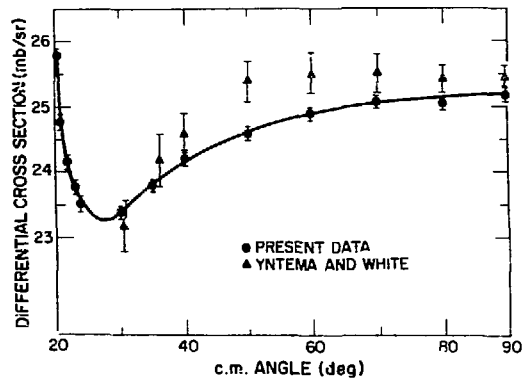


Figure B-1. Proton-proton scattering cross sections at 19 MeV.

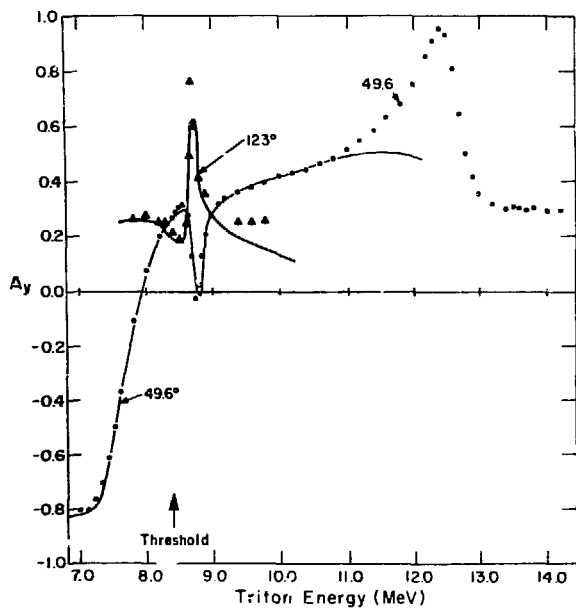


Figure B-2. Excitation function for the ${}^4\text{He}(t,t){}^4\text{He}$ analyzing power.

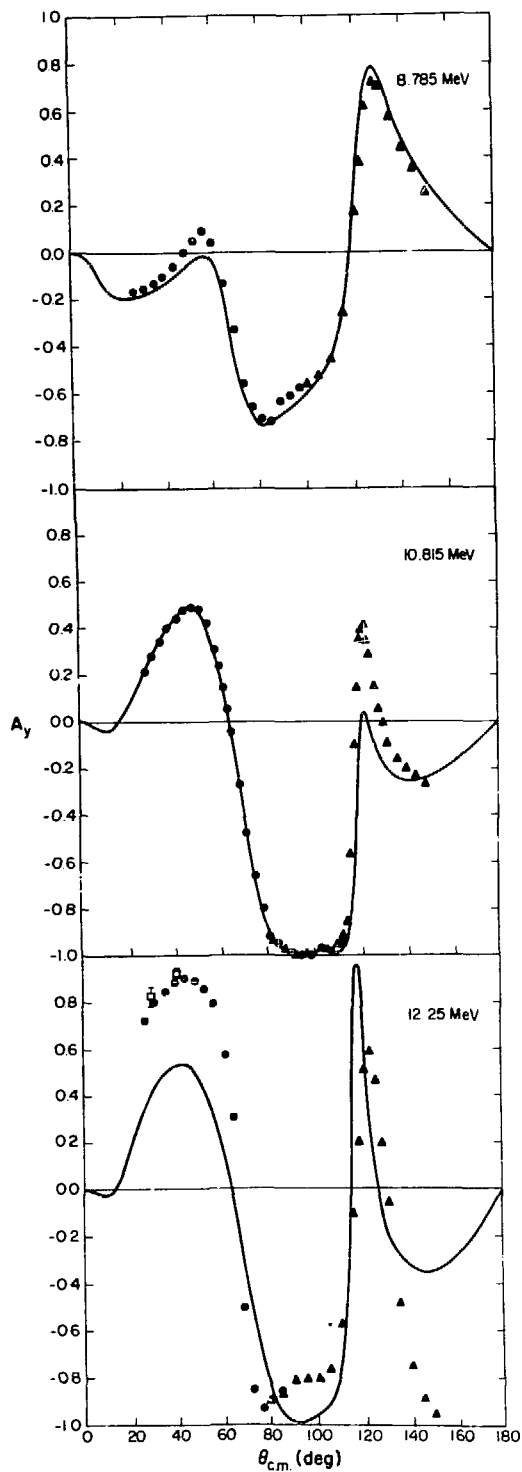


Figure B-3. Angular distributions of the analyzing power for ${}^4\text{He}(t,t){}^4\text{He}$ elastic scattering. The open square points at low angles at 12.25 MeV are from the double-scattering measurements of Keaton et al.

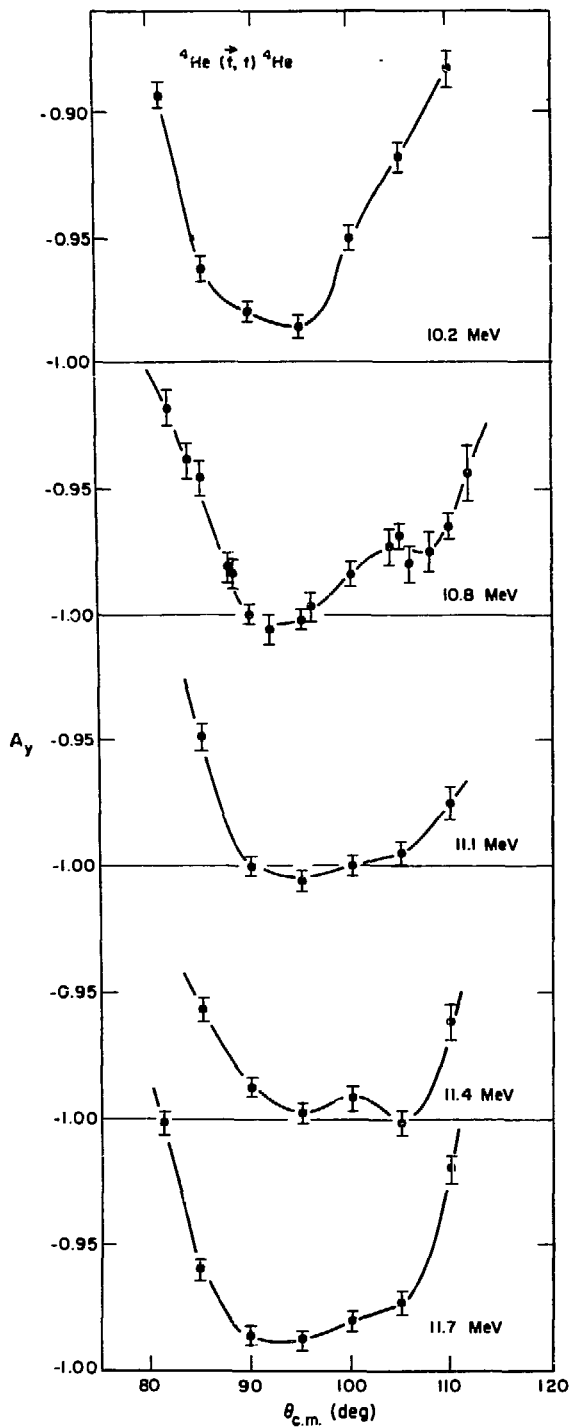


Figure B-4. Angular distributions of the analyzing power for ${}^4\text{He}(t,t){}^4\text{He}$ elastic scattering near $A_y = -1$. Solid lines only connect data points as a visual guide.

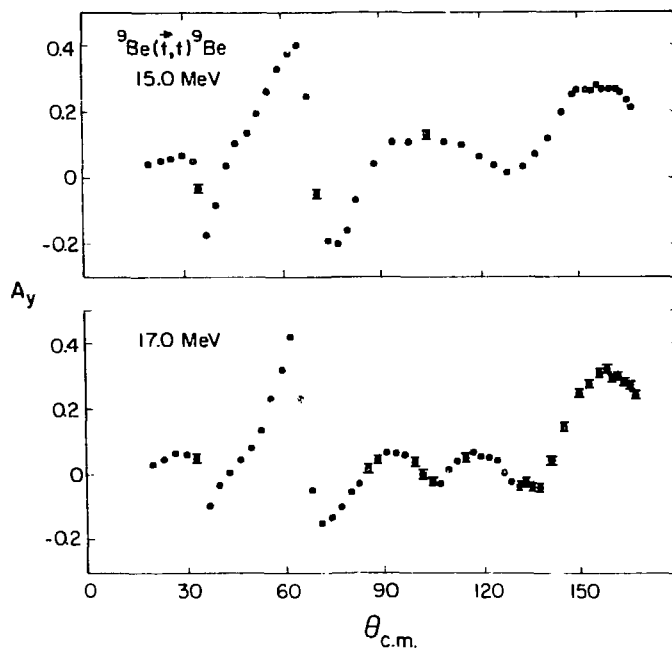


Figure B-5. The analyzing power A_y for the ${}^9\text{Be}(\vec{t},t){}^9\text{Be}$ scattering at 15 and 17 MeV.

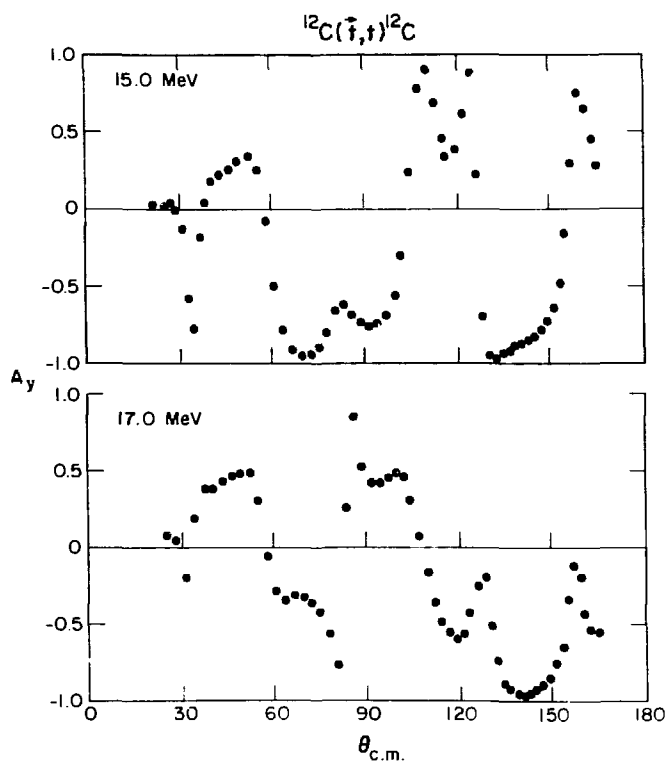


Figure B-6. The analyzing power A_y for the $^{12}\text{C}(\bar{t},t)^{12}\text{C}$ scattering at 15 and 17 MeV.

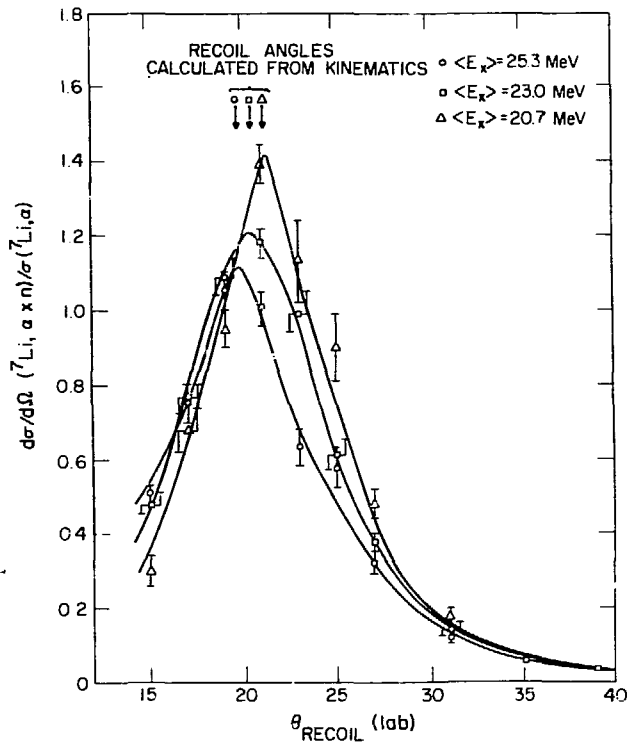


Figure B-7. Evaporation residue angular correlation
 $^{197}\text{Au}(^7\text{Li}, \alpha xn) \theta_\alpha = 120^\circ$.

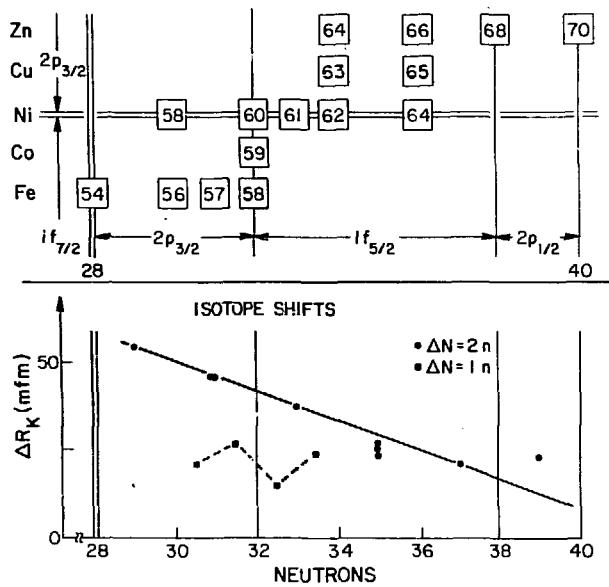


Figure B-8. Isotope shift results for Fe, Co, Ni, Cu, and Zn nuclei.

C. EVALUATIONS

1. Light-Element Standards (Hale, Stewart, and Young)

The evaluation of the neutron cross sections for ^{10}B has been modified somewhat to accommodate changes in the preliminary $^{10}\text{B}(n,\alpha\gamma)$ cross-section measurements of Schrack.¹ The main effect of the changes is that the calculated $^{10}\text{B}(n,\alpha\gamma)$ cross section decreases less rapidly with energy above 500 keV. We are currently preparing complete ENDF/B files for both ^{10}B and ^6Li that incorporate the R-matrix results, and which contain detailed covariance information for the cross sections below 1 MeV.

A report has been issued² that describes in detail the light element standard cross sections included in Version IV of ENDF/B.

2. ^4He System (Hale and Dodder)

In addition to containing several reactions of interest in applications [$^3\text{He}(n,p)\text{T}$, $\text{D}(d,n)^3\text{He}$, and $\text{D}(d,p)\text{T}$], the ^4He system is of interest theoretically since many of its reactions are related by charge symmetry and therefore provide a test of the charge independence of nuclear forces when the data are analyzed in a charge-independent framework.

We have begun a charge-independent R-matrix analysis of reactions in the ^4He system at low energies that uses the isospin 1 ($T=1$) parameters from an earlier analysis of the ^4He system,³ allowing only a single shift (~ 400 keV) of the level energies to allow for Coulomb differences between ^4He and ^4Li . Our present fit, obtained by searching over fewer than 20 $T=0$ parameters, accounts for most of the measured data available for the $\text{T}(p,p)\text{T}$, $\text{T}(p,n)^3\text{He}$, $^3\text{He}(n,p)\text{T}$, and $^3\text{He}(n,n)^3\text{He}$

¹ R. A. Schrack, G. P. Lamaze, O. A. Wasson, and A. D. Carlson, "The $^{10}\text{B}(n,\alpha\gamma)^7\text{Li}$ Cross Section from 5 to 800 keV," Proc. of the International Conference on the Interactions of Neutrons with Nuclei, Lowell, Mass., CONF-760715-P2 (1976) p. 1345.

² G. M. Hale, L. Stewart, and P. G. Young, "Light Element Standard Cross Sections for ENDF/B Version IV," Los Alamos Scientific Laboratory report LA-6518-MS (1976).

³ G. M. Hale, J. Devaney, D. C. Dodder, and K. Witte, "An R-Matrix Analysis of the $p\text{-}^3\text{He}$ Scattering Below $E_p = 19.5$ MeV," Bull. Am. Phys. Soc. 19, 506 (1974).

reactions at energies corresponding to E_p below 5 MeV. The well-established 0^+ resonance at ~ 20.3 -MeV excitation energy, along with its associated threshold effect, shows up clearly in our fits to the $T(p,p)T$ data (see Fig. C-1). In addition, we also confirm the existence of 0^- and 2^- $T=0$ levels at somewhat higher excitations and see evidence of higher 1^+ and 2^+ levels above the energy range over which data are currently being analyzed. We expect to obtain firm information about these levels as the energy range of the analysis increases. Figure C-2 shows the fits to preliminary new ${}^1\text{H}(t,t){}^1\text{H}$ cross section and polarization data⁴ taken recently with the Los Alamos Scientific Laboratory polarized triton source.

Data for the $D(d,n)$ and $D(d,p)$ reactions at deuteron energies below 1 MeV have been added to the two-channel analysis described above. While the cross-section and polarization data for the proton branch of the $D+d$ reaction are adequately represented, the charge-independent fit has difficulty reproducing the larger cross section and 0 to 90° cross-section asymmetry observed for the neutron branch above $E_d = 100$ keV. Although we are able to obtain a slight enhancement of the neutron branch at energies near 1 MeV due to the presence of isospin-one levels, it is not as large as measurements indicate. We are continuing study of this problem.

3. $n + {}^9\text{Be}$ Evaluation (Young and Stewart)

An evaluation of $n + {}^9\text{Be}$ cross-section data has been completed, with particular emphasis on adequate representation of secondary neutron spectra as measured recently at Los Alamos.⁵ Because the present ENDF/B formats and procedures do not permit accurate representation of energy-angle correlations in emitted neutrons from the ${}^9\text{Be}(n,2n)$ reaction, we were required to devise a special format. The multigroup processing code NJOY will be modified appropriately to permit processing of data in the revised format. The new evaluation will be available for comparison with the official ENDF evaluation.

⁴ R. F. Haglund, Jr., D. Fick, P. A. Schmelzbach, G. G. Ohlsen, N. Jarmie, and R. A. Brown, " ${}^1\text{H}(t,t){}^1\text{H}$ Scattering at Low Energies," Bull. Am. Phys. Soc. 21, 989 (1976); and private communication.

⁵ D. M. Drake, G. F. Auchampaugh, F. D. Arthur, C. F. Ragan, and P. G. Young, "Double Differential Beryllium Neutron Cross Sections at Incident Neutron Energies of 5, 9, 10.1, and 14.2 MeV," Los Alamos Scientific Laboratory report LA-6257 (1976); to be published in Nucl. Sci. Eng.

4. Reaction Theory Model Code Development (Arthur and Young)

We have continued development of the statistical-preequilibrium nuclear model code GNASH. Emphasis has been placed on evaluating the usefulness of different global optical model sets, improving level density and gamma-ray strength parameterizations, and incorporating mass tables, decay chains, etc. into the code so that complicated calculations up to energies of 40-50 MeV require minimal input.

We have calculated charged-particle cross sections and spectra induced by 15-MeV neutrons on stainless steel 316 in order to compare with the recent measurements of Haight et al.⁶ Proton and alpha spectra were calculated for ⁵⁴Fe, ⁵⁶Fe, ⁵⁰Cr, ⁵²Cr, ⁵⁸Ni, and ⁶⁰Ni using global parameters and combined appropriately for SS 316 (see Fig. C-3). For protons our calculations indicate a low-energy shoulder at approximately 1.4 MeV resulting from (n,np) reactions on ⁵⁶Fe and ⁵²Cr. Because of the thickness of the stainless steel foil used in the measurements (6.7 mg/cm²), and because an E-ΔE detector system was used, we believe the threshold for proton detection would have been too high to see this effect. (The calculated proton spectrum is dashed in the region where uncertainties exist in the measurement due to finite target and ΔE detector thicknesses.) The alpha spectrum comparison indicates a need for more accurate transmission coefficients in this mass region.

As part of a Cross Section Evaluation Working Group model-code comparison effort, we have calculated neutron-induced reactions on ⁵⁹Co from 35 keV to 40 MeV. In addition, we have calculated (n,n'), (n,2n), (n,3n), (n,p), (n,α), and (p,n) reaction cross sections for comparison with experimental data on a variety of other nuclei.^{7,8} Shown in Fig.

⁶ R. C. Haight, S. M. Grimes, and J. D. Anderson, "Hydrogen and Helium Production Cross Sections for 15 MeV Neutrons on Stainless Steel 316 and 304," UCRL Preprint 78783 (1976); to be published in Nucl. Sci. Eng.

⁷ E. D. Arthur and P. G. Young, "Calculations of (n,2n) and (n,3n) Spectra and Cross Sections," Proc. of the International Conf. on the Interactions of Neutrons with Nuclei, Lowell, Mass., CONF-760715-P2 (1976), p. 1453.

⁸ E. D. Arthur and P. G. Young, "A New Statistical-Preequilibrium Nuclear Model Code," Trans. Am. Nucl. Soc. 23, 500 (1976).

C-4 are comparisons of measured⁹⁻¹² and calculated (p,n) cross sections for ⁴⁵Sc, ⁸⁹Y, ¹⁶⁹Tm, and ¹⁹⁷Au. These results support our conclusion, reached in other studies,^{7,8} that cross section calculations using global neutron and proton parameters in the present model are generally accurate to ± 20 -25% up to projectile energies near 25 MeV. We plan to test the models at energies above 25 MeV by further use of charged-particle-induced measurements.

5. Distribution of Fission-Product Yields (Madland, England)

a. Pairing Influence

The existence of a significant ($\pm 20\%$, or larger) even-odd Z pairing influence on ²³⁵U and ²³³U independent thermal fission yields is now well known. In preparation for Version V of ENDF/B, which will contain yield data for at least 11 fissionable nuclides at one or more neutron fission energies (≥ 20 yield sets), we have developed a model for including even-odd Z and N pairing effects in fission-product yields.¹³ ²³⁵U independent yields at 2 neutron energies (see Fig. C-5 for pairing effects at thermal energy) were used to develop the model parameters. The pairing effects were calculated for 17 fissionable nuclides at 7 neutron energies up to 14 MeV.

⁹ R. G. Thomas, Jr. and W. Bartolini, "Neutron Production in Ag, Ta, Au, Pt, and Pb by the Interactions of 7.5-14 MeV Protons," Phys. Rev. 159, 1022 (1967).

¹⁰ T. McGee, G. L. Rao, G. B. Saba, and L. Yaffee, "Nuclear Interactions of ⁴⁵Sc and ⁶⁸Zn with Protons of Medium Energy," Nucl. Phys. A150, 11 (1970).

¹¹ C. Birattari, E. Gadioli, E. Gadioli Erba, A. M. Grassi Strini, G. Strini, and G. Tagliaferri, "Pre-equilibrium Processes in (p,n) Reactions," Nucl. Phys. A201, 579 (1973).

¹² L. F. Hansen, R. C. Jopson, Hans Mark, and C. D. Swift, "¹⁸¹Ta(p,n)¹⁸¹W and ¹⁹⁷Au(p,n)¹⁹⁷Hg Excitation Functions between 4 and 13 MeV," Nucl. Phys. 30, 389 (1962).

¹³ D. G. Madland and T. R. England, "The Influence of Pairing on the Distribution of Independent Yield Strength in Neutron-Induced Fission," Los Alamos Scientific Laboratory report LA-6430-MS (July 1976); D. G. Madland and T. R. England, "Pairing Effects on the Distribution of Fission-Product Yields," Trans. Am. Nucl. Soc. 24, 462 (1976).

b. Isomeric State Yields

In the absence of measurements and a model, the independent yield for each Z,A had previously been equally distributed between isomeric and ground states in ENDF/B evaluations. A simple one-parameter model has been constructed using, primarily, experimental data from $^{131,133}\text{Te}$ and $^{133,135}\text{Xe}$ for estimates of the parameter value and its energy dependence. Yield branchings were calculated for 144 nuclides having isomeric states ($T_{1/2} \geq 0,1$ s), at three neutron fission energies.¹⁴ Figure C-6 shows a model comparison with the remaining (limited) experimental data, as well as with the Te and Xe measurements used to parameterize the model.

6. Fission-Product Data and Source Terms (England, Stamatelatos, and Wilson)

a. Data Libraries

Cross Sections: A basic 154-group neutron absorption library for 181 fission products was processed from ENDF/B-IV using the NJOY Code.¹⁵ This library has been collapsed to various few-group structures and combined with other decay parameters. A report on the library is being prepared; a basic 4-group library for use in thermal reactors is included in a report prepared for the Electric Power Research Institute.¹⁶

Decay Parameters and Spectra: Decay parameters, except for spectra, have been processed from ENDF/B-IV and tabulated into an extremely compact form¹⁷ for 711 nuclides. The tabular listing also includes σ_{2200} and resonance integrals for 181 nuclides including 113

¹⁴ D. G. Madland and T. R. England, "Distribution of Independent Fission Product Yields to Isomeric States," *Trans. Am. Nucl. Soc.* **24**, 461 (1976) and Los Alamos Scientific Laboratory report LA-6595-MS (Nov. 1976).

¹⁵ R. E. MacFarlane and R. M. Boicourt, "NJOY: A Neutron and Photon Cross Section Processing System," *Trans. Am. Nucl. Soc.* **22**, 720 (1975).

¹⁶ T. R. England, W. B. Wilson, and M. G. Stamatelatos, "Fission Product Data for Thermal Reactors Part 1," and "Fission Product Data for Thermal Reactors Part 2," to be issued by Electric Power Research Institute.

¹⁷ T. R. England and R. E. Schenter, "ENDF/B-IV Fission-Product Files: Summary of Major Nuclide Data," Los Alamos Scientific Laboratory report LA-6116-MS (ENDF 223) (Sept. 1975).

that are stable for a total of 824 nuclides having tabular data. 180 nuclides have beta end-point energies, gamma energies and intensities. For these, a 75-group beta and 150-group gamma library have been constructed.¹⁸

b. Source Terms

The above libraries have been used to construct an extensive chain library for CINDER-10, which is an extended version of CINDER-7¹⁹ being developed for a variety of applications.

Figures C-7 and C-8 show recent comparisons of beta spectra after several hundred seconds of cooling and an initial irradiation of 15 ms and 8 h.²⁰ Figure C-9 shows a typical comparison with the recent gamma spectra measured at LASL (E. Jurney, measurements are preliminary and unpublished).

Decay heat calculations have been compared with recent benchmark measurements at ORNL,²¹ IRT,²² and LASL.²³ Data reduction

-
- ¹⁸ T. R. England and M. G. Stamatelatos, "Multigroup Beta and Gamma Spectra of Individual ENDF/B-IV Fission Product Nuclides," Los Alamos Scientific Laboratory report LA-NUREG-6622-MS (Dec. 1976).
- ¹⁹ T. R. England, R. Wilczynski, and N. L. Whitemore, "CINDER-7: An Interim Report for Users," Los Alamos Scientific Laboratory report LA-5885-MS (April 1975).
- ²⁰ N. Tsoulfanidis, B. W. Wehring, and M. E. Wyman, "Measurements of Time-Dependent Uranium-235 Fission Fragments," Nucl. Sci. Eng. 43, 42 (1971).
- ²¹ J. K. Dickens, T. A. Love, J. W. McConnell, R. M. Freestone, J. F. Emery, and R. W. Peelle, "Fission Product Beta and Gamma Energy Release Quarterly Progress Report for July-September 1976," Oak Ridge National Laboratory report ORNL/NUREG/TM-65 (December 1976).
- ²² S. J. Friesenhahn, et al., "²³⁵U Fission Product Decay Heat From 1 to 10⁵ Seconds," Elec. Power Research Institute report EPRI NP-180 (Febr. 1976).
- ²³ J. L. Yarnell and P. J. Bendt, "Decay Heat from Products of ²³⁵U Thermal Fission by Fast-Response Boil-Off Calorimetry," Los Alamos Scientific Laboratory report LA-NUREG-6713 (Draft 1/15/77).

from the measurements is still in progress but essentially final. In general, the calculations agree with measurements within 2 to 3% over the cooling range of 20 to 10^5 s.

Photoneutron spectra from ^9Be and ^2H have been calculated and reported in Ref. 24, and absorption buildup comparisons are given in Ref. 16.

7. Neutron Transport Cross Sections for Radiotherapy Applications
(Wilson, Foster, and MacFarlane)

A 60-group cross-section library has been developed for use in fast neutron (≤ 60 MeV) radiotherapy shielding and in-phantom transport calculations. The P₅ library combines processed ENDF/B-IV data and medium energy cross-section data calculated with the intranuclear-cascade and evaporation code CROIX. The 60-group structure was based on sensitivity studies with iron shielding. The library²⁵ includes H, B, C, N, O, Si, Fe, and W.

²⁴ M. G. Stamatelatos and T. R. England, "Fission-Product Gamma-Ray and Photo-Neutron Spectra and Energy-Integrated Sources." Los Alamos Scientific Laboratory report NUREG-0155 (LA-NUREG-5345-MS) (Dec. 1976).

²⁵ W. B. Wilson, J. B. Smathers, D. R. Harris, D. G. Foster, Jr., R. E. MacFarlane, "Neutron Multigroup Cross Sections for Radiotherapy Shielding Applications," Trans. Am. Nucl. Soc. 23, 633 (1976).

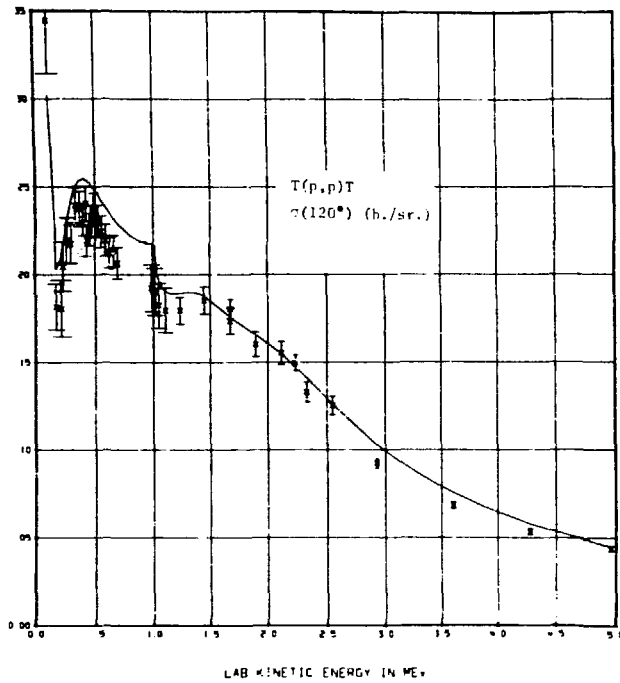


Figure C-1. Excitation curve for the $T(p,p)T$ differential cross section at $\theta_{cm} = 120^\circ$. The R-matrix calculation (solid curve) is compared to measurements by Jarmie, Ennis, and Haglund.

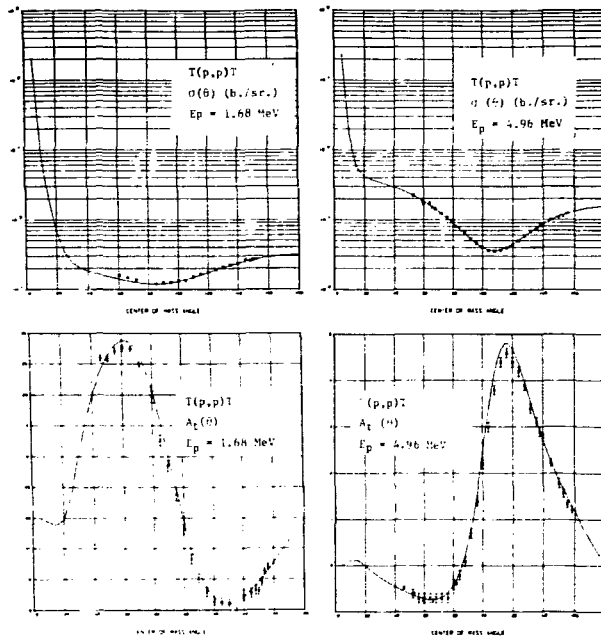


Figure C-2. Differential cross sections and triton analyzing powers for $t-p$ scattering at proton energies of 1.68 and 4.96 MeV. The data are those of Haglund et al.

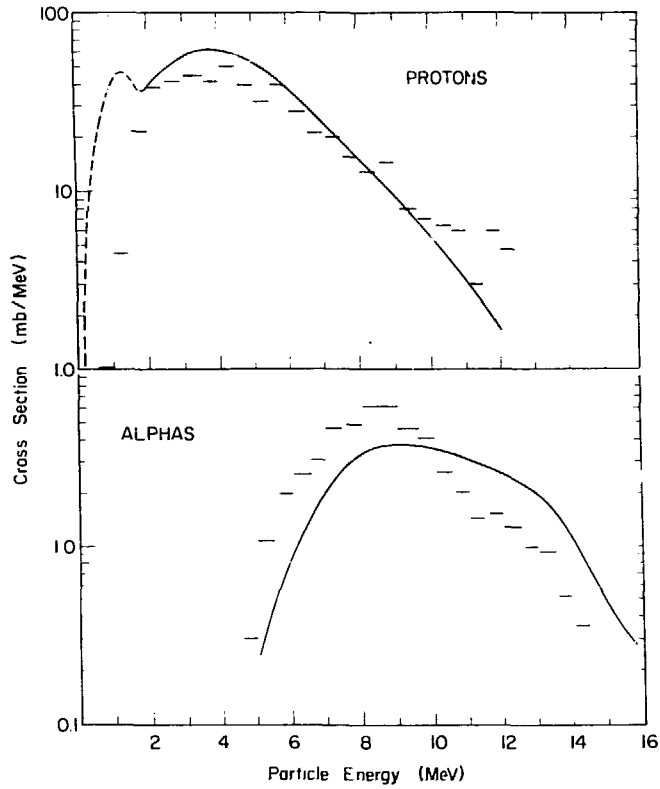


Figure C-3. Measured and calculated proton and alpha spectra from 15-MeV neutron bombardment of stainless steel 316. The calculated results are represented by the curves.

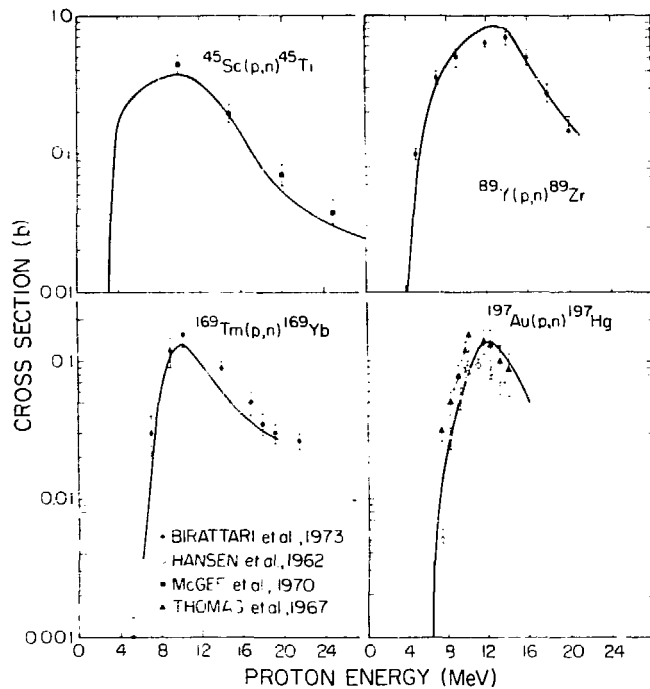


Figure C-4. Measured and calculated cross sections for (p,n) reactions on ^{45}Sc , ^{89}Y , ^{169}Tm , and ^{197}Au .

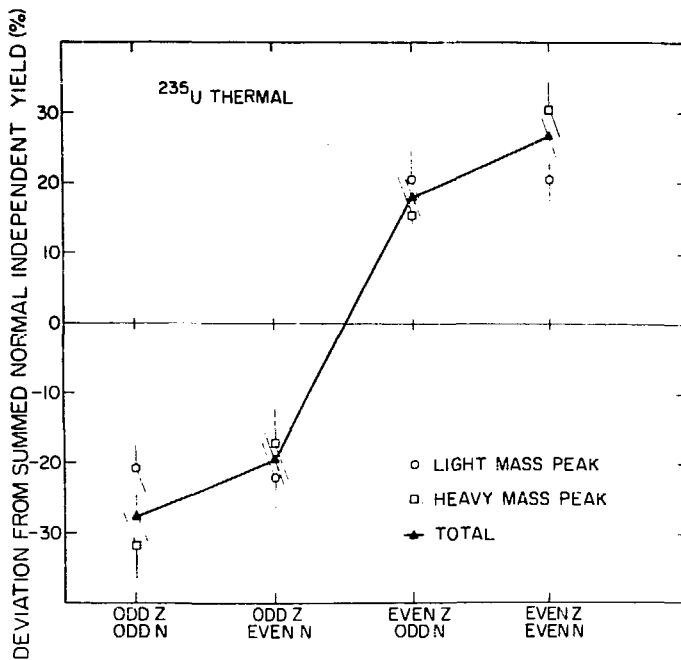


Figure C-5. Deviation of the summed IY from the summed NIY for odd-odd, odd-even, even-odd, and even-even fission products, and for the light mass peak, heavy mass peak, and the total mass distribution, in ^{235}U thermal fission.

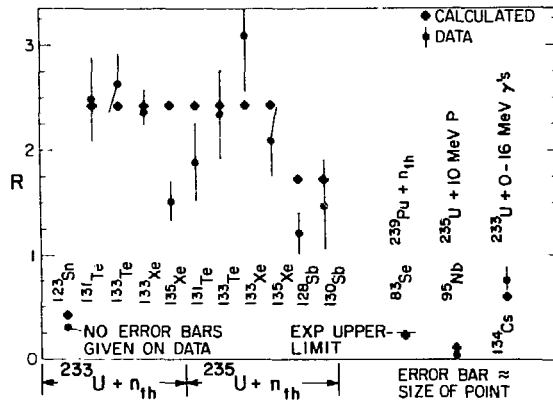


Figure C-6. Comparisons of calculated and experimental isomeric-state/ground-state independent yield ratios.

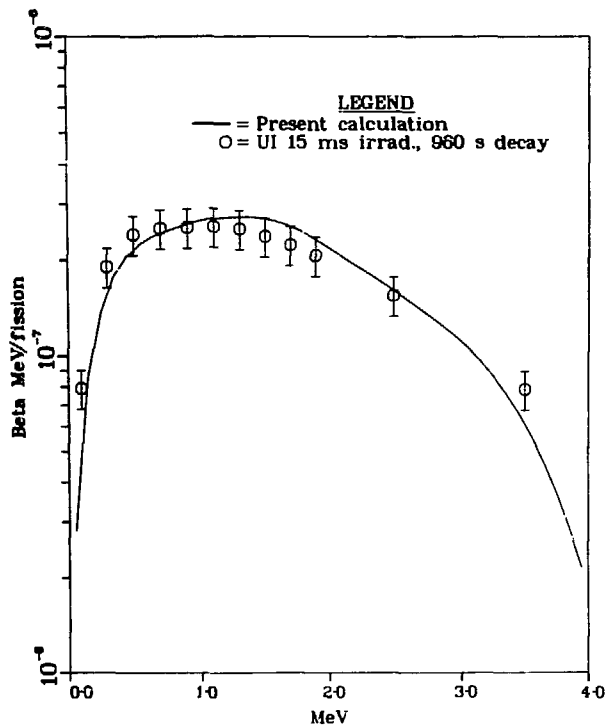


Figure C-7. Measured and calculated beta energy per fission for thermal fission of ^{235}U with 15 ms irradiation and 960 s delay.

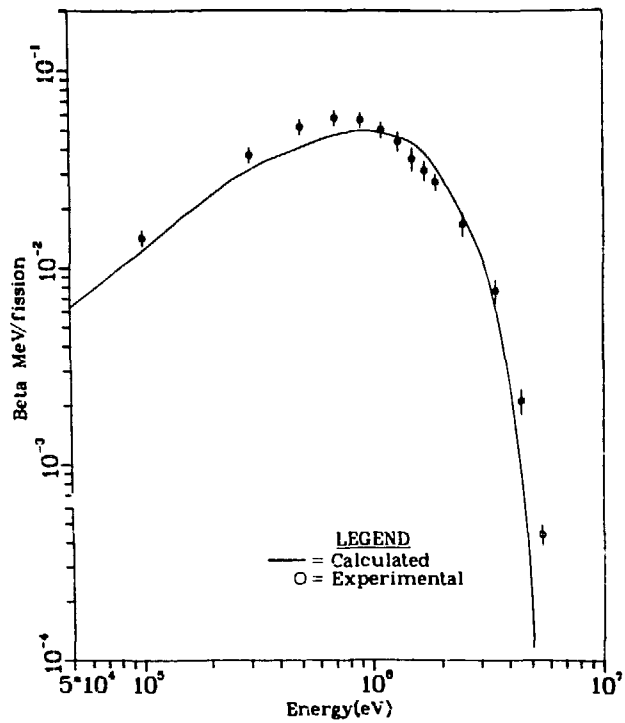


Figure C-8. Beta MeV/fission at 8 hrs. irradiation and 960 sec. cooling.

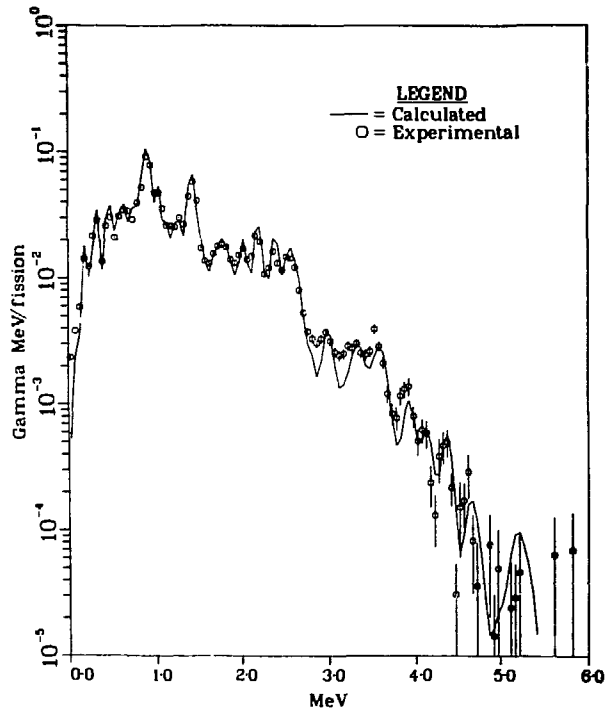


Figure C-9. Fission-product gamma MeV/fission/bin at 5.56 hrs. irradiation and 660 sec. cooling.

D. Sources, Facilities, and Applications

1. The T(d,n)⁴He Reaction as a Calibrated Polarized Neutron Source and the Analyzing Power of ⁴He(n,n)⁴He from 20 to 30 MeV
(Lisowski, Walter, Duke Univ.; Ohlsen, Hardekopf)

Experimental results for the zero-degree analyzing power and for the longitudinal vector polarization transfer coefficients for the reaction ${}^3\text{H}(d,n){}^4\text{He}$ have been obtained.¹ These data and unique properties of the reaction ${}^3\text{H}(\vec{d},\vec{n}){}^4\text{He}$ initiated by longitudinally polarized deuterons allowed a calibration of the neutron polarization to an absolute accuracy of $\pm 2\%$. Measurements of the analyzing power of ${}^4\text{He}$ at $\theta = 69^\circ, 80^\circ, \text{ and } 128^\circ$ (c.m.) were taken using the calibrated neutron beam for E_n in the range 20 to 30 MeV.

2. Accurate Neutron Source Reaction Cross Sections (Jarmie and Jett)

Accurate differential cross sections have been measured for the reactions ${}^2\text{H}(d,{}^3\text{He})n$ at 12.305 MeV, for ${}^3\text{H}(p,{}^3\text{He})n$ at 13.600 MeV, and ${}^2\text{H}(t,{}^4\text{He})n$ at 20.000 MeV. The center-of-mass angular range of the data is 25° - 100° . The relative error for most of the data is on the order of 1% and the scale error is less than 1%. The data are used to give absolute normalizations to the measured neutron source reaction spectra from these reactions^{2,3,4,5} and will be useful in the analysis of mass-4 and mass-5 systems.

¹ P. W. Lisowski, R. L. Walter, G. G. Ohlsen, and R. A. Hardekopf, Phys. Rev. Letters 37, 809 (1976).

² D. K. McDaniels, M. Drogg, J. C. Hopkins, and J. D. Seagrave, Phys. Rev. C7, 882 (1973).

³ D. K. McDaniels, M. Drogg, J. C. Hopkins and J. D. Seagrave, Phys. Rev. C6, 1593 (1972).

⁴ M. Drogg and D. M. Drake, Los Alamos Scientific Laboratory report LA-5732-MS (1974).

⁵ M. Drogg, R. K. Smith and R. Woods, Los Alamos Scientific Laboratory report LA-6262-MS (1976).

3. Intense Neutron Source Facility - Status (Emigh)

A description of possible uses of the INS facility for obtaining nuclear data using 14-MeV neutrons was presented in USNDC-7. These objectives remain part of the experimental program associated with the operation of the facility. Funds for the INS facility have been authorized and appropriated for construction, and Title I Architect-Engineering activities began in January 1977. The schedule calls for the facility to become operational early in 1981. The facility will contain two 14-MeV neutron sources, each capable of producing 10^{15} neutrons/s with a maximum flux of $\sim 10^{14}$ neutrons/cm² s on a continuous basis.

4. Decay Heat from Products of ²³⁵U Thermal Fission by Fast-Response Boil-Off Calorimetry (Yarnell, Bendt)

A major reactor-safety design problem is the avoidance of core melt-down following a loss-of-coolant accident. In principle, the heat flux in the core as a function of time after such an accident can be calculated by taking into account the β and γ energy released (as a function of time) by the decay of the fission products present in the fuel. However, these complex calculations need to be tested experimentally.

At the Omega West Reactor, decay heat from the products of thermal fission of ²³⁵U, for an irradiation of 2×10^4 s at constant flux, and for cooling times from 10 to 10^5 s, has been accurately measured with a cryogenic boil-off calorimeter. The β and γ radiations which compose the decay heat were absorbed in a 52-kg copper block, and this heat was used to evaporate liquid helium. The flow of boil-off gas was used to calculate the decay heat. The time constant of the calorimeter was 0.85 s. The number of fissions in the ²³⁵U samples was determined radiochemically. The energy loss due to γ leakage from the absorber was found to be $\leq 3\%$; a correction for this loss was made by Monte Carlo calculations based on experimentally determined γ spectra. The overall uncertainty (1σ) in the experimental data is $\leq 2\%$ except at the shortest cooling times, where it rises to about 4%. The data agree within the errors with summation calculations based on the ENDF/B-IV data base. The experimental data were extended to the case of infinite irradiation by means of summation calculations. The extended data for infinite irradiation are in good agreement with the summation calculation. For short cooling times, the results are $\approx 7\%$ below the current ANS Decay Heat Standard. The uncertainty of this experiment is an order of magnitude smaller than that assigned to the ANS standard.

Figure D-1 shows the experimental and calculated decay heats for 2×10^4 s irradiations, and Fig. D-2 shows their ratio. Figure D-3 shows the extended experimental data, the calculation, and the present

ANS Decay Heat Standard, for the infinite irradiation case. This standard plus 20% is currently used in reactor safety evaluations.

5. Analysis of Uranium and Plutonium in Urine by Delayed Neutron Counting (Minor, Ide, Moss, and Campbell)

One of the required radiation monitoring procedures carried out by the Health Division at LASL is the quantitative determination of uranium and plutonium in urine samples. A new method of performing such assays, based on delayed-neutron counting, has been initiated at the Omega West Reactor. The counting system was developed mainly for use in ERDA's National Uranium Resource Evaluation (NURE) program. The method has the advantages of being fast, inexpensive, and nondestructive to the sample.

Forty cubic centimeters of urine are placed in a plastic tube and irradiated for one minute in a thermal neutron flux of 1.2×10^{13} n/cm² s. After a 30-s delay, the delayed neutrons emitted by certain fission products are counted for 60 s with an array of ³He proportional counters embedded in a cylinder of polyethylene. The sensitivities observed for ²³⁸U, ²³⁵U, and ²³⁹Pu are: 0.5 µg/liter, 0.5 d/m/liter, and 300 d/m/liter, respectively. Since thermal neutrons cause fission of ²³³U, ²³⁵U, and ²³⁹Pu and the detector cannot distinguish between these isotopes, assumptions based on operational conditions must be made to determine the individual's exposure. Aside from this limitation, the technique is invaluable for screening large numbers of samples, with only the high values being checked by the traditional (and more costly) wet chemistry assay methods.

6. Instrumental Epithermal Neutron Activation Analysis (Gladney and Hensley)

A limited number of applications of instrumental epithermal neutron activation analysis (IENAA) have been reported over the past 10 years. The principal advantage of using IENAA is the drastic reduction relative to thermal neutron activation of gross activities resulting from (n,γ) reactions on isotopes such as ²³Na and ²⁷Al. In addition the epithermal (n,γ) cross section for some other isotopes is increased relative to thermal neutron cross sections (e.g. U, Th, As). Normally these irradiations are conducted in the thermal column of a reactor in Cd lined containers. At the Los Alamos Omega West Reactor (OWR) a special epithermal irradiation facility was constructed several years ago which uses an Al-B alloy to enclose the end of the rabbit tube and to reduce the thermal flux to low levels. This epithermal facility is superior to Cd wrapping since short-lived activities may be more easily studied.

The OWR epithermal facility has been used for measuring As, Sr and U in soils and vegetation. This instrumental procedure has greatly enhanced accuracy, precision and detection limits for all three elements relative to those obtained using thermal neutron activation analysis. Unlike delayed neutron counting for U determination, IENAA method can be used to measure U abundances in matrices containing variable U isotopic abundances.

7. Pulsed Neutron Facility - WNR

The WNR facility is approaching a state of operational readiness. An 800 MeV proton beam has been transported from LAMPF to the end of the 200 m channel which serves the facility and tuning tests are being conducted in a target area at this location. The 90° vertical bend system which directs protons onto the main neutron production target is approaching completion, as are the target facilities themselves. Two neutron flight paths for fast and resonance neutron experiments are under construction, and a third for experiments using thermal neutrons is in the design stage. The present schedule anticipates tuneup beam on the neutron production target by the end of April, 1977, and the experimental program beginning by July 1. Much of the initial effort will be concerned with a determination of neutron spectra and backgrounds for various target and moderator configurations.

8. Determination of Sulfur in Environmental Materials (Curtis, Gladney, Journey)

Conventional analytical techniques for sulfur usually prove to be complicated and time consuming. Because the cross section for producing a radioactive product is low, neutron activation analysis is not sufficiently sensitive to be useful in many practical cases. We have investigated the quantitative determination of S in complex matrices by thermal-neutron-induced prompt gamma rays using NBS and Illinois State Geological Survey standard samples. The technique provides a rapid, non-destructive analysis for as little as 100 µg of S.

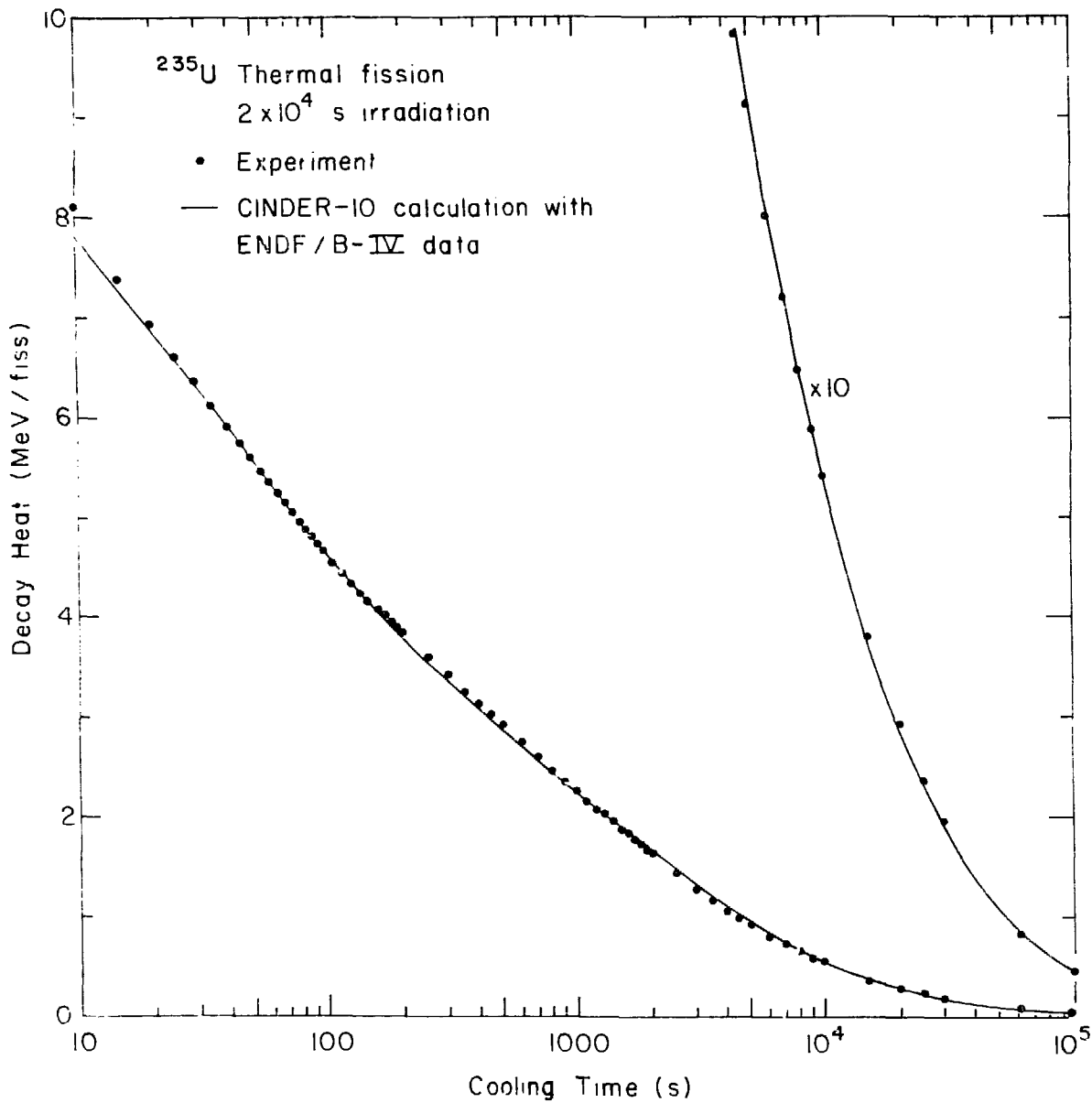


Figure D-1. Experimental and calculated decay heats for 2×10^4 s irradiations.

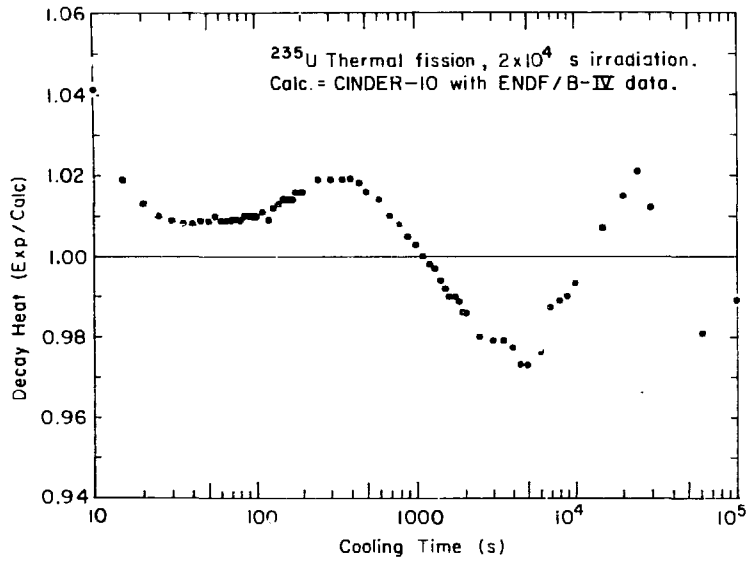


Figure D-2. Ratio of experimental to calculated decay heats.

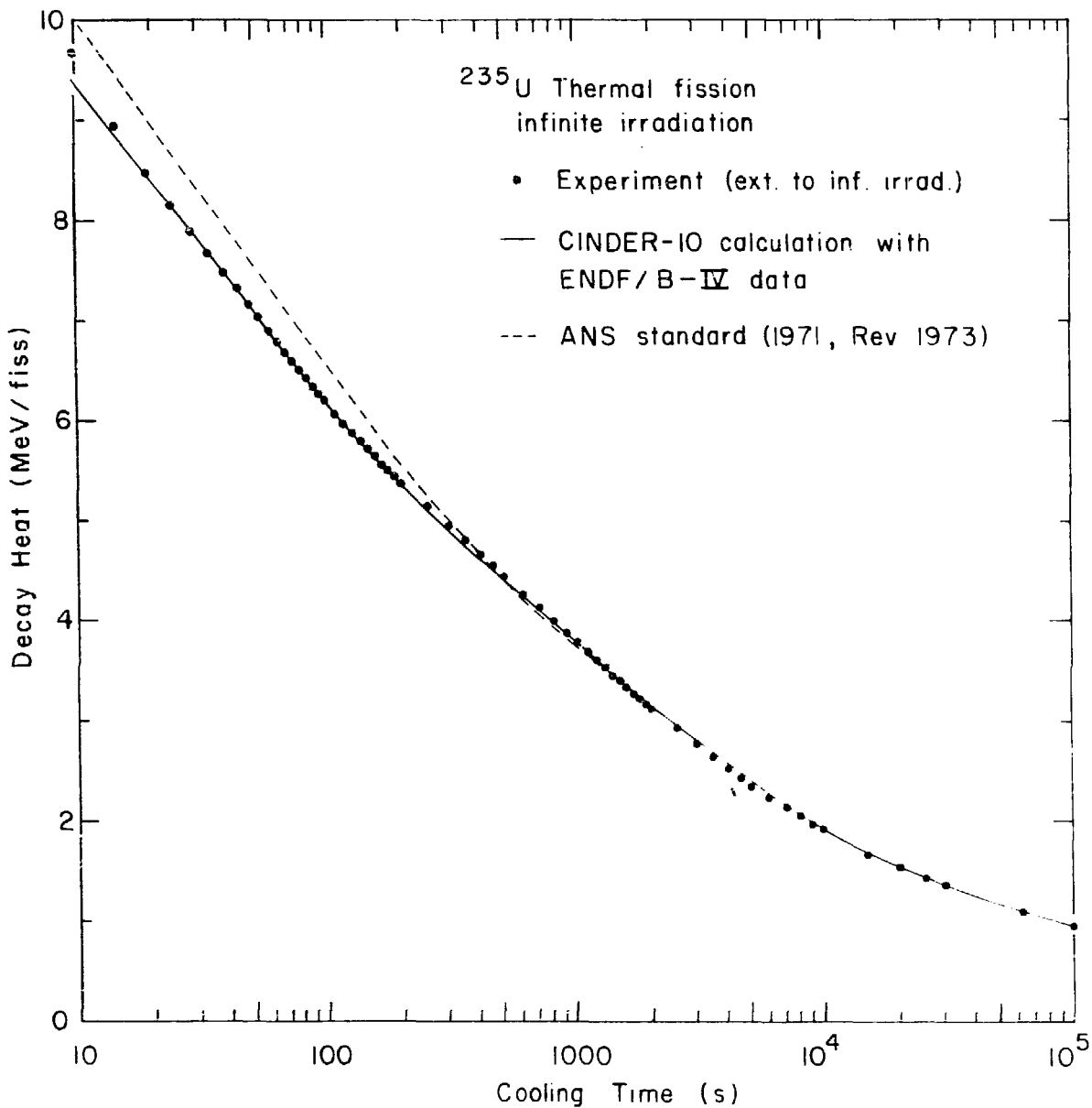


Figure D-3. Extended experimental data, the calculation, and the present ANS decay heat standard for the infinite irradiation case.

NUCLEAR PHYSICS GROUP
UNIVERSITY OF LOWELL

Faculty Staff: B.K. Barnes, L.E. Beghian, G.P. Couchell, J.J. Egan, P. Harihar, G.H.R. Kegel, S.C. Mathur, T.V. Marcella, A. Mittler, D.J. Pullen, W.A. Schier, and E. Sheldon.

Research Assistants: A. Bird, J. Chang, J. Correia, D. Donati, P. Karatzas, R.V. LeClair, Y. Liu, J. Nardini, N. Sullivan, S. Traiforos, J. Wang.

A. NEUTRON SCATTERING CROSS SECTION MEASUREMENTS*

The University of Lowell nuclear physics group is continuing its program of elastic and inelastic neutron scattering cross section measurements for elements primarily involved in the fuel, cladding, structural and coolant materials of LMFBR reactors. For the lighter elements (Na, Si, Ti, Cr, Mn, Fe, Co and Ni) the neutron cross sections are inferred from gamma-ray production cross sections obtained with the $(n, n'\gamma)$ reaction, whereas in the case of U measurements are made using both the (n, n') and $(n, n'\gamma)$ reactions.

1. $(n, n'\gamma)$ Studies

In most of the studies described in this section the absolute gamma-ray differential cross sections were measured at only one angle. The angle integrated cross sections were deduced from these using theoretical angular distribution shapes calculated with the code MANDY, which is based on a statistical compound nuclear model. The inferred neutron scattering cross sections are corrected for neutron multiple scattering and for neutron and gamma-ray attenuation effects. Except for the uranium study, the sample scatterers were right circular cylinders, typically 2.54 cm in diameter and 5 cm high. For uranium, a disc-shaped scatterer was used having a thickness of 0.53 cm and a diameter of 1.91 cm.

a. $^{23}\text{Na}(n, n'\gamma)$

Gamma-ray production cross sections have been measured for ten gamma transitions over the incident neutron energy range 0.52 to 4.23 MeV, and from these the neutron inelastic scattering cross sections have been inferred for six levels in ^{23}Na . Gamma-ray angular distributions were also measured at several incident energies and from these the magnetic substate populations were evaluated for the 440-keV($5/2^+$) and 2078-keV($7/2^+$)

*This project is supported in part by the National Science Foundation.

states in ^{23}Na . Comparisons have been made between the distributions and magnetic substate populations calculated from compound-nuclear and direct-interaction theories, the former yielding better agreement in the interpretation of experimental results.

This work has been submitted for publication in Phys. Rev. C.

b. $^{28}\text{Si}(n,n'\gamma)$

The neutron scattering cross section for the 1780-keV(2^+) first excited state of ^{28}Si has been deduced from the gamma-ray production cross section measured at 125° in the incident energy range $E_n = 1.97$ to 4.18 MeV. Even with a relatively coarse energy resolution of approximately 100 keV, considerable structure is evident in the excitation function.

c. $\text{Ti}(n,n'\gamma)$

Production cross sections have been measured at 125° for the following gamma-ray transitions in the naturally occurring titanium isotopes: 889 keV in ^{46}Ti ; 160 keV in ^{47}Ti ; 983-, 1312-, and 1438 keV in ^{48}Ti ; 1623 keV in ^{49}Ti ; and 1554 keV in ^{50}Ti . Neutron scattering cross sections have been determined for the following states: $E_x = 889$ keV(2^+) in ^{46}Ti ; $E_x = 983$ keV(2^+), 2295 keV(4^+), and 2421 keV(2^+) in ^{48}Ti ; and $E_x = 1554$ keV(2^+) in ^{50}Ti . The energy ranges are from threshold to $E_n = 3.4$ MeV.

d. $\text{Cr}(n,n'\gamma)$

Gamma-ray production cross sections have been measured at 125° for over 20 gamma-rays produced by neutron scattering from chromium in the incident energy range 0.84-3.97 MeV. Neutron inelastic scattering cross sections have been deduced for 22 levels in the four natural chromium isotopes $^{50,52,53,54}\text{Cr}$. These data have recently been reanalyzed and will supersede earlier results sent to the NNCSC (EXFOR 10492.006, .007 May 1975). The earlier results did not include corrections to the angle integrated gamma production cross sections resulting from gamma-ray angular distributions with contributions from Legendre polynomial terms $A_{2n} P_{2n}(\cos \theta)$ with $n > 1$. For some transitions such higher order terms are found to be significant, especially near the threshold region. In addition, several new transitions were found which were missed in the original analysis, and also the effective neutron energy for each measurement has been adjusted downward (9 keV at low incident energies to 24 keV at high energies) to account for the kinematic energy spread of incident neutrons produced by the $\text{T}(p,n)^3\text{He}$ reaction. In many cases the deduced level cross sections are in good agreement with the ENDF/B-IV evaluation for chromium. In most cases where there is significant disagreement, our results are lower. Such discrepancies are usually most pronounced in the threshold

region of the excitation function. The most notable, if not the largest, discrepancy was observed in the threshold behavior of the 1434-keV(2^+) first excited state of ^{52}Cr (83.76% abundance). Below 2 MeV incident neutron energy the ENDF level cross section is generally 20-50% higher than our results. Considering that this level accounts for more than half the inelastic scattering cross section in natural chromium over this energy region, this difference is rather significant in neutron slowing down calculations. The present results are being prepared for publication and will be submitted to the NNCSC.

e. $^{55}\text{Mn}(n, n'\gamma)$

Gamma-ray production cross sections (at 125°) have been measured for 19 transitions from levels up to and including $E_x = 2429$ keV in ^{55}Mn over the incident energy range $E_n = 1.0$ -3.6 MeV. Angular distributions were also measured for 6 of these transitions. Total neutron inelastic scattering cross sections have been extracted for 12 levels up to $E_x = 2429$ keV. Comparisons with calculations using the statistical compound nucleus theory provide good agreement with the accepted J^π -assignments for the first four levels at 126 keV($7/2^-$), 984 keV($9/2^-$), 1292 keV($11/2^-$), and 1530 keV($3/2^-$), and narrows the range of probable J^π -values for eight levels above 1.8 MeV excitation to at most two values in each case.

This work has been submitted to Nuclear Physics for publication.

f. $\text{Fe}(n, n'\gamma)$

Neutron inelastic cross sections for levels in natural iron have been deduced from measurements of the gamma-ray production cross section at 125° over the incident neutron energy range 0.88-3.97 MeV. Level cross sections were obtained for the first ten excited states of ^{56}Fe ($E_x = 847$ keV to 3450 keV) as well as for the first four excited levels of ^{54}Fe and the 367-keV level in ^{57}Fe . Earlier results of this study were sent to NNCSC (EXFOR 10519.003, .005). These data are now being revised to include contributions to the gamma-ray angular distribution of $A_{2n}P_{2n}(\cos \theta)$ terms with $n > 1$ as well as a small adjustment in the effective incident energy arising from kinematic effects (see chromium).

Our measured cross sections have been compared with the ENDF/B-IV compilation for natural iron. In most cases the agreement is good. One notable exception is the excitation function for the 847-keV(2^+) first excited state of ^{56}Fe (91.66% abundance). In the first 1 MeV above threshold our measurements are generally 10-35% lower than ENDF. Our estimated uncertainty in this region is no more than $\pm 10\%$. Between 1 and 2 MeV incident neutron energy this level accounts for at least 90% of the total inelastic neutron scattering cross section of iron. The revised results are being prepared for publication and will be submitted to the NNCSC.

g. $^{59}\text{Co}(n,n'\gamma)$

Total neutron inelastic scattering cross sections have been extracted for 19 levels in ^{59}Co up to $E_x = 3.0$ MeV in the incident energy range $E_n = 1.11$ - 3.32 MeV. These were deduced from measured gamma production cross sections for 36 transitions. Excitation functions were measured at 90° and 125° , and angular distribution measurements were made at $E_n = 1.41, 1.76, 1.91, 2.32$ and 2.83 MeV. Comparisons with compound nucleus statistical model calculations provide good agreement with previous J^π assignments for the first nine levels, and suggest probable J^π -values for ten levels between $E_x = 2.1$ and 3.0 MeV.

h. $\text{Ni}(n,n'\gamma)$

Gamma-ray production cross sections (at 125°) have been measured for 15 transitions from levels up to $E_x = 3420$ keV in ^{58}Ni and 3123 keV in ^{60}Ni , over the incident energy range $E_n = 1.4$ - 3.9 MeV. These data are currently being analyzed to extract total inelastic neutron scattering cross sections for 13 levels.

i. $^{238}\text{U}(n,n'\gamma)$

A study is in progress to determine total inelastic neutron scattering cross sections for levels near 1 MeV excitation or higher in ^{238}U using the $(n,n'\gamma)$ technique. Very little experimental data is available for inelastic scattering close to the thresholds for these higher excited states. In view of the high level density in this region it is difficult to resolve these states in (n,n') time-of-flight measurements, and furthermore the TOF technique does not have the sensitivity to clearly resolve low energy neutron groups from the background at high incident energies. Our preliminary measurements of the $(n,n'\gamma)$ reaction in the range $E_n = 1.0$ - 1.5 MeV have established the feasibility of this technique to this excitation region in ^{238}U .

2. $^{238}\text{U}(n,n')$ Studies

a. Low Energy Measurements

A detailed study of neutron inelastic scattering from ^{238}U at low incident neutron energies ($E_n \leq 0.2$ MeV) has recently been initiated¹ at this laboratory using a high resolution time-of-flight spectrometer and a disc-shaped scatterer. The 45-keV(2^+) first excited state is mainly

¹See, e.g., Couchell et al, Proc. Int. Conf. on the Interactions of Neutrons with Nuclei, Univ. of Lowell, 1976, U.S.E.R.D.A. Report CONF-760715-P2, p. 1332.

responsible for inelastic scattering in this energy region, and is the only contributor below the threshold for the 148-keV(4^+) second excited state. Feasibility studies have shown that the 45-keV group can be clearly resolved from the elastic peak in scattered neutron time-of-flight spectra at incident energies as low as 0.1 MeV. A five-point excitation function for this level has been measured over the region $0.10 \text{ MeV} < E_n < 0.15 \text{ MeV}$. Measurements have been corrected for finite sample effects which are rather large in this energy region. The inelastic cross section has been placed on an absolute scale by normalizing the measured elastic yield to the differential elastic cross section listed in ENDF/B-IV. Uncertainties in the inelastic measurements are estimated to be $\pm 15\%$. A comparison of these preliminary results with inelastic cross sections given in ENDF indicates our measurements to be about 20% higher at 0.1 MeV and about 60% higher at 0.15 MeV, with a suggestion of structure in the excitation function in the vicinity of the latter energy.

We plan to modify the present experimental arrangement before proceeding with more detailed studies. The repetition rate of the pulsed beam will be reduced from the present value of 5 MHz to 1-2 MHz in order to allow longer flight paths without low-energy wrap-around in the time-of-flight spectrum. Longer flight paths will also permit more substantial shielding of the neutron detector to reduce problems with neutron decay in the present shielding arrangement. New commercially available scintillators having a greater light output for low energy neutrons will also be tested in order to improve the system time resolution. Improvements in this area will help to resolve the inelastic and elastic peaks at perhaps lower energies than the present measurements.

b. High Energy Measurements

Neutron scattering cross sections for the ground and first two excited states in ^{238}U have been measured at incident energies in the range $E_n = 0.9\text{-}3.1 \text{ MeV}$. Corrected excitation functions and preliminary uncorrected angular distribution data have already been presented.¹ The latter data are currently being corrected for multiple neutron scattering and for neutron attenuation effects. The final results will shortly be submitted for publication and to the NNCS.

3. Future (n,n') and (n,n'\gamma) Studies

We plan to extend these neutron cross section measurements to include ^{232}Th , ^{239}Pu , and possibly ^{235}U . The level spacing in ^{232}Th is similar to that in ^{238}U and its study should be straightforward. In ^{239}Pu

¹Egan et al, Proc. Conf. on Nuclear Cross Sections and Technology, Washington, D.C., 1975, N.B.S. Special Publication 425, p. 950; also Proc. Int. Conf. on the Interactions of Neutrons with Nuclei, Univ. of Lowell, 1976, U.S.E.R.D.A. Report CONF-760715-P2, p. 1331.

our resolution will not be adequate to separate the ground state and first excited state ($E_x=8$ keV). However, neutron groups from the next four states should be well resolved for incident neutron energies up to 2 MeV. Substantial improvements in energy resolution will be necessary before undertaking a study of ^{235}U . However, we expect these improvements to be realized during the next twelve months.

B. (n, α) REACTION STUDIES

We have recently initiated studies of the (n, α) reaction on the alloying elements of stainless steel. In a reactor environment this reaction is known to lead to the formation of helium in sufficient quantities to cause swelling and the formation of "bubbles" in stainless steel. A clear understanding of this effect requires a knowledge of the energy dependent (n, α) cross section. A moderate resolution, high sensitivity pulse ionization chamber has already been constructed for measuring these cross sections. Preliminary results for nickel should be available within the next few months.

C. IRRADIATION-INDUCED CREEP MEASUREMENTS

We propose to expand our program to include studies of neutron irradiation-induced creep in reactor structural materials, as well as those intended for first wall applications in fusion devices. Neutron irradiation will be simulated using proton bombardment, and the proposed method involves incorporating the target directly into the wall of the irradiation chamber to provide effective cooling. The sample creep will be measured using a laser interferometer with the irradiated sample as one of the reflecting surfaces. Some advantages of this method are, i) the sample temperature can effectively be maintained at a predetermined constant value, or alternatively can be provided with a controlled, time-dependent behavior to simulate reactor accidents caused by coolant loss, ii) the samples are exposed to biaxial stress, iii) the creep sensitivity is high, and iv) the sample creep is monitored continuously during irradiation.

THE UNIVERSITY OF MICHIGAN

A. INTRODUCTION

The cross section project at The University of Michigan continues to stress the measurement of absolute neutron cross sections. Since our techniques do not rely on the input of any other fast cross section data, we intend to provide absolute normalization points for relative data provided by linacs and other TOF facilities.

All our measurements are conducted relative to the secondary national neutron standard source NBS-II. Our measurements also stress the use of limited solid angle counting for reaction products in which the counting efficiency is determined by accurate geometric measurements. Since our neutron sources are small, they are easily calibrated in The University of Michigan manganese bath facility. The source is normally positioned between dual target foils during the measurement of the reaction rate to minimize the dependence of the summed reaction yield on small geometric uncertainties in the actual position of the source. These techniques have largely been detailed in previous progress reports.

We feel that the value of the data given in this report is enhanced by the fact that each individual measurement is part of a larger set of data which incorporates many of the same measurement techniques. For example, the same manganese bath calibration facility has been used for all the measurements reported here. Similarly, the target foils and standard source NBS-II are common to many of the measurements. Each additional data point therefore adds to the background information against which prior measurements must be evaluated. It is particularly significant that this report includes a description of a measurement of ν -bar for ^{252}Cf . Since our reported value is based on the same NBS-II normalization as our other cross section data, any systematic error in its assumed emission rate would be reflected in both measurements.

B. FISSION CROSS SECTION MEASUREMENTS USING PHOTONEUTRON SOURCES (M. C. Davis, G. F. Knoll, J. C. Robertson)

We have now completed a set of differential fission cross section measurements on ^{235}U and ^{239}Pu using each of four photoneutron sources (Na-Be, La-Be, Na-D, and Ga-D). Some of these results have been given in previous reports, but the entire set will be reproduced here for completeness. These values include the measurement for ^{235}U at 964 keV which was carried out primarily by D. M. Gilliam.

Fission events were accumulated with the source positioned symmetrically between two identical foils (1.1 mg cm^{-2} thickness) and detectors in an experiment package suspended in a low albedo laboratory. Fission fragments passing through limited solid angle apertures were recorded on polyester track-etch films. The accumulated tracks were displayed on the screen of a projection microscope and counted by hand. The masses of the foil deposits were determined by microbalance weighings and confirmed by thermal fission and alpha counting. The neutron flux at the targets was calculated from the experimental geometry and by using a manganese bath to compare the source yield with the standard source NBS-II. Considerations of scattering, target thickness, and angular and spatial distributions in neutron production were included in the vacuum streaming calculations. Careful analysis of the kinetics of manganese activation and mixing delays were required in comparing relative source strengths in the bath. The room-scattered flux contribution to the total flux was determined from different source-detector spacing runs. These backgrounds typically contributed less than 1% of the total fission rate at the closest source-target spacings used in the measurement. Neutron spectra were calculated by Monte Carlo for each photoneutron source, and the cross section reduced to the median source energy by using published data on the cross section shape.

Values of 1.471 ± 0.024 , 1.274 ± 0.020 , 1.162 ± 0.022 and 1.210 ± 0.025 barns were obtained for the ^{235}U fission cross section at nominal neutron energies of 140, 265, 770, and 964 keV. Corresponding values of 1.469 ± 0.041 , 1.515 ± 0.035 , 1.670 ± 0.037 and 1.643 ± 0.033 barns were obtained for ^{239}Pu . Subsequent fission ratios of 0.999 ± 0.031 , 1.189 ± 0.30 , 1.437 ± 0.040 and 1.358 ± 0.032 are free of any source yield dependencies.

These results were presented at the NEANDC/NEACRP Specialists Meeting on Fast Fission Cross Sections held at Argonne National Laboratory on June 28-30, 1976. Further details are given in the Proceedings of this meeting (NEANDC (US) - 199/L, 225).

C. FISSION CROSS SECTIONS OF ^{235}U AND ^{239}Pu AVERAGED OVER ^{252}Cf Neutron Spectrum (M. C. Davis, G. F. Knoll)

A series of measurements have been carried out to derive values for the spectrum-averaged fission cross sections of ^{235}U and ^{239}Pu for ^{252}Cf fission neutrons. Values of 1.215 ± 0.017 barns for ^{235}U and 1.790 ± 0.034 barns for ^{239}Pu were obtained for the fission cross sections, corresponding to a ratio value of 1.473 ± 0.033 .

The same target foils and general experimental configuration used for our earlier photoneutron measurements were also applied to this determination. These include registration of fission fragments on polyester track-etch films through limited solid angle apertures, and calibration of the ^{252}Cf source against NBS-II in our manganese bath. Latent tracks in the films were etched and manually counted using a projection microscope. Separate runs were made with different source-foil spacings to permit evaluation of the room-scattered flux contribution at the center of the low-albedo laboratory.

The deposit masses were uncertain to an estimated $\pm 0.5\%$ for ^{235}U and 1.4% for ^{239}Pu . Other significant uncertainties included $\pm 0.8\%$ associated with track counting statistics, reproducibility, and discrimination between fragment tracks and alpha pits. Uncertainties in the angular distribution of fission fragment emission weighted over the ^{252}Cf spectrum amounted to $\pm 0.7\%$. Neutron calibration by the manganese bath technique required corrections with residual errors for absorption in the source dry well and in the source itself ($0.6 \pm 0.2\%$), fast capture by $^{32}\text{S}(n,p)$ and $^{160}\text{O}(n,\alpha)$ reactions ($0.7 \pm 0.2\%$), and neutron streaming and penetration ($0.2 \pm 0.1\%$).

Table 1 gives a comparison of this work with that of Heaton, et al.,³ and various differential data weighted over the Cf spectrum. Spectrum-averaged measurements of this type can serve as a useful check on various data sets, particularly in terms of their normalization level in the 0.5 to 5.0 MeV range. Since many features of the present measurements (target foils, counting apertures, manganese bath, etc.) are in common with previous measurements at Michigan, they also support the validity of results reported earlier using photoneutron sources.^{1,2}

¹D. M. Gilliam and G. F. Knoll, A. of Nucl. Energy, 2, 637 (1975).

²M. C. Davis and G. F. Knoll, "Absolute Measurements of ^{235}U and ^{239}Pu Fission Cross Sections with Photoneutron Sources", NEANDC/NEACRP Spec. Mtg. on Fast Neutron Fission Cross Sections, Argonne (1976). NEANDC (US) - 199/L, 225.

³Heaton, Gilliam, Spiegel, Eisenhauer, Grundl, "Fission Cross Sections of ^{235}U , ^{238}U , and ^{239}Pu Averaged Over the ^{252}Cf Neutron Spectrum", NEANDC/NEACRP Spec. Mtg. on Fast Neutron Cross Sections, Argonne (1976). NEANDC (US) - 199/L, 333.

Table 1
Comparison of ^{252}Cf Spectrum-Averaged Cross Sections

<u>INTEGRAL</u>	Cross Section Values (barns)		Ratio
	$^{235}\text{U}(n,f)$	$^{239}\text{Pu}(n,f)$	$^{239}\text{Pu}/^{235}\text{U}$
This work	1.215 \pm 0.017	1.790 \pm 0.034	1.473 \pm 0.033
Heaton	1.205 \pm 0.027	1.808 \pm 0.045	1.500 \pm 0.024
ENDF/B-III	1.239 \pm 0.002 ^a	1.819	1.468
ENDF/B-IV	1.241	1.789	1.442
ENDF/B-V	1.233	--	--

a. Error due only to the uncertainty in the Cf spectrum.

D. NU-BAR OF ^{252}Cf (H. Bozorgmanesh, G. F. Knoll)

A measurement of the average number of neutrons per fission (nu-bar) for the spontaneous fission of ^{252}Cf has been completed. Results were presented at the meeting of the Standards Subcommittee of CSWEG in October of 1976, but this report constitutes the first publication of the final result.

The measurement was carried out by independently determining the absolute fission rate and absolute neutron yield from a small plated foil of Californium. The neutron source emission rate was obtained in The University of Michigan manganese bath. The nature of the background, the statistical error associated with the bath, and the desired accuracy of the measurement (~0.5 percent) required a source with a neutron emission rate of 10^6 per second. The associated fission rate (2.7×10^5 per second) and decay rate (8.1×10^6 per second) clearly were too high for accurate 2π geometry counting of the fission fragments. Therefore, fragments were counted using a restricted solid angle near the normal to the plane of deposit and using a heavy-ion silicon surface barrier detector behind variable defining apertures. For this purpose a fission chamber was designed so that all angular and axial positioning and all aperture changes were performed remotely. The source to aperture distance could be observed directly to within 10^{-4} inches.

Table 1

Comparison of ^{252}Cf Spectrum-Averaged Cross Sections

<u>INTEGRAL</u>	Cross Section Values (barns)		Ratio
	$^{235}\text{U}(r,f)$	$^{239}\text{Pu}(n,f)$	$^{239}\text{Pu}/^{235}\text{U}$
This work	1.215 \pm 0.017	1.790 \pm 0.034	1.473 \pm 0.033
Heaton	1.205 \pm 0.027	1.808 \pm 0.045	1.500 \pm 0.024
ENDF/B-III	1.239 \pm 0.002 ^a	1.819	1.468
ENDF/B-IV	1.241	1.789	1.442
ENDF/B-V	1.233	--	--

a. Error due only to the uncertainty in the Cf spectrum.

D. NU-BAR OF ^{252}Cf (H. Bozorgmanesh, G. F. Knoll)

A measurement of the average number of neutrons per fission ($\bar{\nu}$) for the spontaneous fission of ^{252}Cf has been completed. Results were presented at the meeting of the Standards Subcommittee of CSWEG in October of 1976, but this report constitutes the first publication of the final result.

The measurement was carried out by independently determining the absolute fission rate and absolute neutron yield from a small plated foil of Californium. The neutron source emission rate was obtained in The University of Michigan manganese bath. The nature of the background, the statistical error associated with the bath, and the desired accuracy of the measurement (~ 0.5 percent) required a source with a neutron emission rate of 10^6 per second. The associated fission rate (2.7×10^5 per second) and decay rate (8.1×10^6 per second) clearly were too high for accurate 2π geometry counting of the fission fragments. Therefore, fragments were counted using a restricted solid angle near the normal to the plane of deposit and using a heavy-ion silicon surface barrier detector behind variable defining apertures. For this purpose a fission chamber was designed so that all angular and axial positioning and all aperture changes were performed remotely. The source to aperture distance could be observed directly to within 10^{-4} inches.

Potential competing processes which can lead to pulses in the low amplitude tail of the fission fragment distribution are:

- a. multiple pile-up of decay alpha particles
- b. low-angle scattering of fission fragments
- c. energy loss of fission fragments with the source
- d. long-range alpha (LRA) particles from tertiary fission (3.27×10^{-3} per binary fission)

Multiple alpha pile-up into the energy region of interest was eliminated by restricting the solid angle, such that the corresponding alpha rates were less than a few hundred per second. Fragment scattering was minimized by tailoring the shape of the aperture edge and by avoiding observation angles near the plane of the foil. The thin deposit ($1.5 \mu\text{g}/\text{cm}^2$) and evaporated gold cover ($50 \mu\text{g}/\text{cm}^2$) led to minimal fragment energy loss in the direction of the aperture.

The LRA energy spectrum was recorded separately by stopping the fission fragments and decay alphas in an aluminum foil of approximately $3 \text{ mg}/\text{cm}^2$ thickness. Pulse height analysis of the transmitted long-range alphas produced a broad peak centering around 16 MeV (corrected for energy loss in the aluminum absorber). The count rate of LRA was then obtained from this integrated spectrum. The aluminum absorber was removed and the complete spectrum was recorded under the same geometrical conditions. The fission rate was determined from the integrated fission spectrum (all counts above the upper tail of LRA).

By changing both the aperture diameter and the foil-to-aperture distance, a series of 44 independent fission rate measurements were carried out. The solid angle for counting fission fragments ranged from 2×10^{-5} to 60×10^{-5} steradians over this set. The self-consistency of this data was used as a gauge of geometric uncertainties in the fission counting.

The manganese bath source-comparison technique was used to determine the neutron emission rate of the ^{252}Cf source. The calibration of the manganese bath was performed by observation of the saturated activity induced by the standard NBS-II photoneutron source. The neutron emission rate of NBS-II has been established by the absolutely calibrated manganese baths at ANL, NPL, BIPM, and NBS.

The correction factors for neutron rate determination in The University of Michigan manganese bath were then thoroughly examined. A long counter was employed to directly determine the neutron leakage rate of the NBS-II photoneutron source, as well as a $5 \mu\text{g}$ ^{252}Cf source.

The efficiency of the long counter was experimentally examined by the source comparison technique. ANISN modeling of the bath and the ^{252}Cf source resulted in a leakage correction factor in good agreement with the experimental value. A portion of the Californium neutron spectrum consists of fast neutrons with energies above the thresholds for charge particle reactions $^{16}\text{O}(n,\alpha)^{13}\text{C}$ and $^{32}\text{S}(n,\alpha)^{29}\text{Si}$. Since neutrons captured in these charged particle reactions do not contribute to the measured activity of ^{56}Mn , corrections must be made for "oxygen loss" and "sulphur loss".

These parasitic absorptions in the bath, as well as source and support self-absorption corrections, were calculated with the transport code. These values were compared to published results under similar conditions. Several neutron emission rate determinations were conducted prior, after, and in the course of fission rate determination period. A consistent value of neutron emission rate relative to NBS-II was obtained within statistical uncertainty.

The average number of neutrons per fission of 3.744 ± 0.023 was obtained from the ratio of independent measurements of absolute neutron emission rate and absolute fission rate.

E. $^6\text{Li}(n,\alpha)$ CROSS SECTION (J. C. Engdahl, J. C. Robertson)

We have made significant progress toward a new $^6\text{Li}(n,\alpha)$ cross section measurement at 24 keV. Methods have been developed for the registration of reaction product tracks on cellulose nitrate film with essentially 100% efficiency. A Sb-Be source similar to our previous photoneutron sources has been constructed and irradiated for the first time.

In order to eliminate dependency on angular distribution information, multiple targets and detector orientations will be used to average out reaction product anisotropy.

First measurements at 24 keV will take place shortly. Additional measurements using our other sources will follow.

NATIONAL BUREAU OF STANDARDS

A. NEUTRONS

1. International Neutron Flux Intercomparison (M. M. Meier, O. A. Wasson, and K. C. Duvall)

The NBS Van de Graaff Laboratory participated in the international flux intercomparison sponsored by BIPM in December 1976. Seven national standards laboratories measured the efficiencies of a BF_3 counter imbedded in a polyethylene sphere and a ^3He proportional counter at their respective neutron flux facilities. The NBS participated at 250 and 565 keV and monitored flux with the "black" detector. The results will be presented by V. D. Huynh at the International Specialists Symposium on Neutron Standards and Applications.

2. Black Detector Calibration (M. M. Meier)

The differential efficiency as a function of pulse height for the black detector has been measured using the associated particle technique at neutron energies of 870, 700, and 500 keV. A Monte Carlo program written by Poenitz¹ which calculates the same function has been modified to include the effects of the Poisson statistics of photoelectron production. A comparison of the experimental and calculated response is shown in Fig. A-1. The efficiencies calculated at the bias levels shown agree to better than two percent. This work is being continued with a somewhat improved experimental design in expectation of reducing this discrepancy to the one percent level and extending the energy range to 250 keV.

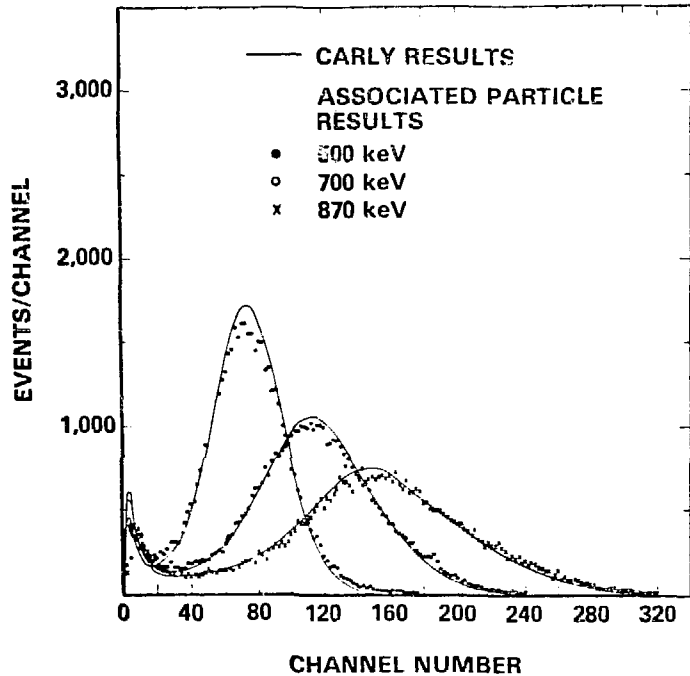
3. Nanosecond Wide Pulses of eV Neutrons (K. C. Duvall, O. A. Wasson, M. M. Meier, and C. D. Bowman)

We have repeated the (p,n) experiment of Lefevre and Ross² on the target ^{64}Ni which was reported to yield 100 n/microcoulomb within a 4° half angle in a 400-700 eV wide band. The reaction is of particular interest owing to the effective kinematic collimation, the relatively high yield, and the short pulse width which is limited only by the capabilities of the accelerator. The collimation reported by Lefevre and Ross has been verified, but our preliminary results on yield indicate nearly three times as many neutrons as they report.

¹ W. P. Poenitz, Argonne National Laboratory Report No. 7915 (1972).

² H. W. Lefevre and E. W. Ross, Phys. Rev. C13, 2083 (1975).

Figure A-1.
Black detector calibration.



4. High Resolution Total Cross Sections (H. T. Heaton II, C. D. Bowman, and A. D. Carlson)

Attempts to use a single rf pulse from the NBS electron linear accelerator in conjunction with the 200 meter flight path to make high resolution (~ 15 keV at 20 MeV) neutron total cross section measurements have not been as successful as initially anticipated primarily due to the small amount of charge available when operating in this mode. To date the best which has been achieved is a linac pulse containing three microstructure pulses with a relative charge distribution of 1.0 to 3.4 to 1.1 and an average current of $\sim .15$ μ A. Using the gamma flash incident on a 3 cm thick plastic scintillator to measure the timing resolution, a 450 psec resolution has been achieved using the center 2.5 cm portion of a 12.5 cm photomultiplier tube as shown in Fig. A-2. This resolution increases to about 700 psec when using 10 cm of the phototube. Current attempts to achieve high resolution data involve developing suitable techniques for unfolding a pulse containing many microstructure pulses from the data.

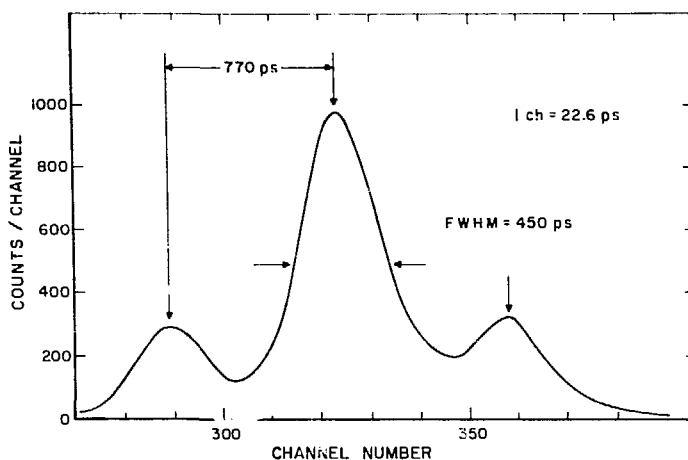


Figure A-2. Measured time resolution.

5. A Measurement of the ${}^6\text{Li}(n,\alpha)\text{T}$ Cross Section from 3 - 800 keV
(G. P. Lamaze, O. A. Wasson, and R. A. Schrack)

The ${}^6\text{Li}(n,\alpha)\text{T}$ cross section has been measured from 3 to 800 keV neutron energy at the NBS Linac above ground neutron time-of-flight facility. The experiment was conducted along the 200 meter drift tube. The ${}^6\text{Li}(n,\alpha)\text{T}$ events were detected at 69.25 m in a 0.5 mm thick ${}^6\text{Li}$ loaded glass scintillator (NE912) coupled to an RCA 8850 photomultiplier tube. The neutron flux was monitored at 200 m with a 5.08 cm x 60.96 cm hydrogen filled proportional counter. Both pulse height and flight time were recorded for each event in each detector. The peak cross section was determined to be $3.15 \pm .09$ barns at 241 ± 3 keV. The results have been included in the ENDF-B/V evaluation and are in excellent agreement with an R-matrix analysis of the ${}^7\text{Li}$ system performed by G. Hale of LASL. A paper has been prepared for submission to Nuclear Science and Engineering.

6. A Measurement of the ${}^{235}\text{U}(n,f)/{}^6\text{Li}(n,\alpha)\text{T}$ Cross Section Ratio
from 6 eV to 30 keV (G. P. Lamaze)

The ${}^{235}\text{U}(n,f)$ cross section has been remeasured from 6 eV to 30 keV relative to ${}^6\text{Li}(n,\alpha)\text{T}$ at the 20 m flight path of the NBS linac above ground time-of-flight facility. The fission events were detected in a 10.16 x 17.78 cm parallel plate fission chamber with a total mass of 173 mg of ${}^{235}\text{U}$. The ${}^6\text{Li}(n,\alpha)\text{T}$ events were detected in a .5 mm thick ${}^6\text{Li}$ loaded glass scintillator. Background was measured continually with resonance filters of ${}^{238}\text{U}$, Na, and Al. The data are currently being

analyzed and the results will be compared with a previous NBS $^{235}\text{U}/^6\text{Li}$ ratio measurement reported at the Proceedings of the NEANDC/NEACRP Specialists meeting of Fast Neutron Fission Cross Sections of ^{233}U , ^{235}U , ^{238}U , and ^{239}Pu held at Argonne (June 1976).

7. $^{235}\text{U}(n,f)$ and $^{237}\text{Np}(n,f)$ Cross Section Measurements in the MeV Energy Region (A. D. Carlson and B. H. Patrick)

Relative measurements of the ^{235}U and ^{237}Np fission cross sections in the energy range from about 0.7 to 3.5 MeV are nearing completion. These measurements are being carried out at the 60 m flight path of the linac neutron time-of-flight facility. The uranium and neptunium are contained in separate parallel plate ionization chambers with deposits of $\approx 100 \mu\text{g}/\text{cm}^2$ on each side of five plates. The neutron flux is determined using a Si(Li) detector to record recoil protons from neutrons which scatter in a thin polyethylene film. The detector is shielded from the direct beam by a thick tapered lead cylinder. The data from the flux detector and the fission chambers are obtained during the same linac run using a multiexperiment, 2-parameter (time and pulse height) data acquisition system. The data already collected are in the process of being analyzed. The measurements on ^{235}U will provide a tie in with the recently completed NBS measurements from 5 to 800 keV neutron energy. The present measurements are the first phase of a program for the determination of the ^{235}U and ^{237}Np fission cross sections. The second phase will extend the energy region up to ≈ 20 MeV.

8. Kerma Factors for 19 Elements or Nuclides up to 30 MeV
(R. S. Caswell, J. J. Coyne, and M. L. Randolph, ORNL)

Tables of calculated kerma factors for neutrons (kerma per unit neutron fluence, where kerma is the energy transferred to secondary charged particles) have been completed for 19 elements or nuclides: H, ^6Li , ^7Li , B, C, N, O, F, Na, Al, Si, P, S, Cl, Ar, K, Ca, and Fe. The chief source of nuclear data is the Evaluated Nuclear Data File ENDF/B-4 up to 20 MeV. From 20 MeV to 30 MeV reaction cross sections have been extrapolated from lower energy cross sections using total cross section information and optical model cross sections as a guide. The kerma factors will appear in a report, Neutron Dosimetry for Biology and Medicine of the International Commission on Radiation Units and Measurements (ICRU, in press). It is intended to publish a more complete description of the calculations and underlying assumptions in the near future. Comparison will be made to other calculated kerma factors.

9. Chemical Effects on Uranium Fission (R. A. Schrack,
D. M. Gilliam, G. P. Lamaze, C. D. Bowman)

A reported chemical effect on the neutron induced fission cross section of ^{235}U prompted an attempt to observe the effect using the NBS double fission chamber.¹ The fission foils of the NBS chamber are .005" platinum discs with a deposit of UO_2 (99.7% ^{235}U) about $500 \mu\text{g}/\text{cm}^2$ thick covering an area of about 1 cm^2 in the center of the fission foils. Two foils of approximately equal mass were chosen. One of the fission foils was baked to oxidize it to U_3O_8 . The fission yields were measured using the external thermal beam of the NRS reactor. The fission chamber was rotated to remove any effects due to chamber asymmetries. The ratios of U_3O_8 to UO_2 yield obtained were:

$$.9794 \pm .00085$$

$$.9795 \pm .00029$$

with a weighted average of $.97948 \pm .00027$

The other UO_2 foil was then removed and baked in the same manner as the first and the ratios of U_3O_8 to U_3O_8 yield were then obtained:

$$.9774 \pm .00022$$

$$.9763 \pm .00025$$

$$.9763 \pm .00025$$

with a weighted average of $.9767 \pm .00014$

To eliminate the effect of the mass difference of the two foils, the ratio of the above yields gives the relative yield of $\text{U}_3\text{O}_8/\text{UO}_2 =$

$$\frac{.97948 \pm .00027}{.97670 \pm .00014} = 1.0028 \pm .00032$$

All errors are from counting statistics only. Systematic errors are not known but are believed to be significantly greater than the statistical errors. A measure was made of the α -particle yields from the foils to determine any mass difference. The ratio of this mass difference before and after the second baking is $1.0011 \pm .002$ and is thus not sufficiently accurate to determine if there was any mass loss or not. If any mass

¹ J. A. Grundl, D. M. Gilliam, N. D. Dudey, R. J. Popek, Measurement of Absolute Fission Rates. Nuclear Technology 25, 237-257 (1975).

were lost however in the $UO_2 \rightarrow U_3O_8$ conversion, the observed effect would have been increased. Other systematic errors have not been investigated. Samples of U_3O_8 and UO_2 are now being prepared for further measurements that will measure the relative yield of fission products by measuring γ ray and delayed neutron yields.

10. Absolute Measurement of the $D(t,n)He^4$ Thick Target Yield in Deuterium for $E_t = 191.3$ KeV (R. F. Fleming, R. B. Schwartz, and M. P. Unterweger)

We have developed a technique for the measurement of thick target yields for charged particle reactions using a thermal neutron beam. The technique has been applied to the D-T fusion reaction by using a deuterium proportional counter with a small addition of He-3 gas. When placed in a thermal neutron beam, 191.3 KeV tritons are produced by the reaction $He^3(n,\bar{\nu})T$. As these tritons slow down in the deuterium gas the D-T reactions take place producing an energetic alpha particle. The thick target yield is just the ratio of the alpha count rate to the He-3 count rate.

The corrections for detector end effects, pulse pileup, etc. are now being made. If accurate data for the stopping power of hydrogen ions in deuterium can be obtained, our result will provide an absolute normalization for the D-T cross section.

11. Personnel Dosimetry Program (R. B. Schwartz and I. G. Schroder)

The three beam filters, producing neutron beams of 2, 25, and 144 keV, have been installed at the NBS Reactor. All three are in tangential beam tubes: the scandium filter (2 keV) views a manganese resonant scatterer, and the iron (25 keV) and silicon (144 keV) filters view a graphite scatterer. This arrangement reduces the gamma-ray background and the contamination with "wrong" energy neutrons, at the cost of lower intensity. The beam characteristics are given in Table 1.

The beams are being used primarily for neutron dosimeter calibrations. In the case of the 25 keV and 144 keV beams, there is good agreement with calibrations obtained using accelerator neutron sources*. (There are, of course, no appropriate accelerator sources of 2 keV neutrons.)

* D. E. Hankins, private communication.

Table 1 Neutron Beam Characteristics

<u>En</u> (keV)	<u>Filter</u> <u>material</u>	<u>diam.</u> (cm)	<u>Intensity</u> (n/sec)	<u>% of other</u> <u>energy</u> <u>neutrons</u>	<u>γ</u> <u>intensity</u> mR/hr
2	110 cm sc 1 cm Ti	1.7	6×10^5	3%	8
24	30 cm Fe 30 cm Al	2.5	1×10^6	0.3%	9
144	136 cm Si 2 cm Ti	2.5	2.2×10^6	~0	40

12. Absolute Measurement of the ^{235}U Mass in a Large Volume Multiplated Fission Ionization Chamber (O. A. Wasson, M. M. Meier, D. M. Gilliam, and R. B. Schwartz)

It is essential to know the ^{235}U mass contained in the large volume, 10 deposit, fission ionization chamber used in measurements of the absolute ^{235}U neutron fission cross section at the NBS Van de Graaff. The absolute mass of the approximately 200 mg ^{235}U in the chamber was measured relative to two standard ^{235}U fission deposits mounted in the NBS double fission ionization chamber¹ by means of tailored, large diameter, uniform thermal neutron beam from the thermal column at the NBS reactor. The neutron flux was uniform within $\pm 0.75\%$ throughout a 30 cm diameter which irradiated both chambers. The relative neutron induced fission rates of both chambers were measured at the same position. The mass measurement was independent of the geometrical area and density variations of the deposits, the absolute neutron flux, the neutron energy distribution, and the neutron cross sections. The ^{235}U in the large chamber was 173.1 mg with a one standard deviation systematic error of 1.8%.

¹ J. A. Grundl, D. M. Gilliam, N. D. Dudey, and R. J. Popek, Nucl. Technol. 25, 237 (1975).

13. Neutron Irradiation and Calibration Services (V. Spiegel)

The following activation detectors were irradiated at the ^{252}Cf irradiation facility to a maximum fluence of about 10^{13} neutrons: three irradiations of sulfur disks; one irradiation of nickel, titanium, and aluminum disks; three irradiations of transistors, and one irradiation of ^{235}U , ^{238}U , ^{237}Np , and ^{232}Th dosimeters. Six neutron sources were calibrated during the past year at the Manganese Sulfate Bath facility.

14. Compendium of Benchmark Neutron Fields for Reactor Dosimetry (J. A. Grundl and C. M. Eisenhauer)

The identification of neutron fields with proper characteristics for referencing reactor neutron dosimetry measurement methods is in progress under a new program initiated by the IAEA. An international survey to compile information on such benchmark neutron fields is complete and a first-round report has been prepared. It summarizes for each benchmark in the form of a compendium a physical description of the facility, characteristics of the neutron field, assigned neutron spectrum, selected reaction rate ratios both measured and predicted, and availability of the field for dosimetry referencing irradiations.

The first compilation is restricted to standard and reference neutron fields understood within the context of the following characteristics:

1. Simple and well-defined geometry
2. Adequate neutron fluence and stable flux density
3. Reproducible and accurately characterized neutron spectra based on spectrum measurements and/or reliable calculations
4. Sustained availability for measurements.

The compendium was presented at the IAEA Consultants Meeting on Integral Cross Section Measurements in Standard Neutron Fields for Reactor Dosimetry held in Vienna, November 1976. Manuscript copies are available.

15. A Californium-252 Fission Spectrum Irradiation Facility for Neutron Reaction Rate Measurements (J. A. Grundl, V. Spiegel, C. M. Eisenhauer, H. T. Heaton II, D. M. Gilliam, and J. Bigelow (ORNL))

Spontaneous fission sources of ^{252}Cf lightly encapsulated and with neutron source strengths approaching 10^{10} n/sec, have been developed

especially for integral cross section measurements and neutron reaction rate calibrations. An irradiation facility at the National Bureau of Standards makes use of these sources in two well-investigated geometries. A free-field neutron flux in the range of 10^7 n/cm² sec and fluences of up to 10^{13} n/cm² are established at the facility based only upon a distance measurement and the absolute source strength of the national standard Ra-Be photoneutron source. The error in the ²⁵²Cf source strength ($\pm 1.1\%$) dominates the total free-field flux uncertainty of $\pm 1.4\%$ (1σ). Neutron scattering effects in the source capsule and support structures, and neutron return from concrete and earth boundaries have been calculated and investigated experimentally. In the worst case they contribute $\pm 0.7\%$ to the total flux response uncertainty for all observed neutron reaction rates, including those with sensitivity to low-energy neutrons.

Fission cross section measurements with ²⁵²Cf fission neutrons have been carried out with double fission chambers and the NBS set of reference and working fissionable deposits. Recently completed fissionable deposit isotopic mass intercomparisons and comparisons of observed and calculated anisotropy of source capsule transmission provide an updated experimental result for the fission cross section of ²³⁵U:

$$\bar{\sigma}_f(^{235}\text{U}, \chi_{\text{Cf}}) = 1205 \pm 27 \text{ mb.}$$

This value falls below that calculated with the ²³⁵U(n,f) energy dependent cross sections of ENDF/B-IV by 3.0%. The error in this cross section validation measurement attributable to ²⁵²Cf fission spectrum uncertainties is less than $\pm 0.2\%$.

Calibration irradiations in the Big Ten Critical Assembly at Los Alamos, a benchmark for breeder reactor fuels and materials dosimetry, have been monitored with the NBS double fission chambers. One component of these measurements was to establish a neutron flux level in such an environment by means of a direct flux transfer from the NBS ²⁵²Cf fission neutron field. The transfer to the central Big Ten field, accomplished with a ²³⁹Pu-loaded fission chamber, does not depend significantly upon any neutron reaction cross section. Since the ²³⁹Pu fission cross section is largely independent of energy for both spectra, the spectrum correction for the flux transfer, $\bar{\sigma}_f(^{239}\text{Pu}, \chi_{\text{Cf}}) / \bar{\sigma}_f(^{239}\text{Pu}, \text{Big Ten})$, is close to unity; the calculated value is 1.11 ± 0.015 . The neutron flux level for Big Ten irradiations of high-power activation dosimeters was established at 8.2×10^{10} n/cm² sec with a total error exclusive of cavity perturbations of less than $\pm 2\frac{1}{2}\%$ (1σ).

An absolute spectrum-averaged cross section for $^{238}\text{U}(n,f)$ may be obtained on the basis of this flux transfer measurement. For the center of Big Ten the cross section determined with a ^{238}U fission chamber containing a natural uranium deposit of known mass is

$$\bar{\sigma}_f(^{238}\text{U}, \text{Big Ten}) = 50.7 \pm 1.5 \text{ mb}$$

The computed value for the Big Ten spectrum based on new calculations using ENDF/B-IV cross sections is 52.3 mb vs a previous computed value of 46 mb based on ENDF/B-III cross sections. The new inelastic cross sections for ^{238}U in ENDF/B-IV have removed a long-standing disagreement between integral cross section measurements and the results of neutron transport calculations in a basic reactor physics critical.

16. A Gamma Ray Laser Using Existing Technology (C. D. Bowman)

In exploring the influence of solid state on neutron physics several unexplored phenomena were recognized which have an analog with the influence of solid state on the physics of γ -ray interactions and transport. From these studies has emerged a concept for a γ -ray laser based on nuclear transitions and using the above phenomena for control (focusing, dispersion, reflection, background reduction) of the laser is based on the 9.3 keV transition in ^{83}Kr which apparently can be pumped either by (γ,n) or (n,γ) reactions with our most intense presently available laboratory sources of neutrons and bremsstrahlung or by nuclear explosions. Since the concepts based on nuclear explosions and laboratory sources are entirely different, two reports are being prepared describing approaches along these two lines.

17. Doppler-Free Neutron Spectroscopy (C. D. Bowman and G. P. Lamaze)

For many years the obtainable experimental resolution in neutron spectroscopy has been much finer than the broadening introduced by thermal motion of target nuclei. The purpose of this work is to demonstrate that the Doppler effect can be avoided by three different techniques--none of which have been theoretically or experimentally explored. All three methods involve the measurement of elastic scattering. The first is simply small angle forward scattering at angles of about 15° or less. At these angles, the nuclear recoil energy is small enough that Mossauer-like binding of the nucleus in the lattice can take place. The second is by coherent scattering at neutron resonances. Near the resonances the coherent scattering can become very large. The atoms acting coherently and therefore without recoil scatter neutrons strongly at the Bragg angle. The third is by resonance "total" reflection which takes place at the interface of two media when the index of refraction

(which depends on the scattering length at resonance) of the two media differs. These three effects exist also in the nuclear scattering of γ -rays.

Experiments at the NBS linac to positively identify these effects have not yet been successful. Studies of the small angle scattering had initially led us to conclude that the required combination of neutron intensity and resolution could not be obtained at NBS. However recent studies into the details of phonon transfer show that the experiment was not properly designed. Meanwhile Poortmans at BCNM has reported effects in total cross section measurements on ^{238}U which he believes can only be associated with this effect. Owing to special laboratory geometry at the LLL linac, it appears possible to do a feasible experiment on the second (coherent scattering) method. Finally, a tungsten reflector has been polished for an attempt at NBS to verify the total reflection concept.

18. Influence of Molecular Vibrations on the Shape of Neutron Resonances in Gases (C. D. Bowman and R. A. Schrack)

We have performed calculations showing that the shape of neutron resonances in gaseous samples is influenced not only by the usual Doppler effects but also by molecular excitations. We follow the approach taken by Lehtohov (Phys. Rev. A12, 1954 (1975)) in calculating such effects for nuclear absorption or scattering of γ -rays and apply it to neutron reactions with molecules of the form XY_6 for the atom X located at the center of mass of the molecule.

These molecules have two normal modes involving the X atom. For UF_6 these modes carry an energy of $\hbar\omega = 23$ and 78 meV. For a molecule in the ground state, the probability of exciting these vibrations in various combinations is given by

$$P_{\alpha_1, \alpha_2, \alpha_3, \beta_1, \beta_2, \beta_3} = \frac{1}{2\pi} \frac{Z_\alpha^{(\alpha_1+\alpha_2+\alpha_3)} Z_\beta^{(\beta_1+\beta_2+\beta_3)} e^{-(Z_\alpha+Z_\beta)}}{\alpha_1! \alpha_2! \alpha_3! \beta_1! \beta_2!}$$

$$\cdot B(\alpha_3+\beta_3+1/2, \alpha_1+\alpha_2+\beta_1+\beta_2+1) B(\alpha_2+\beta_2+1/2, \alpha_1+\beta_1+1/2)$$

where the α_i are quantum numbers associated with one normal mode and β are the quantum numbers associated with the other normal mode. The quantities Z_α and Z_β are constants involving the mass and force constant associated with the normal mode and the neutron energy. The B term is the Beta function.

The influence on resonance shape has been calculated for several resonances in ^{238}U . The result for capture in the 20.9 eV resonance is compared in Fig. A-3 for a solid and for UF_6 gas at room temperature. The effects are manifested in the shape and also in the position of the resonance which is shifted somewhat higher in energy. It appears that this effect would be easy to observe in comparative transmission experiments on uranium metal and UF_6 .

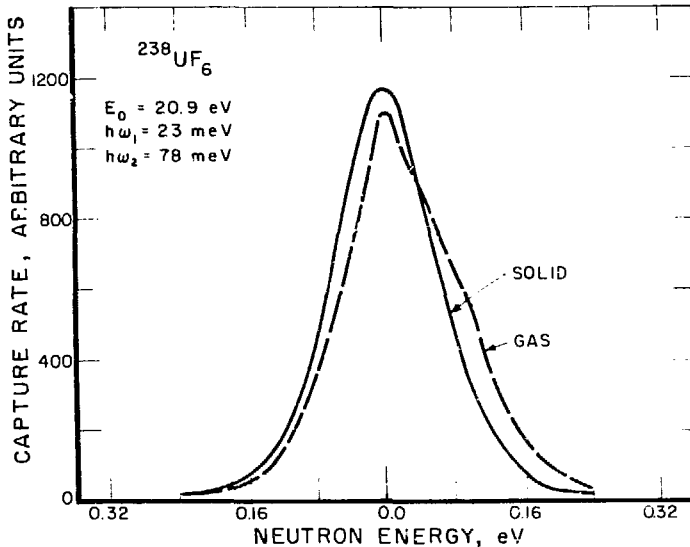


Figure A-3. Shape of 20.9 eV resonance.

19. Phonon Transfer Effects on Low Energy Fission Cross Sections (C. D. Bowman and R. A. Schrack)

The influence of phonon transfer on low energy neutron reaction cross sections for solid materials has been calculated for the special case of $T=0$ and for arbitrary temperatures. At $T=0$ the Debye approximation to the phonon spectrum was used and at higher temperatures the Einstein (delta function) approximation was assumed. At higher temperatures the cross section can be represented by the expression

$$\sigma_{(n,f)} = 4\pi \lambda^2 g \Gamma_n \Gamma_f W'(E)$$

$$W'(E) = e^{-b(2\alpha+1)} \sum_{n=-\infty}^{\infty} \frac{[\alpha/(\alpha+1)]^{n/2} I_{(n)} \{2b\alpha(\alpha+1)\}^{1/2}}{(E-E_0+n\epsilon)^2 + \Gamma^2/4}$$

where $b = \pi E/M\epsilon$, I is the imaginary bessel function of the first kind,

$\alpha = [\exp(\epsilon/kT) - 1]^{-1}$ and ϵ is the average energy of the phonon transferred. This equation can be transformed to the same form as given in the Jackson and Lynn paper with the exception of an apparent typographical error in their expression. Note that the phonon transfer can be expressed simply as the sum of a number of unbroadened B-W relations displaced by the energy $n\epsilon$ and weighted with the proper coefficient.

In Fig. 1 the comparison of the fission cross section for ^{235}U is shown with and without phonon transfer by displaying their ratio. Several different temperatures are shown with kT expressed in meV. The value for ϵ was taken to be 14 meV although the results are relatively insensitive to the value of ϵ . The effects appear to be small at thermal energies but not entirely negligible compared to presently claimed accuracies. At higher energies, the effects increase into the 0.5 to 1% range. Note the relatively large difference predicted between $T=0$ and $T=25$ meV.

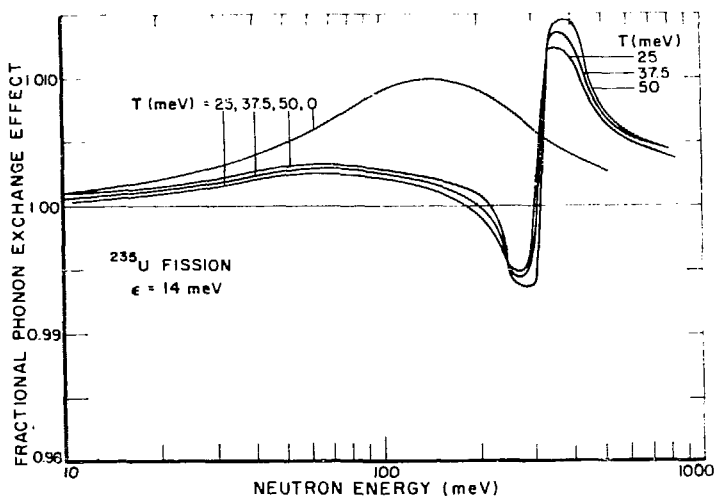


Figure 1. Effect of phonon exchange in ^{235}U .

For ^{239}Pu the effects as shown in Fig. 2 at thermal energy appear to be entirely negligible, but near the 0.3 eV resonance differences of about $\pm 5\%$ are encountered. The dashed line shows the effect of Doppler broadening at $T=25$ meV calculated using the usually applied gas model. Note that not only are the magnitudes incorrect, but the cross section on the low energy side is even changed in the opposite direction from our calculation.

During the coming year we hope to conduct experiments verifying these prediction.

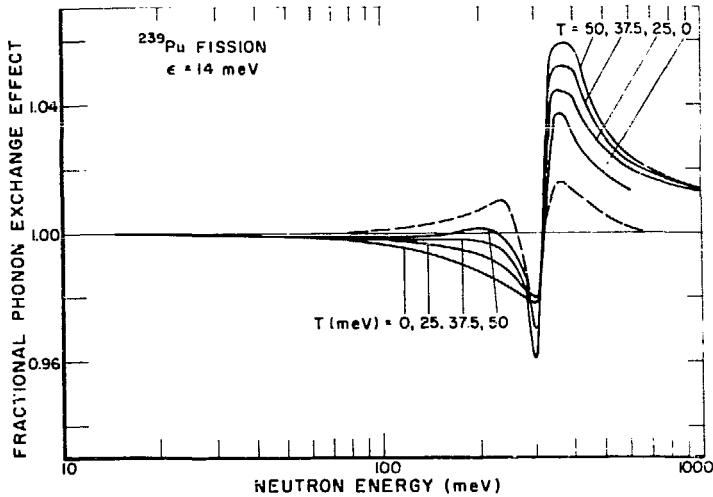


Figure 2. Effect of phonon exchange in ^{239}Pu .

These calculations do not include the effect of phonon exchange on the energy dependence in the neutron entrance channel ($r_p = r_p^0 \sqrt{E}$). The effects of including this term are now being calculated and are expected to be negligible in the several hundred millivolt range, but below 50 meV should be as large as several tenths of one percent.

20. Measurement of the Neutron-Flux at the APFR Pulsed Reactor
(E. D. McGarry, D. M. Gilliam, A. H. Rozi, and G. S. David)

A flux-transfer technique has been used to measure the total neutron flux to an accuracy of 5% at the Army Pulse Radiation Facility (APRF) fast pulse reactor.¹ Use was made of ^{239}Pu -loaded fission chambers developed by the National Bureau of Standards (NBS) and calibrated against a ^{252}Cf source at NBS. Advantages of the method were that it used a standard source for calibration, that it was independent of errors in fission foil masses, and that the effects of cross-section errors were minimized by the need to use only cross-section ratios.

¹ E. D. McGarry, A. H. Rozi, G. S. David, D. M. Gilliam, "Absolute Neutron-Flux Measurement at Fast Pulse Reactor with Calibration Against Californium-252," IEEE Conf. on Nuclear and Space Radiation, San Diego (July 1976).

The results show that previous dosimetry was 18% too high in the APRF in-core irradiation facilities, and 21% too high at core surface. Flux calibrations have also been made by using ^{237}Np , several uranium isotopes, and the $^{32}\text{S}(n,p)^{32}\text{P}$ reaction. Fluxes from all measurements agreed to 7%. The (>10 keV/ >3 meV) flux ratios determined for the 'glory holes' and leakage spectra were 8.4 ± 0.6 and 7.3 ± 0.5 , respectively.

21. Intercomparison of Fission Rate Measurements: Karlsruhe Reactor Physics and Los Alamos Radiochemistry (D. M. Gilliam and J. A. Grundl)

Fission rate measurement scales at two laboratories engaged in quite different branches of nuclear energy development have been intercompared via NBS initiative and cooperative execution. The Reactor Physics Group at GfK (Gesellschaft für Kernforschung) in Karlsruhe, Germany, submitted fissionable deposits for direct comparisons with NBS reference deposits, and the Radiochemistry Group at Los Alamos participated in joint fission rate measurements with NBS at Los Alamos. For the basic uranium fissionable isotopes, both laboratories are within 2% of the NBS fission rate measurement scale. This is marginally adequate for some programmatic goals; more serious, however, is a discrepancy between Los Alamos and NBS of nearly 6% for ^{239}Pu fission rate measurements.

With the cooperation of Dr. Werner Scholtyssek of GfK, fissionable deposits of ^{235}U , ^{239}Pu , and normal uranium were sent to NBS for comparisons with the corresponding NBS reference deposits. The mass assay of the NBS reference deposits has been described in detail by Grundl, et al.¹

Table 1 shows the results of the comparison and the estimated uncertainties. The largest uncertainties were the quoted errors (1.2% to 1.5%) for the NBS reference deposits themselves.¹ Other systematic errors contributed about 0.5% uncertainty or less.

¹ J. A. Grundl, D. M. Gilliam, N. D. Dudey, and R. J. Popek, "Measurement of Absolute Fission Rates," Nuclear Technology 25, 237 (1975).

Table 1 Comparison of results

Principal Isotope	Mass Determined by NBS μg	Mass Determined by GfK μg	Mass Scale Ratio GfK/NBS
^{238}U	$325.1 \pm 1.6\%$	325	0.9997
^{235}U	$309.4 \pm 1.3\%$	311	1.0052
^{239}Pu	$28.62 \pm 1.3\%$	28.98	1.0126

The intercomparison of absolute fission rate measurements between NBS and the Radiochemistry Group responsible for weapons diagnostics at Los Alamos Scientific Laboratory (LASL) was carried out at LASL. After calibrations and temperature effects testing at the National Bureau of Standards Reactor, double fission chambers developed at NBS were operated in the BIG-10 critical facility at LASL simultaneously with the irradiation of an activation fission foil pack which was later destructively analyzed by the Radiochemistry Group. Table 2 shows the results of the comparison. The striking discrepancy in ^{239}Pu fission rates is receiving careful study by both groups.

Table 2 Fission rates (per nucleus) in BIG-10 Test C-LASL

	Isotope Studied			
	^{235}U	^{238}U	^{237}Np	^{239}Pu
NBS Measurement ($10^{-15} \text{ sec}^{-1}$)	$110.4 \pm 1.5\%$	$4.14 \pm 1.8\%$	$35.2 \pm 1.9\%$	$132.3 \pm 1.6\%$
LASL Measurement ($10^{-15} \text{ sec}^{-1}$)	$112 \pm 1.6\%$	$4.21 \pm 3.8\%$	$35.3 \pm 5\%$	$140 \pm 2\%$
LASL/NBS	1.014	1.017	1.003	1.058

22. Fast Reactor Fission Yields (D. M. Gilliam and J. A. Grundl)

The Interlaboratory LMFBR Reaction Rate (ILRR) program¹ has achieved accuracies in the range of 1.9% to 2.5% in the measurement of selected fission product yields which are of interest in fuels and materials dosimetry for fast breeder reactors. For fast neutron induced fission in the major fuel isotopes ^{239}Pu and ^{238}U , results are reported for the fission products ^{95}Zr ($t_{1/2} \approx 64\text{d}$), ^{103}Ru ($t_{1/2} \approx 39\text{d}$), and ^{140}Ba ($t_{1/2} = 12.8\text{d}$). Since some energy dependence was indicated in the yield of ^{103}Ru from ^{235}U , only ^{95}Zr and ^{140}Ba yields are reported for ^{235}U fission. Accuracies in the range of 3.6% to 5% were achieved for fission yields from ^{237}Np .

The ILRR fission yield results are summarized in Table 1. Table 2 gives the decay scheme data used in deriving the results of Table 1. Taken together, these two tables provide a consistent basis for fission rate measurements which is independent of the gamma-ray intensity data.

Table 1 Recommended Fission Yields for a Fast Reactor Spectrum

ILRR Yield and Total Error		Principal Isotope of Fission Foil			
		^{235}U	^{238}U	^{239}Pu	^{237}Np
Fission Product Nuclide	^{95}Zr	0.0647 <u>+2.2%</u>	0.0521 <u>+2.6%</u>	0.0480 <u>+2.3%</u>	0.0593 <u>+5.0%</u>
	^{103}Ru	Energy de- pendance	0.0635 <u>+2.5%</u>	0.0708 <u>+2.3%</u>	0.0592 <u>+4.3%</u>
	^{140}Ba	0.0606 <u>+1.9%</u>	0.0599 <u>+2.2%</u>	0.0530 <u>+2.0%</u>	0.0571 <u>+3.6%</u>

¹ W. N. McElroy, Nuclear Technology, Vol. 25, Feb 1975, p. 177.

Table 2 Decay Scheme Data and Errors

Fission Product Nuclide	Half-life* (days)	Gamma-Ray* Energy (keV)	Gamma-Ray Intensity* (%)	Resultant Yield Uncertainty (%)
⁹⁵ Zr	54.1 ± 0.3	724.179	44.1 ± 0.5	} 1.1
		756.710	54.6 ± 0.5	
¹⁰³ Ru	39.43 ± 0.10	497.08	89.0 ± 1.0	1.2
¹⁴⁰ Ba	12.789 ± 0.006	537.35	24.4 ± 0.3	} 0.2
¹⁴⁰ La	1.6775 ± 0.0008	1596.18	95.40 ± 0.08	

Table 3 shows the differences in the results from two different fast neutron spectra which were employed in these measurements. BIG-10 is a very well characterized fast critical facility at the Los Alamos Scientific Laboratory. The fast neutron field in the CFRMF¹ critical facility is achieved by means of a zoned-core configuration with a water-moderated thermal neutron driver. In Table 3, the 2.4% difference for the ¹⁰³Ru yield of ²³⁵U is significantly large with respect to the experimental precision; therefore, no single precise value can be stated for that case. All of the other differences are within the experimental error.

¹ W. N. McElroy, Nuclear Technology, Vol. 25, Feb 1975, p. 177.

* These data (in columns 2, 3, and 4) were given in a private communication from R. G. Helmer, Nuclear Physics Branch, Aerojet Nuclear Company, Idaho National Engineering Laboratory, Sept. 1, 1976. An earlier review by Helmer and R. C. Greenwood was published in Nuclear Technology, 25, No. 2, February 1975., p. 258.

Tabel 3 Ratio of Fast Fission Yields: CFRMF/BIG-10

CFRMF Yield - 1 BIG-10 Yield		Principal Isotope of Fission Foil			
		²³⁵ U	²³⁸ U	²³⁹ Pu	²³⁷ Np
Fission Product Nuclide	⁹⁵ Zr	0.1 %	0.8 %	0.3 %	4.5 %
	¹⁰³ Ru	-2.4 %	-1.0 %	-0.6 %	-0.5 %
	¹⁴⁰ Ba	-0.2%	-0.7 %	0.6 %	1.3 %

23. Intermediate-Energy Standard Neutron Field (ISNF)
(D. M. Gilliam, J. A. Grundl, and C. M. Eisenhower)

a. Physical Description

The initial ISNF has been set up in the graphite thermal column of the NBS reactor. A square opening, 30 cm x 30 cm provides access to the center of the graphite column (parallelepiped 1.4 x 13. x 0.94 meter, density 1.71 g/cm³). Split graphite blocks containing the ISNF cavity and cylindrical access penetrations may be inserted through the biological shield of the reactor and into the thermal column opening with the reactor at full power. A detailed schematic cross section of the ISNF arrangement within the cavity is shown in Fig. 1.

Fission neutrons from the fission converter disks are partially moderated in the surrounding graphite. Those which return to the cavity are transmitted by the boron-10 shell (along with an uncollided component from the source disks) to produce the ISNF neutron field at the center of the cavity.

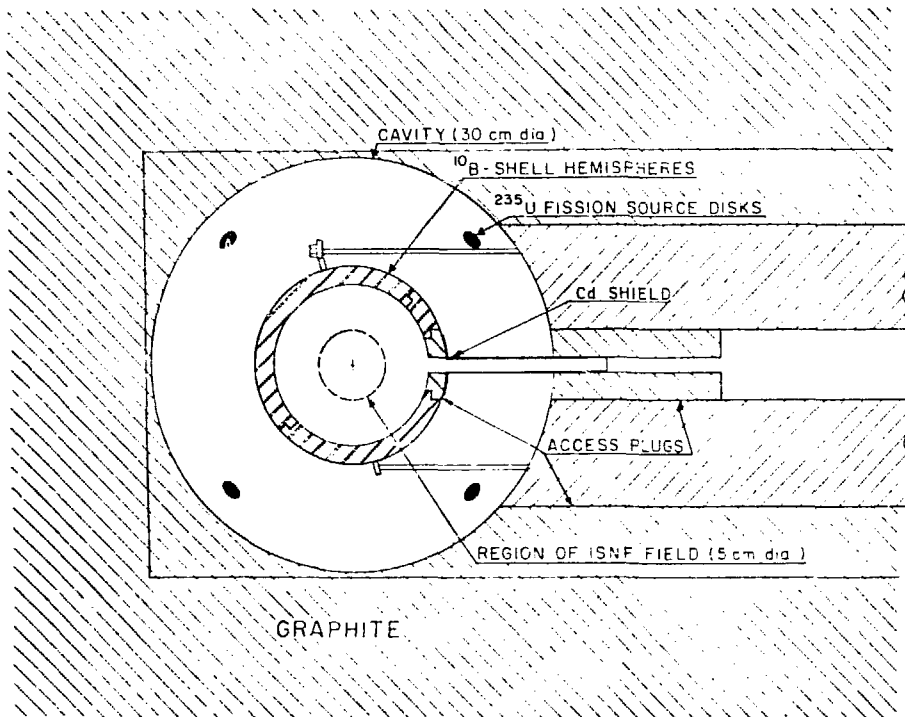


Figure 1. ISNF geometry.

b. Neutron Flux and Fluence

The thermal neutron flux in the cavity is $\sim 1 \times 10^{11} \text{ cm}^{-2}\text{sec}^{-1}$ and each disk operates at a fission power of about one watt. Eight disks are used in normal operations so that the total neutron source strength in the thermal column cavity is about $6 \times 10^{11} \text{ sec}^{-1}$. The resultant flux and fluence at the center of the cavity are as follows:

Total neutron flux intensity: $\sim 1 \times 10^9 \text{ n}\cdot\text{cm}^{-2}\cdot\text{s}^{-1}$

Typical maximum fluence: $\sim 1.5 \times 10^{14} \text{ n}\cdot\text{cm}^{-2}$

Neutron Field gradient: $\sim 2\%$ over 4 cm

Average and median neutron energies: 1.0 MeV and 0.56 MeV respectively

Spectrum energy range: 90% between 8 keV and 3.5 MeV

Response range of $1/\nu$ -detector: 90% between 0.5 keV and 1.5 MeV

Specific neutron flux intensities are established by flux transfer from the NBS ^{252}Cf source using $^{239}\text{Pu}(n,f)$ as the transfer reaction.

c. Neutron Flux Monitoring

Flux monitoring for routine irradiations will be accomplished by means of fission chambers and/or activation foils located inside of the boron-10 shell.

d. Neutron Spectrum

Assignment of the ISNF spectrum is based solely on neutron transport calculations which are subject to sensitivity studies. The cross sections used in calculations carried out at NBS through 1976 are based on ENDF/B-III spectrum averaged in a 40-group energy structure. The spectrum at the center of the ISNF was calculated with the discrete ordinates code ANISN (S8, P3 approx.) and is shown in Fig. 2.

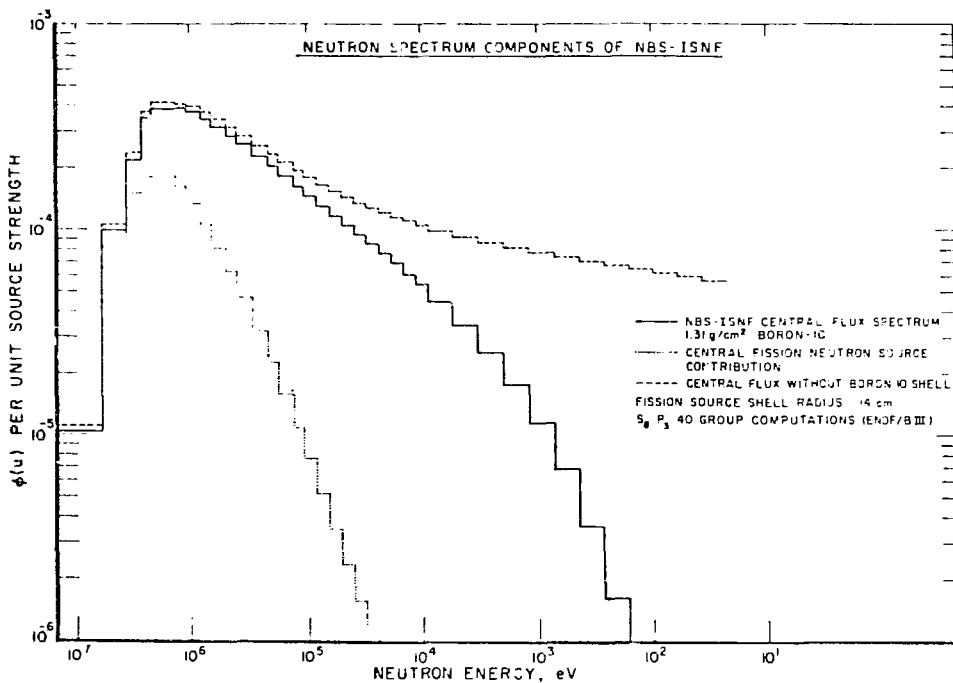


Figure 2. Neutron components.

The sensitivity of the calculated spectrum to variations in several parameters has been investigated. For example, a 1% increase in graphite density increases the flux around 10 keV by about 1%. An uncertainty of about 7% in source position produces only 1% uncertainty in the flux below 200 keV. Effects of uncertainties in the angular distribution of scatter in graphite and perturbations due to aluminum in the system have also been investigated. Uncertainties due to cross section data and energy-group structure are currently under investigation by means of new 240-group calculations. The latest calculations make use of ENDF/B-IV cross sections.

e. Unique Features

The ISNF was designed so that the spectrum at the center could be calculated to arbitrary accuracy. This was accomplished by designing it as a one-dimensional spherically symmetric configuration containing mainly ^{10}B and C, whose cross sections are among the best known of all materials.

f. Results of Initial Experiments

Flux (by transfer from calibrated ^{252}Cf field):

$$0.3 \times 10^9 \text{ neut/cm}^2\text{sec}$$

at a nominal reactor power of 10 MW

Fission Cross Section Ratios:

$$\bar{\sigma}_f(^{239}\text{Pu})/\bar{\sigma}_f(^{235}\text{U}) = 1.15 \pm 4\%$$

$$\bar{\sigma}_f(^{238}\text{U})/\bar{\sigma}_f(^{235}\text{U}) = 0.093 \pm 4\%$$

B. FACILITIES

1. Installation of Standard Neutron Beam Line on the 3 MV Van de Graaff (D. A. Wasson, M. M. Meier, and K. C. Duvall)

An additional beam line to be used for the production of standard neutron beams in the energy region from 100 keV to 2 MeV has been installed in the NBS Van de Graaff laboratory. The neutrons from the $^7\text{Li}(p,n)$ or $^3\text{H}(p,n)$ reactions are collimated to a cone shaped beam with a 4.5° half angle by means of a removable insert in a large movable shield as is shown in Fig. B1. The shield is mounted on an air bearing to permit rapid access to the end of the beam pipe for target changes.

The neutron flux is measured by the Black Neutron Detector which is described in an accompanying report and is positioned in a separate shield behind a precision collimator located 5.6 m from the neutron source. The beam diameter at 120 cm is 18.9 cm with a non-uniformity of less than 1%. For a 20 keV thick ${}^7\text{Li}$ target the neutron flux for a 4 μA proton beam is 5×10^3 n/cm²sec for 500 keV neutrons with 0.1% epithermal neutron and 0.1 mR/hr γ ray background. The facility became operational in December 1976 and is being used for standard neutron cross section measurements and for neutron dosimetry.

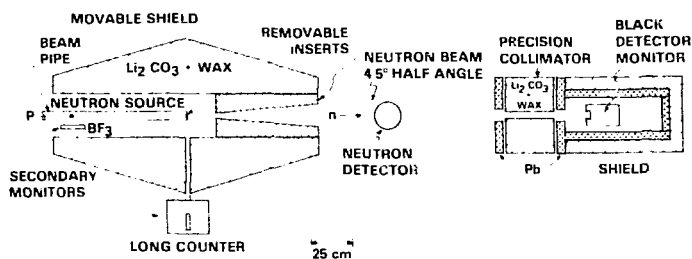


Figure B1. Standard neutron beam line geometry.

2. 3 MV Positive Ion Van de Graaff (M. M. Meier, K. C. Duvall, and O. A. Wasson)

Machine operation has been satisfactory. The primary source of down time is routine maintenance associated with ion source replacement. A third beamline is now instrumented and in use for cross section and dosimetry experiments.

The computer system for data acquisition and analysis has now been upgraded to include two magnetic tape units, a 2.7 10^6 bytes disc, high speed teletype and 32 K of core. New CAMAC instrumentation includes a 1024 channel MAC and a two parameter multiplexer. A second multiplexer is under construction, so that two two-parameter experiments can be done simultaneously.

3. A Tagging System Using Positron Annihilation Radiation, (E. Hayward, W. R. Dodge, and B. H. Patrick)

A tagging system for producing monoenergetic photons, using the two-photon annihilation-in-flight of high energy positrons, has been developed at the NBS Linac. This has been used to study the response function of a large 10" x 10" NaI(Tl) spectrometer with NE 110 anti-coincidence shield. A smaller 5" x 5" NaI(Tl) crystal located at 20⁰

to the incident, momentum-analyzed positron beam detected the lower energy (5-7 MeV) photons. The larger spectrometer viewed the Be annihilation target through a series of well-defined collimator holes located at angles in the range 4° - 11° to the incident beam direction. At these angles the background bremsstrahlung is much less important than in the forward direction. The pulse height analyzer associated with the large spectrometer was gated on by a coincidence between the two detectors. Figure B2 is the pulse height distribution produced by 31 MeV photons incident on the spectrometer. The lower histogram represents those photons rejected by the anticoincidence shield. Similar distributions have been obtained for 9.4 and 15.1 MeV incident photons.

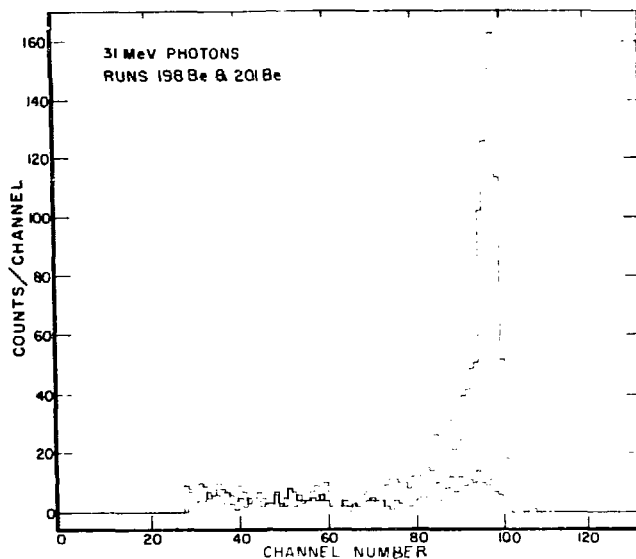


Figure B2. 31 MeV γ ray spectrometer response.

In principle, the efficiency of the large NaI(Tl) spectrometer can be calculated simply by using the absorption coefficients of NaI(Tl) and of all the filters in front of it. This allows the efficiencies of less well-understood detectors to be determined when they are also gated on by a coincidence with the smaller detector.

C DATA COMPILATION

1. X-Ray and Ionizing Radiation Data Center (J. H. Hubbell)

A low-Z evaluation and compilation "Photon Mass Attenuation and Mass Energy-Absorption Coefficients for H, C, N, O, Ar and Seven Mixtures from 0.1 keV to 20 MeV" was accepted for publication by

Radiation Research for the April 1977 issue. The seven mixtures include air, water, polystyrene, methacrylate, polyethylene, bakelite, and amber.

This Data Center also responded to 160 requests for data or information in 1976.

2. Photonuclear Data Center (E. G. Fuller, H. M. Gerstenberg)

The major effort over the last year has been to complete work on a compilation of evaluated photonuclear reaction cross section data for the p-shell nuclei. Of the nine stable nuclides to be included in the final compilation, preliminary evaluations for all except ^{13}C and ^{14}N have been completed and are undergoing internal review. Barring unforeseen complications, the complete evaluation should be submitted for publication to the editor of the Journal of Physical and Chemical Reference Data by the end of June 1977.

At the time of the Gordon Photonuclear Conference in August 1976, the Data Center issued an interim draft index "New Photonuclear Data, January 1973-May 1976." In addition to indexing the data published since the cutoff date for inclusion in NBS Special Publication 380, Photonuclear Reaction Data, 1973, this report contains a complete index to the 1100 data sets now in the Center's digital cross section library. This report is an interim version of the first supplement to NBS SP-380 which will include an index to data publishing through 1976. This is planned for publication in late spring.

The Center has continued to respond to an average of about 1.5 requests per month from various segments of the scientific and technological community for information from its files. During the last year, the results of a calculation based on data provided as a result of one of the more unusual requests, were published in The Astrophysical Journal 205, 638 (1976). The paper, by J. L. Puget, F. W. Stecker, and J. H. Bredekamp of the NASA Goddard Space Flight Center, gives the results of a calculation of the interaction of ultrahigh energy cosmic ray nuclei (^{56}Fe and lighter) with the intergalactic radiation fields. These fields, when Lorentz-shifted into the rest frame of the nuclei, contain appreciable fluxes of photons capable of inducing photonuclear reactions.

D. RADIOACTIVITY

1. Plutonium-239 Half-Life Measurement (L. L. Lucas and J. R. Noyce)

The Radioactivity Section participated in a Safeguards-related program in which plutonium-239 sources, prepared from a plutonium sample whose isotopic composition was similar to that found in nuclear fuel, were sent to several laboratories and intercompared. Our measurements of total-alpha-particle specific-activity, combined with the isotopic-abundance and calorimetric measurements carried out elsewhere, will be used to resolve a previous discrepancy between half-life values measured by calorimetry and alpha counting.

2. Measurement of Gamma-Ray Probabilities Useful for Detector Calibrations or Activity Determinations (Radioactivity Section)

Calibrated germanium and silicon detectors have been used to measure the emission rate of selected gamma rays and x rays from activity-calibrated sources of ^{123}I , ^{127}Xe , ^{198}Au , ^{145}Pm , ^{201}Tl , ^{99}Mo , ^{152}Eu and ^{208}Tl . This direct determination of the probability per decay, P_γ , eliminates any dependence on other nuclear decay parameters. Differences of 20% from tabulated values for P_γ were observed in some cases.

OAK RIDGE NATIONAL LABORATORY

A. CROSS SECTION MEASUREMENTS

1. Gamma-Ray Production Data

During the reporting period the following gamma-ray production data obtained at ORELA were released:

- a. Neutron-Induced Gamma-Ray Production in ^{208}Pb for Incident-Neutron Energies Between 4.9 and 8.0 MeV, and in ^{209}Bi for Incident-Neutron Energy of 5.4 MeV* (J. K. Dickens)

Interactions of neutrons with ^{208}Pb have been studied by measuring photon production cross sections. γ -ray spectra were obtained at incident-neutron energies of 4.9, 5.4, 6.4, 6.95, 7.45 and 8.0 MeV with a γ -ray detector system utilizing a 48-cc Ge(Li) detector. Nearly monoenergetic neutrons were obtained from the D(d,n) reaction using deuterons obtained from the (pulsed) Oak Ridge National Laboratory 5-MV Van de Graaff accelerator. Time of flight was used to discriminate against pulses due to neutrons and background radiation. Extracted differential and total inelastic cross sections have been compared with previous comparable measurements and with data from the ENDF/B evaluation with generally satisfactory results. New information on the level structure of ^{208}Pb is reported.

Data were also obtained at $E_n = 5.4$ MeV for a sample of natural bismuth, and new information on the level structure of ^{209}Bi was obtained. Differential γ -ray production cross sections were obtained, and the total inelastic cross section at $E_n = 5.4$ MeV was deduced from these data.

- b. The Mn(n, γ) Reaction Cross Section for Incident Neutron Energies Between 0.2 and 20.0 MeV**,† (G. L. Morgan)

Differential cross sections for the neutron-induced gamma-ray production from natural manganese have been measured for incident neutron energies between 0.2 and 20.0 MeV. The Oak Ridge Linear Accelerator (ORELA) was used to provide the neutrons and a NaI spectrometer to detect the gamma rays at 125° . The data presented are the double differential cross section, $d^2\sigma/d\Omega$, for gamma-ray energies between 0.22 and 10.6 MeV for coarse intervals in incident neutron energy. The integrated yield of gamma rays of energies greater than 220 keV with higher resolution in the neutron energy is also presented. The experimental results are compared with the Evaluated Neutron Data Files (ENDF).

*Submitted for publication in Nuclear Science and Engineering.

**Abstract of ORNL/TM-5531.

†Relevant to request No. 74287.

c. A Re-Measurement of the Neutron-Induced Gamma-Ray Production Cross Sections for Iron in the Energy Range $850 \text{ keV} \leq E_n \leq 20.0 \text{ MeV}$ *,** (G. T. Chapman, G. L. Morgan and F. G. Perey)

Values of the gamma-ray production cross sections for neutron interactions with iron as reported by previous investigators have differed by as much as a factor of 1.5 or more at neutron energies greater than about 5 MeV. Because of this discrepancy, the measurements have been repeated at ORNL using the ORELA as a pulsed source of neutrons with energies between 850 keV and 20 MeV. The data were obtained using a NaI(Tl) gamma-ray spectrometer oriented at an angle of 125 degrees to the incident neutron beam. The sample was positioned in the beam at a distance of 47.35 meters from the neutron source. The resulting data presented as differential cross sections ($d^2\sigma/d\Omega dE$) for gamma rays between 0.7 and 10.5 MeV, show good agreement with some previously published data, but are significantly different from previous ORNL measurements for neutron energies greater than 5 MeV.

d. Cross Sections for Gamma Production by Fast Neutrons for 22 Elements Between $Z = 3$ and $Z = 82$ †,‡ (Dickens, Morgan, Chapman, Love, Newman and Perey)

Cross sections for the production of gamma rays with $0.3 < E_\gamma < 10.5 \text{ MeV}$ have been measured as a function of neutron energy over the range $0.1 < E_n < 20.0 \text{ MeV}$. Results were obtained for 22 elements which are commonly encountered in the calculation of radiation effects. The measurements were made using a heavily shielded NaI detector in conjunction with the white neutron spectrum from the Oak Ridge Electron Linear Accelerator. Incident neutron energies were determined by time-of-flight over a 47-m flight path while gamma-ray energy distributions were obtained from pulse height unfolding techniques. Elemental differential cross sections are presented for Li, C, N, F, Mg, Al, Si, Ca, V, Cr, Fe, Ni, Cu, Zn, Nb, Mo, Ag, Sn, Ta, W, Au, and Pb.

*Abstract of ORNL/TM-5416.

**Relevant to request No. 66022.

†Accepted for publication in Nuclear Science and Engineering.

‡Relevant to request Nos. 62020, 63003, 63004, 66022, 72037, 72052, 74111, 74224, 74230, 74304 and 74313.

2. Capture Cross Sections

- a. Neutron Capture by the Chromium Isotopes*,** (M. J. Kenny,†
B. J. Allen,† A. R. de L. Musgrove,† R. L. Macklin and J. Halperin)

Capture cross sections of the chromium isotopes have been measured up to 350 keV using the capture cross section facility at the 40-m station of the Oak Ridge Electron Linear Accelerator. Resonance parameters have been derived for 180 resonances. A moderate correlation (~ 0.45) is observed between reduced neutron width and radiative widths for s-wave resonances. Calculations of valence widths show that valence capture can only account for a fraction of the observed radiative widths. An additional mechanism such as a 2p-1h doorway state must therefore be occurring.

- b. Resonance Neutron Capture in the Isotopes of Titanium* (Allen,†
Boldeman,† Musgrove† and Macklin)

The neutron capture cross sections of $^{46,47,48,49,50}\text{Ti}$ have been measured from 2.75 keV to 300 keV with ~ 0.2 per cent energy resolution. The reduced neutron widths and radiative widths of the s-wave resonances exhibit correlations which, with the exception of ^{47}Ti , are consistent with the calculated magnitudes of the valence component, assuming the radiative widths contain an additional uncorrelated part. In ^{47}Ti a significant correlation is observed for $J=3^-$ resonances, although the calculated valence component is small.

- c. The Neutron Capture Cross Section of ^{89}Y * (Boldeman,† Allen,†
Musgrove† and Macklin)

The resonance neutron capture cross section of ^{89}Y has been measured between 2.5 and 100 keV with the neutron capture facility at the 40-m flight station on ORELA. A strong valence contribution to the p-wave cross section has been identified which is similar in magnitude to that estimated using the optical model formalism of the Valence Theory.

- d. The 292.4-eV Neutron Resonance Parameters of Zirconium-91†,¶
(R. L. Macklin, J. A. Harvey, J. Halperin and N. W. Hill)

Resonance parameters, particularly the radiative width of the 292.36-eV s-wave level in $^{91}\text{Zr} + n$, have been reinvestigated. The spin assignment $J = 2^+$ is supported. The neutron width $\Gamma_n = (866 \pm 11)$ meV and radiative width $\Gamma_\gamma = (86.8 \pm 2.2)$ meV indicate less neutron capture than do parameters derived from earlier studies. This lower capture, however, is more compatible with integral measurements and a lead slowing down spectrometer measurement.

*To be submitted for publication in Nuclear Physics.

**Relevant to request Nos. 65006, 65007 and 72036.

†Australian Atomic Energy Commission, Lucas Heights, NSW, Australia.

¶Nucl. Sci. Eng. 62, 174 (1977).

¶Relevant to request Nos. 69155, 69156 and 72065.

e. High Resolution Neutron Transmission and Capture for $^{91}\text{Zr}^{*},^{**}$
(Musgrove,[†] Boldeman,[†] Allen,[†] Harvey and Macklin)

The neutron transmission through ^{91}Zr was measured at both 80-m and 200-m stations of ORELA and in combination with a capture measurement at the 40-m station, has resulted in resolved resonance parameters below 20 keV bombarding energy. The average resonance parameters obtained were as follows: $\langle D \rangle_s = 640 \pm 120$ eV, $10^4 S_0 = 0.36 \pm 0.10$, $\langle \Gamma_Y \rangle_s = 140 \pm 8$ meV;

$$\langle D \rangle_p = 300 \pm 50 \text{ eV}, 10^4 S_1 = 5.7 \pm 1.0, \langle \Gamma_Y \rangle_p = 200 \pm 12 \text{ meV}.$$

A correlation between p-wave reduced neutron widths and radiative widths is found which is attributed to valence neutron transitions.

f. Non-Statistical Neutron Capture in $^{140}\text{Ce}^\ddagger$ (Musgrove,[†] Allen,[†] Boldeman[†] and Macklin)

The radiative neutron capture cross section of ^{140}Ce has been measured with high resolution ($\Delta E/E \leq 0.2\%$) at the 40-m station of ORELA. Resonance parameters have been extracted below 60 keV bombarding energy. The average s-wave parameters deduced from the data are as follows: $\langle D \rangle = 1.77 \pm 0.45$ keV, $S_0 = 3.1 \pm 0.9 \times 10^{-4}$, $\langle \Gamma_Y \rangle_s = 7 \pm 10$ meV. A significant correlation $\rho(\Gamma_n^0, \Gamma_Y) = 0.6 \pm 0.2$ is found between reduced neutron widths and total radiative widths indicating the presence of valence neutron capture. However, evidence for energy dependence of the radiative widths is not reflected in the neutron widths and points to a further non-statistical process in neutron capture.

g. Non-Statistical Effects in the Radiative Capture Cross Sections of the Neodymium Isotopes^{*,†} (Musgrove,[†] Allen,[†] Boldeman[†] and Macklin)

The neutron capture cross sections of the stable neodymium isotopes have been measured with high energy resolution in the keV region at the 40-m station of ORELA. Average resonance parameters are extracted for s-wave resonances.

Significant positive correlations are found between Γ_n^0 and Γ_Y for all isotopes. The magnitude of the observed correlation coefficient, particularly for ^{142}Nd ($\rho = 0.9$), cannot be explained in terms of valence neutron capture and additional mechanisms are discussed.

*Submitted for publication in Nuclear Physics.

**Relevant to request Nos. 69155, 69156 and 72065.

[†]Australian Atomic Energy Commission, Lucas Heights, NSW, Australia.

[‡]Accepted for publication in Australian Journal of Physics.

[¶]Relevant to request Nos. 67034-38 and 74094.

The average s-wave radiative widths for the odd-A isotopes were markedly greater than for the even-A isotopes, while the p-wave radiative width for ^{142}Nd was considerably less than the s-wave width.

h. Neutron Capture by ^{208}Pb at Stellar Temperatures* (R. L. Macklin, J. Halperin and R. R. Winters**))

Neutron capture cross section data for isotopically enriched ^{208}Pb were taken at the Oak Ridge Electron Linear Accelerator time-of-flight facility and analyzed for nuclear resonance capture parameters up to 825 keV. Two new capture resonances at energies (43.29 keV and 47.26 keV) near stellar interior temperatures were found. The resonance parameter data lead to improved values for ^{208}Pb neutron capture probabilities calculated for a wide range of stellar interior temperatures.

i. $^{232}\text{Th}(n,\gamma)$ Cross Section from 2.6-800 keV,† (Macklin and Halperin)

Neutron capture by isotopically purified ^{232}Th was measured at the Oak Ridge Electron Linear Accelerator. The pulse height weighting method was used with small liquid scintillators to measure the prompt gamma-ray energy release following neutron capture. Resonance parameters were derived up to 10 keV. The average radiative width was $(19.8 \pm 0.2 \text{ statistical} \pm 0.4 \text{ systematic}) \text{ meV}$ for 50 resonances in the 2.6-4.0 keV interval. Strength functions $10^4 S_0 = 0.365 \pm 0.024$, $10^4 S_1 = 1.078 \pm 0.057$, $10^4 S_2 > 0.842 \pm 0.084$, $\Gamma_\gamma/D_0 = 0.0198/(13.24 \pm 0.71)$ were found to fit the average cross section well (to 105 keV) when allowance was made for p-wave inelastic competition above the ~ 50 -keV threshold. Recent evaluations of the cross section range from 8 to 50 percent higher than the present results.

j. Valence Neutron Capture in ^{54}Fe ‡,§ (Allen,† Musgrove,† Boldeman† and Macklin)

The neutron capture cross section of ^{54}Fe has been measured with 0.2 per cent energy resolution from 2.5 to 500 keV. A large and significant correlation is observed between the s-wave reduced neutron widths and the corresponding radiative widths. The valence model readily accounts for this correlation as well as the magnitude of the s-wave radiative widths.

*Submitted for publication in *Astrophysical Journal*.

**Denison University, Granville, Ohio.

†Submitted for publication in *Nuclear Science and Engineering*.

‡Relevant to request Nos. 62034 and 74204.

§To be submitted for publication in *Nuclear Physics*.

¶Relevant to request Nos. 72039 and 74040-42.

+Australian Atomic Energy Commission, Lucas Heights, NSW, Australia.

This page deliberately left blank.

k. The Neutron Total and Capture Cross Sections of $^{92}, ^{94}\text{Zr}^{*,**}$
(Boldeman,† Musgrove,† Allen,† Harvey and Macklin)

The neutron total and capture cross sections of $^{92}, ^{94}\text{Zr}$ have been measured at the 80- and 40-m flight stations, respectively, on the Oak Ridge Electron Linear Accelerator. Resonance analysis of the total cross sections gave values of s, $p_{3/2}$ and $p_{1/2}$ strength functions. Strong intermediate structure was observed in the $p_{3/2}$ cross section of ^{92}Zr . Significant single particle transitions identified in the p-wave capture cross section indicate the importance of the valence process for both nuclei. It is noted that the intermediate structure in the $p_{3/2}$ total cross section leads to enhanced valence effects in the capture cross section. The effect of non-statistical E1 transitions following particle-hole annihilation in the compound states was not observed in either the ^{92}Zr or ^{94}Zr capture cross sections as they had been in that for ^{90}Zr .

l. Resonance Neutron Capture in $^{56}\text{Fe}^{\ddagger, \S}$ (Allen,† Musgrove,† Boldeman,† Kenny† and Macklin)

The neutron capture cross section of ^{56}Fe has been measured with 0.2-0.3% energy resolution from 2.5 keV up to the inelastic neutron scattering threshold. Results are compared with recent total cross section data and average parameters are derived for s-, p- and d-wave resonances. The low correlation coefficient observed between the s-wave reduced neutron and radiative widths is consistent with the minor contribution of the valence capture mechanism as calculated in the framework of the optical model. Broad E1 and M1 doorway states for s-, p- and d-wave resonances are postulated to explain the cross section data and γ -ray spectra up to 1 MeV.

m. Odd-Even Effects in Radiative Neutron Capture by ^{42}Ca , ^{43}Ca and $^{44}\text{Ca}^{\S, +}$ (Musgrove,† Allen,† Boldeman,† Chan++ and Macklin)

The neutron capture cross sections of $^{42-44}\text{Ca}$ have been measured with high resolution ($\Delta E/E \approx 0.2\%$) at the 40-m station of the ORELA. Resonance parameters have been extracted for levels below 230 keV in ^{42}Ca , below 40 keV in ^{43}Ca , and below 165 keV in ^{44}Ca . The average s-wave resonance parameters obtained from our data are as follows: $\langle D \rangle = 8.6 \pm 1.0$ keV, 1.5 ± 0.2 keV and 16 ± 2 keV for $^{42}, ^{43}, ^{44}\text{Ca}$ respectively. The corresponding s-wave radiative widths for the even-A isotopes are considerably greater than for ^{43}Ca . In addition, p-wave radiative widths in the even-A isotopes are anomalously small.

*Nucl. Phys. A263, 389 (1976).

**Relevant to request Nos. 69142, 69159, 69160 and 69162.

†Australian Atomic Energy Commission, Lucas Heights, NSW, Australia.

‡Nucl. Phys. A509, 170 (1976).

§Relevant to request Nos. 74046-48.

§Accepted for publication in Nuclear Physics.

+Relevant to request Nos. 74029-30.

++Melbourne University, Parkville, Victoria, Australia.

3. Total Cross Sections

a. Measurement of the Neutron Total Cross Section of Fluorine from 5 eV to 20 MeV^{*,**} (Larson, Johnson, Harvey and Hill)

Neutron transmissions through Teflon (CF₂) and carbon have been measured to provide high resolution transmission and cross sections for fluorine from 5 eV to 20 MeV. The Oak Ridge Electron Linear Accelerator was used for the neutron source. The 80-m flight path with a ⁶Li glass detector was used for the low-energy measurements, and the 200-m flight path with a NE-110 detector was used for the higher energy measurements. The various background contributions were carefully studied and are discussed in detail. The 2389 resulting values are tabulated and compared with the current ENDF/B-IV evaluation.

b. Measurement of the Neutron Total Cross Section of Sodium from 32 keV to 37 MeV^{†,‡} (D. C. Larson, J. A. Harvey and N. W. Hill)

The neutron transmission through a 8.1-cm sample of pure sodium has been measured for neutron energies between 32.5 keV and 37.4 MeV. The ORELA was used to provide the neutrons, which were detected at the 200-m flight path by a NE-110 proton recoil detector. The experimental results are tabulated and compared with the total cross section in the ENDF/B-IV file for sodium.

c. Measurement of the Neutron Total Cross Section of Silicon from 5 eV to 730 keV^{¶,§} (Larson, Johnson, Harvey and Hill)

Neutron transmission through natural silicon samples has been measured for neutron energies between 5 eV and 730 keV. The ORELA was used to provide the neutrons. The 80-m flight path with a ⁶Li glass detector was used for the low energy measurement, and the 200-m flight path with a NE-110 detector was used for the higher energy measurements. The 1.488 resulting values are tabulated and compared with the current ENDF/B-IV evaluation.

*Abstract of ORNL/TM-5612 (October 1976).

**Relevant to Request No. 74168.

†Abstract of ORNL/TM-5614 (October 1976).

‡Relevant to request Nos. 74010 and 74011.

¶Abstract of ORNL/TM-5618 (November 1976).

§Relevant to request No. 74171.

4. Scattering and Reactions

a. High Resolution Fast Neutron Gamma-Ray Production Cross Sections for Iron up to 2100 keV*,** (W. E. Kinney† and F. G. Perey)

High resolution gamma-ray production cross sections for the 846-keV gamma ray of iron have been measured up to an incident neutron energy of 2100 keV. The measurements were performed using the Oak Ridge Electron Linear Accelerator as the neutron source and obtained by a ratio measurement to the ${}^7\text{Li}$ 477-keV gamma-ray cross sections. Three NE-213 detectors were used at 30, 90 and 125° to derive the total inelastic cross sections and the angular distributions. The 1250 angular distributions measured with about 0.1 nsec/m resolution show considerable fluctuations as a function of energy over the resonances seen in the inelastic cross sections. The results are compared to the ENDF/B-IV evaluation, high resolution data at 125° and, after suitable averaging, with recent monoenergetic neutron source data which average over the structure experimentally. The general consistency of the data with recent measurements, using different techniques and normalization procedures, indicates that our knowledge of this important cross section for fission reactor applications may now be known to an accuracy better than 10%. This is a significant achievement in view of the wide scatter of earlier data on such a fluctuating cross section.

b. Cross Sections for the Nb(n,xn) and Nb(n,x γ) Reactions Between 1 and 20 MeV† (G. L. Morgan)

Differential cross sections for the production of secondary neutrons and gamma rays from neutron interactions in niobium have been measured at 129 deg. (lab) for incident neutron energies in the range 1 to 20 MeV. An electron Linac was used as the white neutron source. Incident neutron energies were determined using time-of-flight techniques for a source-to-sample distance of 48 m. Secondary spectra were determined by unfolding the pulse-height distributions observed in a NE-213 scintillation counter. The results are compared to the current evaluated data file (ENDF/B-IV, MAT 1189).

c. Angular Momentum Determination of Resonances in ${}^{24}\text{Mg} + n$ by Elastic Neutron Scattering¶ (Horen, Harvey and Hill)

The angular momentum values of fifteen resonances in ${}^{24}\text{Mg} + n$ have been determined by elastic neutron scattering. The change in shape of the differential cross section [i.e., $\sigma_{\ell j}(E, \theta)$] versus angle has been observed for most of these resonances. Assignments of $\ell = 2$ for five resonances could be made on the basis of their distinct interference pattern in the 90° cross section data.

*Submitted for publication in Nuclear Science and Engineering.

**Relevant to request Nos. 66016-17.

†Deceased.

‡Abstract of ORNL/TM-5829; relevant to request No. 74309.

¶To be published in Physical Review C.

d. Giant Magnetic Dipole States in $^{208}\text{Pb}^*$ (D. J. Horen and J. A. Harvey)

From total and elastic neutron cross section measurements up to $E_n = 400$ keV on ^{207}Pb , a large concentration of p-wave strength was observed at ~ 120 keV indicating the presence of a doorway state. This corresponds to an excitation energy of 7.49 MeV in ^{208}Pb and is mainly contained in five $J^\pi = 1^+$ resonances as tabulated. The position of this doorway state and its radiative width ($\Gamma_{\gamma 0} = 7.2$ eV) is in remarkable agreement with the predictions of Ring and Speth for one component of the giant M1 resonance (i.e., $E_x = 7.50$ MeV and $\Gamma_{\gamma 0} = 9.3$ eV).¹

E_n (keV)	J^π	Γ_n (eV)	$\Gamma_{\gamma 0}$ (eV) ²
90.17	1^+	272	2.05
115.17	1^+	923	1.54
127.91	1^+	613	2.51
130.23	$(1)^+$	87	1.1
132.18	(1^+)	55	

e. Measurement of the $^6\text{Li}(n,\alpha)$ Cross Section in the Region of the 244-keV Resonance** (Cleide Renner, J.A. Harvey, N.W. Hill and K. Rush)

The $^6\text{Li}(n,\alpha)$ cross section has been measured at several discrete neutron energies from ~ 100 to ~ 400 keV using a 1.7 cm dia. beam at the 80-meter flight path at ORELA. The neutron beam was filtered through 8" or 12" of armco iron to eliminate the gamma flash and produce several monoenergetic groups of neutrons (~ 2 keV wide). Of particular interest are the Fe-window neutrons at 219, 244 and 274 keV.

The $^6\text{Li}(n,\alpha)\gamma$ events were detected either by a 1 mm thick 25.4 mm dia. piece of ^6Li glass or a 12.7 mm thick, 111 mm dia. piece of ^6Li glass. The ^6Li content of the 1 mm piece of ^6Li glass was determined from the $1/v$ slope of the total cross section measured from ~ 0.05 to 100 eV. The ^6Li content of the 12.7-mm piece was obtained from σ_T measurements from ~ 10 to 1000 eV. Both pieces of ^6Li glass were scanned with a narrow neutron beam and showed that the ^6Li content was uniform to $\sim 1\%$. Pulse height distributions were measured for ~ 20 neutron groups and backgrounds for most groups. Although the efficiency for a neutron interacting in the ^6Li glass detector is quite low, the probability of observing the (n,α) events which have taken place in the ^6Li glass scintillator is very high ($\sim 99\%$) and it can be determined accurately.

The neutron flux was measured with an NE-110 detector either 7.5 or 2.0 cm thick. The pulse height distributions for the same ~ 20 neutron groups and backgrounds were measured for both NE-110 detectors. For the

*Paper to be presented at the Washington APS Meeting, April 25-28, 1977.

**Relevant to request Nos. 69009-11 and 72003-9.

¹Allen and Macklin, Proc. Third Neutron Cross Section and Tech. Conf., Knoxville, Tenn., March 1971, CONF-710301, p. 764.

²P. Ring and J. Speth, Nucl. Phys. A235, 315 (1974).

7.5-cm thick NE-110 flux monitor, the efficiency for a neutron interaction in the detector is very high ($\sim 99\%$ at 220 keV) and can be determined accurately vs neutron energy, but the probability of producing enough light to produce a measurable pulse may be only $\sim 90\%$ and drops sharply below ~ 150 keV. For the 2-cm thick NE-110, the efficiency for a neutron interaction is lower ($\sim 70\%$ at ~ 240 keV) and it can also be determined accurately vs neutron energy, but the probability of detecting the event is higher for the lower energy neutron groups. To determine the overall detection efficiencies of these two monitors detailed comparisons must be made with calculated responses using Monte Carlo techniques. Monte Carlo calculations for the NE-110 detectors and the experimental conditions used in this experiment were made by G. L. Morgan, ORNL, and M. M. Meier, NBS.

f. Angular Distribution of Neutron-Proton Scattering at 27.3 MeV^{*,**}
(J. L. Fowler, J. A. Cookson,† M. Hussain,‡ C. A. Uttley† and R. B. Schwartz¶)

Using the 12 MV Harwell Tandem Generator and the $t(d,n)\alpha$ reaction to produce 27.3-MeV neutrons, we have measured the relative differential cross sections for forward scattering of neutrons. We recorded proton recoils in a small scattering scintillator of plastic in coincidence with the scattered neutron pulses detected by a large NE-102A scintillator at 7 angles between 17° and 57.9° to the incident neutron beam. We measured the absolute efficiency of the large detector using the associated particle method. In addition to the usual corrections for multiple scattering and for loss of protons from the edges of the small scintillator, we also corrected for effects of the $^{12}\text{C}(n,n'\gamma)$ reaction. Our relative cross sections combined with measurements of others for backward scattering of neutrons give a complete differential cross section curve at 27.3 MeV which is in agreement with the prediction of Binstock¹ based on n-p scattering phase shifts.

*Paper presented at Chicago ANS Meeting, February 7-10, 1977.

**Relevant to request No. 72001.

†AERE Harwell.

‡AERE Harwell, on leave from University of Dacca, Bangladesh.

¶AERE Harwell and NBS, Washington, D.C.

¹Phys. Rev. C 10, 19 (1974).

5. Capture γ -Rays

- a. Location of Dipole and Quadrupole Strengths in ^{208}Pb via the $^{207}\text{Pb}(n,\gamma)$ Reaction*.** (Raman, Mizumoto, Macklin, Slaughter, Morgan, Halperin, Chapman and Winters)

We have carried out a detailed investigation of the $^{207}\text{Pb}(n,\gamma)$ reaction in the neutron energy region up to 1 MeV with Ge(Li), NaI(Tl) and total energy detectors. One aim of this study was the identification of primary E2 transitions which are rarely encountered in (n,γ) reactions. At least seven E2 transitions were observed. Radiation widths were also obtained for a large number of dipole transitions to the ^{208}Pb ground state. They were subdivided into M1 and E1 transitions on the basis of parity assignments from recent transmission and scattering measurements.¹ In the 7.37-7.73-MeV excitation region we have located 17% of the M1, 0.3% of the E1 and 0.6% of the E2 strengths in ^{208}Pb .

- b. Neutron Capture Gamma-Ray Studies of Levels in ^{57}Fe and ^{59}Fe *.†‡
(J. C. Wells, Jr.,§ S. Raman and G. G. Slaughter)

We have performed γ -ray measurements on natural Fe and enriched ^{58}Fe targets following resonance neutron capture. From the 1.167-keV $1/2^-$ resonance of ^{56}Fe we have observed 14 primary and 23 secondary γ rays in ^{57}Fe . Of these, 28 have been incorporated into a level scheme. The relative intensities of the primary γ rays are in good agreement with the results of Chrien *et al.*² However, the 6507-keV transition reported in Ref. 1 was absent in our spectra. We have observed 6 primary and 20 secondary γ rays from the 230- and 359-eV neutron resonances of ^{58}Fe . Of these, 17 have been incorporated into a level scheme for ^{59}Fe , which includes a number of levels known from (t,p) and (d,p) reaction studies by McLean *et al.*³ and (n,γ) studies by Bogdanov *et al.*⁴ The neutron separation energy of ^{59}Fe was determined to be 6580.8 ± 2.0 keV.

*Paper to be presented at the Washington APS Meeting April 25-28, 1977.

**Relevant to request No. 74186.

†Relevant to request Nos. 66022 and 74184.

‡Tennessee Technological University, Cookeville.

§D. J. Horer, J. A. Harvey and N. W. Hill, Physics Div. Annual Rept., ORNL-5137 (1976) and private communication.

2R. E. Chrien *et al.*, Phys. Rev. C 1, 973 (1970).

3K. C. McLean *et al.*, Nucl. Phys. A191, 417 (1972).

4A. P. Bogdanov *et al.*, Yad. Fiz. 14, 909 (1971) [Sov. J. Nucl. Phys. 14, 509 (1972)].

6. Actinides

- a. High Resolution Measurement of the ^{238}U to ^{235}U Fission Cross Section Ratio Between 2 MeV and 25 MeV*,** (F. C. Difilippo,† R. B. Perez, G. de Saussure, D. Olsen and R. Ingle)

There are persistent discrepancies among recent measurements of the ^{238}U fission cross section in the region from threshold to about 30 MeV.¹⁻⁵ Some of those discrepancies may be due to errors in the energy calibration of the measurements.

This paper describes a measurement of the $^{238}\text{U}/^{235}\text{U}$ fission cross section ratio. Particular attention was paid to the energy calibration of the data. The results of the measurement are provisionally normalized to an evaluated value at 2.5 MeV,⁶ but further experiments are in progress to obtain an independent absolute normalization.

*Paper presented at Specialists Meeting on Fast Neutron Fission Cross Sections of ^{233}U , ^{235}U , ^{238}U , and ^{239}Pu , June 28-30, 1976, Argonne National Laboratory.

**Relevant to request Nos. 67203 and 69416.

†IAEA Fellow, on assignment from Comision Nacional de Energia Atomica, Argentina.

¹F. C. Difilippo, "SUR, A Program to Generate Error Covariance Files," ORNL/TM-5223 (1976); this document contains a complete list of references on the measurements of the ^{238}U fission cross section.

²J. W. Behrens, G. W. Carlson, and R. W. Bauer, "Neutron Induced Fission Cross Sections of ^{233}U , ^{234}U , ^{236}U , and ^{238}U with Respect to ^{235}U ," Proc. Conf. Nuclear Cross Sections and Technology, NBS Special Pub. 425 (1975), vol. II, p. 591. Also UCRL-76219 (1975) and private communication.

³J. W. Meadows, Nucl. Sci. Eng. **49**, 310 (1972) and Nucl. Sci. Eng. **58**, 255 (1975).

⁴M. S. Coates, D. B. Gayther, and M. H. Pattenden, Proc. Conf. Nuclear Cross Sections and Technology, NBS Special Pub. 425 (1975), vol. II, p. 568.

⁵We are indebted to J. W. Behrens for KFK data obtained by private communication from S. Cierjacks (1976).

⁶W. P. Poenitz, letter to the participants of the CSEWG Task Force Meeting, March 16, 1976.

- b. Precise Measurement, 0.52 to 4000 eV, and Analysis, 0.52 to 108/eV, of Neutron Transmissions Through Seven Samples of ^{238}U *,** (Olsen, de Saussure, Perez, Silver,† Difilippo, Ingle and Weaver)

The transmissions of 0.52 to 4000 eV neutrons through 3.62, 1.08, 0.254, 0.0762, 0.0254, 0.0127, and 0.0036-cm-thick samples of depleted ^{238}U have been measured at 42 m with a 1.0-mm ^6Li -glass detector using the Oak Ridge Electron Linear Accelerator pulsed neutron source. In order to obtain resonance parameters, these seven transmissions from 0.52 to 1086.8 eV have been simultaneously least-squares shape-fitted with a multilevel Breit-Wigner cross section formalism with "picket fence" terms to account for truncation effects. This simultaneous fit yielded a χ^2 per degree of freedom near unity. Averaged over this energy range, an s-wave strength function of $.968 \pm .036 \times 10^{-4}$ and an effective radius of $.944 \pm .005 \times 10^{-12}$ cm were obtained. In addition these transmission data yielded an average radiation width of 23.1 ± 1.0 meV for the 12 lowest-energy s-wave resonances with radiation widths of 23.0 ± 0.8 , 22.8 ± 0.8 , and 22.9 ± 0.8 meV for the 6.67, 20.9, and 36.8-eV resonances, respectively. The derived radiation widths for these three resonances are shown to depend on the cross section formalism employed.

- c. Neutron Capture Cross Section of ^{240}Pu †,¶ (L. W. Weston and J. H. Todd)

The ^{240}Pu average capture cross section was measured from 200 eV to 350 keV. The cross section was normalized at thermal neutron energies (0.02 to 0.03 eV) and this normalization was confirmed at the 1.06 eV resonance by the black resonance technique. The Oak Ridge Electron Linear Accelerator was used as the source of pulsed neutrons. The capture gamma-ray detector used was the "total energy detector" which is a modification of the Moxon-Rae detector. The shape of the neutron flux was measured relative to the $^{10}\text{B}(n,\alpha)$ cross section up to 2 keV and the $^6\text{Li}(n,\alpha)$ at higher neutron energies. The results of the measurement define the average capture cross section of ^{240}Pu over a wide neutron energy range to an accuracy of about 8% which is significantly better than previously known. The results indicate that the ENDF/B-IV evaluation is about 25% low above 30 keV neutron energy. The cross section is important in fast Pu-fueled reactors.

*Accepted for publication in Nuclear Science and Engineering.

**Relevant to request Nos. 69420-22 and 74123.

†Institute for Energy Analysis, Oak Ridge, Tennessee.

‡Submitted for publication in Nuclear Science and Engineering.

¶Relevant to request Nos. 67194, 69390 and 72137.

d. Measurement of the ^{238}U Subthreshold Fission Cross Section for Incident Neutron Energies Between 0.6 and 100 keV* (Difilippo, Perez, de Saussure, Olsen and Ingle)

We have measured the neutron-induced ^{238}U subthreshold fission cross section in the neutron energy range between 0.6 and 100 keV. Twenty-eight fission clusters were identified. The well-known clusters at 721 and 1210 eV appeared resolved into their Class I components.

Average ^{238}U subthreshold fission cross sections were determined and compared with available results in the literature.

We interpreted the measurement in terms of fission doorway (Class II levels) arising from the assumption of the existence of a double-humped fission barrier for the $^{238}\text{U} + n$ compound nucleus at large deformations. On the basis of this model several fission barrier parameters were determined.

e. The Thermal-Neutron Capture and Fission Cross Sections and Resonance Integrals for ^{243}Cm * (C. E. Bemis, Jr., J. H. Oliver, R. Eby and J. Halperin)

The thermal-neutron capture cross section and capture resonance integral for ^{243}Cm have been measured in Co monitored reactor irradiations of nearly isotopically pure ^{243}Cm (99.94%) using cadmium filter techniques. The thermal neutron absorption (capture + fission) cross section and corresponding resonance integral for ^{243}Cm have also been measured in a separate experiment relative to ^{248}Cm . Values of $\sigma_{2200}(n,\gamma) = 130.7 \pm 9.6$, $\sigma_{2200}(n,f) = 609.6 \pm 25.9$, $I(n,\gamma) = 214.7 \pm 20.3$ and $I(n,f) = 1575 \pm 136$ barns are reported.

f. Measurements on ^{245}Cm Fission Cross Section** (J. W. T. Dabbs, C. E. Bemis, Jr., N. W. Hill and S. Raman)

Measurements on the neutron fission cross section of ^{245}Cm have been repeated using a new and much improved $^6\text{Li}(n,\alpha)$ neutron beam monitor. This monitor was developed and used in the recently completed measurements on ^{243}Cm reported at the ICINN Conference. The measurements on ^{245}Cm extended over several months and used the same sample ($\sim 10 \mu\text{g}$) as the previous measurements. A normalization procedure is being developed to utilize both sets of measurements in obtaining the cross section, thus improving the statistical accuracy of the results. Recently proposed ENDF/B-V standards for ^6Li and ^{235}U will be used in reducing the data on both Cm isotopes to cross sections. This work is underway.

*Accepted for publication in Nuclear Science and Engineering.

**Relevant to request No. 67145.

A new fission chamber using 3" dia. parallel plates and a honey-comb separator is being prepared for tests in connection with the measurement of the neutron fission cross section of ^{241}Am . A computer simulation of the behavior of this chamber configuration indicates that pileup of alpha pulses can be tolerated at least to 10^8 α /sec in each section of the chamber and with presently available amplifiers. New low pileup amplifiers are under development with the goal of increasing this limit.

g. The Neutron Total Cross Section of ^{249}Cf (J. A. Harvey, R. W. Benjamin, N. W. Hill and S. Raman)

Transmission measurements have been made upon two small samples containing $\sim 70\%$ ^{249}Cf and $\sim 30\%$ ^{249}Bk . These are the same two samples which were measured ~ 18 months earlier when the sample was 98% ^{249}Bk and only $\sim 2\%$ ^{249}Cf . The transmission measurements were made using a 110-cm diameter, 1.3-cm thick ^6Li glass scintillator located at a 17.8-meter flight path. Some measurements were made with samples cooled with liquid nitrogen and some were made at room temperature. The measurements covered the energy range from 0.005 eV to ~ 1000 eV with an energy resolution of $\sim 0.3\%$.

Of the twenty-four resonances observed up to 20 eV, sixteen are due to ^{249}Bk still present in the sample. The largest resonance in ^{249}Cf is the known one at 0.70 eV. The present data will be analyzed in conjunction with the earlier ^{249}Bk total cross section data and the ORELA fission cross section data of ^{249}Cf measured by Dabbs *et al.*

h. Decay Heat of ^{235}U Fission Products by Beta- and Gamma-Ray Spectrometry*,** (Dickens, Love, McConnell and Peele)

Gamma-ray energy-release data for thermal-neutron fissioning of the fuel element ^{235}U were obtained for waiting times $2 \leq t_w \leq 14000$ sec. These data were processed to give modest-resolution gamma-ray energy spectra vs t_w . The resulting spectra have been integrated to give integral gamma-ray energy-release data. Beta-ray data obtained were processed to give beta-ray energy spectra for waiting times $2 \leq t_w \leq 14000$ sec. Some of these spectra have been compared with existing data; the quality of agreement varies between poor and very good. The beta-ray spectra have been integrated to give integral beta-ray energy-release data.

Total energy-release data were obtained by summing the gamma-ray energy-release data with the beta-ray energy release data. The total

*Paper presented at 4th Water Reactor Safety Information Meeting, September 27-30, 1976, Gaithersburg, Maryland.

**Relevant to request No. 70029.

energy-release data have been compared (a) with the current ANS Decay Heat Standard, (b) with results of computations using current best files of fission-product data, and (c) with results of other recent experiments. These comparisons suggest likely improvement to the current standard for $t_w \leq 400$ sec, as well as reduction of the uncertainties assigned to the standard.

7. Integral Measurements

a. Secondary Neutron Spectra from Neutron Interactions in a Thick Carbon Sample*,** (G. L. Morgan)

The spectra of secondary neutrons produced by neutron interactions in a thick (≈ 3 mean free path) sample of carbon have been measured as a function of the incident neutron energy over the range 1 to 20 MeV. A linac (ORELA) was used as a white neutron source with a 48-m flight path. Incident energy was determined by time-of-flight, while secondary spectra were obtained through pulse-height unfolding techniques. The results of the measurement are compared to calculations based on the current evaluated data file (ENDF/B 1274).

8. Experimental Techniques

a. Transport Calculations of Neutron Wave Experiments in Subcritical Assemblies† (F. C. Difilippo)

A recent neutron wave experiment in a thermal multiplying assembly with and without control rods has been analyzed numerically in terms of transport theory. The code TASK was used for this purpose. The present study dealing with a highly enriched, compact multiplicative system indicates that the dispersion law of the assembly is very sensitive to transport effects and to the estimation of the leakage of the fast neutron population. The present calculations of neutron wave propagation in multiplicative systems show that this technique can be used as a highly sophisticated experiment for integral checks of neutron cross section sets.

b. A Simple Method for Determining Absolute Disintegration Rates for some Radionuclides (J. K. Dickens)

A method is described for determining absolute disintegration rates for certain electron-capture isotopes using x-ray-gamma-ray summing in a single high-resolution detector. The method does not require knowledge of detector efficiencies nor of gamma-ray branching ratios. Results obtained for ^{65}Zn are presented in which a source of 10500 disintegrations/sec was calibrated to an estimated accuracy of 0.9% using a 200 mm² intrinsic Ge detector.

*Abstract of ORNL/TM-5814.

**Relevant to request Nos. 74175-6, 74255 and 74270-1.

†Submitted for publication in Nuclear Science and Engineering.

‡Submitted for publication in Nuclear Instruments and Methods.

c. A Review of Radiation Energy Spectra Unfolding* (D. K. Trubey)

On April 12-13, 1976, the Radiation Shielding Information Center of ORNL convened a seminar-workshop on unfolding radiation energy spectra. More than 20 papers were presented. They describe theoretical approaches and practical experiences in determining neutron and gamma-ray spectra from responses of detectors, such as NE-213, and NaI scintillators and neutron activation detectors. They represent a description of the state of the art.

B. DATA ANALYSES

1. Theoretical Calculations

a. Charged Hadron and Lepton Currents Produced by Low-Momentum (≤ 3 GeV/c) Charged Pions in Al, Fe, and Pb Targets**
(P. S. Beiser,† T. A. Gabriel and J. D. Amburgey)

Calculations have been carried out to determine the spatial dependence of charged hadron and lepton currents produced by low-momentum (≤ 3 GeV/c) charged pions in Al, Fe, and Pb targets. Even at the lowest momentum values considered (0.5 GeV/c), there is little difference between incident positive pions and negative pions with respect to the average spatial dependence of the charged current.

b. Neutron Kerma Factors for H, C, N, O, and Tissue in the Energy Range of 20 to 70 MeV‡ (R. G. Alsmiller, Jr. and J. Barish)

Calculated kerma factors (kerma per unit fluence) in the energy range of 20 to 70 MeV based on nonelastic charged-particle-production cross-section data obtained from the intranuclear-cascade model of nuclear reactions are given for H, C, N, O, and tissue.

c. The Spatial Variation of the Damage Energy and Gas Production in the Experimental Volume of a Li(D,n) Neutron Radiation Damage Facility¶ (R. G. Alsmiller, Jr. and J. Barish)

Calculated results are presented of the variation with position in the experimental volume of a Li(D,n) neutron radiation damage facility of the damage energy and helium and hydrogen production in copper and in niobium when this volume is partially filled with experimental samples. The neutron nonelastic cross-section data at the higher energies (≥ 15 -20 MeV) needed to carry out the transport calculations were obtained from the intranuclear-cascade model of nuclear reactions.

*Abstract of ORNL/RSIC-40.

**Abstract of ORNL/TM-5677 (December 1976).

‡ORAU undergraduate research trainee, Eckerd College, St. Petersburg, FL.

†Abstract of ORNL/TM-5702; submitted for publication in Health Physics.

¶Abstract of ORNL/TM-5554; submitted for publication in Nuclear Technology.

- d. Comparison of Measured Neutron Spectra with Predictions of an Intranuclear-Cascade Model* (Aaron Galonsky,** R. R. Doering,** D. M. Patterson,** and H. W. Bertini)

Neutron spectra resulting from bombardment of targets of ^{48}Ca , ^{90}Zr , ^{120}Sn , and ^{208}Pb with 45-MeV protons have been measured at many angles between 0° and 160° . Intranuclear-cascade, Monte Carlo calculations predict too many high-energy neutrons in the forward direction and too few neutrons, particularly high-energy neutrons, at angles greater than $\sim 45^\circ$. Beyond 90° the underprediction is by factors of 10 to 100. For angle-integrated spectra, however, there is reasonable agreement between theory and experiment.

2. ENDF/B Related Evaluations

- a. Requirements on Experiment Reporting to Meet Evaluation Needs†
(R. W. Peelle)

To define the requirements placed by the evaluation of nuclear cross sections upon the reporting of experimental results, a model of part of the evaluation process is presented. The model is a straightforward application of nondiagonal weighted least-squares estimation to average cross sections in the energy regions where the shape of the cross section is not given by theory. To combine in a logical way the existing evaluated information with one or more new sets of experimental results, the estimated covariance matrix of each experimenter's results needs to be known on an appropriate mesh. The likelihood that each experimenter may underestimate the uncertainties in his results does not remove the need for him to record for users the estimated magnitudes and correlation patterns of these uncertainties.

- b. An Evaluation for ENDF/B-IV of the Neutron Cross Sections for ^{235}U from 82 eV to 25 keV‡ (R. W. Peelle)

Capture and fission cross sections for ^{235}U in the "unresolved resonance" energy region were evaluated to permit determination of local-average resonance parameters for the ENDF/B-IV cross section file. Microscopic data were examined for infinitely dilute average fission and capture cross sections and also for intermediate structure unlikely to be reproduced by statistical fluctuations of resonance widths and spacings within known laws. Evaluated cross sections, averaged over lethargy intervals greater than 0.1, were obtained as an average over selected

*Phys. Rev. C 14, 748 (1976).

**Michigan State University, East Lansing, Michigan 48824.

†NEANDC/NEACRP Specialists Meeting on Fast Neutron Fission Cross Sections of ^{233}U , ^{235}U , ^{238}U , and ^{239}Pu , June 28-30, 1976, Argonne National Laboratory.

‡ORNL-4955, ENDF-233 (May 1976).

data sets after appropriate renormalization. Estimated uncertainties are given for these evaluated average cross sections. The "intermediate" structure fluctuations common to a few independent data sets were approximated by straight lines joining successive cross sections at 120 selected energy points; the cross sections at the vertices were adjusted to reproduce the evaluated average cross sections over the broad energy regions. Data sources and methods are reviewed, output values are tabulated, and some modified procedures are suggested for future evaluations.

Evaluated fission and capture integrals for the resolved resonance region are also tabulated. These are not in agreement with integrals based on the resonance parameters of ENDF/B versions III and IV.

3. Validation of ENDF/B Evaluation Through Integral Measurements

a. Analysis of a Neutron Scattering Integral Experiment on Iron for Neutron Energies from 1 to 15 MeV* (S. N. Cramer and E. M. Oblow)

Monte Carlo calculations were made to analyze the results of an integral experiment with an iron sample to determine the adequacy of neutron scattering cross-section data for iron. The experimental results analyzed included energy-dependent NE-213 detector count rates at a scattering angle of 90 deg and pulse-height spectra for scattered neutrons produced in an iron ring pulsed with a 1- to 20-MeV neutron source. The pulse-height data were unfolded to generate secondary neutron spectra at 90 deg as a function of incident neutron energy. Multigroup Monte Carlo calculations using the MORSE code and ENDF/B-IV cross sections were made to analyze all reported results. Discrepancies between calculated and measured responses were found for inelastic scattering reactions in the range from 1 to 4 MeV. These results were related to deficiencies in ENDF/B-IV iron cross-section data.

b. Analysis of a Neutron Scattering and Gamma-Ray Production Integral Experiment on Oxygen for Neutron Energies from 1 to 15 MeV** (S. N. Cramer and E. M. Oblow)

Monte Carlo calculations were performed to analyze an integral experiment on a liquid oxygen sample to determine the adequacy of the neutron scattering and gamma-ray production data for oxygen. The experimental results included energy- and angular-dependent NE-213 detector count rates and secondary pulse-height spectra for scattered neutrons and gamma rays. The sample was a spherical dewar of liquid oxygen pulsed with a 1- to 20-MeV neutron source. Pulse-height data were unfolded to generate secondary neutron and gamma-ray production spectra as a function of angle in broad incident neutron energy bins. Analysis of all the

*Abstract of ORNL/TM-5548 (November 1976).

**Abstract of ORNL/TM-5535 (September 1976).

reported data was based on multigroup Monte Carlo calculations using the MORSE code. Results indicate that the current ENDF/B-IV neutron and gamma-ray production data for oxygen above 1 MeV appear to be in good order. The only major discrepancy uncovered was related to neutron scattering and gamma-ray production from first level inelastic scattering interactions. Calculated results for the production of 6-MeV gamma rays from the 6-MeV first inelastic level in oxygen appear to be low by around 50% at energies above the inelastic threshold. Likewise, calculated secondary neutron spectra for incident neutron energies above 6 MeV are uniformly low at energies corresponding to neutrons having had first level inelastic scattering events in oxygen. Additional deficiencies in the oxygen cross-section data are indicated for inelastic scattering from the cluster of discrete levels in the 12-13 MeV range and for elastic scattering at very small angles at energies above 2 MeV. The size of the inelastic discrepancies is larger than the 20-30% order of error indicated for these cross sections in the ENDF/B-IV uncertainty files for oxygen.

4. Sensitivity Studies

a. Neutronics Calculations for the Oak Ridge National Laboratory Tokamak Reactor Studies* (R. T. Santoro, V. C. Baker and J. M. Barnes)

Neutronics calculations have been carried out to analyze the nuclear performance of conceptual blanket and shield designs for the Tokamak Experimental Power Reactor (EPR) and the Tokamak Demonstration Reactor Plant (DRP) being considered at the Oak Ridge National Laboratory. These reactor designs represent a sequence in the commercialization of fusion-generated electrical power. All of the calculations were carried out using the one-dimensional discrete ordinates code ANISN and the latest available ENDF/B-IV coupled neutron-gamma-ray transport cross-section data, fluence-to-kerma conversion factors, and radiation damage cross-section data. The calculations include spatial and integral heating-rate estimates in the reactor with emphasis on the recovery of fusion neutron energy in the blanket and limiting the heat-deposition rate in the superconducting toroidal field coils. Radiation damage due to atomic displacements and gas production produced in the reactor structural material and in the toroidal field coil windings were also estimated. The tritium-breeding ratio when natural lithium is used as the fertile material in the DRP blanket and in the experimental breeding modules in the EPR is also given.

*Paper presented at the 9th Symposium on Fusion Technology, Garmisch-Partenkirchen, Federal Republic of Germany, June 14-18, 1976.

b. Monte Carlo Analysis of the Effects of Shield Penetrations on the Performance of a Tokamak Fusion Reactor* (R. T. Santoro, J. S. Tang, R. G. Alsmiller, Jr. and J. M. Barnes)

Calculations have been performed using the Monte Carlo radiation-transport code MORSE to estimate the effects on the performance of a D-T burning Tokamak fusion reactor resulting from radiation that streams through penetrations in the blanket-shield assembly. The number of penetrations, as well as the size of some of these penetrations, is appreciable, so the capability of the blanket and shield in attenuating the plasma neutron and secondary-gamma radiation is reduced. The radiation that streams through these penetrations can lead to intolerable nuclear heating and radiation damage in vital reactor components, particularly the cryogenic toroidal-field coils that surround the reactor and the cryopumping surfaces inside the injector.

This paper summarizes the results of Monte Carlo calculations that were carried out for a representative fusion reactor having a rectangular neutron-beam-injector port (30 x 70 cm²) passing through the blanket and shield.

The nuclear heating and radiation damage to the toroidal-field coils adjacent to the injector port were estimated using forward and adjoint Monte Carlo methods. The presence of the neutral-beam-injector port leads to increases in both the nuclear heating and radiation damage in the toroidal-field-coil windings by factors of 50 to 100 over the same responses in fully shielded windings.

c. Fast Reactor Shield Sensitivity Studies for Steel-Sodium-Iron Systems* (E. M. Oblow and C. R. Weisbin)

A sensitivity analysis of a number of integral measurements on a heterogeneous 6-m steel-sodium-iron fast reactor shield mock-up was performed to determine the adequacy of the basic nuclear cross section data for sodium and iron. The study was based on a fine group ENDF/B-IV neutronics cross section library and utilized the complete sensitivity analysis capabilities of the FORSS code system. Preliminary ENDF/B-V error files for sodium and iron were also used to determine calculational uncertainties for the analysis.

*Paper to be presented at the 5th International Conference on Reactor Shielding, Knoxville, Tennessee, April 18-22, 1977.

d. Application of FORSS Sensitivity and Uncertainty Methodology to Fast Reactor Benchmark Analysis* (Weisbin, Marable, Lucius, Oblow, Mynatt, Peele and Perey)

FORSS is an analytical tool used to study the relationships between cross sections and their uncertainties, integral experiments and their uncertainties, and performance parameter predictions and their uncertainties. This paper presents the first results of applying FORSS to the analysis of fast reactor benchmark. Specifically, for a variety of assemblies (ZPR-6/6A, ZPR-6/7, and GODIVA) and performance parameters, the nuclear data sensitivity is tabulated as a function of nuclide, reaction type, and energy. Nuclear data induced uncertainties are quantified, and results of integral experiments are incorporated in a consistent fashion resulting in improved uncertainty estimates of reactor performance for devices being designed. Although there has been considerable work in this field, many of the results to date have been of limited utility because of the paucity of covariance information for nuclear data, the lack of comprehensive libraries of sensitivity coefficients derived consistently from a recognized nuclear data base (e.g., ENDF/B), and the lack of documented uncertainties (including correlations as well as statistical and systematic errors in the integral experiments.

e. Determining the Accuracy Required of Nuclear Data to Meet Specified Reactor Performance Criteria** (Marable, Weisbin, Oblow and Peele)

The purpose of this work is to determine the accuracy required of multi-group nuclear data to ensure at minimum cost a given accuracy in calculated reactor performance parameters. To determine this, as previous studies of this type have shown, both correlation information and cost functions for proposed measurements are required. Detailed energy-dependent correlation information, only recently developed in a preliminary way, has been incorporated into this present work. The optimization calculation finds the standard deviations required of the experimental measurements in order to find a minimum cost subject to the constraints imposed by performance parameter accuracy requirements.

f. Performance Parameter Uncertainties for a Large LMFBR†
(J. H. Marable and C. R. Weisbin)

This paper reports uncertainties in performance parameters of a large LMFBR which result from uncertainties in both nuclear data and relevant integral experiments. The current effort is the first analysis of this type actually applied to a realistic two-dimensional model of an LMFBR using evaluated covariance files based upon ENDF/B-IV.

*Abstract of ORNL/TM-5563; paper presented at ANS Meeting, Washington, D.C., November 15-19, 1976.

**Paper presented at ANS Meeting, Washington, D.C., November 15-19, 1976.

†Paper to be presented at ANS Meeting, New York, June 12-17, 1977.

Conclusions to be drawn from this study are: (1) Integral experiments are presently required in the design of large LMFBR-type reactors in order to achieve acceptable standard deviations in performance parameters, (2) Error analyses of the integral experiments are extremely important and have a direct bearing on the standard deviations of the calculated performance parameters, and (3) Based on current estimated covariance files for differential and integral data and based on our calculated 2-D sensitivity coefficients, the uncertainties in k and BR performance for the 1200 MWe LMFBR model are 1% and 3%, respectively

g. Sensitivity Analysis of TRX-2 Lattice Parameters with Emphasis on Epithermal ^{238}U Capture (E. T. Tomlinson, G. de Saussure and C. R. Weisbin)

Overprediction of epithermal ^{238}U capture in water moderated lattices using ENDF/B data has been a long standing problem basic to the prediction of neutron economy and conversion ratio in light water reactors.

The objective of this paper is the determination of a recommended representation of the ^{238}U capture cross section based upon available differential and specific integral data and the quantitative determination of the sensitivity of thermal uranium lattice (TRX-2) performance parameters to the cross section shape, magnitude, and representation with *emphasis on the first four resolved s-wave resonances*. Sensitivity profiles and covariance matrices developed for ^{235}U and ^{238}U fission permit a quantitative assessment of performance parameter uncertainties due to concomitant uncertainties in nuclear data.

The main conclusions of this study are that the results of recent measurements suggest a modification of the ENDF/B-IV representation of the low energy cross sections of ^{238}U ; calculations of TRX-2 performance parameters made with the recommended cross sections yield results in fair agreement with the measurements; and uncertainties due to methods are as large or larger than those due to nuclear data.

h. Actinide Transmutation: Cross Sections, Methods and Reactor Sensitivity Studies (G. W. Morrison, T. J. Burns and C. R. Weisbin)

One of the potential techniques of disposal of long-lived radioactive actinide wastes from fission reactors is the transmutation of these nuclides into fissile isotopes in a reactor. Subsequent fission yields highly radioactive but relatively short-lived fission products which can be disposed of using conventional storage techniques. In order to evaluate the feasibility of this method of disposal, one needs to quantify the effect of the transmutation on the actinide hazard and the sensitivity of the fission reactor performance parameters to the actinide recycle.

The effect of actinide recycle on reactor operating performance parameters was analyzed using the generalized linear perturbation capability of the FORSS system. The effect of both the quantity of recycled actinides and their placement within the "transmutation" reactor were considered.

C. NUCLEAR DATA PROJECT ACTIVITIES - 1976

(R. L. Auble,* J. R. Beene, F. E. Bertrand,* Y. A. Ellis, W. B. Ewbank, M. L. Halbert,* J. Halperin,* B. Harmatz, M. J. Martin, M. R. Schmorak, K. S. Toth,* and M. P. Webb*)

1. Evaluated Nuclear Structure Data File (ENSDF)

The coverage of ENSDF has been extended considerably during the last year to include new evaluations by the Nuclear Data Project as well as some older data from the Nuclear Data Sheets. As of January, 1977, ENSDF contains the following data sets:

1571	Adopted levels
1251	Decay schemes
1910	Other data sets (mostly nuclear reactions).

Another 550 data sets are being held in our working file for evaluations in preparation.

At its meeting in Vienna, May 1976, the IAEA Advisory Group on Nuclear Structure and Decay Data adopted the ENSDF formats as a preliminary standard for computer encoding of nuclear structure and decay data. In support of the international evaluation effort, the Nuclear Data Project has prepared two tape copies of the complete ENSDF master file (dated 7/76 and 1/77) for distribution through NNCSC in Brookhaven. Subsets from the master tape have also been sent to a few individual users at their request. The second master tape (1/77) is copied from an improved ENSDF master file, thanks to the added data checking done by these ENSDF users.

The ENSDF formats are also being used by other projects to prepare decay data for specific applications (e.g., a revised NCRP handbook of radioactivity, NRC assessment of environmental effects of radiation). These data are then being used to augment the master file. The NDP program MEDLIST is used to generate standard tables of atomic and nuclear radiations from the standard ENSDF data sets.

*Part-time assignment to Nuclear Data Project.

2. Data Evaluation Networks

An international network for evaluation of nuclear structure data is in the initial stages of organization. The network will lead to a wider distribution of responsibility for evaluated data.

Commitments from other US and non-US laboratories have reduced the evaluation responsibility for the Nuclear Data Project from ~220 A-chains to ~100 A-chains. Evaluation of data for this smaller range of nuclei is scheduled for completion over a three-year period. Combined with non-NDP efforts, this should lead to a maximum time of about four years between successive evaluations for data on each nucleus.

In support of the data evaluation network, NDP provides data listings and reference printouts, and acts as a clearinghouse for standard programs to help with the evaluation. NDP will also assume a major role in establishing uniform standards for evaluation of data and for establishing review procedures for evaluated data submitted for addition to ENSDF.

3. Nuclear Structure References (NSR)

During 1976, over 5000 references to new nuclear structure measurements and calculations were indexed and added to the NDP master file. New entries into the master file are published three times each year in "Recent References" issues of Nuclear Data Sheets.

Requests for special bibliographies from the NSR file continue to be processed at a rate of 2-3 per month. Monthly printouts of new references on specific topics are being sent to 10-15 non-NDP data evaluators, in support of the national and international program.

A special bibliography for even-even nuclei was prepared for a US-Japan compilation project, as a test of several selection procedures. The bibliography contained ~25,000 references sorted by nucleus, and consisted of ~5000 computer pages compressed to only 21 sheets of microfiche.

A tape copy of the master NSR file was sent to the Kurchatov Institute (USSR), as part of US participation in an international exchange of nuclear structure information. The tape was successfully processed in Moscow and a dialog is being established to develop a format for routine exchange of indexed bibliographic information. A tape containing keyword abstracts for results reported at three recent Russian conferences was received from the Soviet Union. These references (in a standard ORNL-ADSEP format) are being merged onto the NSR file.

OHIO UNIVERSITY ACCELERATOR LABORATORY

A. STRUCTURE STUDIES OF LIGHT NUCLEI

1. ${}^6\text{Li}+n$ (H. Knox, R. White, R. Lane)

A good understanding of neutron interactions with ${}^6\text{Li}$ is of great importance to the entire nuclear energy program both because of the use of this material in proposed fusion reactor blankets and its use as a standard for flux normalization. Measurements of the differential cross sections of neutrons scattered from ${}^6\text{Li}$ for $4 \leq E_n \leq 7.5$ MeV were reported earlier.¹ Analysis of these data has been completed. This provides new information in a region where only sparse data existed before. An R-matrix analysis of these and other relevant data will be underway shortly.

With the arrival of new highly enriched scattering samples, measurements of inelastic scattering of neutrons from ${}^6\text{Li}$ will be undertaken. Our studies on ${}^6\text{Li}$ are relevant to Request Nos. 74210 and 84250.

2. ${}^7\text{Li}+n$ (H. Knox, R. White, R. Lane)

Measurements of the differential cross section (elastic + 0.478 MeV level) of neutrons scattered from ${}^7\text{Li}$ were reported earlier in the same range of energies. The analysis of these data including finite geometry, air scattering, minor isotope and multiple scattering corrections has been completed. Though neutrons inelastically scattered from the 478 keV level were never completely separated from the elastic group, the cross sections for scattering to this level have been extracted by a curve fitting method.

In the neutron energy range studied here, all reaction channels other than the elastic and inelastic to the 478 keV level are particle unstable and result in the production of a triton. Subtracting our integrated elastic and inelastic cross sections from the total cross section, values of the important ${}^7\text{Li}(n,n')_{\alpha t}$ reaction cross section can be obtained. Evaluations of existing total cross section measurements are underway currently in order to obtain the best available values.

Further measurements of inelastic cross sections are planned upon arrival of new highly enriched scattering samples. Our work on ${}^7\text{Li}$ is relevant to Request Nos. 74211, 74251, and 74252.

¹H. D. Knox, R. M. White, and R. O. Lane, Proc. of the Intl. Conf. on the Interactions of Neutrons with Nuclei, E.R.D.A. CONF-760715-P2, p. 1307.

3. $^{10}\text{B}+n$ (H. Knox, R. White, R. Lane)

Final analysis of the $^{10}\text{B}+n$ differential cross section data reported earlier has been completed. Analysis of these data was complicated by the presence of a 4% oxygen contaminant in the scattering sample. These final data are somewhat different from the earlier Aldermaston data², especially at forward angles. A new highly enriched and chemically pure ^{10}B scattering sample has been obtained and further measurements of both elastic and inelastic neutron scattering are planned. Work on ^{10}B is relevant to Request Nos. 74003, 74004, 74005, and 74006.

4. $^{11}\text{B}+n$ (R. White, R. Lane, J. Cox, J. Adams, H. Knox)

Recent measurements of elastically scattered neutrons from ^{11}B at Ohio University have extended neutron differential cross section measurements from 4 to 8 MeV. The entire energy region of 0.1 to 8 MeV is being analyzed for the first time with a multichannel, multilevel R-matrix program using j-j coupling. Results of this analysis have confirmed previous assignments up to 2 MeV and have suggested some possible changes in assignments in the 2 to 4 MeV region. Between 4 and 8 MeV several new J^π assignments have been made. Further R-matrix analysis and additional measurements of inelastic neutron scattering are planned. The work on ^{11}B is relevant to Request Nos. 74003, 74004, 74005, and 74006.

B. ELASTIC AND INELASTIC SCATTERING^{*}

1. Nucleon Scattering on T=0 Nuclei (J. Rapaport, R. W. Finlay, D. Bainum, T. Cheema, and J. D. Carlson)

Neutron elastic scattering on Si, S and Ca has been measured at 11, 20 and 26 MeV using the Ohio University 11-MeV Tandem Van de Graaff. A time-of-flight technique was used and the angular distributions covered an angular range from 15° through 155° . The measured cross sections were corrected for dead time, source anisotropy, detector efficiency, finite geometry, neutron flux attenuation, and multiple scattering. Individual as well as global fits to the data using an optical model search code are presented. The comparison of the optical model analysis to the neutron and proton elastic scattering data in the case of ^{40}Ca allows an empirical determination of the Coulomb correction term which may be parameterized as $0.48 Z/A^{1/3}$. It is also shown that the elastic scattering

^{*} Supported in part by the National Science Foundation.

² R. Batchelor and J. Towle, Nucl. Phys. 47, 385 (1963).

and inelastic scattering to the 2^+ states in ^{28}Si and ^{32}S may be fitted using the same optical model parameters obtained for ^{40}Ca using the coupled-channel formalism.

Abstract of paper to be submitted to Nuclear Physics.

2. The Isospin Term; Its Real Part V_1 (J. Rapaport, R. W. Finlay, D. Bainum, T. Cheema, and J. D. Carlson)

In the proposal a study of the radial dependence of V_1 was indicated. Does elastic scattering prefer a volume Woods-Saxon or a surface derivative Woods-Saxon? In all analyses it is assumed to have a volume form factor. The optical model search code GENOA (1) was modified to include in the real part of the potential a term with a derivative Woods-Saxon form factor. The neutron analysis on Ca ($T=0$) was first completed to obtain a central geometry that could be used for other closed-shell nuclei. This geometry $r_R = 1.152$ $a_R = 0.692$ was subsequently used to analyze the $^{92}\text{Mo}(n,n)$ and $^{208}\text{Pb}(n,n)$ data at 11, 20 and 26 MeV. A search was done on the strength of the derivative Woods-Saxon form factor that could be interpreted as $\epsilon V_1(E)$. The preliminary results are quite ambiguous and need further study. Results with a volume Woods-Saxon form factor are indicated in the next sub-section.

3. The Energy Dependence of V_1 (J. Rapaport, R. W. Finlay, D. Bainum, T. Cheema, and J. D. Carlson)

The following (n,n) elastic scattering data were selected for this study:

- | | |
|-------------------------------|---------------------------------|
| a) Ca | $E_n = 11, 20$ and 26 MeV |
| b) $^{92,96,98,100}\text{Mo}$ | $E_n = 7, 9, 11, 20$ and 26 MeV |
| c) ^{208}Pb | $E_n = 7, 9, 11, 20$ and 26 MeV |

Individual fits at each energy gave an average geometry which subsequently gave an overall average geometry which was used in the global optical potential fit to all the 28 cases simultaneously. The resultant value of the isospin $V_1(E=0) = 22$ MeV indicated a linear (assumed) energy dependence of $-0.18E$.

It should be noted that values $V_1 = 6 \pm 1$ MeV were used in the analysis of quasi elastic transitions at 94 MeV from a series of targets from V to Pb by Thurlow. This is in very good agreement with the value $V_1(E=94) \approx 5$ MeV obtained from the present results. A paper describing these results is in preparation.

4. Comparison of (n,n) Data and (p,p) Data at Energies Such that $E_p = E_n + \Delta E_c$ (J. C. Ferrer, J. D. Carlson, and J. Rapaport)

The analysis of elastic scattering of neutron and proton data on the same nuclei at $E_n = E_p = E_n + \Delta E_c$ in terms of the optical model has yielded isospin dependent potentials with isospin parameters $V_{1R} = 22.7 \pm 0.6$ MeV and $W_{1D} = 12.7 \pm 0.8$ MeV.

Abstract of a paper published in Physics Letters 62B (1976) 399.

5. Neutron Scattering on the Mo isotopes (J. Rapaport, R. W. Finlay, D. Bainum, T. Cheema and J. D. Carlson).

Individual and global fits to the $^{92,96,98,100}\text{Mo}$ (n,n) data have been obtained. The energy dependence of the real and imaginary parts have shown interesting results which are described in a paper in preparation.

6. Neutron Scattering on the Sn Isotopes (J. Rapaport, R. W. Finlay, D. Bainum, T. Cheema and J. D. Carlson).

Differential elastic scattering cross sections have been measured at 11 MeV for the isotopes $^{118,120,122,124}\text{Sn}$. Angular distributions over the angular range from 15° to 150° in the laboratory were obtained for each sample. Data analysis will be completed for these samples in the near future and an optical model analysis will be performed. The Sn samples were also used in a preliminary effort to observe anomalies in the excitation function for elastic and inelastic neutron scattering in the vicinity of the doubly-forbidden isobaric analog resonances. Time-of-flight spectra were taken at laboratory scattering angle of 82.5° in steps of 50 and 25 keV. Preparations are being made for the measurement of singly-isospin-forbidden (n,p) reaction on the same target nuclei.

7. Neutron Elastic Scattering at 11 MeV and the Isospin Dependence of the Neutron-nucleus Optical Potential (J.C. Ferrer; J. D. Carlson and J. Rapaport)

Elastic scattering of 11 MeV neutrons from Mg, Al, S, Ca, V, Mn, Fe, Co, Ni, Nb, $^{92,96,98,100}\text{Mo}$, In, ^{120}Sn , Ho, Ta, ^{206}Pb and Bi have been measured with the Ohio University Tandem Van de Graaff accelerator.* The required neutrons were produced by the $\text{D}(d,n)^3\text{He}$ reaction. Standard pulsed beam time-of-flight techniques were employed with a multiple detector system which included five large area liquid scintillators and

*The tabulated cross sections are available as a supplement to the paper and have also been stored in the CSIRS files.

plastic scintillator monitor. Measurements of the incident flux at zero degrees were used to normalize the differential cross sections. Energy resolution was approximately 360 keV (fwhm). The measured cross sections were corrected for dead time, detector efficiency, attenuation, multiple scattering, finite geometry, neutron source anisotropy, contaminants and compound elastic contribution. Relative and normalization uncertainties in the measured cross section are 3-5% and approximately 3.5% respectively. A search for an average set of optical model potential parameters based solely on the measured (n,n) data for the isotopically pure samples and for which inelastic contributions to the elastic data are insignificant yield isospin dependent potential strengths, $V_R = [47.14 - 22.50(N-Z)/A]$ MeV and $W_D = [12.16 - 2.03(N-Z)/A]$ MeV.

Abstract of paper published in Nuclear Physics A275 (1977) 325.

8. Neutron Elastic Scattering on ^{208}Pb (J. Rapaport, R. W. Finlay, D. Bainum, T. Cheema and J. D. Carlson).

A paper is in preparation which will describe the neutron optical model potential parameters obtained. A comparison with the results of the $p + ^{208}\text{Pb}$ optical model analysis obtained by van Oers et al. between $E_p = 15$ and $E_p = 1000$ MeV will be described in terms of potential strengths as well as volume integral per nucleon.

9. Inelastic Neutron Scattering of Single-Closed-Shell Nuclei (J. Rapaport, R. W. Finlay, D. Bainum, T. Cheema and J. D. Carlson, with J. R. Comfort [University of Pittsburgh]).

Theoretical predictions of isospin sensitivity of core polarization effects in inelastic nuclear scattering to the first 2^+ states in single-closed-shell nuclei have been investigated by means of the (n,n') reaction on $N = 50$ nuclei (^{90}Zr and ^{92}Mo) and $Z = 50$ nuclei ($^{118,120,122,124}\text{Sn}$). Analysis of the Sn measurements is not yet complete, but the ^{90}Zr and ^{92}Mo results were presented at the ICINN at Lowell. Preliminary results indicate that the anticipated effect ($\beta_{nn'} > \beta_{pp'}$) is indeed observed for these nuclei, but the conclusion is clouded somewhat by the rather wide range in values of $\beta_{pp'}$ which is found in the literature. We are currently reanalyzing $^{92}\text{Mo}(p,p')$ data at 12 and 15 MeV. New measurements in the $N=50$ region are planned and should shed considerable light on the question. An enriched sample of ^{88}Sr has been ordered from ORNL. In the meantime, analysis of the $Z=50$ data continues. Since in this case the theoretical predictions call for $\beta_{nn'} < \beta_{pp'}$ an additional sensitive test will soon be available.

A brief report on the preliminary findings is being prepared for publication.

10. Inelastic Neutron Scattering on Double-Closed-Shell Nuclei (J. Rapaport, R. W. Finlay, D. Bainum, T. Cheema and J. D. Carlson).

Inelastic excitation of collective states in ^{40}Ca and ^{208}Pb by 11, 20, and 26 MeV neutrons has been measured in this laboratory and analyzed by W. G. Love (University of Georgia) in terms of a fully microscopic model of inelastic scattering. The effects of direct and exchange amplitudes, imaginary components in the effective interaction and density dependent forces have been examined. A manuscript reporting the results of this study is being prepared for publication.

11. High Energy (p,n) Experiments Conducted at the Indiana University Cyclotron Facility (IUCF) C. D. Goodman, Oak Ridge National Laboratory; B. Anderson, A. Baldwin, J. Knudson, T. Whitten and R. Madey, Kent State University; C. C. Foster, Indiana University; M. B. Greenfield, Florida A&M; and D. E. Bainum and J. Rapaport, Ohio University.

A program has been undertaken to study the isospin composition of the giant resonance by comparing (p,n) and p,p' cross sections on self-conjugate nuclei. Experiments are being performed at the Indiana University Cyclotron Facility using 62 MeV protons and a 20 meter flight path. Spectra of the (p,n) reactions on ^9Be , ^{12}C , and ^{28}Si have been taken using the Ohio University Very Large Detector (BNL NCS-21501,247 May 1976) which demonstrated an overall time resolution ($\leq 1.5\text{ n sec}$) comparable to that of smaller, less efficient conventional detectors. Further experimental work is planned at $E_p = 135\text{ MeV}$.

C. NEUTRON SPECTROMETRY AND ODD-ODD Ag NUCLEI

1. Mass Measurements of ^{104}Ag , ^{106}Ag (C. Brient, K. Devan)

The masses of ^{104}Ag and ^{106}Ag were determined from the $^{104,106}\text{Pd}$ (p,n) reaction Q-values. An absolute time scale was established by measuring the neutrons from the $^{89}\text{Y}(p,n)$ reaction. The relative time scale was determined by using a precision pulser. The Q-values for the ^{106}Pd (p,n) reaction measured relative to the ground state Q-values of $^{89}\text{Y}(p,n)$ (-3.6166 MeV) reaction³ is $-3.7555 \pm .01\text{ MeV}$ and that of the $^{104}\text{Pd}(p,n)$ reaction measured for the first excited state in ^{104}Ag , in comparison with the third excited state in ^{89}Zr (-5.0684 MeV) is $-5.060 \pm .01\text{ MeV}$.

2. $^{104,106}\text{Pd}(p,n,\gamma)$ $^{104,106}\text{Ag}$ Energy Levels (K. Devan, C. Brient, R. Finlay, J. Rapaport)

The gamma-ray spectra from the $^{104,106}\text{Pd}(p,n,\gamma)$ reactions were measured from the threshold to an excitation energy 1400 keV in steps

³Wapstra, Gove, Nuclear Data Tables A, Vol. 9, 1971.

of 20 keV in the case of ^{106}Ag and 50 keV in the case of ^{104}Ag . Smaller steps of the order of 5 keV were taken whenever further distinction of the threshold was necessary. These measurements were done with three Ge(Li) detectors of different active volumes, namely, two co-axial detectors of volume 35 cm^3 and 80 cm^3 and a 5 m.m. thick Low Energy Photon Spectrometer (LEPS). The energy calibration of these detectors was done with the ^{226}Ra , ^{154}Eu , ^{241}Am , ^{57}Co and ^{22}Na sources. The relative efficiency of the 80 cm^3 detector was determined from the known relative intensities of the gamma rays from the ^{226}Ra and ^{154}Eu sources⁴ corrected for the active volume.⁵ A list of gamma-rays, their relative intensities and the uncertainties in the relative intensity measurements at excitation energies 784 keV (^{104}Ag) and 1400 keV (^{106}Ag) are shown in Tables 1 and 2. Gamma-Gamma Coincidence Measurements were performed with the 80 cm^3 detector in conjunction with the 35 cm^3 detector for 12 energies at $E_p = 5.9\text{ MeV}$ (^{104}Ag) and $E_p = 5\text{ MeV}$ (^{106}Ag).

Table 1
Gamma Rays from the $^{104}\text{Pd}(p,\gamma)$ Reaction

Gamma Ray keV	I	δI	Gamma Ray keV	I	δI
74.0	8.54	0.81	323.0	4.89	0.44
83.7	100	10.03	332.5	3.57	0.31
91.0	0.30	0.13	335.8	10.51	1.02
123.8	88.03	4.01	341.2	92.85	5.02
139.0	11.84	0.62	351.0	1.44	0.31
145.9	1.99	0.16	356.4	3.11	0.61
150.5	1.57	0.15	362.2	6.44	0.42
159.1	11.98	0.70	377.6	10.01	0.72
179.0	1.77	0.16	389.8	30.88	2.02
185.3	7.12	0.50	404.3	8.12	0.63
192.3	1.47	0.40	422.3	6.02	0.62
212.1	15.67	1.10	426.8	22.26	1.41
218.6	1.70	0.40	489.0	9.69	0.90
224.4	25.68	1.52	494.8	0.79	0.16
249.0	0.51	0.11	528.1	5.62	0.41
252.1	16.02	1.01	544.9	0.64	0.12
257.59	1.07	0.21	563.8	20.11	1.32
265.4	8.88	0.53	572.7	5.71	0.42
269.7	7.31	0.45	583.3	6.25	0.50
276.3	8.81	0.50	645.2	3.31	0.42
296.7	12.07	0.85	668.6	3.42	0.35
303.0	6.32	1.03	709.6	13.66	0.95
305.8	1.39	0.41	740.4	8.71	0.62

⁴ H. L. Kernell et al., Nucl. Phys. A 176 (1971) 65

⁵ P. D. Kunz, Modified by J. R. Comfort (private communication)

Table 2

Gamma Rays from the ^{106}Pd (p, γ) Reaction

Gamma Ray keV	I	δI	Gamma Ray keV	I	δI
87.3	1.47	0.15	363.4	15.11	0.95
95.0	33.34	3.50	384.3	10.31	0.65
110.6	100	10.02	394.3	1.95	0.16
122.0	1.36	0.12	416.6	13.09	0.85
139.6	1.57	0.13	461.1	0.58	0.16
147.7	2.44	0.18	474.4	5.43	0.35
154.1	9.75	0.65	486.2	5.75	0.36
158.6	0.65	0.13	492.6	4.76	0.33
165.4	1.52	0.13	524.3	2.43	0.20
181.9	0.86	0.11	533.9	4.88	0.31
205.6	1.98	0.16	545.9	1.67	0.17
234.7	9.94	0.60	585.9	1.36	0.15
239.1	13.34	1.02	640.9	4.52	0.30
243.3	5.54	0.45	649.1	1.53	0.13
253.7	11.49	0.71	681.4	5.22	0.30
277.0	83.04	4.82	688.9	1.59	0.12
288.0	0.86	0.13	751.6	1.35	0.11
297.0	0.59	0.14	817.5	0.59	0.13
301.5	1.03	0.16	828.7	1.94	0.13
305.9	8.51	0.51	858.1	0.53	0.11
341.3	10.03	0.61	876.7	6.53	0.41
320.0	3.85	0.25	898.5	0.72	0.11
325.8	9.02	0.55	939.4	1.39	0.12
333.8	2.49	0.21			

3. $^{104,106}\text{Pd}(p,n)^{104,106}\text{Ag}$, Spin, Parity and Structure Studies (K. Devan, C. Brient)

Pulsed proton beams with energies between 5.9 MeV and 6.75 MeV with repetition rates 1.25 and 2.5 MHz were used to measure (p,n) time-of-flight spectra and angular distributions from rolled foils (500 $\mu\text{g}/\text{cm}^2$ and 260 $\mu\text{g}/\text{cm}^2$) of $^{104,106}\text{Pd}$. (Microfoils - Argonne, Illinois.)

The locations of the $5/2^+$, $1/2^+$ and $3/2^+$ isobaric analogue resonances in ^{105}Ag and the $5/2^+$ and $1/2^+$ resonances in ^{107}Ag were determined from the (p,n) excitation functions, measured with a "long counter." The neutron time-of-flight spectra were taken on, above and below each resonance for $^{105,107}\text{Ag}$ leading to final states in $^{104,106}\text{Ag}$. See Figures 1 and 2. The relative (p,n) cross sections were determined by correcting the neutron yield for relative efficiency, air scattering and

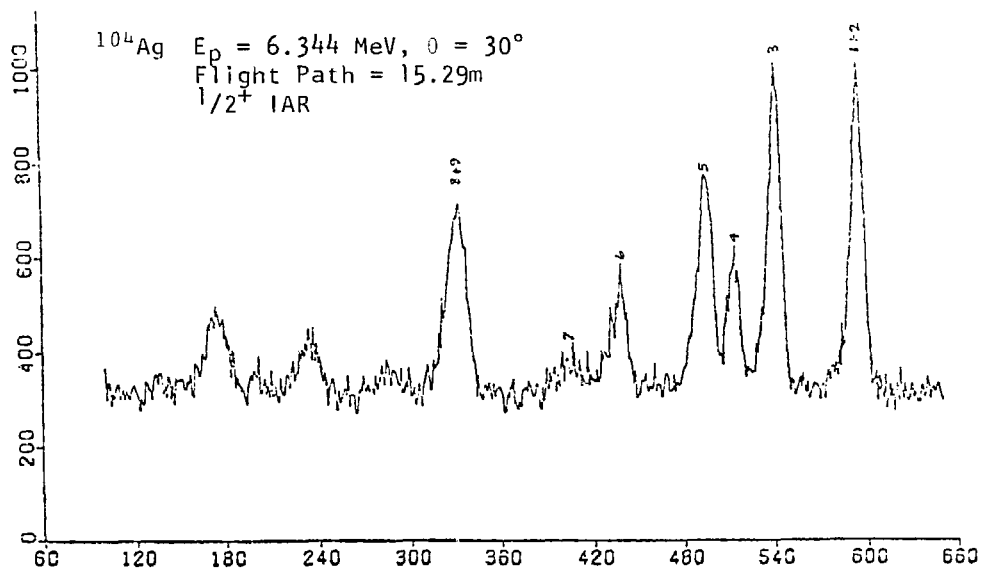


Figure 1. Time of flight spectra on the isobaric analogue resonances.

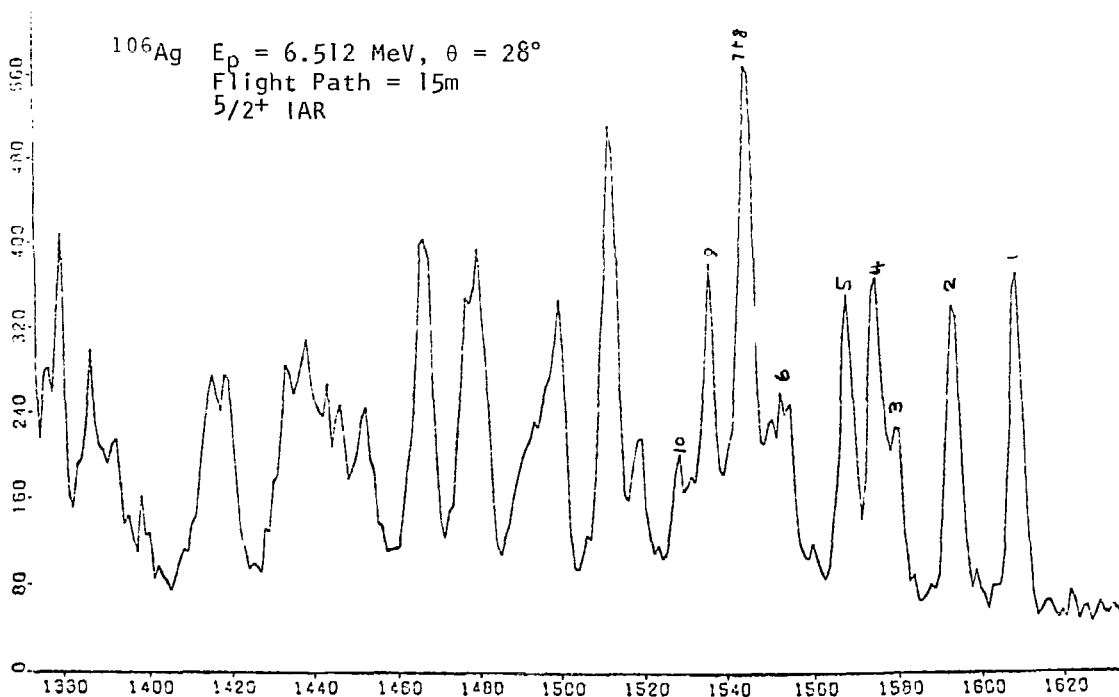


Figure 2. Time of flight spectra on the isobaric analogue resonances.

vacuum changer thickness. The neutron enhancements were determined by subtracting the average off-resonance relative cross section from the analogue on-resonance relative cross section.

Angular distributions of the $^{104}\text{Pd}(p,n)^{104}\text{Ag}$ reaction are shown in Figures 3 to 6. The on-resonance angular distributions are the top curves and the off-resonance distributions are the lower curves. The on-resonance curves were calculated from the relationship^{6,7,8}

$$\sigma(\theta) = \sigma_{\text{CN}}(\theta) + n \sum_{\ell_0 j_0} \omega_{j_0}(\theta) \text{ where}$$

$\sigma_{\text{CN}}(\theta)$ is the Hauser Feshbach cross section

$$\omega_{j_0}(\theta) = \sum \eta_{\nu} (j_p j_p \ell_i j_0) \eta_{\nu} (j_0 j_0 \ell_f j_0) P_D(\cos \theta)$$

where η_{ν} are the Satcheler coefficients,⁹ $T_{\ell j}$ are the transmission coefficients calculated from the computer code - DWUCK.¹⁰ Off-resonance Hauser Feshbach¹¹ cross-sections were calculated with the code "Helene."¹²

The spins and parities of the energy levels in ^{104}Ag were assigned on the basis of (1) the enhancements from three isobaric analogue resonances of different spins; (2) the angular distributions of neutrons from the decay of $5/2^+$ and $3/2^+$ analogue resonances; (3) off-resonance relative cross section in comparison with the Hauser Feshbach calculations; and (4) off-resonance angular distributions in comparison with the Hauser Feshbach calculations. In the case of ^{106}Ag the neutron energies involved were higher and hence the resolution of the time-of-flight spectra was poor for flight path less than nearly 7 m which was the order of flight path available in the angular distribution experimental set-up, therefore no angular distribution measurement was performed for ^{106}Ag . In this case, the spin and parity assignments were made from (1) the enhancements of neutrons from the $5/2^+$ and $1/2^+$ resonances and (2) off-resonance relative cross sections in comparison with the Hauser Feshbach calculations.

The energy level diagrams and the spins and parities assigned are shown in Figures 7 and 8.

⁶ G. Doukellis et al., Nucl. Phys. A 229 (1974) 47

⁷ H. J. Kim and R. L. Robinson, Phys. Rev. 151 (1966) 920

⁸ H. J. Kim and R. L. Robinson, Nucl. Phys. A 167 (1971) 73

⁹ R.L. Kernell et al., Nucl. Phys. A 176 (1971) 449

¹⁰ P. D. Kunz, modified by J. R. Comfort (private communication)

¹¹ W. Hauser and H. Feshbach, Phys. Rev. 87 (1952) 366

¹² S. K. Penny, ORNL-TM-2590

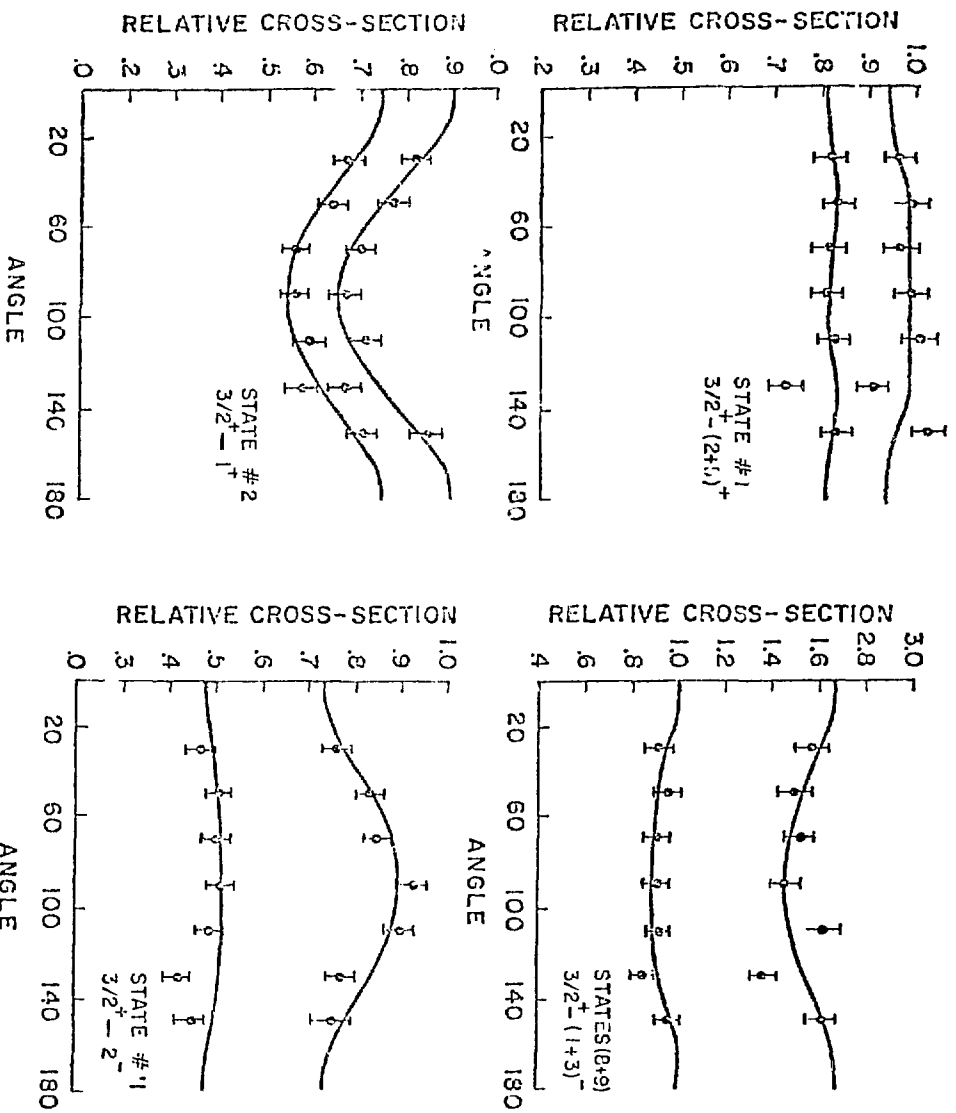


Figure 3.

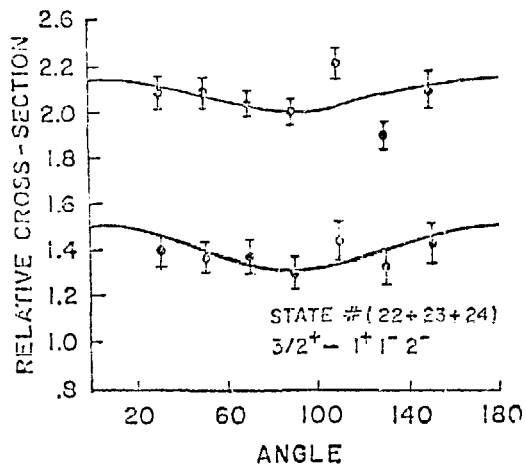
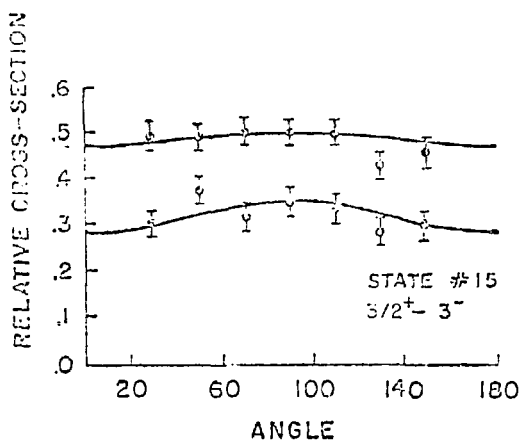
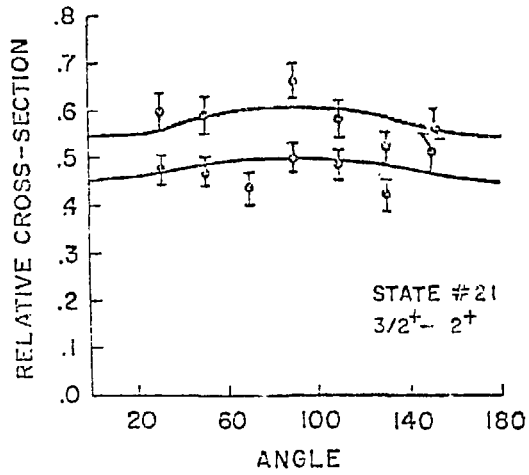
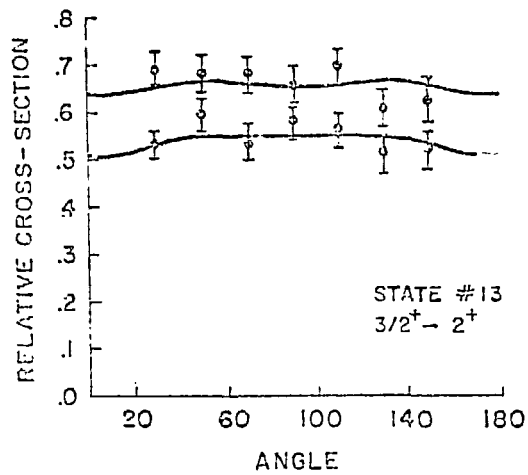


Figure 4.

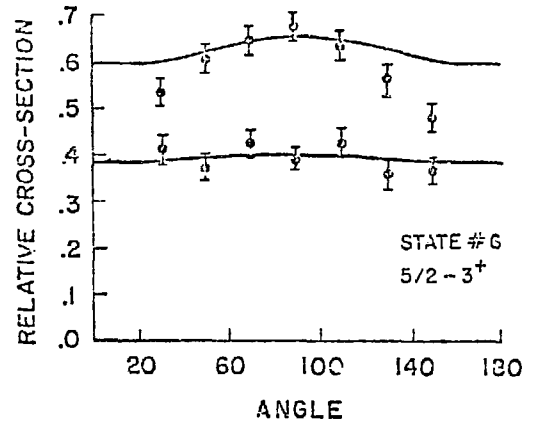
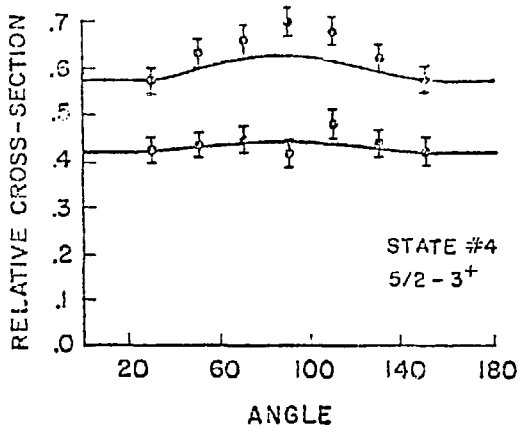
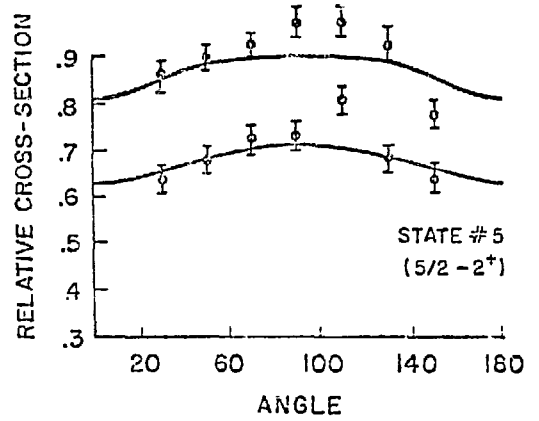
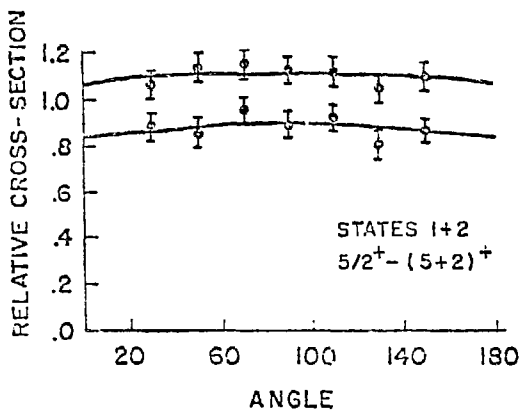


Figure 5.

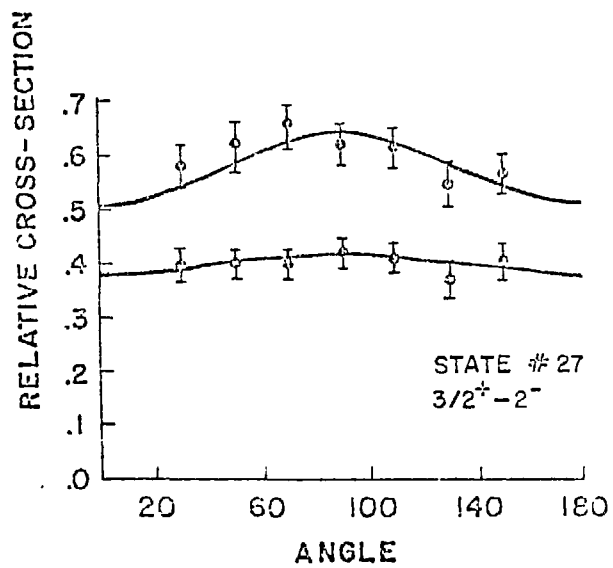


Figure 6.

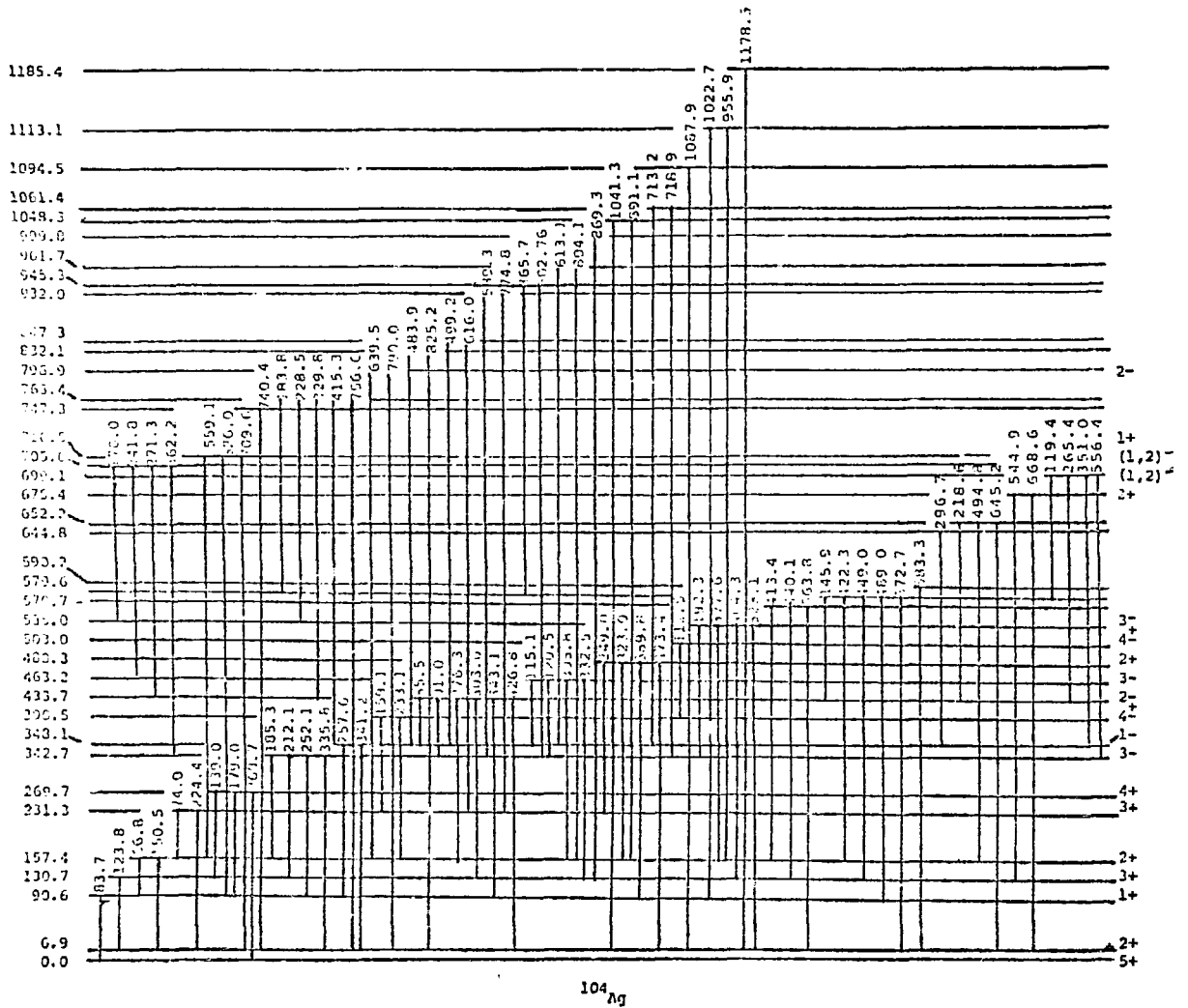
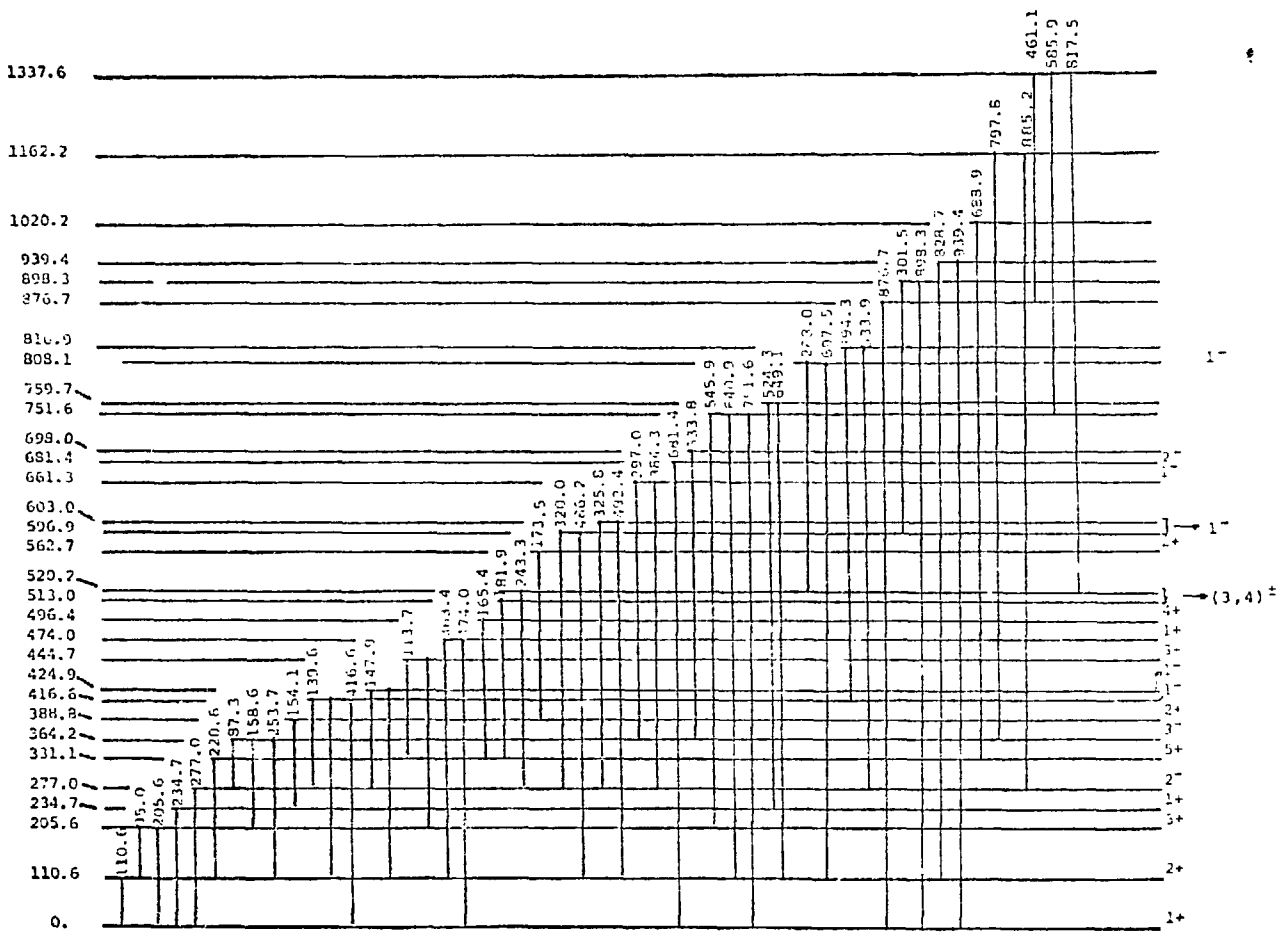


Figure 7.



106_{Hg}

Figure 8.

The structure of these levels can be understood from a detailed study of the odd silver isotopes ranging from ^{105}Ag to ^{111}Ag . In this isotope chain the lowest $1/2^-$ and $9/2^+$ states could be single quasi-particle states $\Pi(g_{9/2})^{-2} P_{1/2}^{-1}$ and $\Pi(g_{9/2})^{-1}$. The $7/2^+$ state has been interpreted as a three-quasi proton state $(g_{9/2})^{-3}_{7/2}$ by Talmi and Unna.¹³ The one phonon-coupled to quasi-particle states are at higher excitation and are not required in the interpretation of the low lying states. The coupling of neutrons to form the odd-odd nuclei $^{106}\text{Ag} - ^{112}\text{Ag}$ would account for most of the spins and parities observed here.

D. HIGH NEUTRON FLUX TARGET (D. Bainum, C. Brient, D. Sturbois, J. Matthews)

A High neutron flux target (about 10^{12} n/sec strad) has been developed at this laboratory. The target uses a beryllium entrance foil and a volume of heavy water in which the beam is stopped and which also acts as a coolant for the entrance foil. The neutron spectrum from this target is nearly identical to that projected to be seen by the first containment wall of a CTR vessel except for the absence of the 14 MeV component (which would be much smaller than the lower energy continuum). Up to 50 μ amps of 8 MeV deuterons have been applied to this target. Local personnel shielding is currently being improved in order that higher beam currents can be run. This system will be used in studies of sputtering on first wall materials.

E. STUDIES OF MAGNETIC FLUX AND CRITICAL CURRENT DISTRIBUTIONS NEAR THE SURFACE IN PROTON IRRADIATED TYPE II SUPERCONDUCTORS (R. Rollins)

The goal of this research is to study the effect of various defects and surface treatments on the critical current density near the surface of type II superconductors. An ac technique developed here is used to study the flux pinning strength (which is fundamentally related to the critical current) as a function of depth from the sample surface. In particular, the effect of irradiation of superconducting materials with 1-8 MeV protons on the critical current density near the surface is being carried out, utilizing the Ohio University Tandem van de Graaff accelerator. The results of the observed flux pinning are then related to calculations based on various models of flux pinning by defects resulting from the irradiation damage. Some of the irradiated samples have been studied using a transmission electron microscope in order to characterize the damage structure. The aim is to characterize the

* Supported by the Air Force Office of Scientific Research.
¹³I. Talmi and I. Unna, Nucl. Phys. 19 (1960) 225.

effect of irradiation damage on the critical current and to increase the basic understanding of critical current and flux pinning mechanisms in superconductors.

F. ELECTRONICS DEVELOPMENT (D. Carter)

A high-speed minicomputer to be used in an on-line data acquisition system has been designed and built. The design objective was to build a high quality on-line system at minimum cost. To meet the above design objective the standard TTL 7400 logic family was chosen.

The system architecture is designed around an 8k by 20 bit memory allowing integer operations in excess of 1 million and all one-word instruction formats. Four general purpose registers are available to the programmer and can be used as index registers, loop counters, accumulators or for temporary data storage. All total instruction execution time are 1 microsecond or less, allowing data input rates in excess of 300 kilohertz when used as a multi-channel analyzer. The instruction set includes 49 basic instructions and has proven highly efficient and easy to use. The four general purpose registers in conjunction with memory-accumulator, register-register and register-memory indexed operations greatly simplify complex programs. Two instructions specifically included in the instruction set for data acquisition purposes are Increment Memory and Increment Memory Indexed. Total instruction execution time for these complex instructions is also 1 microsecond. One level of interrupt has been provided. The interrupt may be software masked and unmasked. This one level of interrupt may be software vectored for an unlimited number of interrupts on the level. Eight twenty-bit input ports and eight twenty-bit output ports are available.

The total system parts cost, including 8K of 20 bit memory and a user interactive panel for initial program development, was approximately \$1,500.

G. ACCELERATOR IMPROVEMENTS (D. Sturbois)

The transmission of the Ohio University Tandem Van de Graaff Accelerator has been significantly increased by the use of very thin carbon stripper foils produced at this laboratory. These foils are less than 2 micrograms per square centimeter and are produced by a method employing an extremely light carbon coating on glass with an iso-amyl acetate coating to facilitate installation. With these foils target currents of 80 μ a of deuterons and 150 μ a of protons are easily obtainable.

UNIVERSITY OF PENNSYLVANIA

PROGRESS REPORT ON GRANT EY-76-S-02-2785.* 000

Principal Investigator: Dr. Fay Ajzenberg-Selove, Professor of Physics

[This progress report covers the period from March 1, 1976 to February 28, 1977.]

A. REVIEW AND EVALUATION WORK

1. A manuscript of A = 13-15 was published in Nuclear Physics as "Energy Levels of Light Nuclei, A = 13-15" by F. Ajzenberg-Selove, Nuclear Physics A268 (1976) 1-204.

2. Preliminary versions of manuscript on A=16 and A=17 were sent to about 200 nuclear physicists for their comments in July 1976 (PPP-3-76) and September 1976 (PPP-4-76). After incorporating comments and new data, the final manuscript on A = 16-17 was submitted to Nuclear Physics in December 1976. It has been accepted for publication in 1977.

3. A preliminary version of A=18 has been sent to 200 colleagues in February 1977 (PPP 1-77). We plan to complete the manuscript on A = 18-20 by the late fall of 1977. We then plan to begin on the nuclei with A = 5-10, again working toward a four-year cycle.

B. EXPERIMENTAL RESEARCH

1. Completed Research

a. At P-9, Los Alamos Scientific Laboratory

Published:

"Energy Levels of ^{62}Co " by F. Ajzenberg-Selove, E. R. Flynn, C. Hansen, J. D. Sherman, N. Stein and J. W. Sunier, Physical Review C14 (1976) 767-771.

"States of ^{34}P " by F. Ajzenberg-Selove, E. R. Flynn, S. Orbesen and J. W. Sunier, Physical Review C15 (1977) 1-3.

Accepted for publication:

"States of ^{54}V and ^{58}Mn " by E. R. Flynn, J. W. Sunier and F. Ajzenberg-Selove, Physical Review (1977).

b. At 88" Cyclotron, Lawrence Berkeley Laboratory

Published:

"Energy Levels of ^{12}N " by C. F. Maguire, D. K. Scott, J. Mahoney and F. Ajzenberg-Selove, Physical Review C13 (1976) 933-936.

c. Older work from Penn Tandem

Published:

" $^{10}\text{B}(^{10}\text{B},\alpha)^{16}\text{O}$ Reaction" by F. Ajzenberg-Selove, R. R. Betts and D. J. Crozier, Physical Review C14 (1976) 357-360.

2. Research Under Way

1. At P-9, Los Alamos Scientific Laboratory

We have completed a first draft of a manuscript on the mass and on the excited states of ^{122}In .

We are completing a study of the (t,p) reactions on the light nuclei.

We have proposed a number of (t, ^3He) experiments to the P-9 group hopefully to be carried out this spring or summer.

2. At the 88" Cyclotron, Lawrence Berkeley Laboratory

We have had three runs this past year to study nuclei far off the stability line. In the most recent of these experiments we have studied the $^{16}\text{O}(\alpha,^8\text{He})^{12}\text{O}$ and $^{20}\text{Ne}(\alpha,^8\text{He})^{16}\text{Ne}$ reactions. This paper will be presented at the 1977 Washington meetings of the APS by G. Kekelis et al.

RENSSELAER POLYTECHNIC INSTITUTE

A. NEUTRON CROSS SECTION MEASUREMENTS

1. Neutron Capture and Transmission Measurements on ^{95}Mo , ^{97}Mo , ^{133}Cs and ^{143}Nd
(R. W. Hockenbury, W. Yip and R. H. V. Gallucci)

Neutron capture and transmission measurements have been made on enriched samples of ^{95}Mo , ^{97}Mo , ^{133}Cs and ^{143}Nd from about 20 eV to 100 keV. The keV capture cross sections were determined to within $\pm 8\%$. Some resonance parameters are given in Table A-1.

The keV data were fitted using the methods of Lane and Lynn¹. Initial values of R , Γ , S^0 and S^1 were taken from various sources. The average level spacing, \bar{D} , was taken from our own capture data. These parameters were then adjusted until reasonable agreement was obtained between experiment and theory. In the fitting process, certain parameters (specific to each isotope) were not allowed to vary excessively depending on their quality. The sensitivity of the final result to the parameters, Γ , \bar{D} , S^0 and S^1 varies with energy. The most important quantities are Γ and \bar{D} . Generally the calculations are less sensitive to S^0 and S^1 , thus these values have a greater uncertainty when determined in this manner. The results to data are given in Table A-2. These values are obviously not unique but represent "best" values as judged by the somewhat subjective fitting process.

^{95}Mo A satisfactory fit was obtained for the parameters listed in Table A-1. The experimental results are also in fair agreement with the theoretical results of Schmittroth and Schenter². However, the data of Kapchigashev and Popov³ are about 10-30% higher proceeding from 10 to 50 keV.

^{97}Mo At low energies, there is reasonable agreement between calculation and experiment, however, at high energies, the calculated values do not decrease as fast as the experimental points. Our data are about 10% lower than Ref. 3 at 10 keV and overlap at about 50 keV. Again, our data are in fair agreement (10%) with Schmittroth and Schenter.

^{133}Cs The calculated curve follows the experimental results fairly well except for the three highest energy groups. At 10 keV, our results are about 10% higher than Popov and Shapiro⁴.

^{143}Nd At this time, no reasonable fit has been obtained and to

our knowledge, there are no other data with which to compare. The magnitude of the cross section is consistent with our previous results for ^{145}Nd (Ref. 5).

1. A. M. Lane and J. E. Lynn, Proc. Phys. Soc. A70, 557 (1957).
2. F. Schmittroth R. Schenter, "Fast Neutron Capture Cross Sections for Fission Product Isotopes".
3. S. V. Kapchigashev and Yu. P. Popov, Conf. on Int. of Neutrons with Nuclei, Dubna, Report No. 1845, 104 (1964).
4. Yu. P. Popov and F. L. Shapiro, Soviet Phys.-JETP 15, 683 (1962).
5. R. W. Hockenbury, W. R. Koste and R. Shaw (To be submitted for publication). Pertinent to Request No. 72072, 74074.

2. Neutron Capture Cross Section Measurements of ^{99}Tc Up to 80 keV
(R. C. Little and R. C. Block)

Capture and transmission measurements were carried out upon ^{99}Tc using the 1.25-m-diam. liquid scintillator tank and the $^{10}\text{B-NaI}$ detector respectively. The sample consisted of 10 grams of ^{99}Tc metal in a double sealed aluminum container. The transmission data were used to normalize the capture yield in the low energy region, and the capture data were reduced to capture yields.

Adamchuk et al.¹ have reported ^{99}Tc resonance parameters up to 1.1 keV. There was good agreement with their data in this region. Eight new resonances were observed below 1.1 keV. There were also 21 new resonances observed above 1.1 keV. They were resolvable up to 1.6 keV. The energy levels and integrated yields of the new resonances are listed in Table A-3.

The capture yield divided by sample thickness is plotted vs. neutron time of flight in Fig. A-1. The method of Schmitt² was applied to the data to correct for self-shielding and neutron multiple scattering in the sample, from which the capture cross section was deduced from 4 keV to 80 keV. These results are plotted in Fig. A-1 along with the ENDF/B-IV evaluated data. Errors in these results are approximately 10%, largely from uncertainties in normalization. It may be seen that the ENDF data underpredicts the cross section by about 15%.

1. Yu. V. Adamchuk, Yu. G. Shchepkin, G. V. Muradyan, M. A. Voskanyan, Conf. Kiev 2, 1972 (May 1973).
2. H. W. Schmitt, "Sample Scattering Corrections in Neutron Beam Experiments", Oak Ridge National Lab. (1960).

Table A-1

Neutron Widths from Transmission Data Analysis

Isotope	Resonance E_0 (eV)	Γ_γ (meV)	Γ_n (meV)	Γ (meV)
Mo-95	898.2	161.	300.	461.
Mo-95	680.4	161.	1020	1180
Mo-95	554.2	161.	127.	288.
Mo-95	358.2	161.	230.	391.
Mo-95	159.4	161.	14.2	175.
Mo-97	557.5	128.	538.	666.
Mo-97	396.9	128.	76.0	204.
Mo-97	285.8	128.	119.	247.
Mo-97	70.8	128.	21.0	149.
Cs-133	295.5	119.	120.	239.
Cs-133	220.6	119.	28.5	148.
Cs-133	201.3	119.	22.8	142.
Cs-133	146.2	119.	22.8	142.
Cs-133	94.2	119.	28.1	147.
Cs-133	82.7	119.	6.70	126.
Cs-133	47.5	119.	21.4	140.
Nd-143	708.3	72.8	366.	438.
Nd-143	657.7	72.8	456.	528.
Nd-143	306.1	72.8	791.	864.
Nd-143	158.3	72.8	1240	1310
Nd-143	55.2	72.8	42.1	115

3. Neutron Total and Capture Cross Section Measurements on Fission Product Pd.

(U. N. Singh, Y. Nakagome, R. C. Block)

Neutron total and capture cross section measurements on elemental and fission product Pd have been made using the Gaerttner Laboratory electron linear accelerator. The sample (9.254 grams) was obtained on loan from the Petten laboratory, The Netherlands. The chemical analysis of the fission product sample showed:

^{104}Pd - 1.41%, ^{105}Pd - 48.82%, ^{106}Pd - 22.38%, ^{107}Pd - 15.70%,

^{108}Pd - 8.94%, ^{110}Pd - 2.75%

These measurements were undertaken due to the absence of data¹ for ^{107}Pd .

The measurements used the capture tank detector at 25.63 meters

Table A-2

Sample	Nuclear Radius (cm)	Target Nuclear Spin	Radiation Width (eV)	Observed Spacings (eV)	s-wave Str. Ftn. (eV) ^{-1/2}	p-wave Str. Ftn. (eV) ^{-1/2}
MS-105	$.52 \times 10^{-12}$	$\frac{7}{2}$	0.0728	41.6	$.9 \times 10^{-3}$	$.2 \times 10^{-3}$
MS-05	$.7 \times 10^{-12}$	$\frac{5}{2}$	0.16	50	$.1 \times 10^{-4}$	$.7 \times 10^{-3}$
MS-07	$.69 \times 10^{-12}$	$\frac{5}{2}$	0.128	29	$.9 \times 10^{-5}$	$.6 \times 10^{-3}$
MS-103	$.61 \times 10^{-12}$	$\frac{7}{2}$	0.113	20	$.9 \times 10^{-4}$	$.7 \times 10^{-3}$

Radiation Width : Averaged BNL Values

Observed Spacings: R.F.I. Data

s-Wave Str. Ftn. : Best Fitting Value

p-Wave Str. Ftn. : Best Fitting Value

Table A-5
New Resonances Observed in ^{99}Tc

<u>Energy (eV)</u>	<u>$\int \frac{Y}{N} dE$ (b-eV)</u>
210.3	6.04
465.3	7.61
578.1	15.77
717.5	9.89
916.1	5.11
944.7	8.78
982.0	10.46
1010.5	10.27
1138.3	104.82
1180.8	111.20
1203.0	135.48
1215.7	55.28
1268.7	74.71
1284.1	90.23
1399.7	73.13
1310.8	62.06
1329.7	63.71
1333.5	36.64
1346.7	44.95
1370.3	47.64
1405.1	118.29
1426.6	61.19
1444.9	151.92
1478.8	166.86
1494.2	40.33
1533.9	53.46
1150.2	114.40
1564.7	48.59
1598.6	119.09

and the $^{10}\text{B-NaI}$ transmission detector at 28.32-m flight path. Earlier measurements² were made at R.P.I. on a Pd sample enriched in ^{105}Pd (94.51%) under similar conditions. These earlier capture measurements are plotted at the top of Fig. A-2 and are compared with the present fission product Pd capture measurements shown at the bottom of the figure. We have tentatively assigned all resonances not reported in Refs. 1 and 2 to ^{107}Pd , and these are listed in Table A-4 and some of these are labeled in Fig. A-2.

According to the Table A-4 16 resonances are assigned to ^{107}Pd below 200 eV, an energy above which we seem to be missing levels. Ref. 1 reports 17 resonances in ^{105}Pd below 200 eV. Since ^{105}Pd and ^{107}Pd have similar binding energies and the same spins and parities, it is expected that these two target nuclei would have similar level densities, in agreement with the present measurements. Pertinent to Request No. 67020, 74084.

4. Capture Cross Section Measurements of Pr and Kr
(P. S. Feigenbaum, H. T. Maguire, Jr., U. N. Singh,
Y. Nakagome and R. C. Block)

Capture measurements have been carried out from a few eV to over 100 keV upon elemental samples of Pr and Kr. A 0.079-cm-thick metallic sample of Pr was used for the Pr measurements, and a 30-cm-long by 7.62-cm-diam. aluminum cell filled with Kr at approximately 2.5 atm pressure was used for the Kr measurements.

The Pr data has a good signal-to-background ratio up to ≈ 100 keV, so that the keV capture cross section can readily be obtained up to this energy. Neutron transmission measurements have also been made for Pr to enable the capture data to be normalized to low-energy resonance capture in Pr.

The Kr data are characterized by many isolated resonances up to several keV, and many new resonances have been observed. These Kr resonances are listed in Table A-5. These data will be combined with future measurements upon isotopically-enriched ^{78}Kr ; the ^{78}Kr sample is scheduled for measurement during the Spring of 1977.

-
1. Neutron Cross Sections, vols. I and II, Brookhaven National Laboratory Report No. BNL-325 (third edition).
 2. R. W. Hockenbury, private communication.

Table A-4

Neutron Resonance energies (below 1 keV) assigned to ^{107}Pd

<u>E_0(eV)</u>	<u>E_0(eV)</u>	<u>E_0(eV)</u>	<u>E_0(eV)</u>
5.20	114.9	211.4	472.3
6.83	126.5	232.6	489.2
41.33	132.2	272.0	538.7
58.95	140.5	292.1	587.2
(73.43)	152.4	325.5	(877.3)
84.20	172.7	369.2	(900.2)
88.48	181.7	376.3	(907.6)
100.6	196.3	380.7	

Table A-5
Kr Resonances

<u>E_0(eV)</u>	<u>BNL-325</u>	<u>Assigned Nuclide</u>
28.06	27.9+0.3	^{83}Kr
40.05	39.8+0.5	^{82}Kr
105.9	106+2	^{80}Kr
232.3 (triplet)	233+6	^{83}Kr
313.9		
(451.8)		
(477.0)		
514.9	519+20	^{84}Kr
643.4	640+25	(^{78}Kr) ^{80}Kr
711.7		
808.8		
918.7		
983.6		
1098		
(1169)		
1413		
1478 (triplet)		
1556		
1609		
1677 (triplet)		
1927		
2123		
2230		
2410		
2794		
(3440)		

Table A-5 (Cont'd)

E ₀ (eV)	BNL-325	Assigned Nuclide
5329		
5651		
6470		
6879		
8341		
11480		

Pertinent to Request No. 74092.

5. $^{238}\text{U}(n,f)$ Measurements Below 100 keV

(R. E. Slovacek, D. S. Cramer, and E. B. Bean (KAPL) and
J. R. Valentine, R. W. Hockenbury and R. C. Block)

This work is now complete and a paper describing this research has been accepted for publication in Nuclear Science and Engineering. The abstract to the paper is as follows:

The $^{238}\text{U}(n,f)$ cross section has been measured from 3 eV to ≈ 100 keV with the RINS 75-ton lead slowing-down spectrometer at the Gaertner Laboratory. Four fission ionization chambers containing a total of ≈ 0.8 gm of ^{238}U (4.1 ppm ^{235}U) were used for the measurements. The fission widths of the 6.67, 20.9, and the 36.8 eV resonances were measured as (10 ± 1) , (58 ± 6) , and (12 ± 2) nanoelectronvolts respectively. By combining these fission results and published resonance parameters, the ^{238}U thermal fission cross section contribution from positive energy resonances was determined to be $2.7 \pm 0.3\mu\text{b}$. The resonance fission integral from 0.4 eV to 100 keV was determined to be (1.30 ± 0.15) mb.

6. $^{232}\text{Th}(n,f)$ Measurements in RINS

(R. C. Block, Y. Nakagawa, P. A. Bicknell, and R. E. Slovacek)

New measurements have been carried out in the RINS 75-ton lead slowing down spectrometer with several additional Th fission chambers. Measurements were carried out with bare and B_4C shielded Th, ^{238}U and ^{235}U detectors to shed light upon what background effects may be present in the Th fission data. In the 1 to 100 eV region, where the B_4C effectively removes all low-energy neutrons from reaching these detectors, we observed that the ^{232}Th and ^{238}U fission counting rates are in the ratio of their photofission cross sections for 7 MeV gamma rays. We conclude that this is caused by $\text{Pb}(n,\gamma)$ gamma rays, and in the 1 to 100 eV region this is predominantly $^{207}\text{Pb}(n,\gamma)$ capture which produces a single gamma ray of 7.368 MeV to the ground state.

The photofission counting rate in the 1 to 100 eV region is equal to (36 ± 9) % of the Th fission counting rate. Correcting for this background, we obtain, below 100 eV, a $1/v$ neutron-induced fission cross section of $56 \sqrt{0.0253/E}$ μb with an error of approximately $\pm 20\%$. This is in good agreement with the older thermal fission cross section measurements carried out at Dubna¹ and Mol² but not in agreement with the recent measurements from Grenoble.³

1. Korneev, Skobkin and Flerov, Sov. Ph. JETP 10, 29 (1960)
2. M. Neve de Mevergnies and P. del Marmol, Proc. of Neut. Sections and Tech. Conf., Wash. D.C., March 1968, NBS Spec. Publ. 299, Vol. I. pg. 611.
3. Wagemans, D'Hondt, Deruytter, Emsallem and Ashgar, Nucl. Phys. A-259, 423 (1976).

7. A Fission Chamber for Cross Section Measurements with $\leq 1 \mu\text{g}$ Samples
(P. A. Bicknell, R. C. Block, Y. Nakagome and G. Krycuk, RPI)

A small ionization chamber has been developed for fission cross section measurements with the RPI 75-ton lead slowing-down neutron spectrometer. The extremely high neutron flux obtained with this spectrometer enables measurements to be made with $\leq 1 \mu\text{g}$ of highly alpha-active fissile samples. The chamber consists of a 0.64-cm-dia. inner hemisphere of stainless steel and a 1.10-cm-dia. outer hemisphere of aluminum, and is operated at 200 Volts and at 1 atm pressure of methane. A charge-sensitive preamplifier was designed for this chamber to operate inside the linac room and drive a 50-ohm cable. Since the chamber and preamplifier must operate in the intense gamma flash produced when the electron beam strikes the photo-neutron target inside the spectrometer, a test for electronic gain shift was carried out under operating conditions with a chamber coated with $\approx 1 \mu\text{g}$ of ^{252}Cf . The gain of the system recovered to within 1% of normal gain in less than 1 μs . Thus measurements can be made up to 100 keV neutron energies.

8. Neutron Total Cross Section Measurements of the 2 keV Minimum in ^{45}Sc and the 24 keV Minimum in ^{56}Fe
(R. C. Block, U. N. Singh (RPI), K. Kobayashi (KUR), R. E. Chrien (BNL) and H. I. Liou (BNL))

Accurate measurements of the neutron total cross section near the resonance-potential interference minima are required to optimize the design of filtered reactor beams.

Neutron time-of-flight transmission measurements were carried out at the Gaertner Linac Laboratory with kg quantities of ^{45}Sc and ^{56}Fe samples which were obtained from the filters for the Brookhaven National Laboratory HFBR reactor. The ^{45}Sc (99.9% pure) measurements were carried out both with and without a thick ^{45}Sc filter in the neutron beam, and transmission samples of $N^{-1} = 0.922, 1.844, 11.7, 50.8$ and 152.5 barns/atom were used. For the major minimum near 2.0 keV, we obtain a minimum cross section of 0.71 ± 0.02 barn, in sharp contrast to a previously reported value of ~ 0.05 barn. The ^{56}Fe measurements were carried out with an Fe filter in the beam and a ^{56}Fe (99.8%) transmission sample of $N^{-1} = 0.174$ barns/atom. The cross section at the 24.4 keV minimum is 0.057 ± 0.003 barn. The results of this experiment provide vital information for the design of high-flux filtered beams using these extremely expensive filter materials. Pertinent to Request No. 74037-9.

9. Temperature-Dependent Self-Indication Measurements in ^{238}U *
(K. Kobayashi (KUR), D. R. Harris, S. H. Kim and R. C. Block)

Self-indication measurements have been completed for the shielding sample at 77°K , 293°K and 873°K and with the self-indication sample at 293°K . All data have been reduced to capture yields and the analysis is concentrating upon determining from these data the resonance parameters of the five lowest energy s-wave resonances at $6.67, 20.9, 36.8, 66.15$ and 80.9 eV. The experimental yield data for the three lowest energy resonances are shown in Figures A-3 to A-5, where the thickness and temperature of the shielding sample is indicated upon each figure. The effects of Doppler broadening and resonance interference are quite apparent in the widths of the 'blacked' out central regions and the asymmetry of the peaks on either side of the central region. In Fig. A-6 the experimental yield for the 20.9 -eV resonance is compared to the prediction of the ENDF/B-IV resonance parameters using a multilevel formalism. It is apparent that the ENDF/B-IV data generally predicts too large a capture yield for all shielding sample thicknesses and that the resonance parameters must be changed.

Preliminary analysis with the 77°K and 293°K data indicates that the radiation width of the three lowest energy resonances should be reduced below the ENDF/B-IV values.

Pertinent to Request No. 69286-9.

* Supported by the Electric Power Research Institute

Figure Captions

- Figure A-1 Neutron capture cross-section vs. time of flight. The straight line is ENDF/B-IV data, while the histogram is RPI data.
- Figure A-2 A comparison of neutron time of flight data between channels 3000 and 4000 for earlier ^{105}Pd measurements (upper figure) and present fission product Pd measurements (lower figure).
- Figure A-3 The self-shielded capture yield of ^{238}U .
- Figure A-4 The self-shielded capture yield of ^{236}U .
- Figure A-5 The self-shielded capture yield of ^{238}U .
- Figure A-6 A comparison of the measured self-shielded capture yield of ^{238}U with the prediction of a multilevel formalism using ENDF/B-IV resonance parameters.

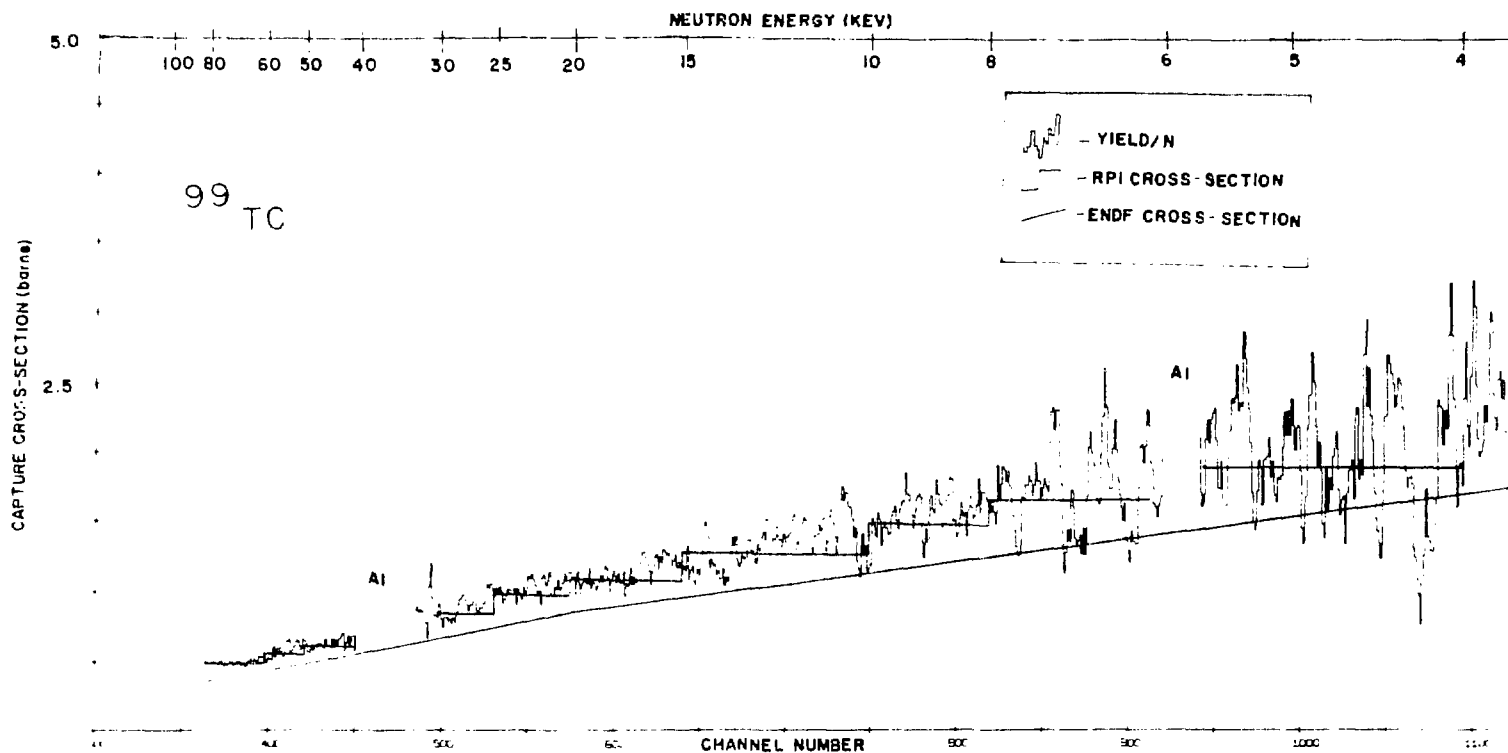


Figure A-1. Neutron capture cross-section vs. time of flight. The straight line is ENDF/B-IV data, while the histogram is RPI data.

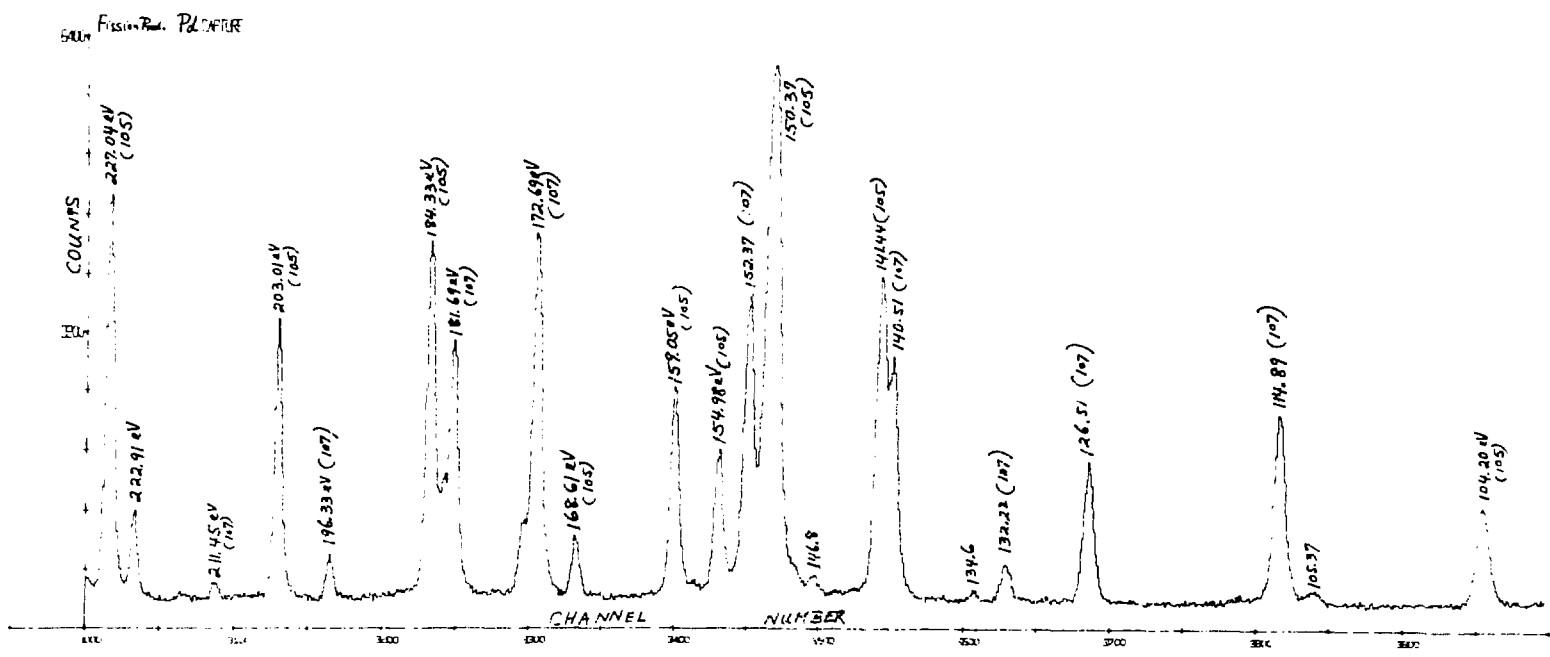
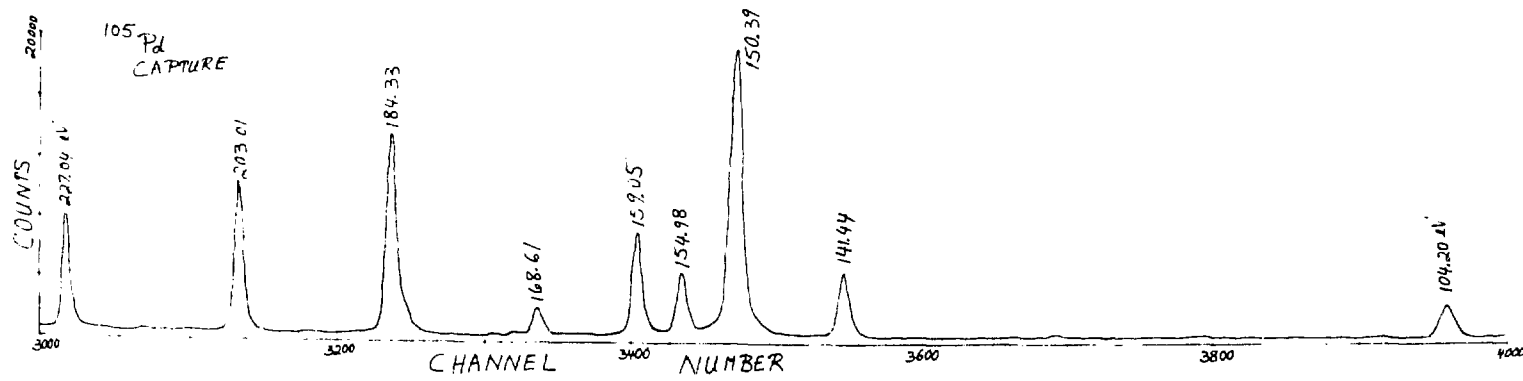


Figure A-2. A comparison of neutron time of flight data between channels 3000 and 4000 for earlier ^{105}Pd measurements (upper figure) and present fission product Pd measurements (lower figure).

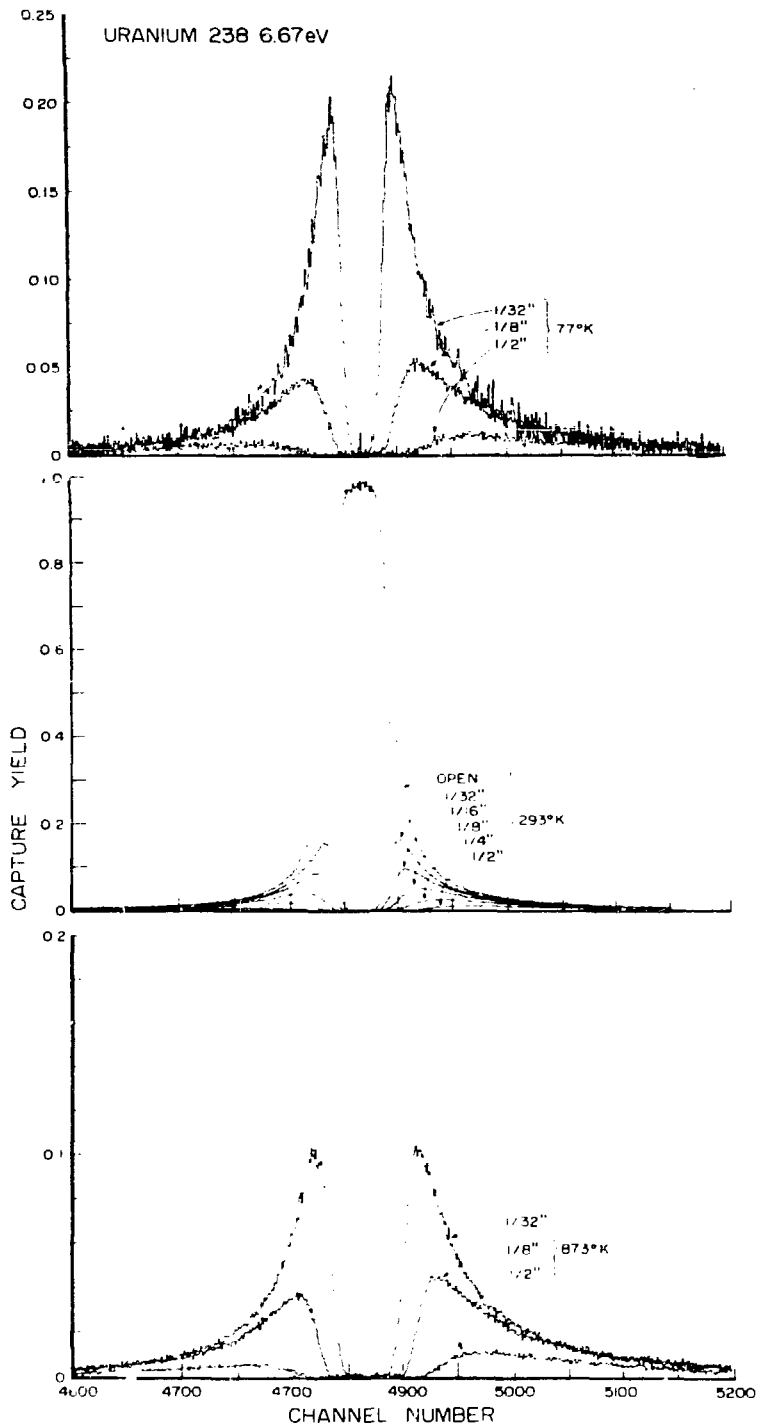


Figure A-3. The self-shielded capture yield of ^{238}U .

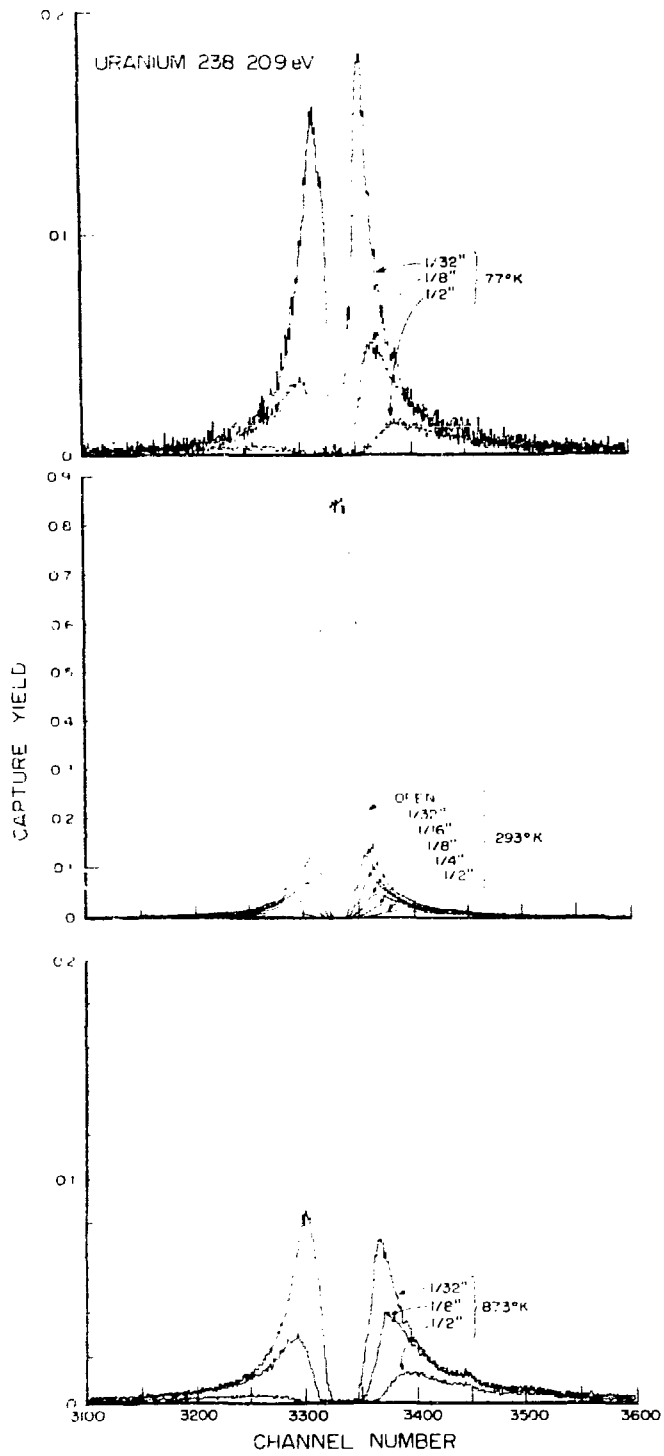


Figure A-4. The self-shielded capture yield of ^{238}U .

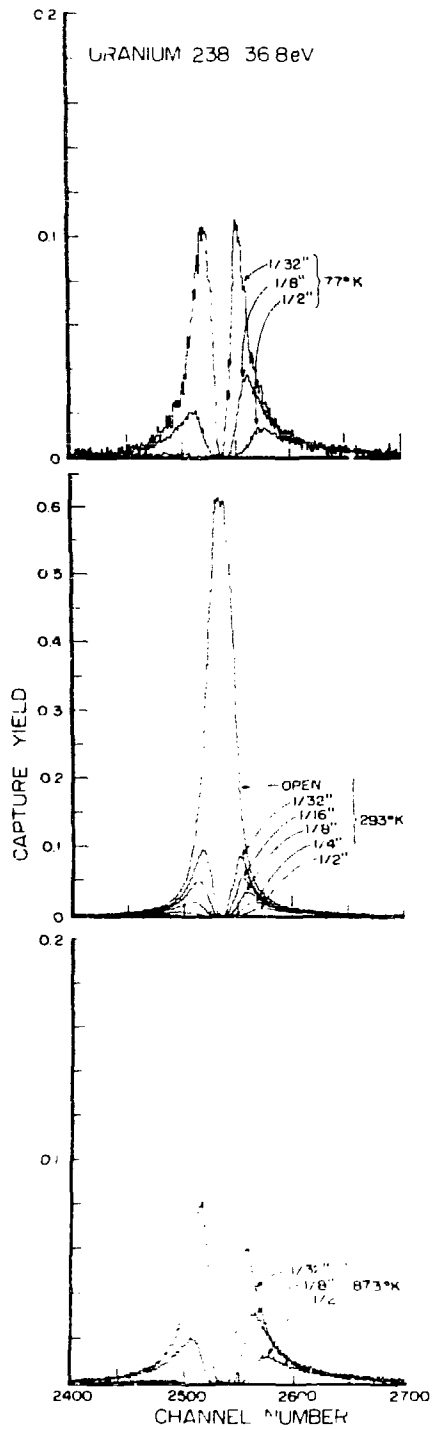


Figure A-5. The self-shielded capture yield of ^{238}U .

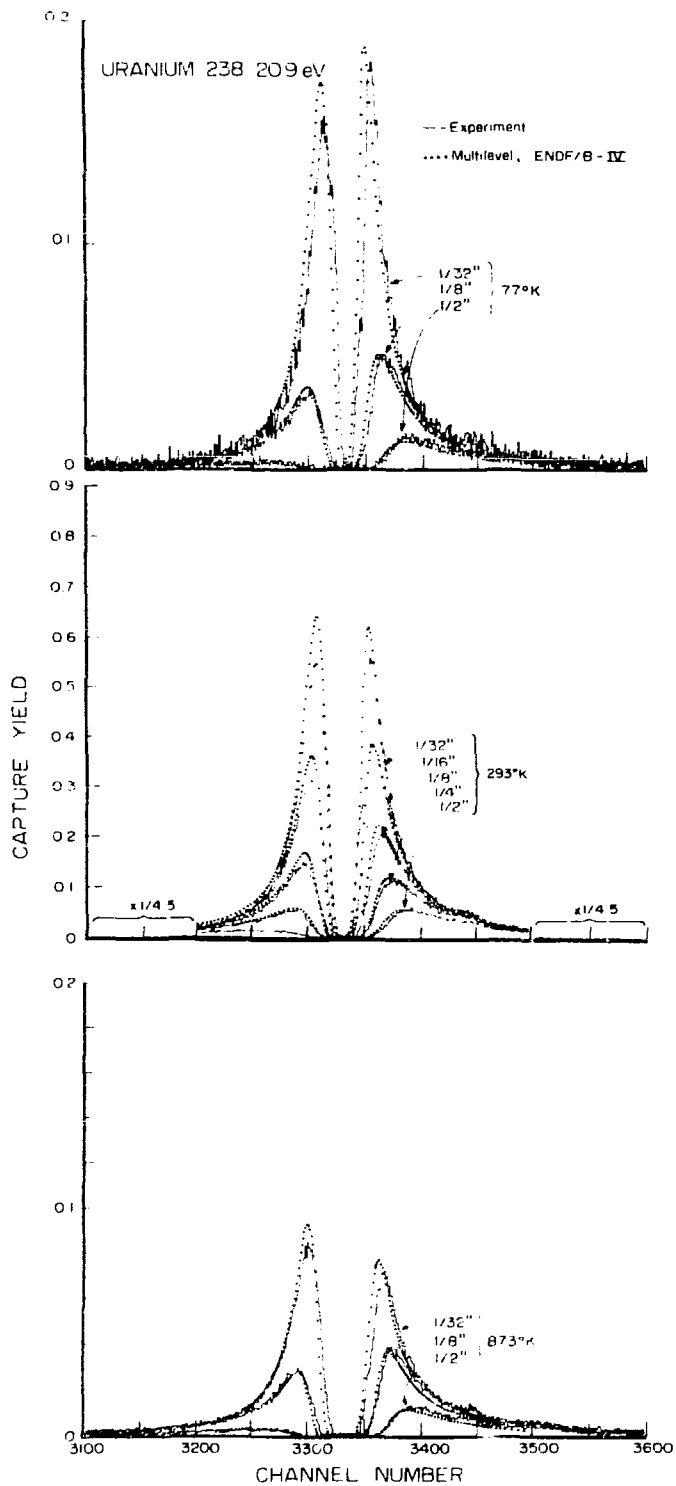


Figure A-6. A comparison of the measured self-shielded capture yield of ^{238}U with the prediction of a multi-level formalism using ENDF/B-IV resonance parameters.

B. INTEGRAL CROSS SECTION CALCULATIONS AND THEORY

1. Sensitivity Analysis for Shielding Data Evaluation by Interactive Graphics Computing (A. Parvez and M. Becker)

Sensitivity studies are being carried out to determine the impacts of cross section uncertainties on the results of neutron transport experiments for several materials.

A very simple and direct approach has been adopted at RPI where a parametric variation of the input data is carried out to determine the consequences of data uncertainties. The problem of data handling and manipulation has been overcome through the development of a sophisticated interactive graphic analysis system. The system operates on a PDP-15 computer associated with a View Tube. To increase the interactive capabilities of the system, a Hardware Dialogue Unit (HDU) has been interfaced to the PDP-15⁽¹⁾. Hardware and software for the system modifications were designed and implemented at RPI.

The processed data (normally SUPERTOG⁽²⁾ output) is transferred directly from a large remote computer to the local computer. The interactive graphic program automatically creates displayable files from this data and allows the user to display, manipulate, and modify any cross section on the screen at the selection of push buttons from the HDU. Along with the original data the errors or uncertainties associated with the data also are displayed.

In addition to displaying and modifying the individual cross sections, the program also provides the capability to interactively modify the secondary distribution on a selective basis or through a variety of pre-defined gross adjustment schemes.

The usefulness of the system is increased through the development of approximate but viable calculational models (continuous slowing down theory⁽³⁾ in this case) to allow a rapid survey by calculating the results following a data change, and graphically comparing them with the integral measurements. Initial conclusions reached on the basis of the approximate model are then tested by carrying out a precise calculation at the remote computer.

By using this strategy, we have successfully interpreted the discrepancies between the calculated and measured spectra in uranium,^(4,5) where both the total inelastic cross section and the secondary distribution have been modified (compared to ENDF/P-IV) to bring the calculation in line with experiment.

Efforts are continuing to analyse and interpret the integral measurements in iron and sodium. For iron the ENDF/B-IV data appears to yield generally satisfactory results, but work is continuing in connection with the uncertainty in multigroup constants where the cross sections show substantial structure, and the impact of this uncertainty on the details of the final spectrum. Investigations recently have been initiated relative to sodium.

-
1. M. Danchak, W. R. Moyer and M. Becker, "The Rensselaer Interactive Graphic Analysis System," Trans. Am. Nucl. Soc. 18, 159 (1974).
 2. R. Q. Wright, J. L. Lucius, N. M. Greene and C. W. Craven, Jr., "SUPERTOOG, A Program to Generate Fine Group Constants and P_n Scattering Matrices from ENDF/B," ORNL-TM-2679, Oak Ridge National Laboratory (1969).
 3. F. E. Dunn and M. Becker, "Improvements to Neutron Slowing Down Theory for Fast Reactor," Nuc. Sci. Eng. 47, 66 (1972).
 4. A. Parvez and M. Becker, "Direct-Data Adjustment for U^{238} by Interactive Graphic Computing," Trans. Am. Nucl. Soc., 22, 717, (1975).
 5. A. Parvez and M. Becker, "Sensitivity of Uranium Spectra to Inelastic Matrix Perturbation," Trans. Am. Nucl. Soc. 23, 505, (1976).
 2. Assessment and Evaluation of Sodium Cross Sections on the Basis of Integral Flux Measurements
(A. Parvez and M. Becker)

At RPI and elsewhere neutron flux measurements have been carried out in individual materials to provide a benchmark in assessing neutron data.^(1,2) For sodium, the neutron spectral flux has been measured by Mallen⁽³⁾, and the preliminary calculations with earlier ENDF/B files have been carried out by Malaviya et al.⁽⁴⁾

In this summary, we present the results of an analysis based on ENDF/B-IV where direct data adjustment has been made to improve the theory-experiment agreement.

For this work the multigroup cross-sections have been generated by using the computer code SUPERTOOG⁽⁵⁾. The weighting spectra employed in these calculations is based on B_n approximation⁽⁶⁾. A discrete ordinate, one-dimensional solution to the Boltzmann equation is obtained through the DTF-IV code.⁽⁷⁾ Figure B-1 shows the results of these calculations against the measured spectra.

Above 2 Mev, there is a gross disagreement between the calculated and measured results. The nature of disagreement varies with the

direction and location of measurement and is typically the same as the one found in iron⁽⁸⁾. Rather small sensitivities obtained from a sensitivity analysis on angular distribution of elastically scattered neutrons leave the perturbation caused by reentrant holes in the experimental assembly as the possible cause of these discrepancies. Further investigations along this direction appear warranted, particularly including the application of Monte Carlo techniques to solve the Boltzmann equation.

In the energy region below 2 MeV, the overall agreement between the measured and calculated spectra is by and large acceptable, but some discrepancies exist in predicting the details of the spectrum.

To get a better perspective, another calculation was performed by using a group structure which placed most of the groups between 100 keV and 1 MeV. The theory shows satisfactory comparison with experiment except around 700 keV and between 250 and 100 keV. The interactive data adjustment facilities⁽⁹⁾ developed at RPI were used to perform a sensitivity analysis and look for suitable data changes to resolve these discrepancies.

The investigations pointed out that a decrease in the elastic cross section in a particular group increases the flux in that group and at the same time results in a decrease in the flux in the lower group because fewer neutrons are slowing down to these groups. This secondary effect is more pronounced in sodium than in other materials like uranium or iron. It does not come as a surprise because sodium is a low atomic weight material and neutrons lose more energy in a single elastic collision with sodium than they do in iron or uranium. In certain situations, it appears more desirable to manipulate the flux in a particular group by changing the elastic down-scattering from higher groups. This fact provides an important guideline in adjusting the elastic cross section.

The adjusted cross sections are shown in Fig. 5-7 against the ENDF/B-IV values. Near the 297 keV minimum, the deviation of the adjusted cross sections from ENDF/B-IV shows qualitative agreement with differential measurements recently reported.⁽¹⁰⁾ It should be noted here that this energy region is roughly where spectrum peaks in fast reactors. This study, therefore, points out towards a need for re-measurement and/or reevaluation of the elastic cross section in the areas where the required adjustments differ substantially from the ENDF/B-IV.

In summary, the ENDF/B-IV data are shown to be in need of revision. In general, a satisfactory behavior is observed but a few well-defined changes in the elastic and hence the total cross section have been suggested.

1. N. N. Kaushal, B. K. Malaviya, M. Becker, E. T. Eurns, and E. R. Gaertner, "Measurement and Analysis of Fast Neutron Spectra in Uranium Depleted in the Uranium-235 Isotope," Nucl. Sci. Eng., 41, 330 (1972).
 2. R. E. Maerker, F. J. Muckenthaler, and R. L. Childs, "The ORNL Benchmark Experiment for Neutron Transport in Thick Sodium," Nuclear Technology, 22, 275 (1974).
 3. A. N. Mallen, "Measurement and Analysis of Fast and Intermediate Neutron Spectra in a Sodium Assembly," Ph.D. Thesis, Rensselaer Polytechnic Institute, Troy, (1973).
 4. B. K. Malaviya, E. R. Gaertner, A. N. Mallen, and N. N. Kaushal, "Measurement and Analysis of Fast Neutron Spectra in Sodium," Trans. Am. Nucl. Soc., 16, 304, (1973).
 5. R. Q. Wright, et al., "SUPERTO, A Program to Generate Fine Group Constants and Pn Scattering Matrices from ENDF/B ORNL-TM-2674, Oak Ridge National Laboratory, (1969).
 6. M. Becker, "Influence of Deep Minima on Multigroup Cross Section Generation," Nucl. Sci. Eng., 57, 75 (1975).
 7. K. D. Lathrop, "DTF-IV, A Fortran IV Program for Solving the Multigroup Transport Equations with Anisotropic Scattering," LA-3373, Los Alamos Scientific Laboratory (1965).
 8. A. Parvez and M. Becker, "An Assessment of ENDF/B-IV for Iron Based on Integral Measurements," Trans. Am. Nucl. Soc. 24, 454 (1976).
 9. A. Parvez and M. Becker, "Direct Data Adjustment for U²³⁸ by Interactive Graphics Computing," Trans. Am. Nucl. Soc., 22, 717 (1975).
 10. P. H. Brown, B. L. Quan, J. J. Weiss, R. C. Block, "Measurement of Neutron Total Cross-Section of Sodium Near Minima," Trans. Am. Nucl. Soc., 21, 565, (1975).
3. An Assessment of ENDF/B-IV for Iron Based on Integral Measurements
(A. Parvez and M. Becker)

Fast-neutron spectra in iron have been measured at RPI¹ and

elsewhere.² The experimental results are then compared with theoretical predictions to help evaluate nuclear data and calculational techniques. Previous papers¹⁻³ have discussed analysis and interpretation of these experiments with early ENDF/B files. This paper describes an assessment of ENDF/B-IV data based on comparison with the integral measurement.

The calculations are carried out by approximating the experimental assembly with a sphere and employing the one-dimensional transport theory code DTF-IV⁴ in S_{16} quadrature. Cross sections are in a 49-group structure with P_8 approximation for differential cross sections. The multigroup cross sections and the 8 terms of Legendre expansion are generated from ENDF/B-IV through SUPERTOG.⁵

The choice of a proper weighting function is important in the generation of effective multigroup constants for iron. This is particularly true because of the better resolution that has been achieved in ENDF/B-IV to describe the high keV scattering resonances and the 25-keV s-wave minima. Under these circumstances a weighting spectrum based on B_n approximation and given by

$$\phi(u) = \frac{1}{\sigma_t + \frac{2B}{N\pi}}$$

has been found to give better results^{6,7} than the generally used

$$\phi(u) = \frac{1}{\sigma_t + DB^2/N}$$

weighting spectrum. The pointwise total cross section (σ_t) used in the weighting function was obtained from ENDF/B-IV by using the RESEN⁸ code and was Doppler broadened to room temperature through the program SIGMAL.⁹

To facilitate interpretation of discrepancies observed between detailed transport calculations and measured results, use is made of the interactive graphic system developed at RPI for this purpose and applied previously to assessment of uranium data.^{10,11}

Figure B-3 shows the ENDF/B-IV predicted spectra against the measured spectra in three different (forward, transverse, and backward) directions at a distance of 10 in. from the source.

The figure shows that the high-energy (>4MeV) agreement is satisfactory only in the forward direction, while in the backward and the transverse directions the calculations underestimate the flux. The good agreement in the forward direction implies that the high-energy multigroup scattering cross sections and the average cosine of the

scattering angle ($\bar{\mu}$) are acceptable.

The only other regular systematic discrepancy is the overprediction of calculated spectra at each dip in the multigroup elastic cross section, pointing towards the fact that the effective multigroup cross sections do not adequately represent the resonance behavior.

The interactive analysis,¹⁰ in which inferences are drawn on the basis of continuous slowing-down theory, has revealed that better agreement can be obtained by using decreased fluctuation ratios in the multigroup elastic-scattering cross sections.

The same interactive analysis also indicates that the overall shape of the total inelastic cross section is satisfactory and, apparently, there is no reason to believe that any disagreements might have been caused by the uncertainties in the inelastic cross section.

In summary, an evaluation of ENDF/B-IV data for iron has been made on the basis of RPI integral measurements. The group cross sections generated from ENDF/B-IV provide a satisfactory overall agreement. Further work appears required in defining group constants for resonance cross sections, and in treatment of anisotropy at high energies.

-
1. B. K. Malaviya, N. N. Kaushal, M. Becker, E. T. Burns, A. Ginsberg, and E. R. Gaerttner, "Experimental and Analytical Studies of Fast Neutron Transport in Iron," Nucl. Sci. Eng., 47, 329 (1972).
 2. Isiro Kimura et al., "Assessment of Neutron Group Constants for Iron and Stainless Steel Through Measurements and Analysis of Energy and Space Distribution of Neutrons in Test Assemblies," Proc. Conf. Neutron Cross-Section and Technology, Vol. I, p. 184, Washington (1975).
 3. B. K. Malaviya, N. Kaushal, M. Golay, and E. R. Gaerttner, "Integral Test and Evaluation of Cross-Section Data from Studies of Fast Neutron Transport in Bulk Media," Proc. Conf. Neutron Cross-Section and Technology, 3rd. Vol. 1, p.91, Knoxville, Tennessee (1971).
 4. K. D. Lathrop, "DTF-IV, A Fortran-IV Program for Solving the Multigroup Transport Equations with Anisotropic Scattering," LA-3373, Los Alamos Scientific Laboratory (1965).
 5. R. Q. Wright, J. L. Lucius, N. M. Creene, and C. W. Craven, Jr., "SUPERLOG, A Program to Generate Fine Group Constants and Pn Scattering Matrices from ENDF/B," ORNL-TM-2679, Oak Ridge National Laboratory (1969).

6. M. Becker, "Influence of Deep Minima on Multigroup Cross-Section Generation," Nucl. Sci. Eng., 57, 75 (1975).
7. R. F. MacFarlane and M. Becker, "Self-Shielding of Elastic Transfer Matrices," Trans. Am. Nucl. Soc., 22, 717 (1975).
8. Odelli Ozer, "Program RESEND," BNL-17134, Brookhaven National Laboratory (Jan. 1972).
9. D. E. Cullen, "Program Sigmal (Version 74-1)," UCID-16426, Lawrence Livermore Laboratory.
10. A. Parvez and M. Becker, "Direct Data Adjustment for ^{238}U by Interactive Graphic Computing," Trans. Am. Nucl. Soc. 22, 717 (1975).
11. A. Parvez and M. Becker, "Sensitivity of Uranium Spectra to Inelastic Matrix Perturbation," Trans. Am. Nucl. Soc., 23, 505 (1976).
4. Fuel Cycle Sensitivity Analysis System for Light Water Reactors*
(M. Becker, D. R. Harris, J. Parillo, A. Parvez and J. M. Ryskamp)

A sensitivity analysis system has been developed for assessing the economic implications of uncertainties in nuclear data and methods for light water reactors. This sensitivity information can be used to indicate directions for worthwhile improvement in data and methods.

The overall structure of the sensitivity analysis system is determined both by the complexity of the nuclear design process and by the large number of relevant nuclear data. The system relates nuclear data to costs by two sequences of operations broken at the few-group cross section level. In Path A, the basic nuclear data are processed to multigroup cross sections and collapsed to few-group cross sections. In Path B, the few-group cross sections are used in depletion of a fuel batch at batch power levels determined by a nodal calculation, and the fuel cycle cost is determined from computed nuclear inventories before and after exposure.

Cost implications of uncertainties at the few-group level are determined first by Path B surveys facilitated by use of the RPI interactive graphics system.¹ Then Path A investigations relate basic data and methods to the few-group cross sections that are found to be important from Path B. Here we report Path B direct methods and results.

* Sponsored by Electric Power Research Institute

A nonlinear perturbation theory technique for Path B was reported earlier.² For both techniques few group, exposure-dependent microscopic cross sections are provided by a reference LASER,³ CHEETAH,⁴ or EPRICELL⁵ calculation.

Direct Path B investigations are carried out by codes FASTCELL, FASTCORE, and COST. FASTCELL utilizes the few-group microscopic cross sections provided by the reference calculation to compute few-group fluxes and nuclide inventories during batch exposure. For an assumed batch power history, FASTCELL provides k_{∞} and migration area to a few-node FASTCORE. FASTCORE computes batch power sharing for given core power demand in the equilibrium fuel cycle. The new batch power history is reintroduced into FASTCELL and the process is repeated to convergence. Preexposure and discharge inventories then are used to compute fuel cycle cost and unit power cost by the code COST. COST computes the present worths of cost components⁶ for ore purchase, conversion, enrichment, fabrication, reprocessing, and credits, assuming fixed payment schedules. Present worths are referred to center-of-exposure for a single fuel batch or to a reference year for a reactor or class of reactors. These codes are fast, for example, FASTCELL costs less than \$1 for a full PWR batch exposure in contrast to about \$700 for the reference LASER run on an IBM-36C/50. Path B codes are operable on the RPI interactive graphics computing system.¹ This fact enables us to make effective surveys and obtain answers to a variety of sensitivity questions.

Some illustrative results of Path B sensitivity calculations are shown in Table B-1. Column 1 shows changes imposed on selected individual few-group cross-sections. Columns 2 and 3 show the changes in annual front end and back end present-worthed expenditures that result. The net change is given in Column 4. When the changes of Column 1 are imposed, equilibrium cycle enrichment is changed so as to maintain cycle length. The material and separative work charges associated with this enrichment change make up the front end costs.

Designers sometimes adjust certain parameters, such as the neutron yield in fission $\bar{\nu}$, so as to force their input data to predict mock-up critical experiments. Columns 5-7 provide results analogous to those of Columns 2-4 for the situations where the data changes of Column 1 are replaced by small ($< 1\%$) compensating changes in $\bar{\nu}$. Compensation is based on preserving fresh fuel multiplication factor, since critical experiments generally are essentially free of fission products and plutonium.

Two observations may be made regarding the specific cases in Table B-1. First, it is possible for net changes to be small differences of large numbers associated with front-end and back end costs and credits. Changing circumstances (e.g. to a throwaway cycle) could

Table B-1

Sensitivity of 1980 PWR Fuel Cycle Expenditure to Changes in Nuclear Data

Column 1 Data <u>Change</u>	<u>Uncompensated</u>			<u>Compensated by \bar{v} Changes</u>		
	Column 2 Front End <u>Cost Change</u>	Column 3 Back End <u>Cost Change</u>	Column 4 Net Cost <u>Change</u>	Column 5 Front End <u>Cost Change</u>	Column 6 Back End <u>Cost Change</u>	Column 7 Net Cost <u>Change</u>
+ 5% in Group 2 (1.855-5530 eV) U^{238} Capture	\$867,000.	-\$102,900.	\$164,000. (65%)	-\$1,089,700.	-\$36,300.	-\$1,126,800. (-4.4%)
+ 10% in Group 2 Zr Capture	\$104,700.	-\$30,300.	\$68,400.	\$300.	-\$1,200.	-\$900.
+ 10% in Group 1 (> 5530 eV) U^{235} Fission	\$23,100.	\$ 2,400.	\$20,700.	\$1,000.	\$5,400.	\$6,400.
+ 1% in Group 3 (< 1.855 eV) U^{235} Fission	-\$191,000.	\$89,100.	-\$102,000.	\$284,700.	-\$71,100.	\$213,600.

affect assessment of importance of a particular change. Second, it is possible for implicit error compensation to lead to cost implications larger in magnitude than the original and possibly even opposite in sign. Compensation is most suspect when applied to data that affect the depletion and conversion processes significantly, but can be effective when applied to data whose impacts are relatively constant, as with zirconium.

-
1. M. Danchak, W. R. Moyer, M. Becker, "The Rensselaer Interactive Graphics Analysis System," Trans. Am. Nucl. Soc. 18, (1974).
 2. D. R. Harris and M. Becker, "Nonlinear Perturbation Technique for the Nuclear Fuel Cycle," Trans. Am. Nucl. Soc., 23, 534 (1976).
 3. C. G. Poncelet, "LASER, a Depletion Program for Lattice Calculations Based on MUFT and THERMOS," WCAP-6073 (1966).
 4. "CHEETAH-P," Nuclear Associates Corporation (1974).
 5. G. Ozer, private communication.
 6. K. E. Assurussen, P. Broglie, and B. W. Southworth, "Manual on Fuel Cycle Cost Calculations, the GACOST Code," GA-10593 (1971).
 5. Analysis of Sensitivity of PWR Fuel Cycle Costs to Uncertainties in Nuclear Data*
(M. Becker, D. R. Harris, A. Parvez and J. M. Ryskamp)

A sensitivity analysis system has been developed for assessing the economic implications of uncertainties in nuclear data and methods for light water power reactors.¹⁻³ We report here the results of a comprehensive analysis of sensitivity of PWR fuel cycle costs to nuclear data at the few group level. This sensitivity information is used to indicate directions for worthwhile improvement in data and methods. Benefits from improvements in data and methods are related to reduction of margins that are provided to ensure meeting reactor and fuel objectives.

Sensitivities are calculated using the code system FASTCELL-FASTCORE-COSTR linked for interactive application.¹⁻³ The cell code FASTCELL depletes a fuel batch, FASTCORE determines overall core properties in the equilibrium cycle, and COSTR computes reactor costs. A cross section or other parameter is changed from a base case, and a corresponding change in fresh fuel enrichment is determined as required

*Sponsored by Electric Power Research Institute

to maintain core reactivity at end of a cycle of fixed length at demand power. Exposure dependent microscopic few group cross sections were supplied to FASTCELL from a LASER⁴ computation for a pressurized water reactor. Power sharing among batches loaded into the core was obtained for FASTCORE from an analysis of PWR power distributions.

Sensitivities of fuel cycle cost through the year 2000 were determined with respect to some ninety nuclear parameters both for a fuel cycle with reprocessing and for a throwaway fuel cycle. Tables B-2 and B-3 show computed sensitivities of fuel cycle cost (with reprocessing) for 1% changes in few group capture and fission cross sections. These costs are for 1980 in 1980 dollars for a PWR batch of 30,000 KgU costing \$27.M. Sensitivity coefficients $\sigma / \sigma_{fcyc} \delta C_{fcyc} / \delta \sigma$ are listed in parenthesis. Computed sensitivities range widely, the larger values indicating economic justification for improvement in data and methods. Particularly important data include thermal capture and fission cross sections and fission energy yield for PU239 and U235, and fast fission and resonance capture cross sections for U238.

-
1. M. Becker, D. R. Harris, J. Parillo, A. Parvez and J. M. Ryskamp, "Fuel Cycle Sensitivity Analysis System for Light Water Reactors", Trans. Am. Nuc. Soc. 24, 216 (1976).
 2. D. R. Harris, "Sensitivity of Nuclear Fuel Cycle Costs to Uncertainties in Nuclear Data and Methods", Ph.D. Thesis, Rensselaer Polytechnic Institute, October 1976.
 3. J. M. Ryskamp, "FASTCELL, a Code for Fast Computation of Reactor Cell Characteristics Over a Fuel Cycle", M. S. Thesis, Rensselaer Polytechnic Institute, December 1977.
 4. C. G. Poncelet, "LASER, a Depletion Program for Lattice Calculations Based on MUFT and THERMOC", WCAP-6073 (1966).

Table B-2

Table B-2 Changes in Fuel Cycle Cost Per Batch for 1% Increases in Neutron Capture Cross Sections

Capturing Material	Fast Neutron Group (25500 eV)	Resonance Neutron Group (1.8 eV-5530 eV)	Thermal Neutron Group (<1.8 eV)
U 235	11,842 (.007)	342,141 (.180)	662,762 (.230)
U 236	110 (.001)	11,011 (.009)	31,428 (.001)
		(.001)	

U-238	\$11,299 (.42)	\$35,108 (.130)	\$11,833 (.048)
Pu 239	\$ 814 (.003)	\$25,873 (.099)	\$198,046 (.733)
Pu 240	\$ - 31 (- .000)	\$ -652 (- .002)	\$ 1,950 (.007)
Pu 241	\$ 362 (.001)	\$ 4,031 (.015)	\$28,061 (.104)
Pu 242	\$ 34 (.000)	\$ 3,098 (.012)	\$ 155 (.001)
Xe 135	\$ 0 (.000)	\$ 0 (.000)	\$ 7,378 (.027)
Sm 149	\$ 0 (.000)	\$ 0 (.000)	\$ 6 (.000)
Fission Products	\$ 0 (.000)	\$16,915 (.063)	\$ 31,664 (.117)
B 10	\$ 24 (.000)	\$ 466 (.002)	\$ 3,963 (.015)
Hydrogen	\$ 121 (.000)	\$ 2,739 (.010)	\$ 29,051 (.108)
Oxygen	\$14,924 (.055)	\$ 0 (.000)	\$ 36 (.000)
Zirconium	\$ 6,623 (.025)	\$ 6,460 (.024)	3,479 (.013)

Table B-3

Changes in Fuel Cycle Cost per Batch for 1%
Increases in Fission Cross Sections

Fissioning Nuclide	Fast Neutron Group(>5530 eV)	Resonance Neutron Group(1.8 eV- 5530 eV)	Thermal Neutron Group (<1.8 eV)
U 235	- \$ 4,716 (.017)	- \$24,181 (- .085)	- \$100,910 (- .373)
U 236	- \$ 4,784 (- .019)	0 (0.)	0 (0.)
U 238	- \$91,999 (- .340)	0 (0.)	0 (0.)

(cont'd)

Pu 239	- \$ 4,785 (- .018)	- \$ 18,108 (- .104)	- \$236,277 (- .874)
Pu 240	- \$ 1,008 (- .004)	- \$ 25 (.000)	0 (0.)
Pu 241	- \$ 1,126 (- .004)	- \$10,583 (- .039)	- \$ 41,665 (- .154)
Pu 242	- \$ 140 (- .001)	0 (0.)	0 (0.)

C. THERMAL HYDRAULICS STUDIES

1. Two-Phase Flow Phenomena in Nuclear Reactors

(R. T. Lahey)

An extensive research program is underway to: (1) develop accurate and reliable two-phase flow instrumentation, (2) develop an in-depth understanding of phase separation and distribution phenomena in nuclear reactor geometrics, and, (3) investigate transient parallel channel effects during hypothetical nuclear reactor accidents.

The data, analysis and instrumentation developed should make a significant contribution to the understanding of nuclear reactor performance and safety.

Figure Captions

- Fig. B-1 Comparison of measured spectra in sodium with DTF-IV calculations using ENDF/B-IV.
- Fig. B-2 Sodium elastic cross section adjustments on the basis of integral measurements.
- Fig. B-3 Comparison between the measured and calculated angular flux at a radius of 10 in. from the source and in different directions.

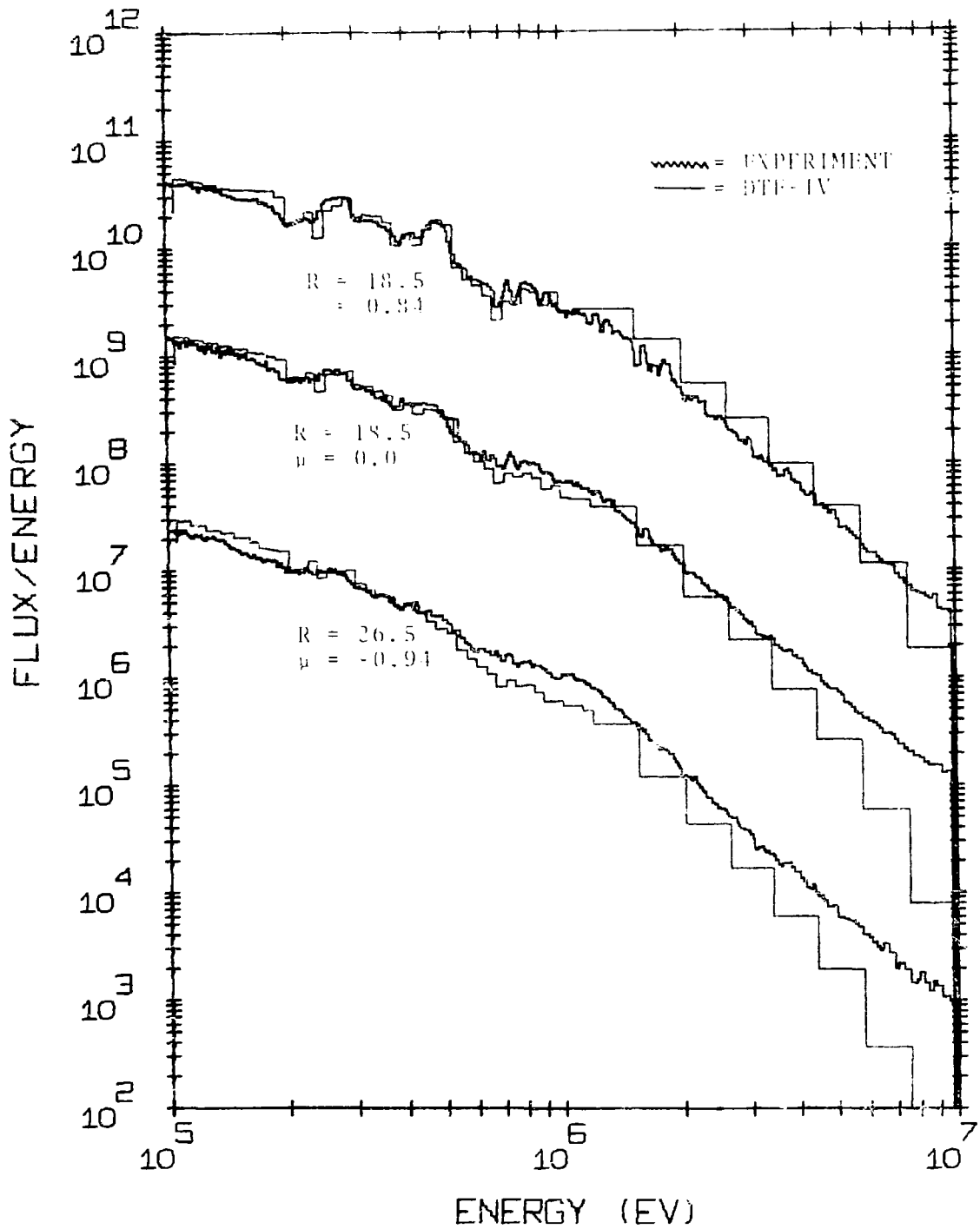


Figure B-1. Comparison of measured spectra in sodium with DTF-IV calculations using ENDF/B-IV.

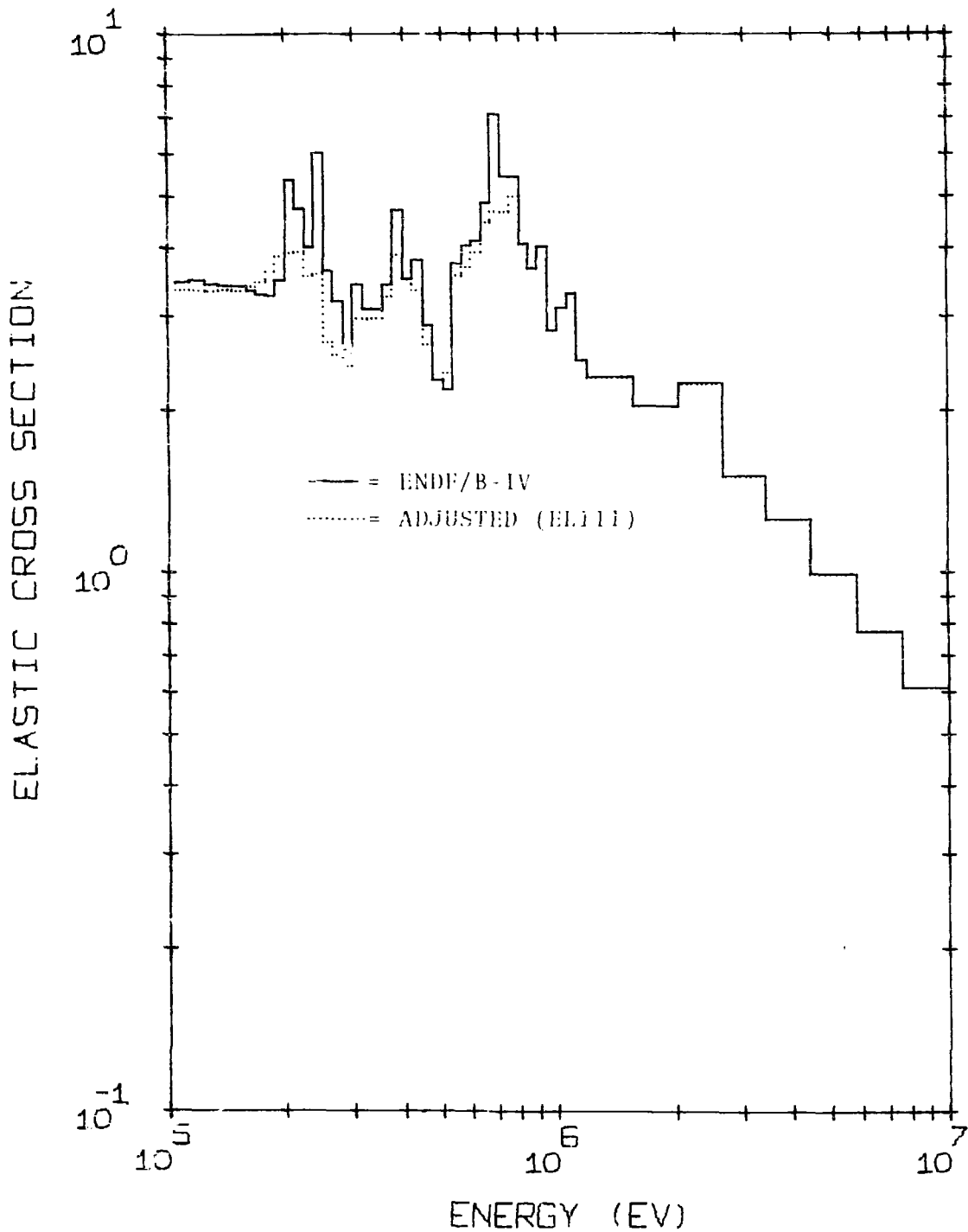


Figure B-2. Sodium elastic cross section adjustments on the basis of integral measurements.

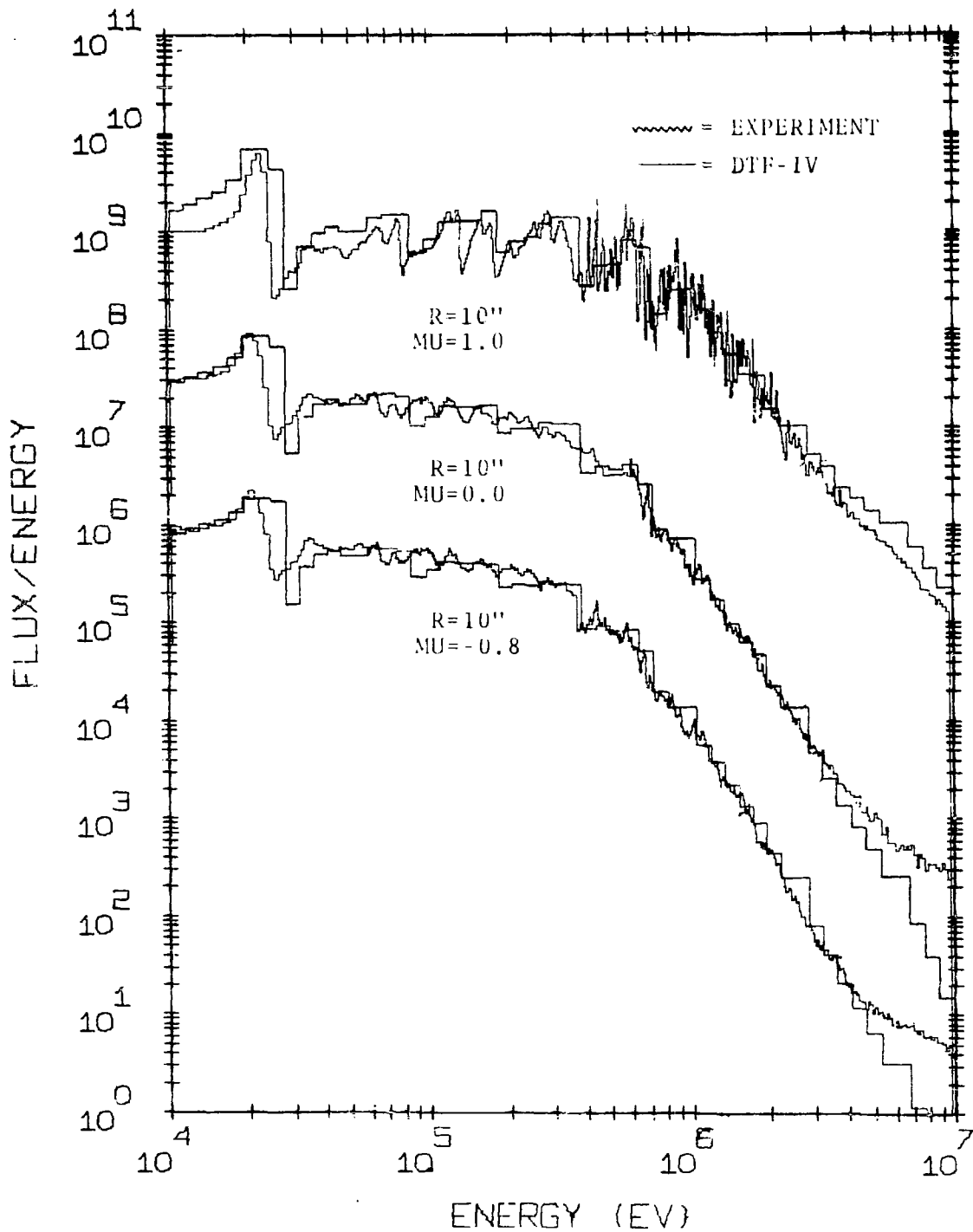


Figure B-3. Comparison between the measured and calculated angular flux at a radius of 10 in. from the source and in different directions.

TRIANGLE UNIVERSITIES NUCLEAR LABORATORY

A. INTRODUCTION

This report to the ERDA Nuclear Data Committee is a summary of research at TUNL in areas of particular interest to the Nuclear Data Committee at the present time. It has generally been excerpted from the TUNL annual progress report dated 31 December 1976, but where additional data are now available appropriate sections have been revised to reflect the new work. Those interested in other aspects of research being carried out at TUNL are referred to the annual report whose table of contents is attached as appendix 1.

B. NEUTRON AND FISSION PHYSICS

1. Fast Neutron Differential Cross Sections (F.O. Purser, C.R. Gould, P.W. Lisowski, L.W. Seagondollar, C.E. Nelson, P. Von Behren, W. Tornow, H.H. Hogue, S.G. Glendinning, Sadig El. Kadi, E.G. Bilpuch, H.W. Newson)

A. Experimental

(1) New Neutron Detector

During this report period design work was completed and construction has begun on an additional neutron detector and shield for use in the neutron time-of-flight program. The massive new shield will contain 2700 kg of a 50/50 lithium carbonate and paraffin mixture, 600 kg. of copper, and approximately 900 kg of lead. The collimator is of the Langsdorf double truncated cone design adapted for a 12.7 cm. diameter NE-213 detector.

The angular carriage for the new detector is under construction by a local contractor. The carriage is designed to allow neutron flight paths ranging from 2.0 to 6.0 meters with an angular range from 0° to 165° . The carriage will traverse an elevated iron track similar in design to that in use with our 4 meter detector. The 4 meter track is being extended to cover a full 360° to allow operation with this detector on either side of the target beam line. Delivery of the new angular carriage is anticipated in January of 1977, with final installation of the new detector scheduled for mid to late Spring.

(2) Tritium Gas Target Capability

Experimental requirements for some of the CTR related measurements planned dictate use of the $T(p,n)^3He$ reaction as the monoenergetic neutron source. A tritium gas handling system and a system of safeguards to allow use of tritium targets in a university environment has been designed. The system incorporates fast acting valves to isolate tritium spills to the beam line, LN_2 -activated charcoal trapping of pumping stations with vacuum pumps exhausted to an external exhaust stack, and additional air handling equipment in target rooms to allow emergency evacuation in the event of a room spill. Vented storage capacity for tritium contaminated parts and a vented glove box for repair of essential tritium contaminated beam line components are provided. Tritium monitors in the exhaust stack and target room will be installed with remote readouts and permanent tritium level recording in the control room.

b. CTR Related Measurements

(1) Natural Carbon

These data have been published in Nuclear Science and Engineering, vol. 61, page 521, December 1976.

(2) Beryllium 9

The elastic and inelastic data are being prepared for publication and will be submitted to Nuclear Science and Engineering.

Additional measurements on Beryllium were undertaken during this report period to measure the continuum neutron production cross sections at incident neutron energies of 7.0 and 7.5 MeV. For these measurements the bias level of the detector was set at 1/10 the pulse height of the ^{137}Cs gamma or approximately 450 keV neutron energy. Analysis of these data and application of various self consistency checks is in progress.

(3) Lithium 6

Seven elastic and inelastic ($Q = -2.18$) cross section angular distributions have been measured for incident neutron energies of 7.5, 9.0, 10.0, 11.0, 12.0, 13.0 and 14.0 MeV. Preliminary data are shown in Fig. 1. Final data analysis has now been completed and the data have been forwarded to the NNCSC. Integrated cross section results for the elastic and inelastic groups are given in Figure 2.

(4) Lithium 7

Eight elastic plus first inelastic ($Q = -0.478$) and

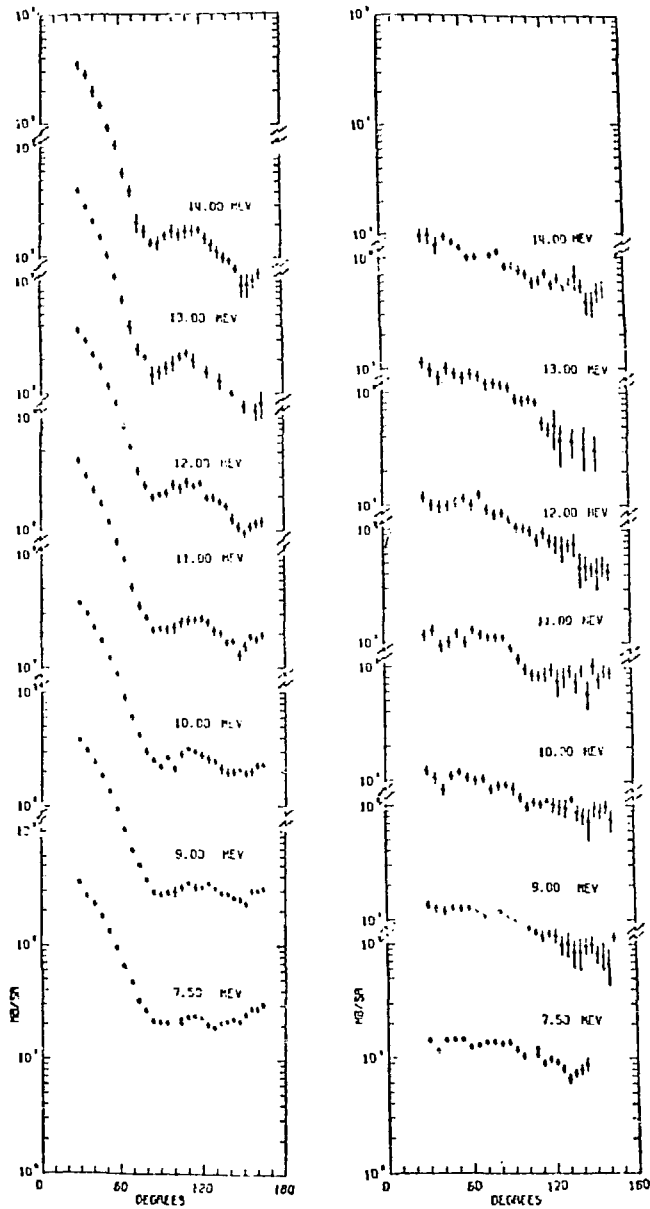


Figure 1. Elastic and inelastic ($Q = -2.184$ MeV) neutron scattering angular distributions for ${}^6\text{Li}$. The large error bars assigned to the inelastic data at back angles are due to large background subtraction uncertainties.

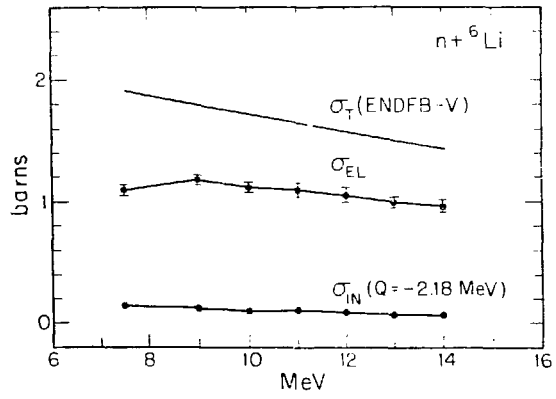


Figure 2.

second inelastic ($Q = -4.63$) cross section angular distributions have been measured. The preliminary data are shown in Figs. 3 and 4. Final data analysis has now been completed and the data have been forwarded to the NNCSC. Integrated cross section results as a function of energy are given in Fig. 5.

(5) Oxygen 16

Twelve elastic scattering angular distributions for ^{16}O have been measured for incident neutron energies from 9.25 MeV to 15.0 MeV. The scattering sample used is a $3/4$ " diameter by 1" high cylinder of BeO . Backgrounds were measured and the effect of the beryllium removed from the spectra by using a cylinder of pure beryllium as the "out" count scatterer. Preliminary data at a few energies, uncorrected for geometric and multiple scattering effects are shown in Fig. 6.

(6) Boron 10 and Boron 11

Scattering samples for these isotopes are on hand. Data accumulation will begin in February 1977.

(7) Small Angle Measurements

This program has been inactive for the present report period. However, the data acquisition electronics set up has been modified to be more compatible with the high levels of raw counting rates associated with this type of measurement. A scattering sample of ^{93}Nb has been provided by A.B. Smith of ANL and small angle measurements ($30^\circ < \theta_L < 150^\circ$) of this isotope are scheduled for Spring 1977.

c. Search for States of High Excitation (>13 MeV) in ^7Li
(P. Von Behren and C.E. Nelson)

Neutron elastic and inelastic differential cross sections to the first excited state in ^6Li are being measured to determine the existence of a possible broad (>4 MeV) state in ^7Li at 16.8 MeV excitation energy. Excitation functions at two angles, 89° and 108° in the laboratory, have been measured in 250 keV steps from $E_n = 10.5$ to 13.0 MeV. The elastic data showed no structure at the backward angle and at 89° the structure was indeterminate due to background problems. The inelastic data at both angles show a peak at approximately 11.2 MeV incident neutron energy which corresponds to an excitation energy of 16.9 MeV in the ^7Li system. The indicated resonance width is uncertain but is greater than 1.0 MeV. The excitation energy of 16.9 MeV agrees well with the value of 16.8 MeV observed in (γ, n) data.

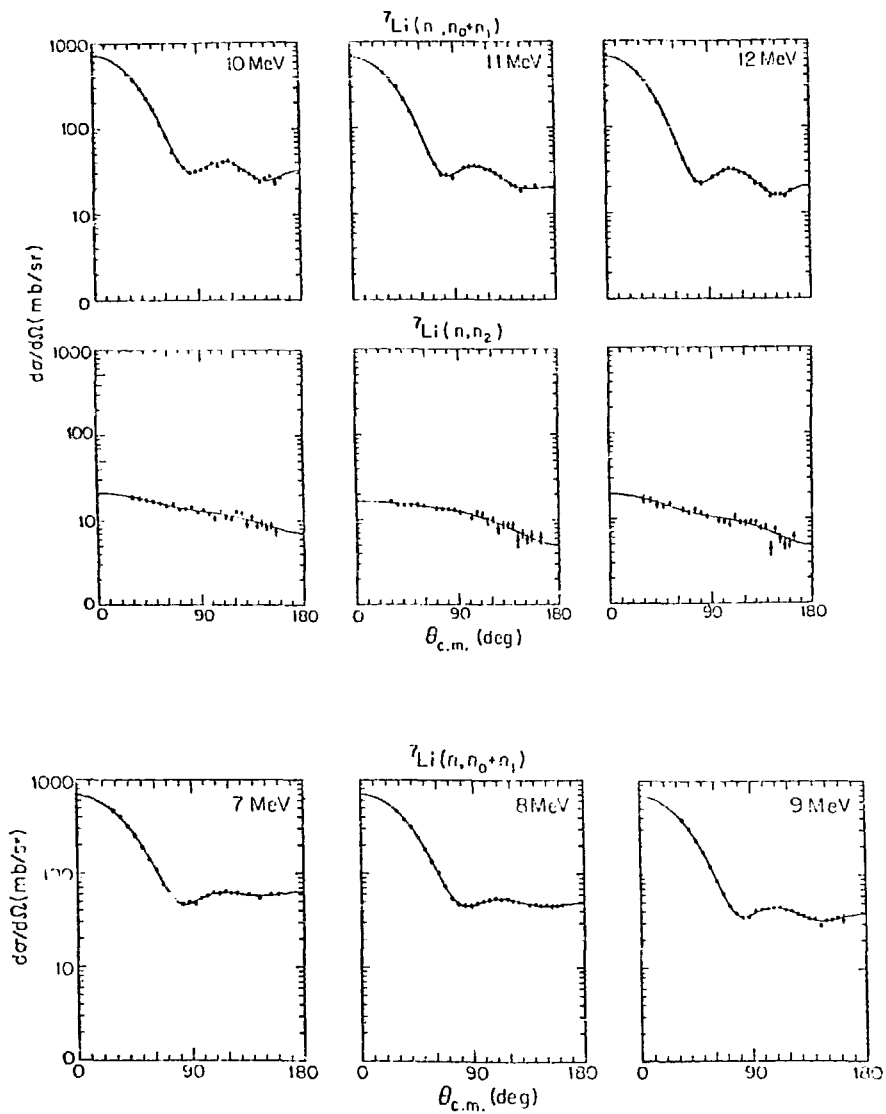


Figure 3. Neutron elastic and inelastic ($Q = -4.63$ MeV scattering angular distributions from ${}^7\text{Li}$. Contributions from the 0.478 MeV state were non-separable from elastic scattering and are included in the elastic data.

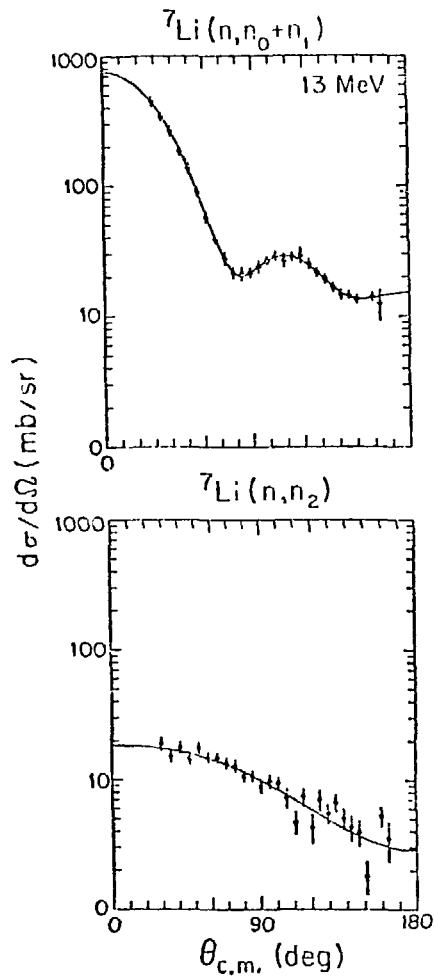


Figure 4. Neutron elastic and inelastic ($Q = -4.63$ MeV scattering angular distributions from ${}^7\text{Li}$. Contributions from the 0.478 MeV state were non-separable from elastic scattering and are included in the elastic data.

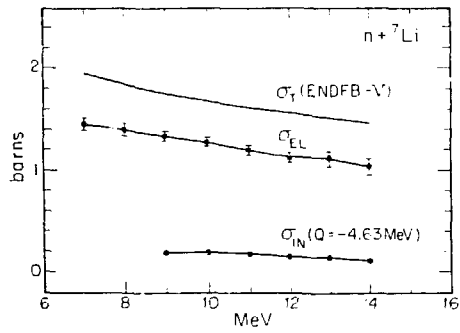


Figure 5.

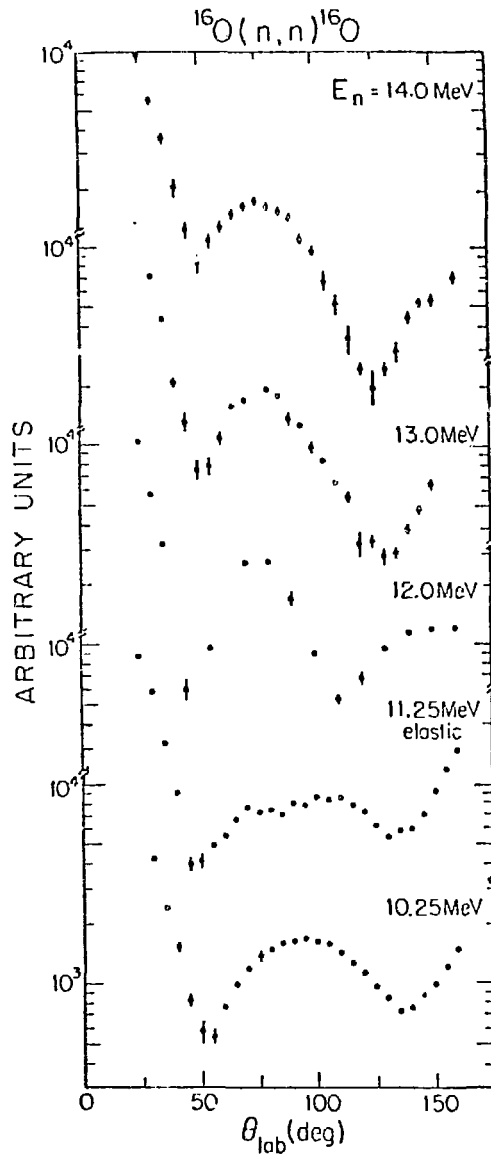


Figure 6. Partial and preliminary results for neutron elastic scattering from ^{16}O . These data have not been corrected for finite geometry or multiple scattering effects and have not been converted to absolute cross sections.

There are predictions of possible levels at these higher excitation energies in ${}^7\text{Li}$. R-matrix calculations¹⁾ suggest $1/2^+$, $3/2^+$ and $5/2^+$ states in the region of interest while resonating group theory calculations²⁾ predict a $1/2^+$ resonance in neutron elastic scattering from ${}^6\text{Li}$ at 11.7 MeV incident neutron energy. It is important to the understanding of the structure of ${}^7\text{Li}$ to determine if such levels do exist. We plan to improve the neutron energy resolution of measurements and extend our data to both higher and lower excitation energies in ${}^7\text{Li}$.

d. Computer Program Development for Neutron Data Correction

Neutron scattering studies generally employ relatively large scattering samples to obtain adequate counting rates. Thus the measured data must be corrected for such effects as finite angular resolution, flux attenuation and multiply scattered neutrons. Monte Carlo simulation techniques are usually employed to calculate the necessary corrections for these effects.

The program Mulcat previously used at TUNL to make these corrections was originally written to correct neutron scattering data for relatively heavy elements. For these cases, due to the negligible kinematic energy loss in scattering, the simplifying assumptions were made that: (1) the angular distributions of all scattered neutrons were constant with energy; and, (2) that all neutrons scattered into the detectors were counted. These assumptions are invalid for scattering from light elements, when kinematic energy losses can be substantial, and are totally inappropriate for measurements in which the continuum neutron spectra are of interest.

The following approach has been used at TUNL to attack this problem.

First: the program Mulcat¹⁾ has been extensively rewritten to incorporate all kinematic energy loss effects exactly. A library of up to 80 distinct angular distributions covering the kinematic energy range applicable has been incorporated, together with appropriate interpolation procedures. In addition, simulated data are accumulated in a time of flight presentation so that the calculation can utilize the energy windows and/or bins corresponding to those used in the experiment. Final data analysis for ${}^6\text{Li}$, ${}^7\text{Li}$ and ${}^9\text{Be}$ is now in process utilizing

1) G.M. Hale, private communication

2) W. Laskar and B. Remaud, *Le Journal de Physique*, vol. 34, p. 783(1973)

1) W.E. Kinney, *Nucl. Instr. and Meth.* 83 (1970) 15

this revised code.

Second: A new and faster version of the computer code MONTE SAMPLE^{2,3)} has been acquired which contains the above mentioned requirements. In addition, this Monte Carlo code embodies a true analog of the scattering experiment without the assumptions inherent in the Mulcat logic. It is presently being modified to incorporate a finite, extended, non-isotropic neutron source routine and due to the longer computer running times required will be used to spot check results from Mulcat.

Third: A completely new Monte Carlo code similar in logic to MULCAT, except that all collisions are forced, has been developed. It has the features that the total calculation has been divided into several smaller calculations which permits the code to be run on our in-house off-line computer. The code is also designed to handle multi-element scattering samples. Results from this code have been exhaustively checked against results from MULCAT and are in excellent agreement. Data reduction with this code will produce substantial fiscal savings over analysis with MULCAT, which requires the use of off-site computer facilities.

2. Resolved Neutron Total Cross Sections and Intermediate Structure
(J. Clement,^{*} B.-H. Choi,^{**} W.F.E. Pineo⁺, M. Divadeenam,⁺⁺ H.W. Newson)

The paper entitled "Intermediate Structure in the $^{28}\text{Si} + n$ Reaction: R-Matrix Interpretation of Experimental Data" will appear in Vol. 102, No. 2 (1977) of Annals of Physics as Part Xf(i) of our series "s- and p-wave Neutron Spectroscopy". The revised abstract follows:

"A multi-level R-matrix analysis of Si neutron cross section data measured at NBS has been performed up to about 4.5 MeV neutron energy. Only a small fraction

²⁾ P. Guenther, A.B. Smith, J. Whalen, Phys. Rev. 12 (1975) 1797

3) A.B. Smith, private communication

^{*} Rice University, Houston, Texas

^{**} Pacific Lutheran University, Tacoma Washington

⁺ Meadville, PA.

⁺⁺ Brookhaven National Laboratory, Upton, New York

of the p- and s-wave s.p. strength is observed, but both exhibit local concentrations of strength indicative of doorway structure around 1 MeV and 0.2 MeV respectively. Besides the well known 180 keV, strong, $1/2^+$ resonance, the s-wave resonance structure is of moderate strength and widely distributed. The f- and d-wave assignments are not unambiguous, but $J > 3/2$ resonances show strong signs of intermediate structure at least for d-waves. A possible correlation between neutron and gamma decay channels and the connection between the states observed in (n,n), (d,p), (n, γ) and (γ ,n) channels is discussed. A core-particle doorway interpretation for s- and p-waves is presented in the same issue of the Annals of Physics."

3. Theoretical Investigation of Neutron Cross Section Measurements
(M. Divadeenam,^{††} S. Ramavatarum,^{††} B. Castel,^{††} D. Halderson,^{††} H.W. Newson)

S- and P-wave Neutron Spectroscopy: Part Xf(ii) Intermediate Structure in the $^{28}\text{Si} + n$ Reaction: Doorway State Calculation. The abstract follows.

"A core-particle calculation developed to describe the low-lying structure of ^{29}Si is extended above neutron threshold energy to yield information on the structure of doorway states indicated by the $^{29}\text{Si} + n$ reaction. The recent experimental evidence for a $J = 3/2^-$ doorway state common to the $^{28}\text{Si} + n$ and the $^{29}\text{Si} + \gamma$ channels is supported by the calculation which also reproduces correctly the magnitudes of the neutron escape widths and the E1 radiative strengths of the $1/2^-$ and $3/2^-$ doorway states."

4. A Selectively Excited and Distorted [Liquid] Drop (SEXDD) Fission Model (H.W. Newson)

These Selection Rules have been simplified as follows:

- I. THE EXCITED NUCLEONS AT SCISSION ARE DISTRIBUTED IN THE ORBITS STATISTICALLY FAVORED FOR DEFORMABLE FRAGMENTS, IF (AT LEAST FOR SPONTANEOUS FISSION)

^{††} Brookhaven National Laboratory, Upton, New York

^{††} Universite de Laval, Quebec, Canada

II. THE FINAL BARRIER SELECTS IN THE TWO INCIPIENT FRAGMENTS THE MAXIMUM COMBINED NUMBER:

- a) OF FILLED MAJOR SHELLS WHICH ARE CONSERVED SELECTIVELY BY KINEMATIC EFFECTS AND
- b) OF PAIRS OF NUCLEONS MOST OF WHICH ARE EFFECTIVELY CONSERVED IF

III. THE LIQUID DROP MODEL (LDM) DESCRIBES THE COLLECTIVE ASPECTS OF THE FISSION PROCESS ADEQUATELY, AT LEAST AFTER THE FINAL BARRIER.

Rule III should certainly be acceptable to the conventional wisdom, and it includes, of course, the statics of the collective states. Since individual nucleons in excited orbits can not be ruled out, consideration of their statistics as in Rule I is necessary. Note that, unlike references 1 and 2, Rule I does not assume a priori that the spherical shell model is applicable at scission. Rule IIb is reasonable to the extent that pairing of all nucleons should help to penetrate the fission barrier and a complex potential implies a slow breakup of pairs relative to the fast transition between barrier and scission predicted by the LDM.

However, Rule IIa is radical in that it implies a spherical shell effect at a saddlepoint which we visualize as highly distorted and conservation even of the pairs (e.g., $s^{1/2}$, $p^{1/2}$, $d^{3/2}$) with lower pairing energies than some of the valence nucleons. Since we define Rule II for very improbably barrier penetrations we have assumed only a residual shell effect, and some of the closed subshells (e.g., $g^{9/2}$, $h^{11/2}$, etc.) should be very strongly conserved, but if Rule IIa is to be useful, it should be a valid approximation for thermal neutron, as well as, spontaneous fission.

We have therefore devised a simple test: If Rule IIa is valid at all excitation energies, the average, median, and/or maximum fission yield should never be less than $50 + 82 = 132$ in the heavy fragment since Rule IIa requires that the $82N$ and $50Z$ shells be filled in the majority of heavy fragments. Also if Rule IIb is valid, there should be sufficient events in which all nucleons are paired in one slightly excited fragment to observe fine structure since the even-even fragments which most nearly satisfy the equation $A_L/A_L = A_H/Z_H$ are energetically favored and are known to be the most prolific primary fragment in each even mass chain. One primary fragment in all odd mass chains satisfies <UCD> so well that little fine structure is expected in them.

Data³⁾ taken by the ORNL group have been reanalyzed to form a family of adiabatic curves which give the yield as a function of mass at various total excitation energies (both fragments) varying between

about ~ 2 MeV and ~ 50 MeV. These were formed from the published contour diagrams by plotting the empirical $Q(A)$ on the same scale, displacing it downward by various amounts between 3 and 50 MeV, and plotting the intersection of the displaced Q values with the contour lines. Since the excitation energy, $E_x(A) = Q(A^-) - E_k(A)$ (the total kinetic energy of both fragments) all points on any resulting yield curves are at the same E_x . The adiabat of the lowest excitation energy is very narrow with a median corresponding to the product ${}^{132}_{50}\text{Sn}82$ with no detectable heavy fragments lighter than ${}^{128}_{50}\text{Sn}$. As excitation energy increases the median and maximum values move toward larger A_H and at $E_x = 25$ MeV the curve is very similar to the total fission yield curve. At higher excitation energies inferred from the more accurate empirical Q , the effect reverses, the median value goes to smaller A_H as excitation energy increases, but the median value does not sink below $A_H \approx 132$ as predicted by Rule IIa. This treatment of thermal fission of U^{233} , U^{235} , Pu^{239} , Pu^{241} , and $\text{Cf}^{252}(\text{sf})$ all showed the same effect.

The above treatment averaged out all signs of fine structure in the yields. In order to eliminate the point scatter in the empirical Q value, Seeger's mass formula was used in a more detailed treatment. This analysis gave adiabats in E_x steps of 6 MeV and showed the expected (Fig. 7c) fine structured peaks at $A_H = 134, 138$ and 144 but none for odd fragments (Fig. 7a). This effect has already been reported using the⁴⁾ fairly good approximation $Q(A) \approx Q(134)$. As excitation energy increases (Fig. 7a) this fine structure nearly dies out before $E_x = \langle E_x \rangle \approx 20$ MeV. At higher excitation energy the smooth behavior persists (Fig. 7b) up to $E_x = 30$ MeV (which includes nearly all of the fission yield) while the median A_H decreases. However, strong fine structure also reappears over a wider range (Fig. 7d) and the adiabat at greatest observable excitation energies ($E_x > 45$ MeV) is very similar to that at $E_x < 5$ MeV. Since fine structure should be most easily observable when all nucleons in one fragment are paired, (a condition which is probable only at low excitation energies), this behavior shows that not only are the major shells at 28, 50, and 82, but also pairs are effectively conserved as predicted by Rule II when one of the fragments is slightly excited. The statistics of Rules I and III modified by Rule II predict little fine structure when $(E_x)_L \approx (E_x)_H \approx E_x/2$ but at sufficiently high

1) H.W. Newson, Phys. Rev. 122 (1961) 1224

2) P. Fong, Phys. Rev. 102 (1956) 439

3) F. Pleasonton, Phys. Rev. 174 (1968) 1500 and previous ORNL data

4) J. Punick, et al., Physics and Chemistry of Fission (1973) Vol. II, p. 19

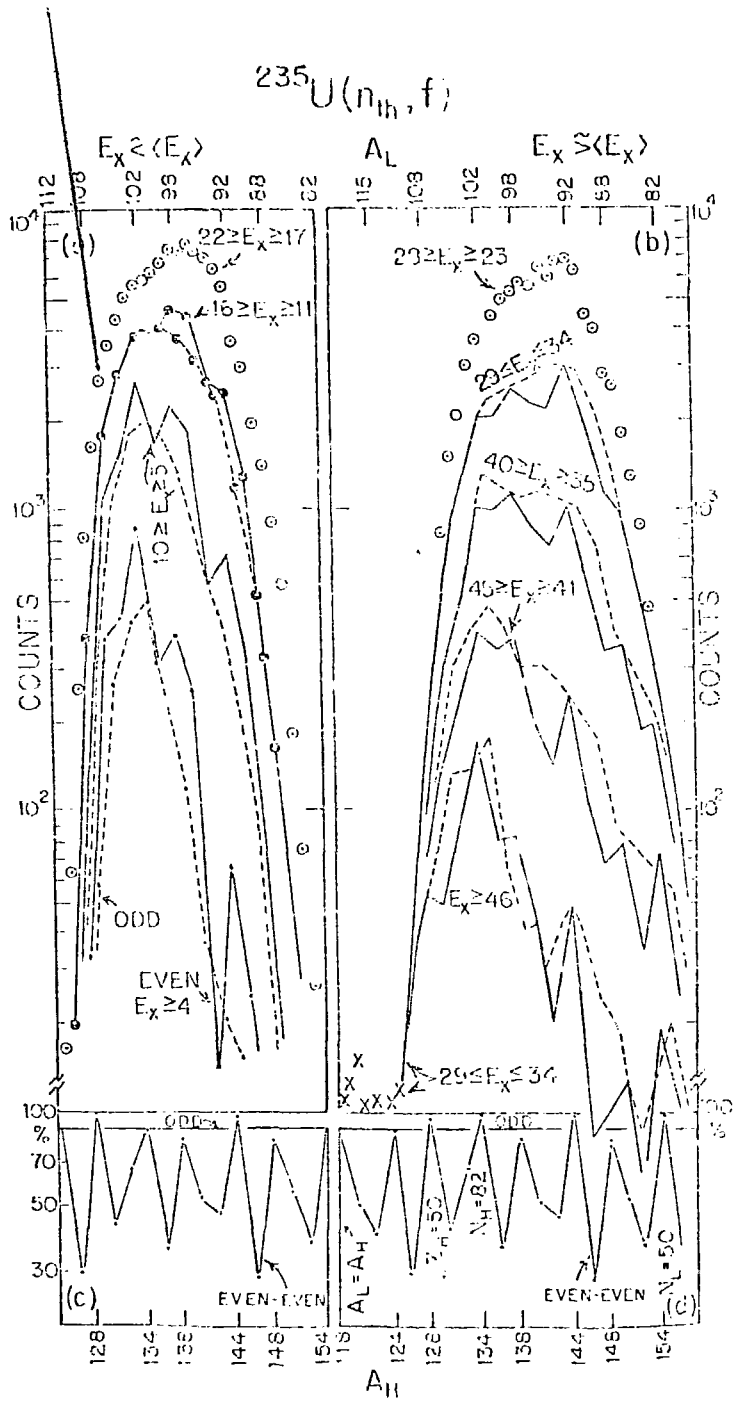


Figure 7.

$E_x (\equiv (E_x)_L + (E_x)_H)$ one fragment should be much more excited than the other which should then be capable of exhibiting obvious fine structure. These statistical arguments are similar to those used in Ref. 1.

Caption Fig. 7: Adiabats (a family of curves of yield as functions of A) for various excitation energies $\langle E_x \rangle \approx E_x \equiv (E_x)_L + (E_x)_H$. Since marked fine structure is expected only for even fragments the curves for lower E_x were interpreted by connecting every other point with a solid line and the remaining points with dashed lines which generate rather smooth curves. We interpret the latter as the odd mass chains. The points connected by solid lines show sharp peaks where fine structure peaks are expected in Fig. 7c which is a plot of the empirical charge distribution expression: $1 / \text{Exp}2(Z_p - Z_{\text{even}})^2$ (where $Z_p = [(236/92)/A^{\text{even}}] - 1 = A^{\text{even}}/2.65$ and Z_{even} is the nearest even Z to Z_p for a given A. Since relatively few primary fission fragments have no unpaired nucleons, the curve in (c) approximates only the most favorable case where E_x approaches zero and even then it should be compared to the difference between the solid and the dashed curves. (b) and (d) show the same interpretation of the data when $\langle E_x \rangle < E_x$. Note that in the upper curves of both (a) and (b) there is also evidence for fine structure, but not much.

5. Charged Particle Fission (F.O. Purser, D.H. Epperson, H.W. Schmitt, E.G. Bilpuch, H.W. Newson)

In order to unfold contributions of sequential fission channels in the fragment mass and kinetic energy distributions of ^{236}Np for excitation energies ranging from subthreshold to 27 MeV it is necessary to have an accurate estimate of the total fission probability as well as the fission probabilities for first, second and third chance fission as functions of excitation energy. The total fission probability was obtained by dividing the experimental fission cross sections of Boyce¹⁾ et al., by the proton total reaction cross sections as calculated by an optical model. Due to the lack of optical model parameters for heavy nuclei at low proton energies it was not surprising that the resulting probabilities in the low energy region did not compare favorably with the direct measurements in the first chance region by Gavron²⁾ et al. In order to get reasonable agreement in this excitation energy region it was necessary to assume that uranium has an effective charge of 94.92 in the spherical optical model formulation utilized to calculate the reaction cross sections.

1) J.R. Boyce et al., Phys. Rev. C10, 231 (1974)

2) Gavron et al., Phys. Rev. C13, 2374 (1976)

The neutron partial decay width Γ_n calculated by Weisskopf³⁾ uses neutron reaction cross sections. In Boyce's work, these cross sections were calculated with the optical model and were assumed identical for all isotopes of Np. It was observed that the experimental cross sections of the uranium isotopes, demonstrated a strong $E_f - B_n$ dependence. A table of neutron cross sections independent on $E_f - B_n$ was generated for the Np isotopes as follows: A search of the ENDL⁴⁾ library of neutron cross sections for the actinides yielded cross sections for nuclei close to Np on the chart of nuclides with similar neutron binding energies and fission barrier heights. From these nuclei a set of neutron cross sections displaying the same $E_f - B_n$ dependence as does the uranium set was obtained and incorporated into the statistical decay model calculation of the first, second and third chance fission probabilities and produced improved agreement with the data.

A comparison of the statistical decay model calculation of the fission probabilities with the Gavron data revealed that at low excitation energies (3-9 MeV) the model was not giving a good approximation. The agreement is good from 9 MeV to 12 MeV where the Gavron data stops. The poor agreement is probably due to the inadequacy of the Gilbert and Cameron⁵⁾ form of the level density at the saddle point of the fissioning nucleus. The calculation was revised to use the experimental fission probabilities of Gavron et al., in the excitation energy range from 3-9 MeV and to match these smoothly with the calculated values from 9-30 MeV.

The reduction of the kinetic energies of correlated fission fragment mass pairs is currently near completion. From these spectra, fragment mass and kinetic energy distributions for a single fissioning nucleus (²³⁶Np) as a function of excitation energy will be extracted using the previously described fission probability calculations to unfold contributions of other than 1st chance fission.

3) V.F. Weisskopf, Phys. Rev. 52, 295 (1937)

4) The LLL Evaluated Nuclear Data Library, UCRL-50400 Vol. 15 Part C (1976)

5) A. Gilbert and A.G.W. Cameron, Can. J. Phys. 43, 1440 (1965)

C. APPLIED TECHNIQUES

1. Neutron Spectra from Deuteron and Proton Bombardment of Thick Lithium Targets (C.E. Nelson,* F.O. Purser, P. Von Behren, H.W. Newson)

The suitability of thick lithium targets as sources of fast neutrons for cancer therapy has been investigated. Incident particle-energy combinations available to the small, "medical" cyclotron source used to determine if such beams when used to bombard lithium targets, lead to an improvement, vis a vis tissue penetration, in the resultant fast neutron spectra. Previous measurements were either non-existent (${}^7\text{Li} + p$) or yielded conflicting results (${}^7\text{Li} + d$).¹⁻³⁾

The relative energy sensitivity of the TUNL neutron time-of-flight facility main neutron detector was measured from 0.7 MeV to 24 MeV neutron energy using the well-known $T(p,n){}^3\text{He}$ and $T(d,n){}^4\text{He}$ neutrons at several charged particle energies,⁴⁾ and by scattering neutrons from hydrogen. The absolute efficiency was obtained by normalizing this relative efficiency curve at $E_n = 4.0$ MeV to a Monte Carlo calculation of the efficiency of the detector done at Oak Ridge National Laboratory.⁵⁾

Fig. 8 shows the neutron energy spectra obtained at zero degrees for 8, 12 and 15 MeV deuterons and 15 MeV protons incident on the thick lithium target. These spectra were integrated for $E_n > 1.0$ MeV to obtain the neutron yield versus laboratory angle data shown in Fig. 9.

Calculations of the average neutron energy for each zero degree spectra showed $E_n = .44E_d$ for the deuteron reactions while $E_n = 4.7$ MeV

* Supported by National Cancer Institute Research Fellowship No. 1 F22 CA00332-01

- 1) A. Pinkerton, et al., Radiology 96 (1970) 131
- 2) F.M. Edwards, et al., Medical Physics 1 (1974) 317
- 3) A.N. Goland et al., Proceedings of the Charged Particle Accelerator Conference, Washington, D.C. 1975, IEEE N521
- 4) D.K. McDaniels et al., Physical Review C (1973) 882
- 5) G. Morgan, private communication

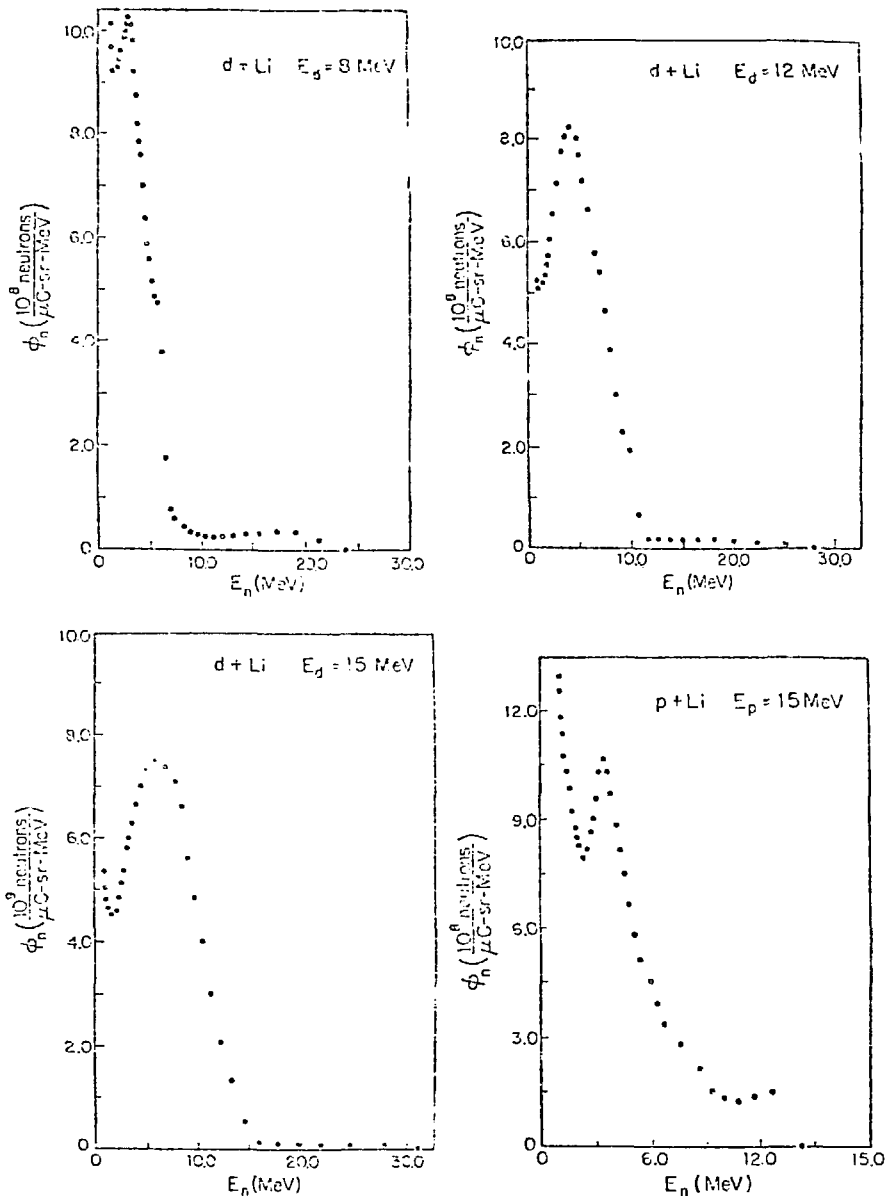


Figure 8. Neutron energy spectra at zero degrees for thick Li target.

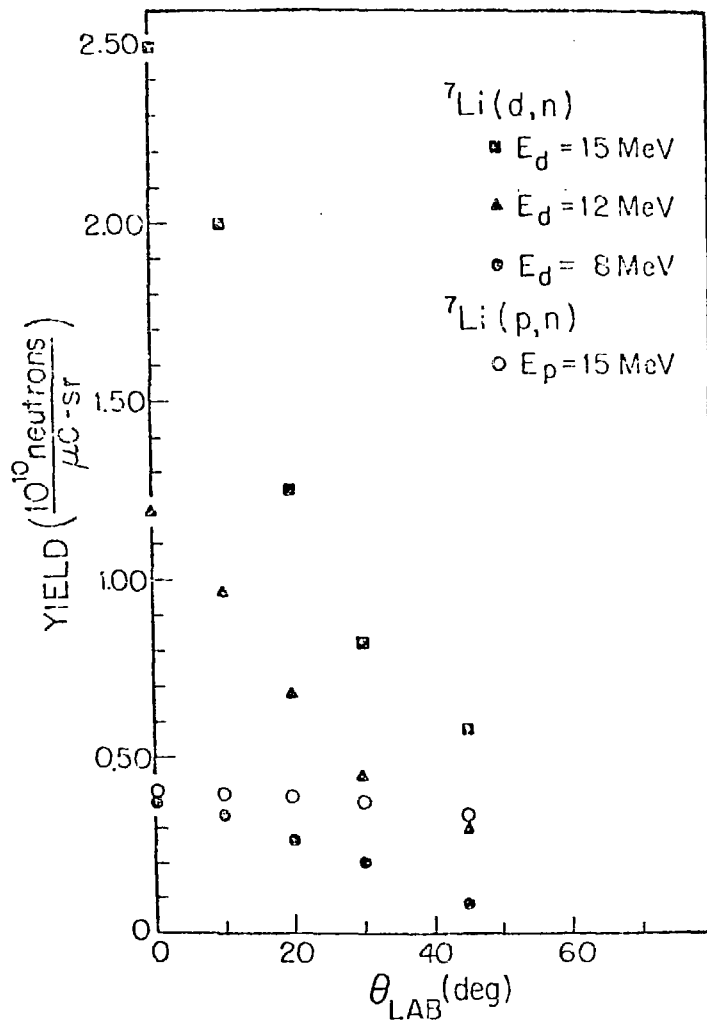


Figure 9. Integrated neutron yield vs. laboratory angle.

for the proton reaction. The results of Weaver⁶⁾ indicated that $E_n = .42 E_d$ for deuterons on beryllium. Thus the lithium target offers essentially no improvement over beryllium with respect to average neutron energy. Since an average neutron energy of at least 8 MeV is required for adequate tissue penetration, the lithium target small cyclotron combination appears to be unsuitable for fast neutron cancer therapy.

This work has been submitted for publication to Physics in Medicine and Biology and has been presented at the following conferences: Interaction Conference on the Interactions of Neutrons with Nuclei, University of Lowell, Lowell, Mass., July 5-9, 1976; Fourth International Conference of Medical Physics, Ottawa, Canada, July 31-Aug. 4, 1976.

2. Development of a Facility for Production of 150 (C.E. Nelson, H.W. Newson, Robert H. Jones*)

A facility for the production and transport of short lived radioactive tracers is being developed in response to Duke University Medical Center interest in pulmonary-cardiovascular research. A specific interest is the use of the Oxygen-15 labelled carbon dioxide for the non-invasive detection of left to right cardiac shunts.

Recent work¹⁾ at the University of Wisconsin has shown the feasibility of producing 150 via the $^{14}\text{N}(d,n)^{150}$ reaction with $E_d=8$ MeV in sufficient quantities such that it can be transported over substantial distances (up to 1/3 mile) if careful attention is paid to gas transport.

Relative yield measurements of the 511 keV coincident gamma rays have been made using the TUNL tandem Van de Graaff. The results indicate that 150 yields similar to those obtained at the University of Wisconsin can be obtained with the 3.5 MeV deuteron beam of the 4 MeV Van de Graaff operating with beam currents of 20 to 25 μA .

In order to improve the operation of the 4 MeV Van de Graaff particularly at such large beam currents, the former mercury diffusion pump has been replaced with a 10" oil diffusion pump, complete with a freon cooled baffle.

* Assistant Professor, Department of Surgery, Duke University Medical Center

6) K.A. Weaver, et al., Nuclear Science and Engineering 52 (1973) 35

1) R.J. Nickles, Bull. Am. Phys. Soc. 17 (1972) 137

Preliminary work, including the testing of various foil-pressure-cell geometries is scheduled for Spring 1977. Also planned are studies done near the production site using animals and counting equipment supplied by Duke University Medical Center.

Further support for this work, including funds to extend gas capillaries to the Duke University Medical Center from the 4 MeV Van de Graaff laboratory are being sought by DUMC via a National Institute of Health Trauma Center Grant.

3. Continuation of PIXE Development for Multielemental Analysis with 3 MeV Protons (R.D. Willis, W. Gutknecht, * R. Shaw, * R.L. Walter)

Our effort to study the competitiveness of proton-induced X-ray emission (PIXE) as a multielemental analytical tool has continued, but at a reduced pace. The cooperation with the departments of medicine and chemistry and the USEPA and NIH still exists, but because of impending personnel changes, the project will be in a "hold" status for a period this Spring. Details of some of our findings, results, and innovations were presented at the First International Conference on PIXE held at Lund, Sweden. Four reports titled: (1) Proton-Induced X-Ray Emission Analysis of Thick and Thin Targets, (2) Wavelength Dispersion Analysis of PIXE Spectra, (3) The Application of Proton-Induced X-Ray Emission to Bioenvironmental Analyses, and (4) Computer Analysis of Proton-Induced X-Ray Emission Spectra. Expanded versions of these talks will appear in Nuclear Instruments and Methods. The main direction for 1977 will probably be in animal toxicity studies and the flow of elements from mothers to fetuses, the accumulation of metals in human lung tissue, element balance for intravenously fed (hyperalimentation) patients, and microprobe developments.

D. DEVELOPMENT

1. High Resolution Development on the Tandem Accelerator (M.E. Bleck, D.A. Outlaw, W.K. Wells, F.O. Purser, H.W. Newson, E.G. Bilpuch, G.E. Mitchell, T.B. Clegg)

a. Terminal Stabilizer

Development work on the energy stabilization system for the TUNL tandem Van de Graaff accelerator described in the 1975 progress

* Department of Chemistry, Duke University

report has continued during the past year. The neutral beam target correction technique has been abandoned in favor of the system shown in Fig. 10. In this configuration the control beam, which is also the target beam, is momentum analyzed by the 90-90 magnets. The focussing properties of these magnets render the control signal derived at the image slits insensitive to position fluctuations of the beam at the object slits. In addition, the superior analyzing power of the system increases the sensitivity of the control loop. It has been found that the control slits must be offset along the beam axis in order to prevent electron crosstalk which overloads the slit preamplifiers.

An isolated $5/2^-$ resonance with $\Gamma_p = 65$ eV in the $^{54}\text{Fe}(p,p)$ reaction has been measured with this system and fitted with an asymmetric resolution function (FWHM - 375 eV). The result is shown in Fig. 11. The contribution to the overall resolution due to beam energy fluctuations is estimated at 250 eV or less.

b. 90-90 Analyzing Magnets

A computer controlled system for stepping the beam energy in a uniform manner has been developed in conjunction with the terminal stabilizer project. The remote master reference "fine" current potentiometer is driven, through a set of reduction gears, by a stepping motor commanded by the computer. The potentiometer is part of a voltage divider that provides a reference signal to the analyzing magnet power supply by scaling the voltage from a set of mercury batteries. These batteries reside in a styrofoam case to minimize temperature drifts. This system steps the master reference much more precisely than was possible by hand. However, preliminary analysis of $^{90}\text{Zr}(p,p)$ data taken over a period of several days indicates that significant drifts in the beam energy, with periods of a few minutes to several hours and with amplitudes of a kilovolt or more, may occur when the magnets are in the current regulated mode. The most attractive solution to this problem is to derive from the NMR fluxmeter a feedback correction signal for the magnet supply. In this way, the magnetic field would be regulated in addition to the current. The stability of such a system depends upon the stability of the RF oscillator which drives the NMR cavity. The existing fluxmeter and power supplies can be operated in this way, so a precision frequency synthesizer accurate to 1 part in 10^8 was obtained on loan for a system test. The beam energy at a given frequency was found to vary no more than ± 150 eV over a period of two days. Stepping the RF in 100 Hz increments provided 70 eV increments in beam energy. The frequency synthesizer is externally programmable and can be computer controlled, although this feature was not used in the test.

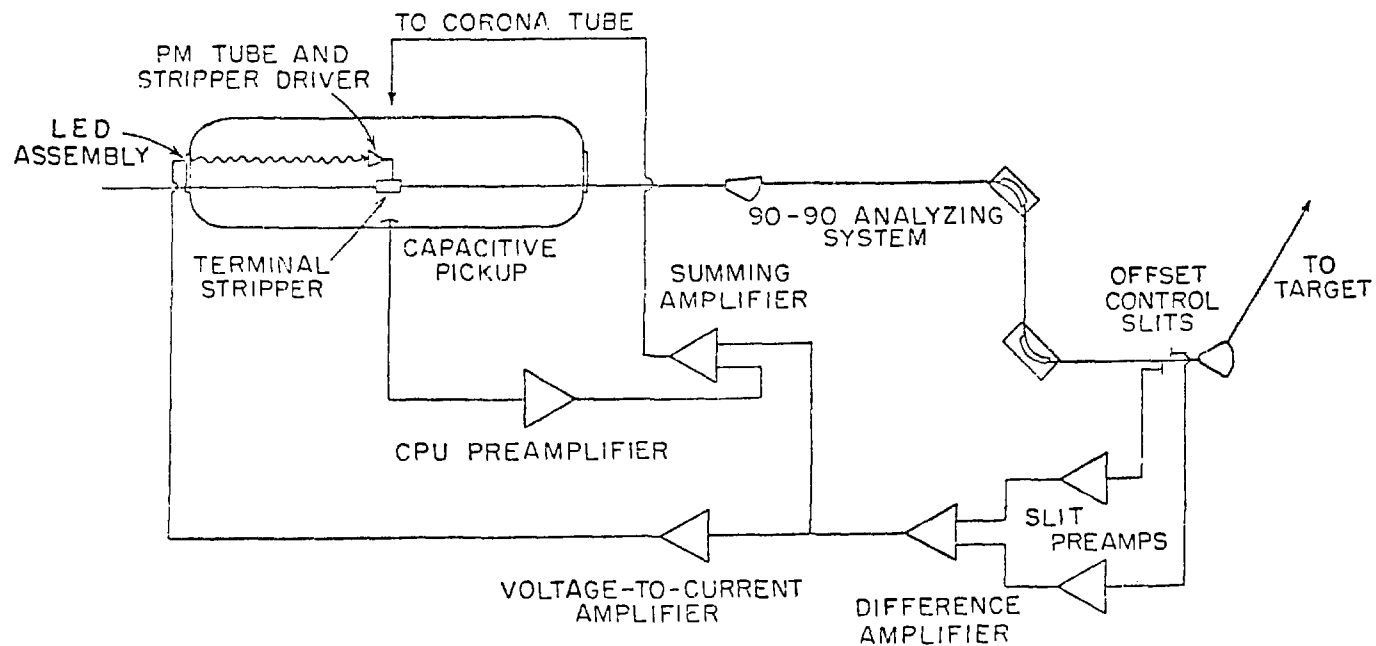


Figure 10. Triple loop control system for tandem accelerator.

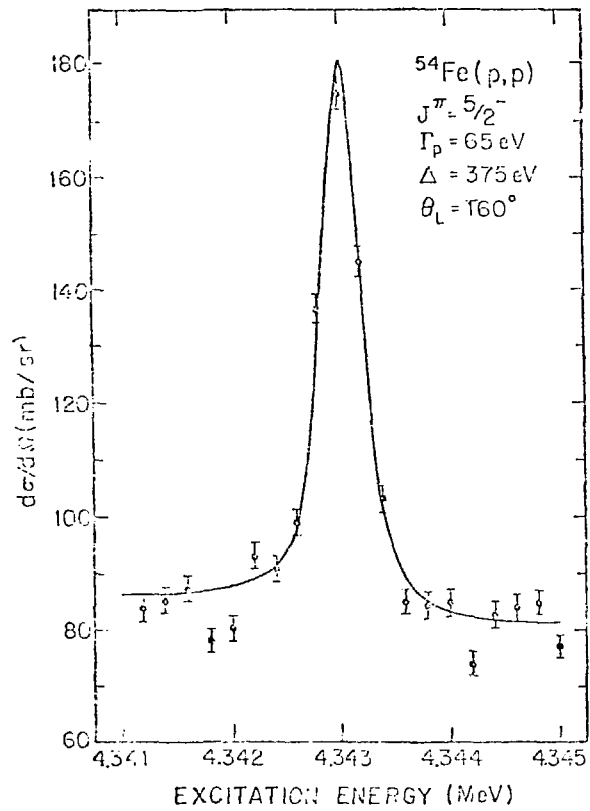


Figure 11. Resonance in the $^{54}\text{Fe}(p,p)$ reaction using the terminal stabilizer.

APPENDIX I

ANNUAL REPORT TUNL XIV

TABLE OF CONTENTS

Major portions of earlier TUNL reports (TUNL I - TUNL XIV) are contained in the reports of USNDC or its predecessor, the AEC Nuclear Cross Sections Advisory Committee.

A.	NEUTRON AND FISSION PHYSICS	1
1.	Fast Neutron Differential Cross Sections	1
a.	Experimental	1
b.	CTR Related Measurements	2
c.	Search for States of High Excitation (713 MeV) in ${}^7\text{Li}$	7
d.	Theoretical Analysis of Neutron Data	7
2.	Resolved Neutron Total Cross Sections and Intermediate Structure	8
3.	Theoretical Investigation of Neutron Cross Section Measurements	8
4.	A Selectively Excited and Distorted [Liquid] Drop (SEXDD) Fission Model	9
5.	Charged Particle Fission	12
B.	NEUTRON POLARIZATION STUDIES	13
1.	Analyzing Power Measurements for n-p Scattering from 10 to 18 MeV	13
a.	Measurements	13
b.	Corrections to the A_y Data	15
2.	Analyzing Power Measurements for n-d Scattering at 12 MeV	15
3.	Analyzing Power for ${}^{12}\text{C}(n,n){}^{12}\text{C}$ Scattering	15
4.	Neutron Polarization and Analyzing Power in the $\text{H}(\vec{\epsilon},\vec{n}){}^3\text{He}$ Reaction Using a Polarized Triton Beam	16
5.	Similarities between $A_y(\theta)$ and $PY(\theta)$ for the ${}^3\text{H}(p,n){}^3\text{He}$ Reaction	16
6.	Remeasurement of PY for the ${}^2\text{H}(d,\vec{n}){}^3\text{He}$ Reaction and Its Implication to the f-wave Admixture of the 2^- State at 22 MeV in ${}^4\text{He}$	19
7.	Neutron Polarization Produced by the Breakup of Vector Polarized Deuterons on ${}^2\text{H}$ and ${}^4\text{He}$	19
8.	Polarization Transfer in the ${}^2\text{H}(\vec{\epsilon},\vec{n}){}^4\text{He}$ Reaction	19
9.	A Calibrated Source of High Energy Polarized Neutrons Obtained from $A_{zz}(0^\circ)$ Measurements for the ${}^3\text{H}(d,n){}^4\text{He}$ Reaction	19

10.	Elastic Scattering of Polarized Neutrons from ^3He	20
11.	Elastic Scattering of Nucleons from ^4He	20
a.	Cross-Section Measurements for $^4\text{He}(n,n)^4\text{He}$	20
b.	$^4\text{He}(\vec{n},n)^4\text{He}$ Analyzing Power Measurements at 14 and 17 MeV	20
c.	$^4\text{He}(\vec{n},n)^4\text{He}$ Analyzing Power Measurements from 30 to 29 MeV with a Calibrated Source of Polarized Neutrons	21
d.	$^4\text{He}(\vec{p},p)^4\text{He}$ Analyzing Power Measurements	21
e.	Phase Shift Analysis of the $^4\text{He}(n,n)^4\text{He}$ and $^4\text{He}(p,p)^4\text{He}$ Scattering Processes	21
12.	Polarization Transfer Studies in (\vec{p},\vec{n}) Reactions	22
a.	Polarization Transfer in the $D(\vec{p},\vec{n})2p$ Reaction from 10 to 15 MeV	22
b.	Polarization Transfer Effects in (\vec{p},\vec{n}) Reactions on Light Nuclei at $\theta = 0^\circ$	22
13.	Comparison of the Polarization and Analyzing Power in (p,n) Mirror Reactions on ^{15}N and ^9Be	22
14.	Cross Sections and Polarizations in $(^3\text{He},n)$ Reactions from ^{12}C and ^{13}C from 8 to 22 MeV	24
15.	Polarization Transfer Studies of $^{12}\text{C}(\vec{d},\vec{n})^{13}\text{N}$, $^{14}\text{N}(\vec{d},\vec{n})^{15}\text{O}$, $^{16}\text{O}(\vec{d},\vec{n})^{17}\text{F}$ and $^{28}\text{Si}(\vec{d},\vec{n})^{29}\text{P}$ at $\theta = 0^\circ$	24
16.	Depolarization Effects in Stripping a Polarized Negative Ion Beam in the Terminal of a Tandem Van de Graaff	25
17.	Pulsed Polarized Beam Studies	25
18.	Sources of Polarized Fast-Neutron Beams--A Status Report	25
C.	HIGH RESOLUTION STUDIES	27
1.	High Resolution Elastic Scattering	27
a.	Review Article	27
b.	^{26}Mg	28
c.	^{30}Si	28
d.	^{34}S	28
e.	^{42}Ca	28
f.	^{54}Ne , ^{58}Ni , ^{60}Ni	28
g.	^{90}Zr	30
2.	High Resolution Proton Capture	30
3.	High Resolution Inelastic Scattering	30
a.	Method	30
b.	^{50}Cr	30
c.	^{56}Fe	31
d.	^{44}Ca	32
4.	Isospin-Forbidden $T = 3/2$ Resonances	32
D.	GAMMA RAY SPECTROSCOPY	34

1.	Mean Lifetimes of Excited States in ^{38}Ca	34
2.	Mean Lifetimes of Levels in ^{55}Co	34
3.	Measurements of Gamma-Ray Angular Distributions and Linear Polarizations for ^{48}V	34
4.	Studies of The Gamma-Ray Decay of Excited Levels in ^{117}Sb	35
5.	A Study of The Low Lying Levels of ^{77}Kr	35
6.	Spin and Parity of The 11.86 MeV Level in ^{24}Mg	35
7.	Magnetic Moment of 738 keV Level in ^{43}K	36
E. CHARGED PARTICLE REACTIONS WITH POLARIZED BEAMS		
1.	The Hamburger Effect in $^{207}\text{Pb}(\vec{d},p)^{208}\text{Pb}$ and $^{207}\text{Pb}(\vec{d},d)^{207}\text{Pb}$	39
2.	The Study of the $^{207}\text{Pb}(\vec{d},t)^{206}\text{Pb}$ Reaction	39
3.	The (\vec{d},α) Reaction on ^{28}Si , ^{37}S and ^{40}Ca	39
4.	The Mechanism of $(\vec{d},^6\text{Li})$ Reactions on Light Nuclei	40
F. RADIATIVE CAPTURE REACTIONS		
1.	General Discussion of The Program	41
2.	Giant Resonance Region of ^{15}N Studied by Polarized and Unpolarized Proton Capture Measurements	41
3.	Giant Dipole Resonance in ^{56}Fe Observed via (p,γ) and (α,γ) Reactions	42
4.	Giant Dipole Resonances in $^{55,57,59}\text{Co}$ Using Polarized Proton Capture	42
5.	Study of The Giant Dipole Resonance Region of ^{31}P	43
6.	Study of The Radiation in The Giant E1 Resonance Region of ^{89}Y with The Reaction $^{88}\text{Sr}(\vec{p},\gamma)^{89}\text{Y}$	45
7.	A Study of The $\text{D}(p,\gamma)^3\text{H}$ Reaction	49
8.	Fast Neutron Capture Progress Report	49
9.	Study of The Giant Dipole Resonance Regions of ^{60}Ni	52
10.	A Study of The $^3\text{H}(p,\gamma)^4\text{He}$ Reaction from $17 < E_p < 30$ MeV	52
11.	Measurement of E2 Strength for The Capture Radiation from ^{56}Fe via The (α,γ) Reaction	54
12.	A Search for the Isovector E2 Resonances in ^{31}P , ^{89}Y and ^{60}Ni	54
G. ATOMIC COLLISION PHYSICS		
1.	Two Electron-One Photon X-ray Transitions ($2e-1\gamma$)	58
2.	K X rays Arising from 20-80 MeV Ion Bombardment of Ti, Mn, Cu and KBr	60
3.	Radiative Electron Capture Resulting from 20-70 MeV Chlorine Ion Bombardment of C, Ti, Mn and Cu	60

H.	HEAVY ION REACTIONS	61
1.	Recoil Ranges and Range Straggling of Nuclei Resulting from $^{59}\text{Co}(^{16}\text{O},\text{X})\text{Y}$ Reactions	61
I.	APPLICATIONS	
1.	Neutron Spectra from Deuteron and Proton Bombardment of Thick Lithium Targets	65
2.	Development of a Facility for Production of ^{15}O	68
3.	Continuation of PIXE Development for Multielemental Analysis with 3 MeV Protons	68
J.	ION SOURCE DEVELOPMENT	70
1.	New Ion Sources for The Tandem Accelerator	70
2.	Intense Metastable Hydrogen Beams	70
3.	A New Polarized Ion Source for SATURNE II	70
4.	Comparison of a Duoplasmatron and a Duopigatron Ion Source	70
K.	ACCELERATOR DEVELOPMENT AND INSTRUMENTATION	71
1.	Injector Cyclotron	71
2.	High Resolution Development on The Tandem Accelerator	71
a.	Terminal Stabilizer	71
b.	90-90 Analyzing Magnets	74
3.	Polarization Monitoring and Beam Control	74
4.	Pulse Beam Time Pick-Off	74
5.	Improvements in Instrumentation in the 3 MeV Laboratory	75
L.	COMPUTER RELATED DEVELOPMENTS	77
1.	The Prime Computer	77
2.	Computer Program Development for Neutron Data Correction	77
3.	Beam Optics Computer Code	78
M.	NUCLEAR THEORY AND PHENOMENOLOGY	79
1.	Studies of Deuteron Scattering Potentials	79
2.	Wave Functions and Wave Packets	79
3.	Polarization Phenomena in Nuclear Reactions	79
4.	Isospin-Consistent DWBA Analysis of (d,t) and (d, ^3He) Reactions	79

5.	A DWbA Transfer-Reaction Code for Small Computers	79
6.	Dissipative Forces in Quantum Mechanics	79
7.	Survey of Nucleon-Nucleus Scattering Potentials	80
8.	Compound-Nucleus Effects and the Nucleon-Nucleus Spin-Spin Interaction	80
9.	Atomic Effects in Nuclear Resonances	80
10.	Projectile-Size Effects in Deformation Measurements	81
11.	Spin-Orbit Coupling in Heavy-Ion Scattering	81
12.	Compound-Nucleus Fluctuation Theory for Polarized Beams	81
13.	The Energy Splitting of the Lowest 6^- , $T = 0$ and $T = 1$ States in the (sd)-Shell	81
14.	Spectroscopic Factors for the $^{28}\text{Si}(p,d)^{27}\text{Si}$ Reaction	82
15.	1975 Mass Predictions	82
16.	Computer Codes for High Accuracy Single Particle States	82
17.	Realistic Single Particle Hamiltonian for Fission and Heavy Ion Calculations	82
18.	Realistic α -Particle Potentials	83
19.	Applications of Group Theory to Rotational Vibrational Bands on Nuclei	83
20.	Exotic Configurations of Super Heavy Nuclei, Bubbles, Torus, etc.	84
21.	Level Density Studies for α Reactions with Targets of $A \leq 40$	84
22.	Dynamics of Heavy Ion Reactions in a Realistic Time-Dependent Hartree-Fock Model	84
23.	Deep Inelastic Heavy Ion Cross Sections in a T.D.H.F. Model	85
24.	Single Nucleon Induced Fission	85
25.	Low Energy Behavior of Fusion Barriers in Heavy Ion Reactions	86
26.	The Griffin Model, Complex Particles and Direct Nuclear Reactions	86

A. DELAYED NEUTRON SPECTRA1. Equilibrium Spectrum (G.W. Eccleston and G.L. Woodruff)

Measurements of delayed neutron spectra at the University of Washington have used a cyclical irradiation-delay-counting sequence that produced a mix of precursors that were close to the equilibrium values.¹ These measurements produced spectra with a large (20%) fraction of delayed neutrons below 100 keV that were significantly softer than a set of equilibrium measurements recently reported by Evans and Krick.² Evans has suggested that the inclusion of more of the shorter half life precursors in their measurements, which may have higher mean energies, in comparison to our near-equilibrium cycle may partially explain the spectral differences.

Recent improvements to the beam monitoring equipment in addition to modifications to the electronic system have enabled measurements using pulsing cycles at the University of Washington which provide an equilibrium mix of delayed neutron precursors. A comparison of the delayed neutron group yields between the original near-equilibrium cycle, the new equilibrium cycle and the cycle used by Evans is listed in Table A-1. In the near-equilibrium cycle one percent of the short half-life precursors, group 6, compose a measured spectrum due to group 6 neutrons. Even though there is a large difference in the group 6 contribution between our previous measurements and an equilibrium measurement, such as Evans, the overall percentage difference between the spectra due to group 6 is not large, less than 1.5 percent. Therefore, the relative differences in the group 6 contributions should not have a strong effect on the overall shape of measured spectra.

The equilibrium delayed neutron spectrum between 20 and 1500 keV has been collected from a ²³⁵U sample and is shown in Figure A-1. The peak at 41 keV is decreased by several percent from previous measurements, however the data still show a significant fraction (20 percent and more) of delayed neutrons in the lower energy (< 150 keV) regions.

¹ G.W. Eccleston and G.L. Woodruff, Nucl. Sci. Engr., in press.

² A.E. Evans and M.S. Krick, Trans. Am. Nucl. Soc., 23:491 (1976).

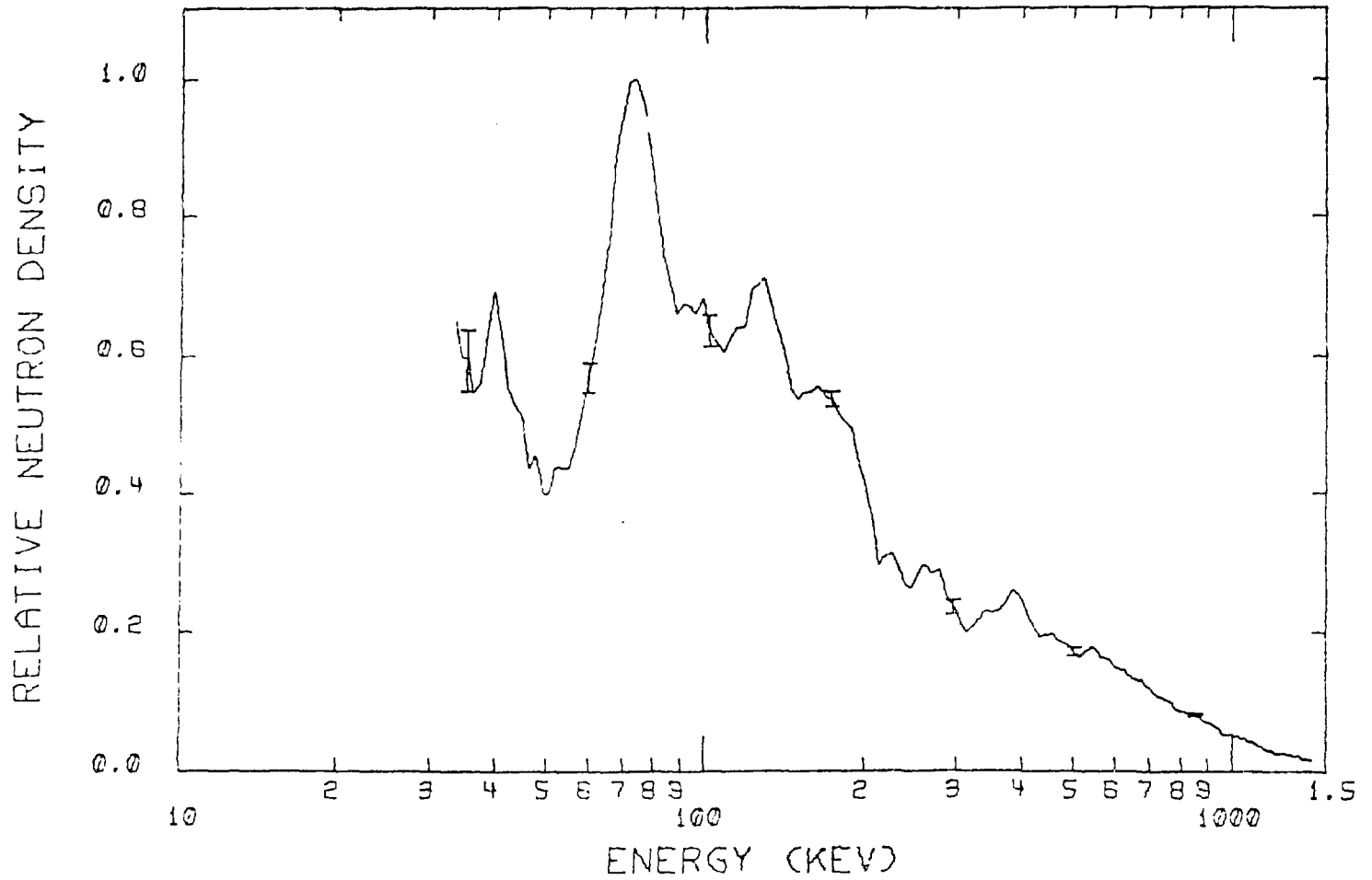


Figure A-1. Equilibrium ^{235}U delayed neutron spectrum.

Measurements of separated precursors by Rudolph, et al.³ have found delayed neutrons at energies as low as 16 keV for the longer half-life precursors with a large portion of the spectrum residing at the lower energies. The results of their measurements in conjunction with ours indicate that delayed neutron spectral measurements should be extended to lower energies than has generally been done.

Table A-1

Comparison Between Delayed Neutron Yields for an Equilibrium Cycle and the Cycles Used in Measurements

Group	Equilibrium Yields	Evans Cycle	Previous Near-Equilibrium Cycle	New Equilibrium Cycle
1	0.038	0.038	0.040	0.038
2	0.213	0.213	0.224	0.213
3	0.188	0.188	0.197	0.188
4	0.407	0.407	0.421	0.408
5	0.128	0.126	0.108	0.128
6	0.026	0.025	0.010	0.025

2. ²⁴⁰Pu Delayed Neutron Spectra

Composite equilibrium delayed neutron spectra have been measured for all nuclides of interest with the exception of ²⁴⁰Pu. The results of all existing delayed neutron spectral measurements are in reasonable agreement for energies above approximately 150 keV. However, at lower energies significant differences exist and recent precursor spectra in addition to our composite measurements indicate a significant fraction of delayed neutrons exist below 150 keV. Presently, a 60 gram sample of ²⁴⁰Pu is being clad at Oak Ridge which will be used to measure the composite equilibrium delayed neutron spectrum between 10 and 1500 keV.

3. Separated Delayed Neutron Precursors

Calculations of composite delayed neutron spectra have recently

³ W. Rudolph, et al., NEANDC(E)-172U, Vol. 5, July 1976.

been accomplished by Saphier, et al.⁴ using as input measured spectra from separated delayed neutron precursors together with the appropriate P_n (neutron branching ratios) and yield data. The importance of these spectra in reactor calculations were evaluated but are limited due to lack of spectral precursor data below 100 keV.

Measurements are planned with a group at Battelle-Northwest Laboratories (BNW), under the direction of Dr. Paul Reeder to obtain data in the lower energy region from separated precursors. Presently, precursors of Rb and Cs are being separated and the yield values may be sufficient to permit measurements to be obtained from ^{93}Rb to ^{96}Rb and ^{142}Cs to ^{144}Cs .

B. EFFECTS OF LEAD SHIELDS ON NEUTRON SPECTRA

Measurements of neutron spectra are usually complicated by intense gamma fluxes and generally require lead shielding to improve the neutron/gamma ratio at the detector, especially at lower energies (< 100 keV). Possible shield bias results from differences in the neutron interaction cross-section with energy and may depend upon both the geometry and the amount of lead in the shield. Previous measurements indicated the effect of spectral bias between 80 and 500 keV was minimal for symmetric lead shields up to 5 cm thick that surround the detector.⁵ A thicker (7 cm) lead shield, described previously,⁶ is presently in use at the University of Washington to enhance measurements of delayed neutron spectra between 10 and 1500 keV. The effects of this cave shield, and a shadow shield of similar geometry, to neutron spectra have been investigated using both Monte Carlo calculations and measurements from an Am-Li source.⁷

Measurements of the neutron spectrum from the Am-Li source were obtained with and without the lead shields using a proton-recoil spectrometry system over an energy range between 10 and 1500 keV. Detected neutron and gamma events were separated based on pulse shape discrimination. Effects of the two shields on the unshielded source spectrum were also calculated using a three dimensional Monte Carlo code; SAM-CE.⁸

⁴ Saphier, Ilberg, Shalev, & Yiftah, Trans. Am. Nucl. Soc., 22:671-672 (1975).

⁵ Fieg, Lalovic & Woodruff, Nucl. Sci. Engr., 58:260 (1975).

⁶ G.W. Eccleston & G.L. Woodruff, Nucl. Sci. Engr., in press.

⁷ G.W. Eccleston & G.L. Woodruff, Trans. Am. Nucl. Soc., 23:19-21 (1976).

⁸ RSIC Computer Code Collection. CCC-187/SAM-CE, Oak Ridge National Laboratory, Oak Ridge, TN.

Computations based on the experimental geometry and lead-detector compositions were completed for 5000 case histories for each shield.

Plots of the spectral data and Monte Carlo calculations corresponding to the two shields are shown in Figure B-1. The source spectrum for Am-Li is significantly softer than reported by others.^{9,10} This may be due in part to both the large size and the experimental orientation of the source which would tend to increase the number of scattering events in the source, for neutrons that reach the detector, and could noticeably soften the spectrum. The shadow shield data for energies below about 200 keV are smaller in magnitude than the source spectrum indicating a significant bias results with this shield. No bias effects are apparent above 20 keV in the cave shield data with the exception of a noticeable shift (one to two per cent) of the small peaks toward lower energies. The accuracy of the Monte Carlo calculations, while not sufficient to confirm differences between the shielded and unshielded measurements, indicate that bias effects are small for the cave shield and not negligible at the lower energies for the shadow shield.

Thick (7 cm) lead shadow shields will introduce a bias to measurements by decreasing the magnitude of the spectrum between about 8 and 30 percent relative to the source spectrum for energies below about 200 keV. This bias can be minimized for energies above 20 keV if the shield geometry is altered to form a cave by placing additional lead (3 cm) on the sides and behind the detector. An additional benefit obtained using this cave shield appears to be an increase in the neutron count rate, compared to the seven centimeter shadow shield, resulting from the additional lead which provides an added increase in the neutron-to-gamma ratio.

C. NEUTRON-GAMMA PULSE SHAPE DISCRIMINATION

Separation of neutron-gamma events in proton-recoil and NE-213 counters is presently being studied using a new method based on an analog divider and biased amplifier arrangement. This system permits a constant fraction bias signal to be formed, independent of the energy pulse, from the amplitude dependent pulse rise time signal, enabling improved neutron-gamma separation to be obtained.

The analog divider is a commercial nuclear instrument marketed by Ortec,* termed a Position-Sensitive Detector Analyzer (PSDA), that

* Ortec, Inc., 100 Midland Road, Oak Ridge, Tennessee 37830.

⁹ Reactor Development Program Progress Report, ANL-7017, p. 39, Argonne National Laboratories.

¹⁰ H. Werle, Karlsruhe Nuclear Research Center, External Report, INR-4170-25, Feb. 1970.

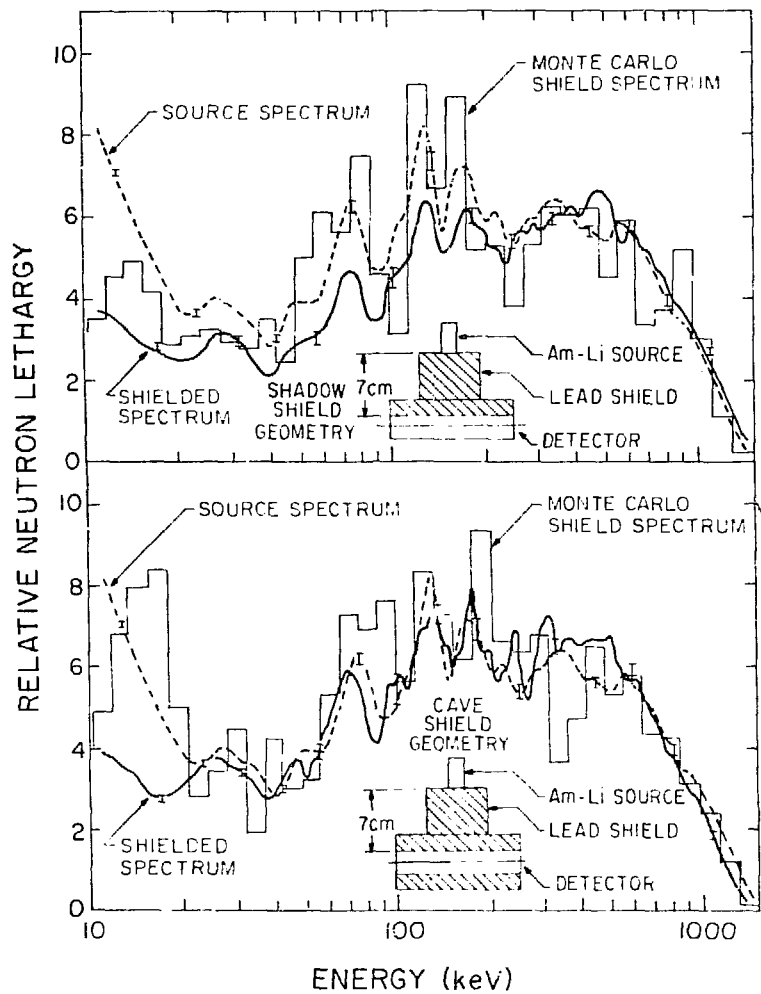


Figure B-1. Am-Li neutron spectra with and without lead shields.

normalizes a position input signal by an energy signal. The normalized output signals can be routed directly into a multichannel analyzer. If the position input is fed by a rate-of-rise signal, such as the fast bipolar output (with appropriate RC time constants) from an Ortec 450 Amplifier, the PSDA will form a specific ionization ratio that directly provides the separation index between neutron and gamma events. This instrument allows several advantages to be realized: (a) Only two basic nuclear instrument modules are required to collect pulse height data and separate it in terms of gamma neutron interactions. These modules are an Ortec 450 Amplifier and an Ortec 464 Position-Sensitive Detector Analyzer. (b) Coupling the output of the PSDA (i.e., the specific ionization ratio) to a biased amplifier permits selection and expansion of events particular to a specific range of rise time values. The net effect is an ability to increase the separation index between neutron and gamma events. (c) Increased neutron and gamma separation allows a larger dynamic range of data to be collected, particularly in situations where the range is limited by inadequate separation.

Measurements are presently underway to provide comparison data between the system using the analog divider and previous methods of pulse shape discrimination. Results to date indicate superior separation is achieved using the analog divider in comparison to a digital division technique or to the method based on the commercial pulse shape analyzing module sold by Ortec. However, one limitation does exist with the analog divider. This unit requires a 10 microsecond conversion time and cannot be used in applications with excessive counting rates.

YALE UNIVERSITY

A. FAST NEUTRON PHYSICS

1. A Global Analysis of n-⁴He Elastic Scattering Data up to 20 MeV
(J. E. Bond and F. W. K. Firk)

An analysis of all recent n-⁴He data up to 20 MeV has been carried out using the R-matrix formalism. Particular attention has been paid to the relationship between the formal and physical parameters obtained. A phase shift analysis indicates small but statistically significant differences for the d-wave phases compared with those obtained in an earlier analysis.¹ Our work has been submitted for publication in Nuclear Physics.

2. Polarization of Neutrons in n-⁶Li Elastic Scattering Between 1.5 and 6 MeV (Y. -H. Chiu and F. W. K. Firk)

Additional measurements of the asymmetries of polarized neutrons elastically scattered from ⁶Li at energies between 1.5 and 6 MeV are being made. These are essential if we are to improve upon the earlier analysis of our polarization data made at four angles.² So far, results at six new angles have been obtained. The available flux of polarized neutrons has been doubled using a thicker graphite polarizer with no appreciable loss of polarization. Monte Carlo calculations are underway to derive the point analyzing powers from the values observed using a new 400 g cylindrical-shell-target of ⁶Li.

3. Polarization of Neutrons in n-⁹Be Elastic Scattering Between 1.5 and 6 MeV (P. McGuire and F. W. K. Firk)

The asymmetries of polarized neutrons elastically scattered from ⁹Be are being measured between 1.5 and 6 MeV at six angles. In addition, the differential cross section will be measured under identical experimental conditions. When combined with our earlier preliminary results, sufficient information will be available to carry out a definitive analysis of n-⁹Be scattering throughout the MeV-region.

¹ Th. Stammbach and R. L. Walter, Nucl. Phys. A180 (1972) 225

² R. J. Holt et al., Nucl. Phys. A237 (1975) 111

B. BICMEDICAL APPLICATIONS*

1. Measurement of X-ray Spectra from High Energy Electron Medical Accelerators (R. Nath** and R. J. Schulz**)

A clinically suitable method for the measurement of x-ray spectra from high energy electron medical accelerators has been developed using the Yale electron LINAC. This precise and practical method uses photonuclear reactions to produce radioactivities in different materials which are sensitive to different photon energy ranges.

2. Measurement of X-ray Spectral Quality in the Range 4 to 30 MeV (R. Nath)

A sensitive and straightforward method for obtaining an index of x-ray spectral quality in the 4 to 30 MeV range has been developed. The method is a clinically feasible solution to an outstanding problem in the dosimetry of high energy x-ray beams used in radiotherapy of cancer⁴

3. A Study of Possible Methods of Enhancement of the Radiation Dose to the Tumor Using High Energy Electrons (R. Nath)

A method for enhancing the dose to a tumor using high energy electron beams and strong magnetic fields is being developed. A positive result would lead to better localization of the dose to the tumor volume and would be of great interest in the clinical practise of radiotherapy with electron beams. This experiment has been set up using the defunct electron scattering beam line at the LINAC.

* Work supported by NCI grant CA-06519

** School of Medicine, Department of Therapeutic Radiology, Yale University.

³ Medical Physics, 3 (1976) 139.

⁴ Medical Physics, 4 (1977) Part I and II.

UNIVERSITY OF KENTUCKY

A. NEUTRON SCATTERING

1. The Elastic and Inelastic Scattering of Neutrons by Isotopes of Molybdenum and Zirconium. (McDaniel*, Sinram**, Chung, Brandenberger⁺, Weil, McEllistrem, Glasgow⁺⁺, and Robertson⁺⁺⁺)

This work includes part of an extensive study of neutron elastic and inelastic scattering in the mass region A=90-100 which has been in progress at this laboratory for several years. The immediate goals of this study are the determination of the level and decay schemes and other nuclear structure properties in this mass region, and accurate measurement of elastic and inelastic differential neutron scattering cross sections at several incident energies. The first of the papers dealing with nuclear structure has been presented¹ first paper describing scattering cross section measurements has also been presented,² and reports measurements at 1.5 MeV incident energy for Mo and Zr isotopes. The other work includes the results of three sets of measurements carried out over a period of three years at incident energies between 2.5 and 6 MeV. The experiments were performed at different times because of limitations on the availability of the isotopically enriched Zr and Mo samples.

Several questions were to be studied through these measurements. First, the behavior of the elastic scattering cross sections as a function of neutron excess in a series of isotopes, and the complementary question of the relationship of Zr and Mo cross sections for nuclei with the same number of neutrons. The variation over a limited number of nuclides was not expected to be great, particularly since all of these nuclei should be spherical, near semi-magic ^{90}Zr . But with sufficiently precise measurements, the influence of changes in Z and N should be discernible. The second question was a related one, whether a consistent complex potential model would fit all of the measurements well. The measurements included are those for neutron elastic and inelastic scattering from ^{92}Mo , ^{94}Mo , and ^{96}Mo at an incident energy (E_n) of 2.52 MeV, from ^{89}Y , ^{92}Zr , ^{98}Mo , and ^{100}Mo at $E_n=2.75$ MeV, and from ^{90}Zr , ^{92}Zr , ^{94}Zr , ^{92}Mo , ^{94}Mo , ^{96}Mo , ^{100}Mo at 3.5 MeV, and from ^{92}Mo , ^{94}Mo , and ^{100}Mo at 6.0 MeV.

The experimental apparatus has been presented in detail elsewhere.² The scattered neutron yields were measured using a dynamically biased time-of-flight (TOF) spectrometer developed at the University of Kentucky³ to reduce backgrounds in wide dynamic range neutron detection. A beam of protons pulsed at a repetition rate of 2.0 MHz and bunched to a pulse width of <1.0 nsec was produced by the University of Kentucky's Van de Graaff accelerator and Mobley beam deflection system. The beam entered a 3.0 cm long gas cell filled with ^3H to 1.0 atm through a 0.00036 cm Mo foil. The proton energy losses in the foil and gas were 180 and 60 keV respectively. The average energy of neutrons produced at 0° was 2.75 MeV with an energy spread of 60 keV full width at half maximum (fwhm). These neutrons were incident on a cylindrical scattering sample mounted with its axis perpendicular to the reaction plane and about 6-8 cm from the center of the neutron source. Scattered neutrons were detected in a heavily shielded and collimated liquid organic scintillator (NE218) mounted between 2 and 4 m from the sample.

Complex potential models and the statistical model were used to obtain fits to the differential elastic scat-

* Now at North Texas University, Denton, Texas

** Now at II, Institut für Experimental Physik, 2-Hamburg-Bahrenfeld Luruper Chaussee-149, W. Germany

+ Now at Los Alamos Scientific Laboratory, Los Alamos, New Mexico

++ Now at Department of Radiology, Washington University, St. Louis, Mo.

+++ Now at Prestonsburg Community College, Prestonsburg, Ky.

1 McEllistrom, Brandenberger, Sinram, Glasgow, and Chung, Phys. Rev. C9, 690 (1974).

2 McDaniel, Brandenberger, Glasgow, and Leighton, Phys. Rev. C10, 1087 (1974).

3 J. D. Brandenberger and T. B. Grandy, Nucl. Instr. and Meth. 93, 495 (1971).

ing cross sections and the total cross sections. Striking similarities were found in the data for ^{90}Zr and ^{92}Mo , and also between the data for ^{92}Zr and ^{94}Mo . The analysis did require a definite i-spin dependence for the real potential, of the form $V-V_0-V_1[N-Z]/A$. The coefficient V_1 was $V_1 \approx 25$, comparable to that required for global fit analyses of proton scattering and some limited neutron scattering surveys. The elastic and inelastic scattering cross sections measured at 6 MeV incident energy are shown in Figs. 1 and 2. The curves shown with the measured points are least squares fits of Legendre Polynomial expansions to the measured cross sections.

2. Structure Studies in ^{92}Zr , ^{94}Zr (Glasgow, McDaniel, Weil, Brandenberger and McEllistrem)

The nuclear level structures of ^{92}Zr and ^{94}Zr are of especial interest because of the proximity of these isotopes in the periodic table to ^{90}Zr , which in its ground state has protons filling the $Zp_{1/2}$ sub-shell at $Z = 40$ and a closed neutron $1g_{9/2}$ shell at $N = 50$. The level structure of ^{92}Zr and ^{94}Zr have previously been studied in transfer reactions, inelastic scattering, β -decay, and thermal neutron capture. The results have been compiled by Wood¹, Kocher and Horen², and Kocher³.

Kocher and Horen's² compilation for ^{92}Zr includes a recently up-dated level scheme. The energies in keV, and spin-parities of the levels below 2.0 MeV, adopted by the compilers², are: 934.46, 2^+ ; 1383.0, 0^+ ; 1495.6, 4^+ ; and 1847.3, 2^+ .

Kocher and Horen² note that above 2.4 MeV, the correspondence between the levels observed in various experiments is not good, primarily because of imprecise energy determinations in the reaction studies. Spins have been tentatively adopted² for four of the levels above 2.4 MeV. While many ^{92}Zr de-excitation γ -rays recently have been identified, excitation functions have been measured only for the nine γ -rays originating from the levels below 2.4 MeV. None have been measured for the γ -rays from the levels above this energy and no γ -ray angular distribution data exists.

Kocher's³ recently released compilation for ^{94}Zr indicates a similar situation for this isotope. The energies, in keV, and spin-parities of the levels of ^{94}Zr adopted by Kocher³, are: 918.24, 2⁺; 1299.99, 0⁺; 1468.34, 4⁺; and 1668.74, 2⁺. Only two spins are known³ for levels above 2.4 MeV.

An additional interest in ^{92}Zr and ^{94}Zr stems from the use of zirconium as a structural material in nuclear reactors. The need for zirconium neutron inelastic scattering cross sections stimulated the recent (n,n' γ) measurements on ^{90}Zr , ^{91}Zr and ^{94}Zr by Tessler, Glickstein, and Carrol.⁴ Neutron time-of-flight studies at Kentucky have recently been made of neutron elastic and inelastic scattering cross sections for ^{90}Zr , ^{92}Zr and ^{94}Zr at 1.5, 2.75, and 3.5 MeV. These neutron time-of-flight experiments provide the most direct measure of the neutron inelastic scattering cross sections, but finite energy resolution prohibits the measurement of cross sections for closely spaced levels. Inelastic scattering cross sections inferred from (n,n' γ) studies provide the best cross section information about the scattering to closely spaced energy levels. This technique can be validated by comparing the inferred values to the cross sections of well-resolved levels measured in time-of-flight experiments.

This work includes the results of ^{92}Zr and ^{94}Zr (n,n' γ) experiments performed to determine the energies, excitation functions, angular distributions, and branching ratios of the de-excitation γ -rays of these isotopes. These experiments consisted of γ -rays excitation function measurements on each isotope using neutrons with energies from 2.22 MeV to 3.70 MeV and angular distribution measurements at incident neutron energies of 3.20 MeV and 3.70 MeV for ^{92}Zr and at 3.10 MeV for ^{94}Zr . Using this information, the ^{92}Zr and ^{94}Zr level structure near and above 2.4 MeV has been investigated and the spins of certain levels uniquely determined or limited to a few choices. Multipole mixing ratios were also determined for many of the γ -rays. These results are compared to previously reported results. Neutron inelastic scattering cross sections inferred from the present measurements are compared to other measurements of these cross sections.

The ^{92}Zr excitation function experiment identified 51 γ -rays, several of which were previously unreported, from 26 levels through 3472.0 keV. Two new levels, 2903.8 keV and 3407.9 keV, were discovered in this study. The remainder of

the level energies measured agree best with those reported by Fanger *et al.*¹² and this agreement aids in clarifying the level structure of ^{92}Zr . The ^{92}Zr 3.20-MeV angular distribution study yielded 24 angular distributions of γ -rays from the levels through 3056.5 keV while the 3.70-MeV study yielded 39 angular distributions of γ -rays from the levels through 3370.9 keV. The analysis of these distributions resulted in the following unique or limiting spin assignments (level energies in keV are followed by the acceptable J values): 2398.0, 3, 4; 2485.1, 5; 2742.6, 4; 2818.0, 2, 3; 2863.6, 3-5; 2903.8 0; 2909.0, 2, 3; 3056.5, 2 3124.4, 1-3; 3177.2, 2-5; 3190.8, 2-5; 3236.2, 2-5; 3262.2, (2); 3275.9, 1-3; 3288.7, 2-4; 3370.9, (1); 3407.9, 2-4; 3452.2, 2-4; and 3472.0, 2-4. Gamma-ray level branching ratios were measured and the γ -ray multipole mixing ratios were obtained for the indicated spin assignments.

The ^{94}Zr excitation studies identified 28 γ -rays, 15 of which were previously unreported, from 20 levels below, 3361.2 keV. A previously reported ambiguity concerning Z^+ and 4^+ levels in the 2320 keV to 2365 keV energy region has been resolved. We have shown that there are two γ -decaying levels in this energy region; a $J = 4$ level at 2329.0 keV and a 2^+ level at 2365.4 keV. New levels were discovered at 2507.6, 2698.0, and 2825.2 keV, and tentatively, 25859.8 keV. The 3.10-MeV ^{94}Zr angular distribution experiment yielded 18 angular distributions of γ -rays from the ^{94}Zr levels through 2887.0 keV. Unique or limiting spin assignments were made to the following five levels of ^{94}Zr for which the spins were previously unknown: 2507.6, 3; 2698.0, 0-3; 2825.2, 2-4; 2859.8, 4(1); and 2887.7, 0-3. The γ -ray multipole mixing ratios were obtained as well as γ -ray level branching ratios.

-
- 1 J. L. Wood, Center for Nuclear Research, Karlsruhe, Germany, External Report 1/72-1 (1972).
 - 2 D. C. Kocher and D. J. Horen, Nucl. Data B7, 299 (1972).
 - 3 D. C. Kocher, Nucl. Data A10, 264 (1973).
 - 4 G. Tessler, S. S. Glickstein, and E. L. Carroll, Jr., Phys. Rev. C2, 2390 (1970); S. S. Glickstein, G. Tessler, and M. E. Goldsmith, Phys. Rev. C4, 1822 (1971).
 5. McEllistrem, Brandenberger, Sinram, Glasgow, and Chung, Phys. Rev. C9, 690 (1974).

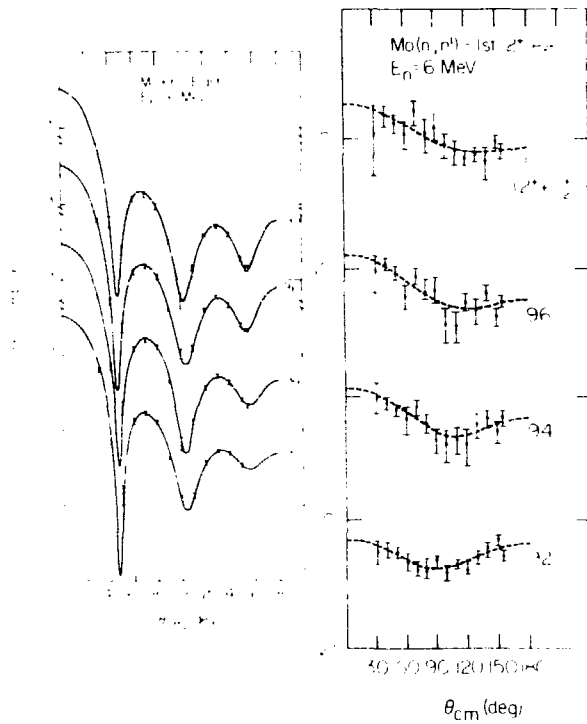


Figure 1. 6 MeV elastic scattering. Figure 2. 6 MeV inelastic scattering.

3. Low Energy Neutron Inelastic Scattering (McEllistrem, Coope, Tripathi, and Schell)

This report extends and supports a recent Physical Review Letter which announced anomalously large neutron inelastic scattering cross sections in certain deformed nuclei. The first publication of these remarkable cross sections was by D. F. Coope, M. C. Schell, S..N. Tripathi, and M. T. McEllistrem. The experimental results are cross sections for inelastic scattering from several even-A Sm isotopes at an incident neutron energy of 2.5 MeV. What is remarkable about these results is evident in the three figures and Table of Ref. 1. Angular distributions of neutrons scattered to the first excited 2^+ levels of ^{148}Sm and deformed ^{152}Sm are shown in Fig. 1. The approximately isotropic results for ^{148}Sm are typical of neutron inelastic scattering angular distributions from many experiments with many nuclei throughout the periodic table. Experiments in several laboratories confirm that, with the exception of scattering to 0^+ excited levels, scattering to other levels showed modest

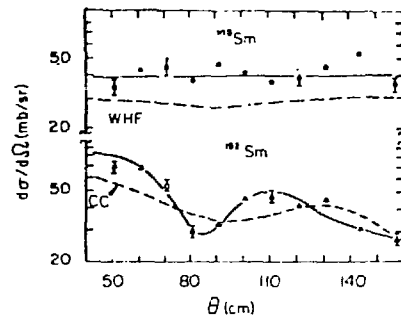


Figure 1. Inelastic scattering cross sections from the first 2^+ states of ^{148}Sm and ^{152}Sm for an incident neutron energy of 2.47 MeV. The cross sections are plotted in center-of-mass coordinates. Solid lines are Legendre polynomial fits to these data; dashed curves represent theoretical calculations described in the text.

anisotropies at low bombarding energies, i.e., for $E_n \lesssim 3$ MeV. The data in Fig. 1 for ^{152}Sm show a quite different pattern, with very pronounced anisotropy. Plotting that data on a semi-log scale, as is done in Fig. 1 of Ref. 1 tends to reduce the appearance of the anisotropy; but one notes that the cross sections vary over a ratio of 3 to 1. A strongly anisotropic distribution such as this is unmistakable evidence of the dominance of a direct interaction process, even at this low incident energy. What is remarkable about

these inelastic cross sections is made even more evident in Fig. 2 and Table I. A γ -ray spectrum gives the relative strengths to several levels with excitation energies above that of the first excited level. One sees strong excitation of a 6^+ level, which is extraordinary, and weak evidence of the 8^+ level in about channel no. 580

For many years discernible direct reaction contributions were inferred as being present in neutron inelastic scattering cross sections, even at low bombarding energies. These contributions were estimated in several publications as being at the 20 to 30 percent level for incident energies from 2.5 to 3.5 MeV. The contributions at low incident neutron energies were difficult to estimate at best, and even the existence of them could be questioned. During the last year we have seen clear evidence of the dominance of direct reactions at 2.5 MeV incident energy clearly established in several experiments with deformed nuclei. The dominance shown for scattering in ^{152}Sm is, we believe, the first publication of the importance of deformations for low energy neutron inelastic scattering.

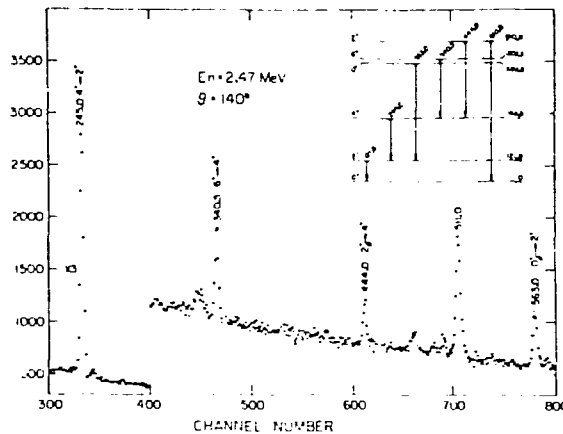


Figure 3. $(n,n'\gamma)$ photon spectra for the rotational nucleus ^{152}Sm . The peaks in the spectrum can be identified with rotational and vibrational transitions in the level scheme shown.

TABLE I. Measured inelastic scattering cross sections for ^{152}Sm compared with CC and WHF calculations. Calculations are described in the text.

Level	Measured		Theory		
	(n,n')	(n,n' γ)	CC	WHF	CC+WHF
2 ⁺	600±40	...	450	140	590
4 ⁺	250±30	262±30	70	90	160
6 ⁺	...	60±10	12	21	33
8 ⁺	...	10±4	...	1	...

not marked on the drawing. The 8⁺→6⁺ transition is more evident in other spectra.

The statistical model (WHF) fails to account for the cross sections by factors of 3 and 4. The coupled-channels model (CC), which should give an excellent description of the direct interaction excitations, fails by similar factors except for the first excited 2⁺ level. Except for the first excited 2⁺ level, even combining the two models fails by a factor of two. Moreover combining them as done in Table I violates unitarity - the WHF values should be reduced at least 25% to correct those values for the cross sections attributed to direct processes with the CC calculations.

4. Sample Size Corrections and Comparisons of (n,n') Cross Sections from n and γ -ray Detection (Glasgow, McDaniel, Weil, Brandenberger, McEllistrem)

As noted above, the neutron inelastic scattering cross sections σ_n inferred from the results of the (n,n' γ) experiments can be compared to those measured directly in (n,n') experiments. These two types of neutron experiments normally have different objectives and usually are not undertaken at the same incident neutron energies. The excitation functions measured in the (n,n' γ) studies can be used to extrapolate the angle integrated γ -ray production cross sections σ_γ to the proper energy so the inelastic neutron cross sections can be inferred and compared to the directly measured values. If the inferred cross sections are to

agree with the directly measured ones, certain criteria must be satisfied. The range of the extrapolation should not be large because the anisotropies of the γ -ray angular distributions can change rapidly with energy. All γ -rays cascading to and emitted from a level must be identified and their angle integrated cross sections accurately measured. Failure to include even one strong γ -ray introduces serious error. Based on excitation function data, $4\pi\sigma_{\gamma}(90^{\circ})$ cross sections often can be used to approximate the cross sections of those γ -rays for which angular distributions were not obtained. However, this approximation introduces additional uncertainties into the inferred neutron inelastic scattering cross sections. Consistent and similar sample-size corrections must be made to the data from the (n,n') and $(n,n'\gamma)$ experiments.

The effects of these corrections for the $(n,n'\gamma)$ measurements on the apparent cross sections are shown in Fig. 1, which shows apparent cross sections for Fe and Pb scatterers as a function of sample diameter. Each panel indicates the element, observed γ -ray energy, and the incident neutron energy, E_n . The height of each sample was equal to its diameter. The upper curve and open points correspond to data corrected only for neutron flux attenuation in the sample. This causes an apparent cross section which increases with sample size, meaning that ignoring multiple processes leads to a severe overestimate of flux removal from the sample. The lower open points and curves show data not corrected for flux attenuation, but corrected for multiple scattering only, which leads to net sample independent. Since no allowance for attenuation has been made, the apparent cross section decreases with sample size. The solid points and middle curves show data corrected both for flux attenuation and multiple scattering, with results essentially sample size independent. We note that the upper and lower curves have positive and negative shapes almost the opposite of each other, which means the two corrections approximately cancel. This is a point made by R. B. Day twenty years ago.

The angle integrated γ -ray production cross sections obtained from the ^{92}Zr 3.20 MeV angular distribution experiment satisfy these criteria and have been extrapolated to 2.75 MeV. Table I compares the inelastic neutron cross sections inferred from these results to those measured directly from an (n,n') experiment at 2.75 MeV, an experiment referred to above. The inferred and directly measured neutron inelastic cross sections for the 934.1- and 1381.9-keV

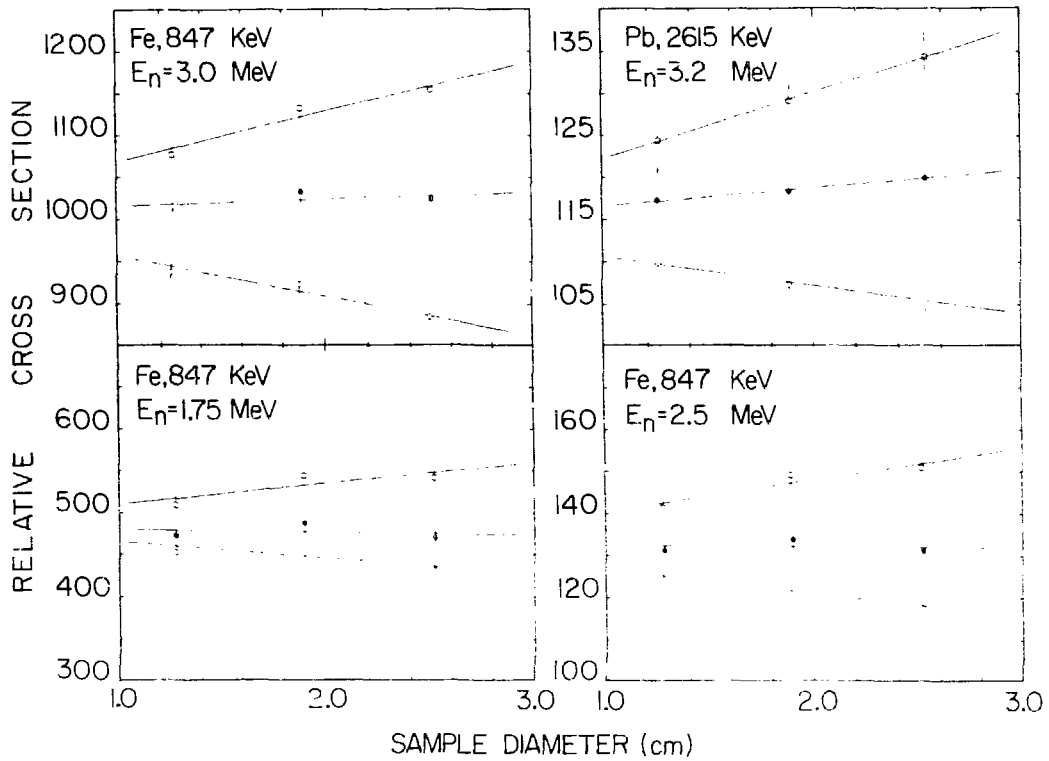


Figure 1. Apparent γ -ray production cross sections as a function of sample size. Each set of points and curve corresponds to results after different corrections, as described in text.

levels agree very well. The cross sections for the remaining three levels agree within their respective uncertainties. The difference between the measured and inferred values for the levels at 1846.4 keV and 2066.1 keV result from insufficient energy resolution to separate the two neutron groups in the (n,n') study. The sum of the inelastic cross sections of these two levels agrees with the sum of those inferred from this study. This is an example of the situation of closely spaced levels mentioned in the introduction, in which the (n,n' γ) technique gives more precise values of the inelastic cross sections than does a direct (n,n') measurement.

Table I. A comparison of ^{92}Zr inferred and directly measured neutron inelastic scattering cross sections at 2.75 MeV. The energy above each column is the incident neutron energy in each experiment.

Level (keV)	Neutron Inelastic Scattering Cross Sections, in (mb), at 2.75 MeV	
	(n,n' γ) 3.20 MeV	(n,n') 2.75 MeV
934.1	633 \pm 68	606 \pm 64
1381.9	198 \pm 12	109 \pm 28
1494.8	183 \pm 22	254 \pm 46
1846.4	240 \pm 26	340 \pm 72
2066.1	240 \pm 25	160 \pm 7

B. DETECTION METHODS

1. A Secondary Standard Neutron Detector for Measuring Total Reaction Cross Sections (Sekharan, Laumer, and Gabbard)

A neutron detector has been constructed and calibrated for the accurate measurement of total neutron-production cross sections. The detector consists of a polyethylene sphere of 24" diameter in which 8- $^{10}\text{BF}_3$ counters have been installed radially. The relative efficiency of this detector has

been determined for average neutron energies, from 30 keV to 1.5 MeV by counting neutrons from ${}^7\text{Li}(p,n){}^7\text{Be}$. By adjusting the radial positions of the BF_3 counters in the polyethylene sphere the efficiency for neutron detection was made nearly constant for this energy range. Measurement of absolute efficiency for the same neutron energy range has been done by counting the neutrons from ${}^{51}\text{V}(p,n){}^{51}\text{Cr}$ and ${}^{57}\text{Fe}(p,n){}^{57}\text{Co}$ reactions and determining the absolute number of residual nuclei produced during the measurement of neutron yield. Details of absolute efficiency measurements and the use of the detector for measurement of total neutron yields from neutron producing reactions such as ${}^{23}\text{Na}(p,n){}^{23}\text{Mg}$ are available.

The detector efficiency is flat to within 2% for neutrons with energies between 30 keV and 1.56 MeV. Tests of detector response at higher energies are encouraging, but presently incomplete. The efficiency of the detector as a function of neutron energy is shown below.

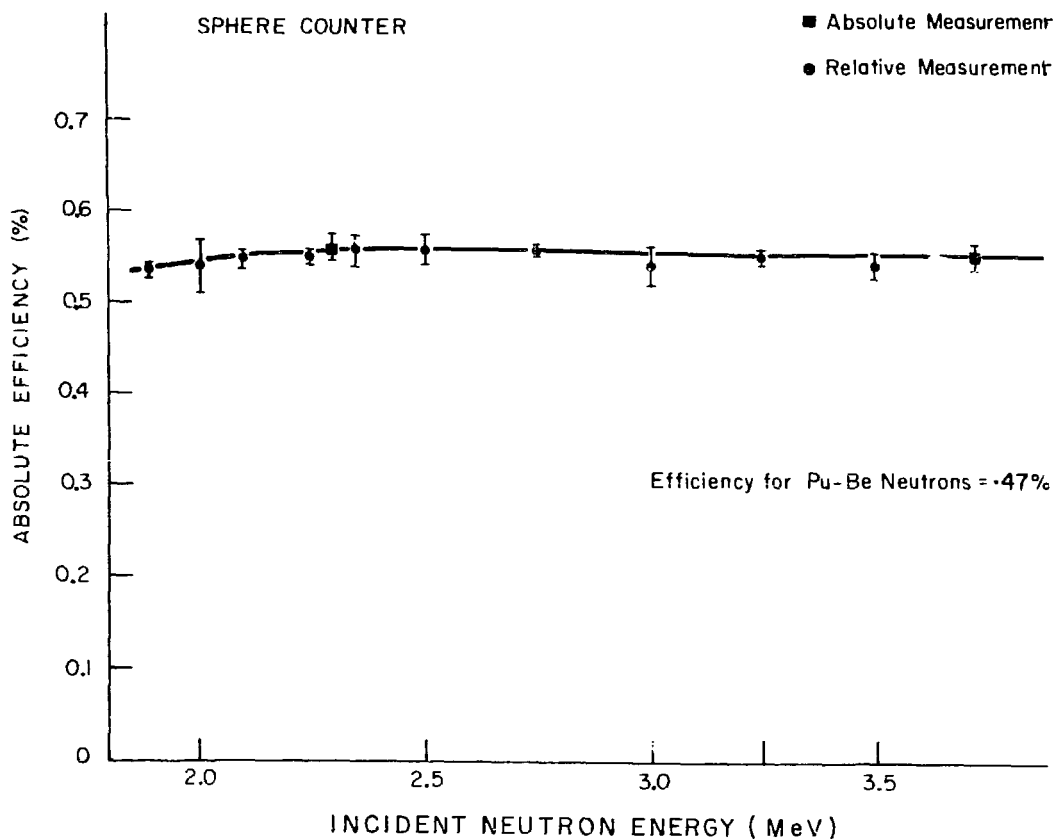


Figure 2. Detector efficiency versus neutron energy.

E. ODD-ODD NUCLEI NEAR A = 90

1. ^{98}Tc Energy Levels (D. E. Miracle, E. C. Hagen, and B. D. Kern)

As a continuation of our study of (p,n) reactions and the structure of odd-Z, odd-N nuclei, the $^{98}\text{Mo}(p,n)^{98}\text{Tc}$ reaction has been studied through observation of the subsequent γ rays.

The results of the analysis of γ -rays singles spectra and γ - γ coincidence spectra are summarized in Fig. 1. The energy level diagram is consistent with levels deduced from the $^{98}\text{Mo}(^3\text{He},t)^{98}\text{Tc}$ and the $^{97}\text{Mo}(^3\text{He},d)^{98}\text{Tc}$ reactions. There are several differences from the results of a concurrent (out previously published) (p,n) study.³

An interesting feature of the ^{98}Tc γ -ray transitions is that they are divided into two groups - one decaying directly or by cascade to the 55.5-keV level (probably even parity) and the other decaying to the 14.6 sec isomeric 90.9-keV level (probably 2^-). The principal configuration of these levels is interpreted as being $[\pi(g_{9/2})^3\nu(d_{5/2})^{-1}]_J^+$ and $[\pi(g_{9/2})^2(p_{3/2})^{-1}\nu(d_{5/2})^{-1}]_2^-$, respectively.

Future internal-conversion electron measurements will be made with the objective of determining the spin-parities of the low-lying levels.

2. Low-lying Levels of ^{94}Nb (E. C. Hagen, D. B. Kern, F. D. Snyder, and D. E. Miracle)

Through the (p,n) reaction it is possible to produce nuclei which are typically not easily produced by other reactions. Their structure can be studied by measurements on the outgoing neutrons by the time-of-flight method, or by the acquiring of gamma-ray spectra. With an even-Z, even-N target, this reaction produces odd-Z, odd-N nuclei which typically have many low-lying levels. Although the description of these levels is more difficult than that for levels of odd-A nuclei, there is theoretical interest in describing the states available to the odd proton and the odd neutron, and the interaction between them.

Computed Hauser-Feshbach (p,n) cross sections have been compared to the cross sections deduced from γ -ray yields and spin-parities assigned on the basis of best fits to the data.

The low-lying low-spin levels of ^{94}Nb have been investigated; these levels were populated via the $^{94}\text{Zr}(p, n\gamma)^{94}\text{Nb}$ reaction with a separate isotope ^{94}Zr foil target (96% ^{94}Zr). Excitation functions of γ rays were obtained at incident proton energies from 1.688 to 3.700 MeV. γ - γ coincidences were observed at $E_p = 3.0$ MeV. The existence of additional levels at 301.5, 450.3, 666.2, and 785.0 keV has been established. Computed Hauser-Feshbach (p, n') cross sections have been fitted to experimental cross sections deduced from the γ -ray data with the resulting best-fit spin-parities: 140.4-keV level, 2^- ; 301.5, 2^- ; 334.2, 3^+ ; 396.3, 4^- ; and 450.3, 3^+ .

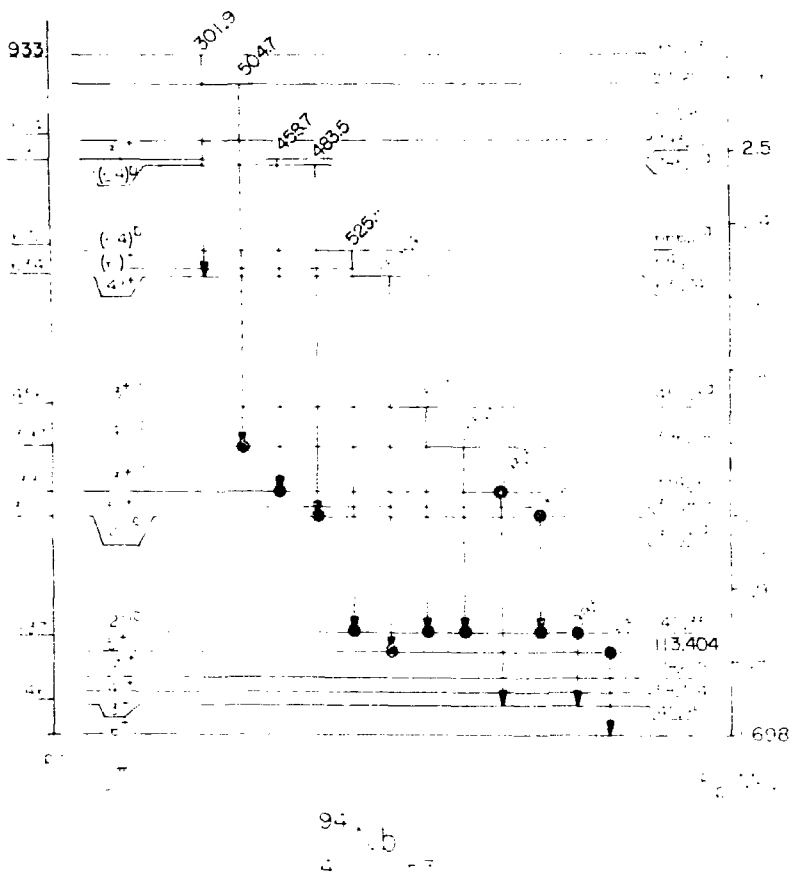


Figure 3. Low lying levels of ^{94}Nb .

4. Neutron Scattering from Separated Tin Isotopes
(Harper, Weil, and Brandenberger)

The differential cross section for elastic scattering of 1.0 MeV neutrons from five separated isotope even-A tin targets has been measured at fourteen scattering angles between 30° and 150°. The scattering samples of $^{116}, ^{118}, ^{120}, ^{122}, ^{124}\text{Sn}$ are all of greater than 90% purity in the major isotope and contain 0.2 to 0.4 moles each. Time-of-flight techniques were used to collect the data and to eliminate background.

The scattered neutron yields have been corrected for multiple scattering, finite geometry, and neutron production anisotropy and attenuation in the scatters. They have been normalized to carbon scattering, which was also measured.

Within the limits of the experimental errors, there is a regular progression in the shapes of the curves with increasing mass number. In particular, the cross section at the minimum near 120° decreases with increasing mass number, while at very forward and backward angles the heavier isotopes have the larger cross sections. Optical model calculations are being made to determine a potential which fits the data. It is planned to make additional measurements at higher bombarding energies to determine the neutron excess dependence of the real and absorptive potentials.